Alma Mater Studiorum - Università di Bologna

DOTTORATO DI RICERCA IN

STUDI SUL PATRIMONIO CULTURALE / CULTURAL HERITAGE STUDIES

Ciclo 33

Settore Concorsuale: 05/B1 - ZOOLOGIA E ANTROPOLOGIA

Settore Scientifico Disciplinare: BIO/08 - ANTROPOLOGIA

THE ONTOGENY OF BIPEDALISM: INSIGHTS FROM THE STUDY OF TALAR GROWTH

Presentata da: Carla Figus

Coordinatore Dottorato

Prof. Raffaele Savigni

Supervisore

Prof. Stefano Benazzi

Co-supervisore

Dr. Timothy M. Ryan

Esame finale anno 2021

A is aiaias,
pro s'esempiu prus bellu de amori, fortza et coraggiu ca deu podia pedi

Alle mie nonne,
Per avermi dato il miglior esempio di amore, forza e coraggio che potessi desiderare

To my grandmothers,
for the brightest example of love, strength, and courage I could wish for

Acknowledgments

Finally, here we are. This is the end of a big journey, for me. As for all the journeys, there were good times, and…well, less good times. I will always remember especially these last, because they gave me the opportunity to learn and grow, as a person and as a young researcher. Also, this last year was crazy, and not even in my worst nightmares I would have imagined to spend the last year of my PhD confined at home during a terrible pandemic which came with pain and so much loss. It was a hard time, truly, and it also amplified the anxiety and the loneliness. It would have been really simple to just get lost in all of this.
Luckily, I was never alone, and I managed to accomplish my doctorate, even if with some difficulties - more than expected - but here I am.

First of all, I'd like to thank my two supervisors, Stefano Benazzi and Tim Ryan, for your guidance and valuable suggestions, and for giving me a chance to learn and experience. I'd like also to thank my supervisor *ad honorem*, Nick Stephens. I couldn't have done anything, without your precious help. I'd like also to thank all my colleagues for their support.

Then, my gratitude goes to my family. My parents, my sister, in particular. They are my pillars. Without you, I wouldn't be the person I am today, and I wouldn't have reached this important goal. I'd like to include my whole family, aunts, uncles, cousins…all of you (well, it's a big one, it's impossible to thank you all one by one!). A special big thank you goes to Zaira, because seeing you growing up help me more than you can imagine.

A giant thank you to all my friends. Again, you are too many to name all but definitely I want to thank, in particular, Cumpa, Martina known as Lucia, and Saretti. Well, you deserve it! For always support me (and, well, to put up with me…). For all the laughter, the crying, the wine. Simply, for always be there for me.

Lastly, a big thank you to Mozart, Beethoven, Vivaldi, Morricone, Tchaikovsky, to name a few. Trust me, I wouldn't be writing these words without you.

Ringraziamenti

Finalmente, ci siamo. È la fine di un lungo e importante percorso e, come per ogni viaggio, ci sono stati i momenti belli e i momenti…meno belli, diciamo. Ma sono proprio i momenti meno belli ad avermi dato la possibilità di crescere, come persona e come giovane ricercatrice, motivo per cui li conserverò a lungo nella mia memoria. Inoltre, l'ultimo anno passato è stato un anno particolarmente difficile, che ha messo a dura prova tutti noi. Mai avrei immaginato che durante l'ultimo anno di dottorato sarebbe scoppiata una pandemia, portando con sé tutti i problemi che, purtroppo, conosciamo bene, come la perdita di persone care, l'isolamento forzato, i problemi socio-economici, la mancanza – molto banalmente – della normalità, e tanto altro. Quest'ultimo anno, dunque, è stato particolarmente difficile, e ha portato con sé nuove difficoltà anche all'interno del mio percorso di dottorato. Ma ce l'ho fatta. Ho portato a termine il mio percorso, anche se vorrei tornare indietro e correggere tutti i miei errori (purtroppo non posso).

Prima di tutto, mi piacerebbe ringraziare i miei due supervisori, Stefano Benazzi e Tim Ryan, per avermi dato la possibilità di portare avanti questo progetto di ricerca, di imparare e fare nuove esperienze, nonché di visitare posti che non avrei potuto vedere altrimenti. Ringrazio anche il mio supervisore *ad honorem*, Nick Stephens, per la pazienza che ha avuto, e per avermi insegnato tantissime cose. Semplicemente, non ce l'avrei fatta senza il suo aiuto. Ringrazio anche tutti i colleghi che in questi anni mi hanno supportata.

Ma soprattutto, ringrazio i miei veri pilastri: la mia famiglia, in particolare i miei genitori e mia sorella. Semplicemente, non sarei qui senza di loro, in tutti i sensi. Includo qui tutta la mia famiglia al completo (davvero troppi da nominare!) ma ringrazio tutti loro. Chi c'è, e chi purtroppo non c'è più, vi ringrazio tutti. Ringrazio Zaira, perché il suo arrivo ha portato una gioia, nelle nostre vite, di cui non sapevamo di aver bisogno.

Un ringraziamento gigantesco va agli amici e alle amiche. Siete tropp* da elencare, ma ognun* di voi sa quanto sia stato prezioso l'aiuto e il supporto datomi in questi anni, anche solo con la vostra vicinanza in più di un'occasione. Però, ci tengo a ringraziare almeno tre persone, che durante questo percorso mi sono state vicino più di altre: Cumpa, una delle mie migliori amiche da…be', da parecchi anni, Martina detta Lucia e Saretti, che invece ho avuto la fortuna di incontrare durante questi ultimi anni. Grazie, semplicemente.

Infine, un grazie di cuore a Mozart, Beethoven, Vivaldi, Morricone, Tchaikovsky, per nominarne alcuni. Diciamo che senza di voi, non starei scrivendo queste parole.

Abstract

One of the most intriguing question in the human evolution field regards the evolution of human bipedalism. The development of bipedal locomotion was gradual during evolution, and with the increase in discoveries of fossils and, in particular, in discoveries of pedal bones, the attention to this problematic has grown in the last decades. Moreover, the discoveries of juveniles fossil foot bones has led the attention to the evolution and the development of bipedal locomotion. The study of the development of human gait in children may help in shedding light to the development of human locomotion. The human talus plays a pivotal role, linking the leg to the foot and receiving and distributing the weight, while permitting a wide range of foot movements. It is also present at birth, and this makes a perfect bone to study to disentangle how the bone structure acts to cope with the changes in locomotion and body weight. Here, I analyze the external and internal morphology of the human talus from the perinatal period to adolescence, to investigate how the different phases of the acquisition of bipedal gait affect talar morphology, and how the bone copes with the weight gain during growth. Results show that the talar internal and external morphologies change in line with the different activities and loading of the foot. Initially, at around birth, the talus has a very globular and immature external shape, with a very dense trabecular architecture, composed of thin, numerous, and densely packed trabeculae, with a rather isotropic structure. External and internal morphologies change in relation to the different loading patterns which follow during growth, showing a more specialized structure, both in the external and internal morphology, linked to the maturation of bipedal locomotion, until the adult-like pattern is reached, during adolescence.

Table of contents

List of figures

Chapter One
Dissertation introduction

1.1. Human Bipedalism: an evolution that took millions of years

One of the most intriguing questions in human evolution concerns the evolution of bipedal locomotion. It is undoubtedly true that the development of human bipedalism was one of the most significant adaptations of the hominin lineage (Harcourt-Smith & Aiello, 2004). Nowadays, modern humans are the only bipedal mammals, and share this characteristic with some extinct hominins that have engaged in obligate bipedal locomotion, and some others hominoid primates that sometimes engage in bipedal locomotion. The term bipeds derives from the latin *bipes,-ĕdis*, and it is used for all the animals that walk on two feet. For example, among vertebrates, also birds and bats are bipeds. But the peculiarity of human bipedalism merits attentions, since it has evolved in a perfect mechanism, unique in its genre. The upright walking is seen as a distinctive feature that marks the divergence between hominins and apes. Humans are considered, after the first few years of life, fully obligate bipeds, since in normal conditions, this is the only form of locomotion. It is general knowledge that obligate bipedalism arose circa 2.5-1.8 Ma, linking its appearance to the genus *Homo*. The more recent hominin species are considered fully bipedal (e.g. *Homo antecessor, H. heidelbergensis, H. neanderthalensis, H. sapiens*) (Harcourt-Smith & Aiello, 2004; Trinkaus, 1983; Aiello & Dean, 1990). Its first appearance in the hominin lineage is still matter of debate, even though *Homo ergaster* (1.8 Ma) is thought to be the first obligate terrestrial biped (Harcourt-Smith and Aiello 2004). Despite no pedal fossil remains have been found yet, this taxon has been considered fully bipedal thanks to both the postcranial evidence (Ruff et al. 1993) and the Ileret footprints (Kenya), which have been associated to *Homo ergaster/erectus* (Bennett et al. 2009). These footprints show the presence of a moderately adducted hallux, with an angle of 14° (with respect to the 8° of modern humans prints and to the 27° from the Laetoli prints), a medial transmission of the weight before push-off and the presence of a medial longitudinal arch (Bennett et al. 2009). These footprints, dated back to 1.51-1.53 Ma, provide one of the earliest evidence of a modern human-like foot anatomy (Bennett et al. 2009). Early hominins, though, may have doubtlessly walked on two legs, but probably this was not their only locomotion (DeSilva, 2009). They were, probably, habitual bipeds. Terrestrial bipedalism has been proposed for australopiths, and confirmed by the Laetoli footprints (3.6 Ma), generally attributed to *A. afarensis* (Ward 2002; DeSilva 2009; Raichlen and Gordon 2017; Drapeau and Harmon 2013; Ryan et al. 2018; Masao et al. 2016). Moreover, the paucity of fossil remains and their fragmentariness represents one of the biggest impediment to our expanding knowledge on the argument, making it even more difficult to infer locomotion behaviors from fossils (Schmitt 2003).

There are three types of bipedalism:

- Facultative bipedalism. This form of locomotion is assumed temporally in order to perform particular tasks, e.g. chimpanzees can carry objects with their hands while walking on two legs;
- Habitual bipedalism. This form of locomotion is typically used, but is not the only locomotion form;

- Obligate bipedalism. This is typical of those hominins where bipedalism is the only type of terrestrial locomotion.

Great apes, like bonobos and chimpanzees, can engage in other type of locomotion such as knuckle-walking, quadrupedalism, and also brachiations, climbing, clinging and swinging. But they can also engage, for short period of times, in bipedal locomotion.

1.1.2. Human gait cycle

The modern human gait cycle is a very complex function that we perform daily without even noticing. It is composed by two main and alternating phases: the stance phase and the swing phase. During these alternating phases, the body weight is transferred from one foot to the other, from side to side. The stance phase begins with an initial contact, e.g. heel-strike, and the foot begins to assume the body's full weight (Moore and Dalley 2018). During this movement, the knee is fully extended and the foot is dorsiflexed to permit the calcaneus to touch the ground first. The forces are transmitted to the ground with the lateral side of the foot, and the foot is flat on the ground, in loading response. This marked the passage to the midstance phase, when the body weight is completely on the bearing foot. At this point, the foot, acting as a lever, passes the forces medially and over to the ball of the foot, then the strong plantarflexors muscle contract, pushing the forefoot down, generating propulsive force and resulting in the push-off, with the anterior part of the foot pushing against the ground and lift off, as the body continues to move forward. During this phase, the toes flex to grip the ground, augmenting the push off initiated from the ball of the foot. As the hallux leaves the ground, this action, known as toe-off, ends, and the leg engages in the swing phase. This phase starts when the toes leaves the ground and ends with the next heel strike. During the swing phase, the foot is off the ground, with the knee and hip both bent to permit the body to move the leg forward, to the next step, e.g. heel strike. Stance phase is a little longer than swing phase.

1.1.3. Development of gait

The acquisition of bipedalism is a complicated process that involves both the musculoskeletal and neuromuscular structures (Chagas et al. 2006). During the first 12-18 months, the fast growing pace, with legs growing faster than the trunk, promotes the development of bipedalism (Adolph and Avolio 2000), during which the disproportion of the cranium and the rest of the body decrease (Chagas et al. 2006). Some important morphological and anatomical differences between juvenile and adults explain some of the differences between immature and mature locomotion. Toddlers have not yet completely developed balance and movement coordination skills (Sutherland 1997), and the instability during gait is one of the most important characteristic of the immature locomotion (Sutherland et al. 1980; Bril and Brenière 1991; Adolph, Vereijken, and Shrout 2003). Toddlers usually have a wider walking base, and produce narrow steps at a slow pace (Levine 2012).

But before standing fully erect, toddlers are not fully bipedal, and often practice also an "on all-four" quadrupedal behavior (i.e., using hands and knees, rarely on hands and feet) (Abitbol 1993). This form of quadrupedalism is different from the one we can observe in other primates, and the similarities are only mechanical, without necessarily implying any phylogenetic relationship (Abitbol 1993). The two main different locomotor behaviors (e.g., human quadrupedalism and bipedalism) are often intermingled for a certain period of time, and the timing differs from child to child (Abitbol 1993; Berger et al.,1984). Moreover, due to the many anatomical differences between species, e.g., the human bigger heads, quadrupedalism requires more muscular energy in humans, than bipedalism. These postures are unique to our species and they appearance varies across cultures (Cowgill and Johnston 2018). Usually, there are some recognizable milestones even if it should be taken into account that individual variability and cultural influence could affect them; nonetheless, children generally start trying to sit upright, with the head well balanced over neck and shoulder at about six months; they then start usually moving on all four at about nine months, and gradually they stand in the upright position and start walking unaided at about twelve months, acquiring the basic skills to perform a stable locomotion during about the first two months of practice (Chagas et al. 2006). During this phase, steps are highly irregular and with a high step-to-step variability, helpful to maintain balance while their muscular control system is still immature (Sutherland et al. 1980; Adolph, Vereijken, and Shrout 2003; Clark, Whitall, and Phillips 1988; Thelen 1992). Between 10 and 17 months, during supported locomotion, children can carry the body and try to propel it forwards but needed to be supported in controlling the equilibrium (Forssberg, 1985). According to Berger and colleagues (1984) infants usually starts to walk gradually unassisted, and initially almost all the efforts are put in trying to hold the body in equilibrium while standing fully erect, rather than in propelling the body forward (Zeininger 2013; Berger, Altenmueller, and Dietz 1984). To cope with the balance issues, infants have a dominance of hip and knee extending moments during stance (Hallemans et al. 2005), with no active push-off at the ankle joint. In this phase, the vastus medialis and gluteus maximus play a pivotal role for balance control, according to Okamoto and colleagues (2003). Mediolateral trunk oscillations are significantly higher in new walkers as well, reflecting variation in joint angles from the ankle through the pelvis (Brenière and Bril 1988; Raichlen et al. 2015). After 3 to 6 months of practice, after the very beginning of locomotion, it is possible to see significant improvements (Bril and Ledebt 1998), and the more they gain experience, the more they grow stronger and with greater control over the movements. Steps become longer, narrower and straighter, and the pattern is more constant, with less step-to-step variability (Sutherland et al. 1980; Forssberg 1985; Adolph, Vereijken, and Shrout 2003; Raichlen et al. 2015). Knees are less flexed (Zeininger, 2013) and the balance skills improved, especially while on one leg (Brenière and Bril 1988; Hilgard and McGraw 1945; Pedersen, Størksen, and Vereijken 2002). Also the pace increases, in correlation with the increase in step length, more than in step frequency (Preis, Klemms, and Müller 2008). Between 2 and 3 years old, children start to gradually assume an adult-like pattern, and the improvements increase more rapidly (Preis, Klemms, and Müller 2008). Other scholars reported that a more mature-like gait is observable after roughly 4 months of unaided walking activity (Okamoto and Okamoto, 2001; Hallemans et al. 2005), while Forssberg and colleagues (1985) reported that no dramatic changes have been observed in the

gait pattern after the beginning of unassisted walking. According to Burnett and Johnson (1971), children's gait patterns resemble the adult ones after circa one year of unaided walking experience, and it slowly continues developing until at least 4 years of age (Ryan and Krovitz, 2006). Finally, other studies reported that bipedalism is not fully developed until 7 or 8 years of age (Bernstein et al. 2000; Brenière and Bril 1988; Sutherland et al. 1980; Bril and Ledebt 1998). Another difference between adult-like locomotion and children pattern, is the absence of the "heel-to-toe" roll-over pattern (Hallemans et al. 2006). To increase the base of support, all the foot touches ground, and the plantigrade-positioned foot is lifted at the end of the stance phase. This help the immature walkers in controlling the equilibrium (Hallemans et al. 2006). The adult-like transfer of the center of pressure from lateral to medial side develops around 18 months (Bertsch et al. 2004), while the heel strike pattern does not develop until 18-24 months, on average (Zeininger 2013). At this age, the muscle associated with plantarflexion are sufficiently strengthened to permit a toe-off phase and a more mature knee flexion and extension (Zeininger 2013). Longitudinal arch is present, even if in a very slight way, at birth (Cunningham, Scheuer, and Black 2016). It is though covered by the fat pad present in the neonatal and toddler foot, that is need to protect the foot. It begins to develop when walking activities starts, and it continues to develop until four to six years (Bertsch et al. 2004). When the longitudinal arch is developing, peak plantar pressures on the fore- and hindfoot increase while pressure is reduced in the midfoot, reaching adult levels between 5 and 6 years (Bertsch et al. 2004; Zeininger 2013; Saers 2017). According to Sutherland and colleagues (1980), numerous other factors can influence the timing and duration of the phases of development of bipedal locomotion, before gait patterns normalize with the finale achievement of mature gait. In fact, children learn day by day how to avoid problems like falls (troubleshooting skills), improving the pace and length of the steps (Adolph, Vereijken, and Denny 1998), adapting their movements to the different ground surfaces (Adolph, Vereijken, and Denny 1998; Adolph et al. 1997; Adolph and Avolio 2000; Bertenthal, Campos, and Barrett 1984; Campos, Bertenthal, and Kermoian 1992). Among the other variables, the increasing body size and the neural maturation are of relevant importance. During the first 2 years of life, the general chubbiness (e.g. the Ponderal Index) is replaced by a slimmer body shape, with an increase in muscle mass (Palmer 1944). According to Adolph (2003), in children neither body dimensions nor gender differences may be directly correlated to locomotion skills, while in adults they are correlated (longer legs, longer steps). In the meantime, the brain continues to grow and it reaches the 70% circa of its adult weight (Thatcher et al. 1996). Johnson (1998) stated that there is a fast activity in the glial cells and a fast synaptic growth in the visual cortex, leading to an increase in electroencephalogram activity in the frontal lobe during the onset of the locomotion activity (Bell and Fox 1998). By age four, the central nervous maturation approaches adult levels, after which gait differences between adults and juveniles come down largely to allometry (Sutherland 1997). However, patterns of muscle activation do not fully resemble those of adults until the child reaches roughly 15 years of age (Sutherland et al., 1980; Sutherland, 1997). All these descriptions highlight the highly variegate patterns in children locomotion, and the difficulty in trying to find common milestones. There is no accordance in the timing of the achieving of the locomotion milestones, due to the high individual variability, and also an interpopulation variability.

1.1.4. Anatomical modifications

During evolution, bipeds went through huge skeletal modification, from the skull to the feet, to perfectly adapt to this new locomotion. Human skeleton is highly specialized, especially in the lower limb and foot. Maintaining balance is more complicated, when walking on two legs, e.g. with less support base area. In the skull, the foramen magnum changes position (Landi et al. 2020), and it is positioned more anteriorly than in quadrupeds, which display also a flattened and horizontally disposed nuchal plane, where the potent nuchal and neck muscles attach. Another important adaptation is seen in the vertebral columns. To cope with the different balance, the human rachis developed two main curvatures: primary and secondary ones. The primary curvatures develop during fetal life in the thoracic and sacral vertebrae. The secondary ones, develop after birth, and are the cervical and lumbar curvatures. These curvatures help maintaining the center of gravity closer on the body's midline, and between the feet. Other primates have a C-shaped spine, and when they engage in a bipedal gait, they must bend the knees to keep balance. The evolution of the lordosis (i.e. the inward curve of the lumbar spine), though, poses other challenging for pregnant females: during pregnancy, lumbar lordosis is accentuated to maintain the center of gravity in the right position, while compensating for the increase weight.

The pelvis also faces numerous adaptations to cope with the different balance. Modern humans coxae, in fact, are short and wide, with a large acetabulum to well accommodate a large femoral head which must support the increase in body weight through the hip during locomotion, and a prominent anterior inferior iliac spine where potent muscles attach, with a short and wide sacrum. The distal part of the femur has a different angle, e.g. valgus, and larger condyles surface. This results in the knees closer together, and the feet directly placed under the center of gravity. In females, the pelvis is wider, to cope with the bigger head size of the human neonates.

1.1.5. The foot

From the hominoid foot fossils from early Miocene (23-5 Ma circa), through the hominid fossils from the Pleistocene, human foot have greatly evolved (McNutt, Zipfel, and DeSilva, 2018), becoming a highly derived and specialized structure, being the only structure that directly made contact with the ground (Harcourt-Smith and Aiello 2004; Holowka and Lieberman 2018; DeSilva et al. 2019; Mcnutt, Zipfel , and DeSilva, 2018). Thanks to its anatomical characteristics, e.g. a stiff longitudinal arch, adducted hallux, short toes, and complex talar structure which, in synergy with muscles and ligaments, significantly participate in forming a stiff lever (Farris et al. 2019), humans perform bipedal locomotion with relative low energetic efforts. The skeletal morphology of the foot is central to reconstructing the evolutionary history of bipedalism. The foot is composed by 26 bones: 7 tarsals, 5 metatarsals, and 14 phalanges. The tarsus, e.g. hind- and mid-foot, comprehends the talus, calcaneus, cuboid, navicular, and the three cuneiforms. The talus, known also as the ankle bone, is of pivotal importance as it has the role to unite the foot and the leg, and receives the weight of

the body from the tibia. It has a body, a neck and a head, and articulates dorsally and medially with the tibia, and laterally with the fibula. Plantarly, it articulates with the calcaneus and, distally, with the navicular. The talus is a very robust bone, and it is the only talar bone without any muscular attachments; its main role is to receive the force from the leg, then transmits the weight posteriorly to the calcaneus, on which the body of the talus rests, and anteriorly to the navicular through the spring ligament, an osseo-ligament that is suspended across a gap between the sustentaculum tali and the navicular bone (Moore and Dalley 2018). The talus is the only foot bone that has no muscular or tendinous attachments. Most of its surface is covered with articular cartilage. The talar body bears the trochlea superiorly and narrows into a posterior process that features a groove for the tendon of the flexor hallucis longus, flanked by a prominent lateral tubercle and a less prominent medial tubercle. The calcaneus is the largest and strongest bone in the foot (Moore and Dalley 2018). It receives the body's weight from the talus and, when standing, it passes the majority of it to the ground. It articulates with the talus and cuboid. The navicular is a little boat-shaped bone that articulates with the talus and the three cuneiforms. This bone is a very important site for tendon attachment and it plays a pivotal role in the longitudinal arch. The cuboid is the most lateral bone in the distal row of the tarsus. The three cuneiform bones (medial, intermediate, and lateral) articulate with the navicular and metatarsals. The lateral articulates also with the cuboid. The metatarsus consists of five metatarsals, numbered from the medial side of the foot, and articulates with the phalanges, through the proximal phalanges.

1.1.5.1. Foot ossification

Together with the development of locomotion, the anatomy of the foot changes, from the initial fetal phases to adulthood, preparing the body, and the foot, to be functional to its roles. There are two types of ossification: during the intramembranous ossification, bones form by a direct differentiation of mesenchymal cells into osteoblasts, while during the endochondral ossification, bones develop by replacing a primitive cartilage model (Long, 2012). The intramembranous ossification is typical of the cranial bones, and it starts towards the end of the second gestational month. Endochondral ossification is typical of the long bones. It initiates first in an avascular environment, where cells differentiate into chondrocytes that secrete cartilage matrix. Then, a thin membrane is formed, to separate the cartilage from the surrounding mesenchyme, called perichondrium (Cunningham, Scheuer, and Black 2016). With different timing for each bone, chondrocytes in the center mature, and start to calcify. Contemporarily, begins the vascularization of the cartilage, and osteoblast commence to secrete the primary bone, which form the bone collar. External loading will stimulate bone response, with the production of secondary trabecular structure (Fazzalari et al. 1997; Ryan and Krovitz 2006). The skeletal elements do not form at the same time, but chondrification occurs in a cranio-caudal direction for the axial skeleton, and in a proximal-distal direction in the appendicular skeleton (Long, 2012). The adult and mature foot, as above mentioned, has 26 foot, excluding accessoria and sesamoids. During growth, though, there are about 46 separate centers of ossification, 26 of which are primary (Cunningham, Scheuer, and Black 2016)(Figure 1). During the fetal period, ossification starts first in the metatarsals, followed, in order, by distal, proximal and middle phalanges. Among the tarsals, the calcaneus is the first to commence ossification,

frequently from two different primary center of ossification, e.g. medial and, often, lateral. The former is probably of endochondral origin, and appears between the 4th and 5th month. The second one, appears a little later, between the 5th and 6th months, and it is of endochondral origins.). The talus (Figure 2) commences ossification after the calcaneus, but it is the first tarsal bone to show evidence of cartilage ossification (Gardner, O'Rahilly, and Gray 1959). The ossification of the talus starts around the 6th-7th months, and it arises usually from one center, but more than one nucleus has been noted (Gardner et al., 1959). The perinatal talus has an oval shape, with two main indentations on the plantar and dorsal surfaces that mark the position of the future sulcus tali and neck, respectively, separating the future articular facets. Laterally, they are separated by a ridge. In the neonatal talus, the angle formed by the neck and head is reported to be around 130-140°, which will increase during growth to reach the adult proportions (150°). According to Scheuer and Black (2004) the reduced appearance of this angle is linked to the inverted appearance of the neonatal foot. The increase of this angle has been associated with the morphological changes linked to the preparation for walking, at about 10-12 months. Around 2.5-3 postnatal months, the neck appears well defined. The ossification of the lateral process and sulcus tali begins around 5 months. At about 2 years of age, the posterolateral wall of the sulcus tali is reported to develop as a downward-projecting triangular process, while the trochlea surface becomes more round in shape (Scheuer and Black, 2004). The neck surface is reported to change direction during growth (Gardner, O'Rahilly, and Gray 1959). Starting from a medial-side direction, during the early fetal life, it changes during gestation, with the increase of the angle between neck and head. The cuboid commences to ossify around birth. Its presence, though, is not a reliable sign of skeletal maturity, and it can also ossify from multiple ossific nodules, which will fuse together. The cuneiforms generally start to ossify from the first year, with the lateral being the first to show ossification signs, followed by the medial cuneiform, from the second year. The intermediate commences ossification around 2.5 year (Scheuer and Black, 2004). The last tarsal bone to start ossification is the navicular, around the end of the second year, and ossification may start from a single nucleus, or multiple foci (Cunningham, Scheuer, & Black, 2016).

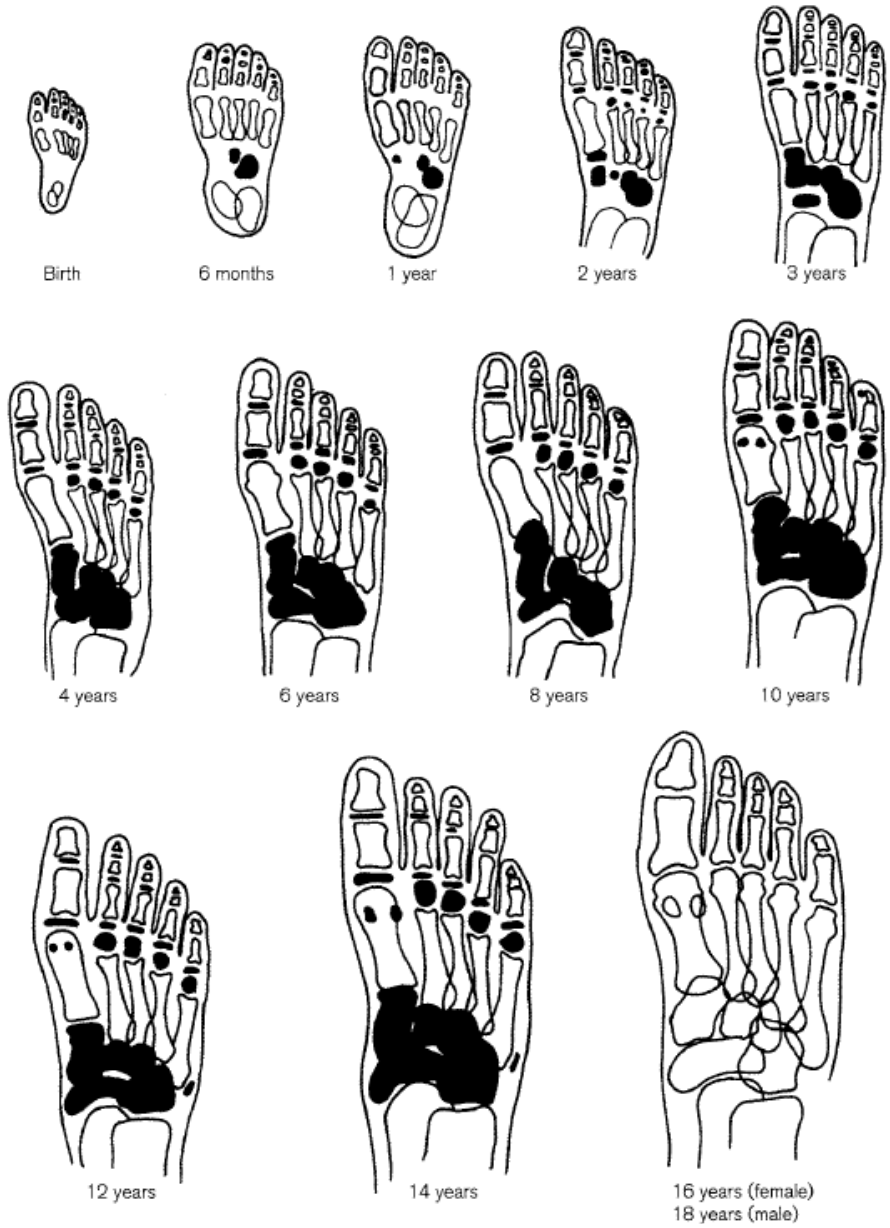

Figure 1 - Stages of foot development. From Cunningham, Scheuer & Black, 2016 (redrawn after Birkner, 1978)

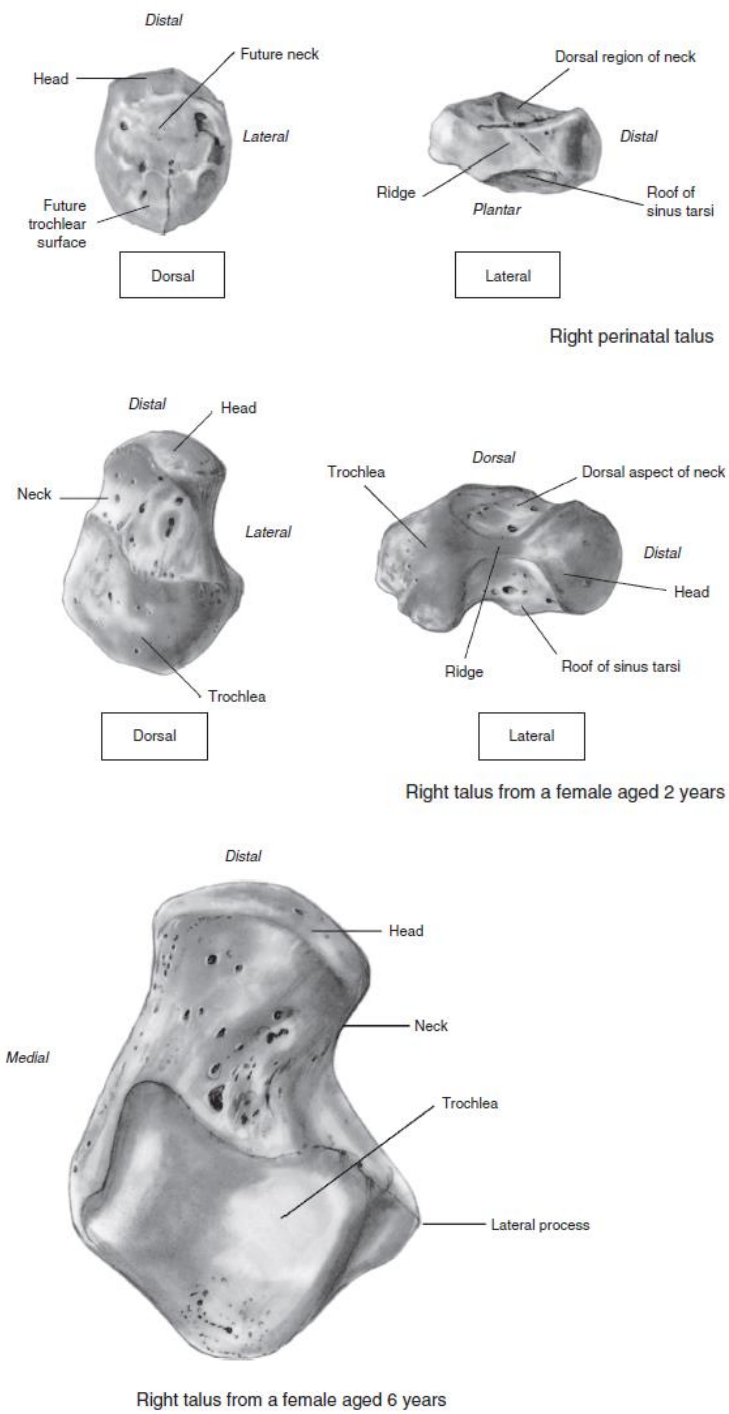

Figure 2 - Anatomy of the growing talus. Top: perinatal; Middle: 2 years old; Bottom: 6 years (dorsal view). From Schaefer, Black, and Scheuer, 2009.

1.1.6. Objectives and chapters summaries

Even though our knowledge about the development of bipedal behaviors have greatly increased during the last decades, there are still many doubts on its origins. The study of the development of bipedal walking could help tracking important developmental milestones, offering a new perspective from which to look at the different locomotor behaviors, and connected morphologies, from the past. Moreover, immature trabecular bone is

highly responsive to functional loading (Ryan and Krovitz 2006; Gosman and Ketcham 2009) and the external morphology is still relatively plastic (Hellier and Jeffery 2006), making an ontogenetic study an excellent way to further explore the relationships between bones and function. Many studies have been conducted on the foot (DeSilva et al. 2019), and many of them have explored the talus, being of pivotal importance (Sorrentino, Stephens, et al. 2020; DeSilva 2009; Saers, Ryan, and Stock 2018; Su and Carlson 2017). It connects the lower leg to the foot, contributes to the formation of the ankle joint, with tibia and fibula, allowing for different movements, e.g. inversion, eversion, dorsiflexion, plantarflexion. In addition, it is a weight receiver and distributor. It receives the weight directly from the tibia, and passes it downwards, through the posterior subtalar joint, to the calcaneus, and forwards, through the anterior subtalar joint and navicular joint, to the calcaneus and navicular, respectively. This makes the talus a perfect bone to study. Nevertheless, there are very few study on its development, and the recent increase in juvenile fossils recoveries makes this problem even more urgent to solve. Studies have been made on the juvenile ilium, for example, on the juvenile tibia, femur, radio. Tanck et al (2001), in their experimental study on the architectural adaptation during ontogeny, found out that, in young pigs, bone density starts to adapt to external load early, during growth, while the trabecular architecture is adapted during later phases of development. They explained the rapid increase of bone density with the weight increase during the early development. Ryan and Krovitz (2006), in their study on the trabecular ontogeny of the proximal femur, found out that the pattern of trabecular structure change during the ontogenetic development of mature bipedal locomotion, with an initially primary cancellous bone being replaced by remodeled bone with fewer, thicker trabecular struts, confirming the previous literature (Fazzalari et al. 1997; Parfitt et al. 2000). Degree of Anisotropy (DA), though, is found to be anisotropic in one of the two Volume of Interests (VOIs) they used (e.g. the inferior volume, with trabeculae oriented in a supero-inferior direction). There is a lack of study on the tarsal bones, except for an analysis of the internal architecture of the juvenile calcaneus (Saers, Ryan, and Stock 2020). A holistic investigation of the juvenile foot bones is missing, and it can be of great help in many fields, not last it could be a framework to which compare the different juvenile fossils. To the knowledge of the author, this is the first study to explicitly examine both external and internal changes in the human talus during the very early phases (from the late gestational weeks). To achieve this goal, a combination of methods is used to better explore the whole patterns of changes: Geometric Morphometric methods (GMM) are used to assess, describe, and quantify the changes in shape and form (shape + size) between different age classes, while trabecular biomechanics is used to better understand how the trabecular architecture adapts to the changing loading linked to the development of locomotion. We decided to use an innovative approach to answer different specific questions linked to age periods, combining these analyses to a "whole-bone approach" in biomechanics, with the analysis of the complete bone combined with a more in-depth analysis that uses pointclouds in order to statistically compare the biomechanics results (DeMars et al. 2020). The main goal of this dissertation is to explore the holistic changes that occur in human talus during growth in a sample of modern humans. In studying the anatomical and functional changes of the talus, I tried to answer to few questions. The most important interrogation is how much the talar morphology changes and when, during growth, and if these changes are linked to the different

locomotor milestones; also, how the anatomical changes covary with the development of the internal trabecular architecture, which, thanks to its faster modeling rate, is thought to be more indicative of the changes in loading behaviors. Though, the difficulties, when coping with so many anatomical changes, make it challenging to directly respond to this big and complex question. This is why I tried to answer these questions one by one.

The obvious, first question was: how does the anatomy evolve during the achievement of the mature gait? How and when the external shell starts to adapt itself to the new locomotor behaviors, and to what extent the trabecular struts capture these changes? Are these changes linked, e.g. does the juvenile talus develop in parallel with the changing in trabecular architecture? In Chapter Two, I tried to provide an answer to these questions. The analysed sample is composed of juveniles from birth to 10 years old, to better explore the differences between non-walkers, immature walkers and mature walkers.

Then, another question arose: how many differences there are between the external and internal morphologies before and after the first bipedal steps? Is it still mainly driven by genetics, and when the epigenetic influence starts to act? In Chapter Three, I tried to better explore this problem. The earliest phases of development are analysed in a sample of modern juveniles from perinates to 3 years old (≤3 years old). The sample is analysed first by age classes, then the sample is divided into two functional groups, e.g. non-loading and loading juveniles, in order to further analyse the differences in morphology and fabric architecture observable during this fundamental timeframe.

Lastly, after the conquest of the mature gait, other forces influence talar morphology. In Chapter Four, I try to address to this problem. Here, the adolescence are included in the sample and the development and orientation of articular facets are explored, to better understand when and how joints adapt themselves to the increased loading due to the locomotion and substrate differences.

Finally, in Chapter Five the results of this dissertation are discussed. Taken together, all this results may help with the study of juvenile fossils, helping us to broaden our knowledge on the origin of bipedalism.

Chapter Two
Insights from morphological and trabecular changes during postnatal growth

2.1. Introduction

Bipedalism is a unique trait of our species, and its evolution has been a hot topic in the paleoanthropological field, and the lower limb – in particular, the foot – has a main role in this quest (Harcourt-Smith 2002; Harcourt-Smith and Aiello 2004; Sorrentino, Carlson, et al. 2020; Mcnutt and Zipfel 2018; DeSilva et al. 2019). Even though many mammals can practice facultative upright positional behavior for short periods of time, only humans can practice upright locomotion permanently. A large amount of study investigated the evolution of bipedalism, mostly focusing on the functional morphology of the adult bone (Sorrentino, Stephens, et al. 2020; Zeininger et al. 2016; Lewton and Scott 2017; Tsegai et al. 2017; Frelat et al. 2012, 2017). Likewise, the study of development of human bipedalism can provide a unique chance to shed light on the evolution of morphology and behavior across species (Colombo et al. 2019; Saers, Ryan, and Stock 2020; Raichlen 2005; Shapiro and Raichlen 2006; Ryan and Krovitz 2006; Gosman and Ketcham 2009; Raichlen et al. 2015). In order to do so, we must determine if and how the skeleton reflects the different loadings that characterize the achievement of human bipedalism (Raichlen et al., 2015). The loading patterns during childhood, irregular at the beginning of the practice and more and more predictable along the way, may capture the shift from unstable to stable locomotion and leave signs in the trabecular architecture and morphology of the bone (Raichlen et al., 2015; Saers et al., 2020). Recent works on the trabecular bone development highlighted the ability of trabecular bone to track ontogenetic signals in the proximal femur (Ryan and Krovitz 2006; Ryan, Raichlen, and Gosman 2017), distal radius (Colombo et al. 2019) proximal tibia (Gosman 2007; Gosman and Ketcham 2009), and calcaneus (Saers, Ryan, and Stock 2020). The correct analyses of these bony signals, in association to the thorough knowledge of the patterns of neuromuscular maturation and changes in muscle strength (McGraw 1935, 1943; Breniere and Bril, 1988; Assaiante and Amblard 1993), may help shed light into the human journey towards a mature and efficient gait (Raichlen et al., 2015). Both cortical and trabecular bone are highly responsive to the loading environments to which they respond through modeling processes (Barak, Lieberman, and Hublin 2011; Wollf 1892; Ruff, 1982; Pontzer et al. 2006; Christopher Ruff, Holt, and Trinkaus 2006; Carlson and Judex 2007). The mechanisms that regulate the bone remodeling during life are well known (Barak 2019), and it has been shown that the rate of bone remodeling during the first two years of life is higher than in adults (Cunningham and Black 2009a,b). Walker (1991) estimates that the neonatal remodeling rate is 50% per annum, while the adult rate is 5%. Numerous longitudinal studies have highlighted the link between bone modeling and gait development (Milovanovic et al. 2017; Ryan and Krovitz 2006; Gosman and Ketcham 2009; Raichlen et al. 2015; Saers, Ryan, and Stock 2020) making it clear that most of the variations we appreciate in adult skeletons actually develop during the post-natal period. Consequently, the understanding of the "when" and "how" these variations appear is crucial (Ryan and Krovitz 2006) and a thorough study of ontogenetic

changes is well suited to better understand the adult anatomy and morphological variations. The external shape is also very informative: it is indeed linked to its function, mainly in the articular areas, that are connected to the joint mobility (Turley and Frost, 2013; Sorrentino, Stephens, et al. 2020; Turley, White, and Frost, 2015). The external shape is also strongly influenced by a genetic blueprint and by its phylogenetic heredity (Kivell 2016; Turley, Simons, and Frost, 2018). Cortical bone model at a slower rate than the cancellous bone (Eriksen 1986; Eriksen 2010) making it easier to catch functional signals in the latter. Due to the slower modeling rate, it could be misleading trying to correctly interpret a particular morphology, without knowing how much it has been determined by genetic and how much by function (Lieberman, 1997). Consider that, the morphological analysis of the external shape should be, in this context, accompanied by the analysis of the internal bone architecture, that can offer important functional insights (Kivell, 2016).

The human talus, being located between the lower limb and the foot, plays an essential role in distributing the weight of the body during walking and standing. One of its most important functions during this process is in allowing for foot movements while efficiently dividing weight between its anterior and posterior portions, where it articulates with the navicular and calcaneus, respectively (Hellier and Jeffery 2006). It is the only bone in the lower limb with no muscular attachment (Detenbeck and Kelly 1969) even if it has many ligamentous attachments. The center of the talus has been recognized as a junctional region for force distribution (Cunningham, Scheuer, and Black, 2016). As such, the talus plays a pivotal role in the different stages of human locomotion, from crawling, to initial bipedal acquisition, to full striding bipedalism at age 8 (Hellier and Jeffery 2006). Unfortunately, little is known about the morphological changes of the talus during the first years of life, when infants acquire upright posture and gait maturation. There are few works on the growing talus, to the knowledge of the authors, and both on a sample of juveniles older than 8 years (Hellier and Jeffery 2006; Turley, Simons, and Frost 2018).

The aims of this chapter are twofold: the first goal is to highlight the ontogenetic morphological changes from birth to about 10 years of age, while the second one is to quantify the trabecular bone properties from early infancy to pre-pubertal age, to better understand how the mechanical forces act on the human talus, ultimately shedding light on the adult bone morphology and functionality. To investigate these changes, a combinative methodological approach, i.e. Geometric Morphometric and trabecular biomechanics, has been used. Based on previous studies on ontogenetic talar changes (Hellier and Jeffery 2006) we predict that the orientation of the articular facets during growth will change to cope with the increase in body weight and to efficiently distribute the forces in a medial direction as gait matures. Based on previous studies on the trabecular biomechanics during growth (Colombo et al. 2019; Saers, Ryan, and Stock 2020; Raichlen et al. 2015; Ryan and Krovitz 2006), we predict also that bone volume fraction (BV/TV) will be higher in the youngest individuals, and it will steadily decrease and then increase again after 3 years of age, following the increase in mechanical strain. Moreover, we predict that the Degree of Anisotropy (DA) values will increase from birth, faster after the onset of locomotion, and then the values will rise slower in the oldest age groups, as stability of gait has been reached.

2.2. Material and Methods

This work analyzes the postnatal development of the human talus. The sample consists of 70 modern juvenile tali aged between 8 postnatal weeks and 10 year old.

Control sample

Fourteen individuals (F=8; M=6), aged between 11 postnatal months and 11 years, came from the Collection of Bologna, Italy, which sex, age at death, and cause of death is known (Belcastro et al. 2017; see Table 1). The collection comprehend Italian skeletal remains from the Emilia-Romagna region and from Sardinia, and they were collected mostly from 1908 to 1953 (Belcastro et al., 2017). The largest part of the Emilia-Romagna cohort was buried in Bologna La Certosa cemetery, the biggest cemetery of the city. The importance of this collection is given by the presence of ante mortem data, information about socioeconomical backgrounds, the generally good state of preservation and the relatively high number of children in the collection. The birth year ranged between 1814 and 1922 (with the majority born after 1850) and they died between 1898 and 1944. For the large part of the individuals, the place of birth were also known. As for the jobs, women were mostly housewives and sewer, while men were employed in different occupations, i.e., farmer, laborer, and mason with more frequency. The great number of non-adults who died before the first year of life highlights the high infant mortality during the mid-19th century (Belcastro et al., 2017), with a decrease of children in the collection from the age of 3. The cohort under study comprehend individuals from Bologna and Parma. Moreover, the cause of deaths of the control sample show that, except for one individual (BO14M), all the children suffered from acute illnesses, and probably died suddenly. This is important, because chronic illnesses may influence the correct acquisition of the locomotor abilities, e.g. lay down, weakness.

Archaeological sample

The rest of the study sample has been selected from different archaeological samples, with a timespan that goes from Neolithic to modern age (Table 1).

The site of Popova zemlja is located near the town of Beli Manastir in Osijek-Baranja County in eastern Croatia. The rescue excavations took place in 2014 and 2015 and covered a surface of approximately 37,000 square meters (Los 2020). Two main cultural layers were identified at the site: a prehistoric layer consisting of several Neolithic and Chalcolithic strata, and a Roman period layer. The prehistoric layers of interest are dated to the Neolithic period in which the remains of a large settlement and 39 inhumation burials were found. According to the available radiocarbon dates a huge majority of Neolithic burials from this site can be dated to the Middle/Late Neolithic, i.e. between 4800 and 4500 BCE. Most of the burials were found in a contracted position on either left or right side with different orientations. In several cases, one or more ceramic vessels were placed by the head of the deceased (Los 2020). Four individuals from this site have been used for the present study.

Thirteen individuals are from the Norris Farms #36 (Illinois, USA) sample, housed at the Pennsylvania State University, for which the age at death was estimated based on tooth crown formation and dental eruption stages

(Milner and Smith 1990). This remains are part of the Oneota culture and dated back to 1300 AD (Millner and Smith, 1990).

The town of Ilok is the easternmost settlement in Croatia, located on the right bank of the Danube River. The samples used in this study come from two locations from this site: Krstbajer (n=4) and Vlatka Kraljevića Street (n=1). Rescue archaeological excavations at the Krstbajer site were carried out between 2015 and 2017 by the Ilok Municipal Museum and the Institute of Archaeology. In total, 188 graves dated between the end of 12th and the transition from the 15th to the 16th century were investigated (Krznar and Rimpf, 2018). These burials most probably belong to the parish cemetery around the church of St. Helen the Queen. In 2016 and 2018, the rescue excavation in Vlatka Kraljevića Street, led by the experts from Ilok Municipal Museum, resulted in a discovery of 24 burials. Archaeological context and direct radiocarbon dates date the use of this cemetery between 1526 and 1668, i.e. during the Ottoman rule over the town (Rimpf and Novak, 2020).

Nineteen individuals came from the Imperial Roman site of Velia. The site, originally founded by Greeks in 540BC (Morel 2006), is located on the Italian west coast, near Salerno (Campania, Italy). Numerous archaeological campaigns have been held, and, during the 2003-2006 campaign (Fiammenghi 2003), a necropolis with over 330 burials. This necropolis, dated back to the I and II centuries AD, yielded both cremation and inhumations, with numerous juvenile burials. The age at death was analyzed based on the assessment of skeletal and dental maturation.

Five individuals came from the sites of Paks and nine from Perkáta-Nyúli dűlő. The two sites are located in – (Hungary), and are stored at the Natural History Museum in Budapest. The cemetery and settlement at Perkáta-Nyúli dűlő represents a population of a Cuman settlement in the Transdanubian region of Hungary, which at the same time preserved a population from the transition period of the Cuman integration (Hatházi 2004). The site was found during a motorway constructions works, between 2009 and 2010 by the Field Service for Cultural Heritage. The cemetery counts more than 4,000 graves. All the individuals dated back to the 14^{th}-16^{th} centuries AD, except for on (3421) that dated back to the 10^{th}-12^{th} centuries AD. Age-at-death was estimated based on the development of the deciduous and permanent teeth (Moorrees, Fanning, and Hunt 1963; Moorrees, Fanning, and Hunt Jr 1963; Smith 1991). When no teeth were available, diaphyseal length (Stloukal and Hanáková 1978) and also epiphyseal fusion (Ferembach 1980) were used (László 2008, 2018; Mesterházy-Ács 2015; Szeniczey et al. 2019)

The church around the cemetery of Paks- Cseresznyés was excavated between April of 2008 and 2009 by the Field Service for Cultural Heritage. According to the buildings and to the archaeological material of the village, it can be dated to the 14^{th} and 16^{th} centuries, which probably became deserted due to the expansion of the Ottoman Empire. The anthropological analysis have been conducted between 2009-2010. The specimens, with a very good state of preservation, belong to 504 individuals, 263 of which were infants (László, 2018).

Table 1. Study sample. The specimens are ordered by age, from the youngest to the oldest.

Site	Specimen	Period	Age at death	Age class	Cause of death	GMM	Trabecular Biomechanics
Norris Farm	821369	1300 AD	8 weeks			✓	✓
Velia	T305 us1344	Roman	0-3 months			✓	✓
Norris Farm	821045	1300 AD	3 months			✓	✓
Velia	T300 us1167	Roman	0-6 months			✓	✓
Velia	T441 us2538	Roman	0-6 months			✓	✓
Velia	T368 us2069	Roman	0.75-1 year			✓	✓
Velia	T398 us2239	Roman	6-8 months	0-1 years		✓	
Velia	T442 us2545	Roman	6-9 months				✓
Norris Farm	821051	1300 AD	7.5 months			✓	✓
Bologna	**BO58_M**	**XX Century**	**11 months**		**Bronchitis**	✓	✓
Bologna	**BO60_F**	**XX Century**	**11 months**		**Acute meningitis (brain fever)**	✓	✓
Velia	T289 us1098	Roman	9-12 months				✓
Velia	T434 us2454	Roman	1-1.5 years			✓	✓
Velia	T415 us2344	Roman	1-1.5 years			✓	✓
Norris Farm	821046	1300 AD	1.5 years			✓	✓
Norris Farm	821014	1300 AD	1.5 years			✓	✓
Bologna	**BO14_M**	**XX Century**	**1 years 5 months**		**Chronic enteritis**	✓	✓
Perkáta-Nyúli dűlő	516	14-16th c.	1.5-3 years			✓	✓
Perkáta-Nyúli dűlő	655	14-16th c.	1-3 years			✓	✓
IlokKralievica	G24	16th-17th century	1.5-2 years			✓	
Velia	T286 us1071	Roman	1.5-2 years			✓	✓
Bologna	**BO14_F**	**XX Century**	**1 year 9 months**	1.1-3 years	**Enteritis**	✓	✓
Norris Farm	821026	1300 AD	2 years			✓	✓
Norris Farm	821207	1300 AD	2 years			✓	✓
Norris Farm	821069	1300 AD	2.5 years			✓	✓
Norris Farm	821113	1300 AD	2.5 years			✓	✓
Perkáta-Nyúli dűlő	639	14-16th c.	2.5-3 years			✓	✓
Perkáta-Nyúli dűlő	3421	10-12th c.	2.5-3.5 years			✓	✓
Ilok	G22	13th-15th century	2-3 years			✓	✓
Velia	T379 us2143	Roman	2-3 years			✓	
Velia	T411 us2319	Roman	2-3 years			✓	✓

Bologna	**BO7_M**	**XX Century**	**2 years 9 months**		**Intestinal gastroenteritis**	✓	✓
BeliManastir	G6	Early/Middle Neolithic	2-3.5 years			✓	✓
Norris Farm	820683	1300 AD	3 years			✓	✓
Norris Farm	819938	1300 AD	3 years			✓	✓
Norris Farm	821214	1300 AD	3 years			✓	✓
Bologna	**BO48_F**	**XX Century**	**3 years**		**Meningitis**	✓	✓
Ilok	G72	13th-15th century	3-4 years			✓	✓
Ilok	G70	13th-15th century	3-4 years				✓
Ilok	G1	13th-15th century	3.5-4.5 years			✓	
Paks TO-18	997	14-16th c.	3-5 years			✓	✓
Paks TO-18	1166	14-16th c.	3-5 years	3.1-6 years		✓	✓
Velia	T209 us1379	Roman	4 years ca			✓	✓
Velia	T342 us1546	Roman	4 years ca			✓	✓
Paks TO-18	1846	14-16th c.	4-5 years			✓	✓
Perkáta-Nyúli dűlő	4263	10-12th c.	4-5 years				✓
Norris Farm	821012	1300 AD	5 years			✓	✓
Velia	T375 us2129	Roman	5 years			✓	✓
Bologna	**BO5_F**	**XX Century**	**5 years**		**Acute meningitis**	✓	✓
Bologna	**Parma7_F**	**XX Century**	**5 years**		**Diphteria**	✓	✓
Bologna	**BO6_F**	**XX Century**	**5 years 10 months**		**Enteroperitonitis**	✓	✓
Bologna	**BO1_M**	**XX Century**	**5 years 8 months**		**Acute enteritis**	✓	✓
BeliManastir	G20	Early/Middle Neolithic	5.5-6.5 years			✓	✓
Paks TO-18	1164	14-16th c.	5-6 years			✓	✓
Ilok	G55	13th-15th century	5-6 years			✓	
Velia	T390 us2207	Roman	5-6 years			✓	✓
Bologna	**BO4_F**	**XX Century**	**5 years**		**Bronchopneumonia, basilar meningitis**	✓	✓
Bologna	**BO11_F**	**XX Century**	**6 years**		**Typhus**	✓	✓
Perkáta-Nyúli dűlő	435	14-16th c.	6-7 years			✓	✓
Velia	T333 us1489	Roman	6-7 years			✓	✓
Perkáta-Nyúli dűlő	1575	10-12th c.	6-8 years			✓	✓
Bologna	**BO6_M**	**XX Century**	**7 years**	6.1-10 years	**Abdominal typhus, peritoneal with perforation**	✓	✓
Paks TO-18	1865	14-16th c.	7-8 years			✓	✓
Perkáta-Nyúli dűlő	752	14-16th c.	7-8 years			✓	✓

Perkáta-Nyúli dűlő	2123	10-12th c.	7-8 years		✓	✓
BeliManastir	G31	Early/Middle Neolithic	7-8 years			✓
Velia	T320 us1431	Roman	7-8 anni		✓	✓
BeliManastir	G1	Early/Middle Neolithic	7-9 years		✓	
Bologna	**BO40_M**	**XX Century**	**9 years**	**Congenital myxedema**	✓	✓
Velia	T138 us1636	Roman	9-10 years		✓	✓
Total of specimens for each analysis					65	64

All the specimens were selected based on their good condition, with minimal or no damages. The left side was preferred; when the left talus was missing or incomplete, the right one was selected instead, and mirrored. All the specimens were scanned in different facilities (see Table 2). Scans were reconstructed as 16-bit TIFF stacks, and Image J was used to inspect the scans and evaluate their quality. When the trabecular bone showed signs of damage or rarefaction due to pathological or diagenetic causes, the specimen was excluded from the analyses. Avizo 9.3 (Visualization Sciences Group, SAS) was used to pre-process the reconstructed scan data (e.g. crop or resample). Where heavy sediment or mummified tissues were present, they were removed in Avizo 9.3 using a Wacom board and the Avizo paint-brush tool in the labels-field. A White Hat filter was applied (to the Norris Farms#36, Beli Manastir, Ilok, and Velia samples) to improve the contrast between bone and the heavy sediment present into the bone. In the cases in which this contrast was impossible to improve, the specimens were excluded from the analyses. Segmentation of the image data was performed using the MIA clustering method (Dunmore, Wollny, and Skinner 2018). In short, this method uses a K-means algorithm to cluster the CT images into specific classes determined a priori by the user. This clustering is based on voxel or pixel intensity. Therefore, a fuzzy c-means algorithm (Dunn 1973; Bezdek et al. 1987) is applied to cope with the scanning artifacts or different levels of mineralization of the specimen or the soil (Dunmore, Wollny, and Skinner 2018), and the class membership probabilities are calculated. Finally, voxels are attributed to the class with the highest membership probability. All the process results in a segmented dataset. All the output used here are raw files, linked to MetaImage files (ITK). The sample was then divided into four age classes, as described in Table 4.

2.2.1. Age Classes

The sample was then subset in four age classes, based on the classifications explained by Swan (2020) (Table 3) as follows:

- Neonates and toddlers (0-1 years). This group includes both infants who are not able to walk independently and infants who engage in a mix of (in)dependent locomotor behaviors, e.g. cruising, crawling, walking with aid.
- Early infancy (1.1-3 years). This stage includes infants who are able to walk independently, engaging in an immature toddling gait.

- Late infancy (3.1-6 years). In this subset, infants engage in an intermediate phase between immature and mature gait.
- Childhood (6.1-10). This stage comprehends children who achieved mature locomotion.

Table 2. MicroCT information: facilities and range of voxel size

Sample	Facility	Voxel size (μ)
Bologna	Center for Quantitative Imaging (CQI), Pennsylvania State University, PA (USA)	20-38
Norris Farms	Center for Quantitative Imaging (CQI), Pennsylvania State University, PA (USA)	12-26
Velia	The Abdus Salam International Centre for Theoretical Physics, Trieste, Italy	18-30
Beli Manastir and Ilok	University of Zagreb, School of Medicine, Zagreb, Croatia	18-29
Paks and Perkata	The Abdus Salam International Centre for Theoretical Physics, Trieste, Italy	18-30

Table 3. Age classes

Age classes	***Group Name***	***Individuals per classes***
0-1 yrs	Neonates and toddlers	12
1.1-3	Early infancy	25
3.1-6	Late infancy	21
6.1-10	Childhood	12
Total		70

2.2.2. Geometric Morphometrics Analysis

To cope with the different morphologies of the growing talus, a minimal template of 236 (semi) landmarks (8 anatomical landmarks, 45 curve semilandmarks, and 184 surface semilandmarks) was created in Viewbox 4 (dHAL Software), on a 1.9 year-old female specimen (BO14-F). The aim of this template is to follow the morphological changes in the gross morphology, related to the ontogeny, from the newborn talus throughout infancy and pre-adolescence (Figures 3 and 4, Table 4-5). The (semi)landmark configurations were applied to all the targets. To be considered geometrically homologous (Mitteroecker et al. 2013; Gunz and Mitteroecker 2013), semilandmarks were allowed to slide on the curves and surface, to minimize thin-plate-spline bending energy (Slice 2006) between template and targets. Then, semilandmarks were allowed to slide against recursive updates of the Procrustes consensus (Rohlf and Slice 1990). The coordinates were then registered with a Generalized Procrustes Analysis (GPA) where the size was removed and the specimens were scaled and translated. The GPA was performed in R, using geomorph (Dean C Adams and Otárola-Castillo 2013).

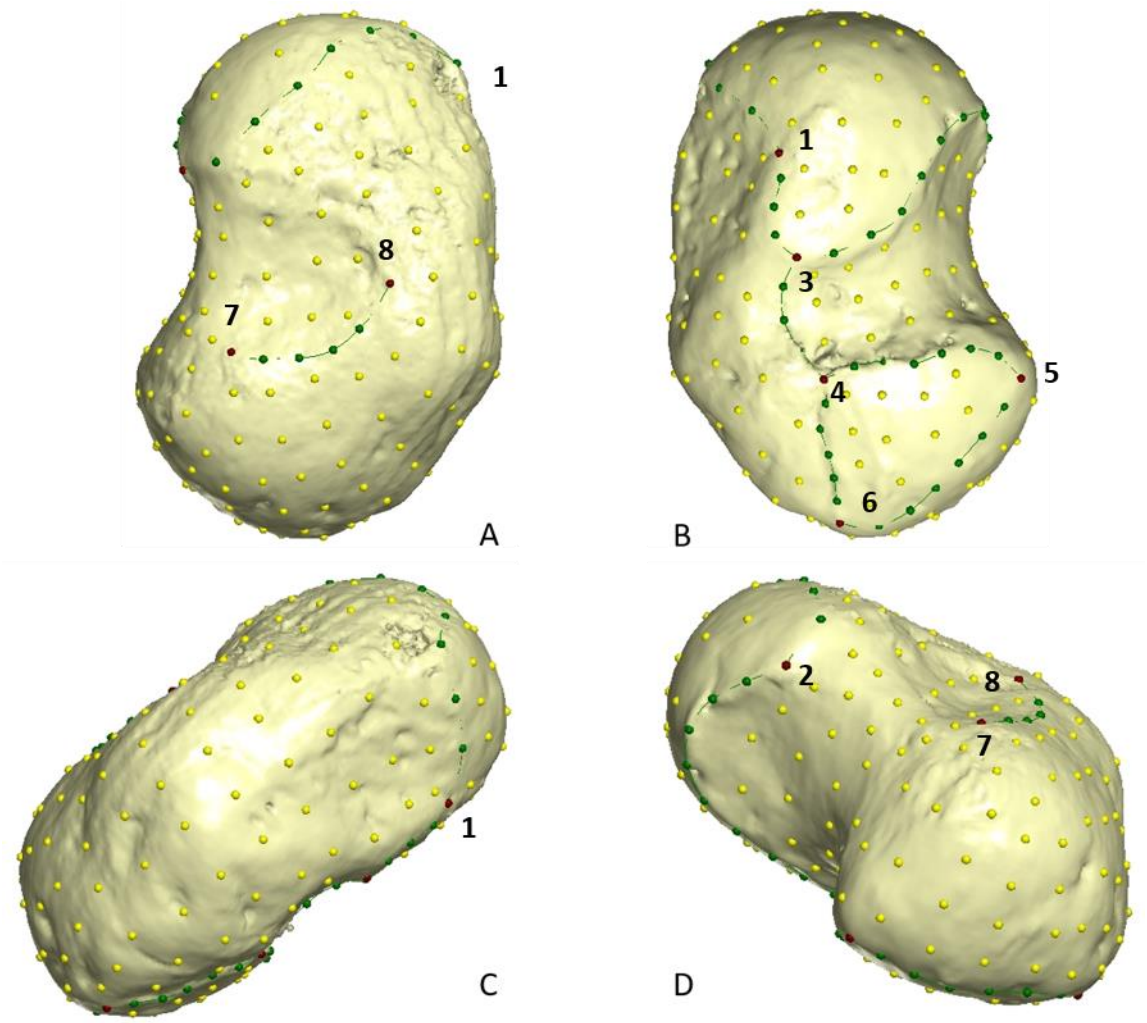

Figure 3 - Configuration of (semi)landmarks. A) Dorsal view; B) Palmar view; C) Medial view; D) Lateral view. Landmarks are represented in purple, curve semilandmarks are in green, and surface semilandmarks are in yellow.

Table 4 – List of anatomical landmarks. Type of landmarks according to Bookstein (Bookstein 1997b)

Label	***Description***	***Type of landmark***
1	Point of contact between head and anterior calcaneal facet	II
2	Point of contact between head and lateral ridge	II
3	The most posterior point of the anterior calcaneal facet	III
4	The most anterior point of the posterior calcaneal facet	III
5	The most lateral point of the posterior calcaneal facet	III
6	The most posterior point of the posterior calcaneal facet	III
7	The most posterior point of the lateral neck	III
8	The most posterior point of the lateral neck	III

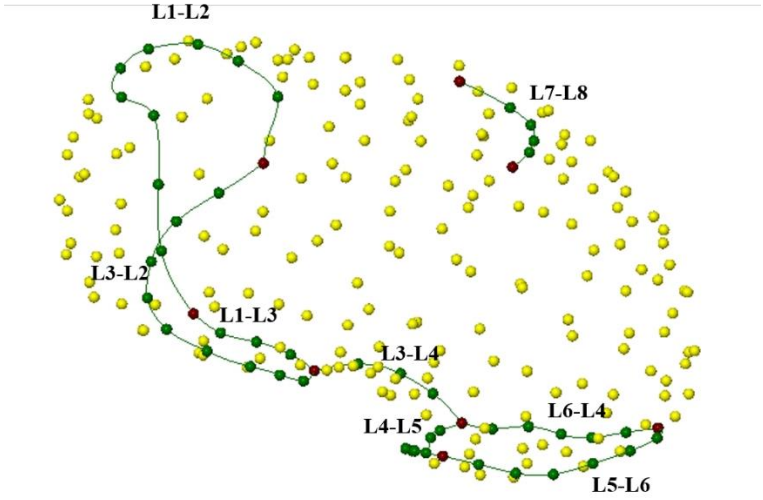

Figure 4 - Configuration of (semi)landmarks. Curves (green points) are highlighted.

Table 5 - semilandmarks

Semilandmarks on curves	N
Curve L1-L2: Head	9
Curve L1-L3: Medial border of the anterior calcaneal facet	3
Curve L3-L2: Inferior Head	9
Curve L3-L4: Sulcus Tali	3
Curve L4-L5: Anterior margin of the posterior calcaneal facet	6
Curve L5-L6: Posterior margin of the posterior calcaneal facet	6
Curve L6-L4: Medial margin of the posterior calcaneal facet	5
Curve L7-L8: Posterior margin of the neck	4
Semilandmarks on surface	N
Neck	10
Head	30
Posterior Calcaneal facets	11
Sulcus Tali	23
Lateral ridge	10
Lateral side	23
Posterior side and trochlea	33
Medial side	35

A shape and form space Principal Component Analysis (PCA) was carried out on the Procrustes coordinates to explore talar shape variation during growth using Morpho (Schlager 2017). First, a Shapiro Normality Test and a Levene test were performed, to assess the distribution of the data and its homoscedasticity. Then, based on the fulfillment of the assumption, the respective parametric or non-parametric tests (Analysis of Variance (ANOVA), Kruskal-Wallis rank sum test, Tukey's post-hoc test, and Dunn's test) were run to find any significance variance between group means along the first three PCs. Pearson's product moment correlation was perform to asses if shape variations were related to size. The variations of size and shape where analyzed in Procrustes form space. Following GPA, patterns of size and shape variation in the talus were analyzed

through PCA in Procrustes form space. The form space PCA reduces shape variation in a few dimensions retaining size information by adding the logarithm of centroid size (lnCS) as an additional variable to Procrustes shape coordinates (Mitteroecker et al. 2004).

2.2.3.Biomechanical analyses

After the above-mentioned segmentation processes, the trabecular and cortical bone were separated following the protocol outlined by Gross and colleagues (2014) using Medtool 4.3 (Dr Pahr Ingenieurs e.U, 2017). Briefly, opening and closing filters (kernel size varies from 3 to 5, depending on the specimen) with a "region growing" function were applied using a customized python-based script within Medtool to remove cortical porosity and facilitate the creation of a uniform shell that is then filled to create three different masks, namely outer (i.e. the outer shell of cortical bone), and inner (i.e. the boundary between cortex and trabecular region), which separates cortical from trabecular bone (Gross et al. 2014; N. B. Stephens et al. 2016, 2018a) (see Figure 5). Then, the inner mask is subtracted from the outer one, creating the cortical thickness mask. For this study, only the inner region, i.e. trabecular bone, was used. Finally, a tetrahedral mesh of trabecular bone was generated using the computational geometry algorithms library CGAL (www.cgal.org), a mesher that creates a 3D finite element model using Delauney triangulation (Delaunay 1934; Gross et al. 2014; Komza and Skinner 2019).

Quantification of bone volume fraction (BV/TV), which is the ratio of trabecular bone voxels relative to the total volume of voxels (Fajardo et al. 2007; Kivell 2016b), and Degree of Anisotropy (DA) which describe the degree of orientation of the trabecular struts (Komza and Skinner 2019), was carried out on the trabecular mesh by moving a sampling 5 mm sphere along a background grid with 2.5 mm spacing for each scan (Pahr and Zysset 2009; Gross et al. 2014). BV/TV (bone voxels/total voxels) is expressed as a percentage, DA is calculated as (1-[eigenvalue3/eigenvalue1]) and is scaled between 1 and 0, where 1 is highly anisotropic and 0 isotropic, following the Mean Intercept Length (MIL). The resulted colormaps were then visualized in Paraview 3.14.1 (Sandia Corporation, Kitware Inc). Mean trabecular thickness (Tb.Th, mm), trabecular numbers (Tb.N), and mean trabecular spacing (Tb.Sp, mm) were calculated (Hildebrand and Rüegsegger 1997; Stephens et al. 2018).

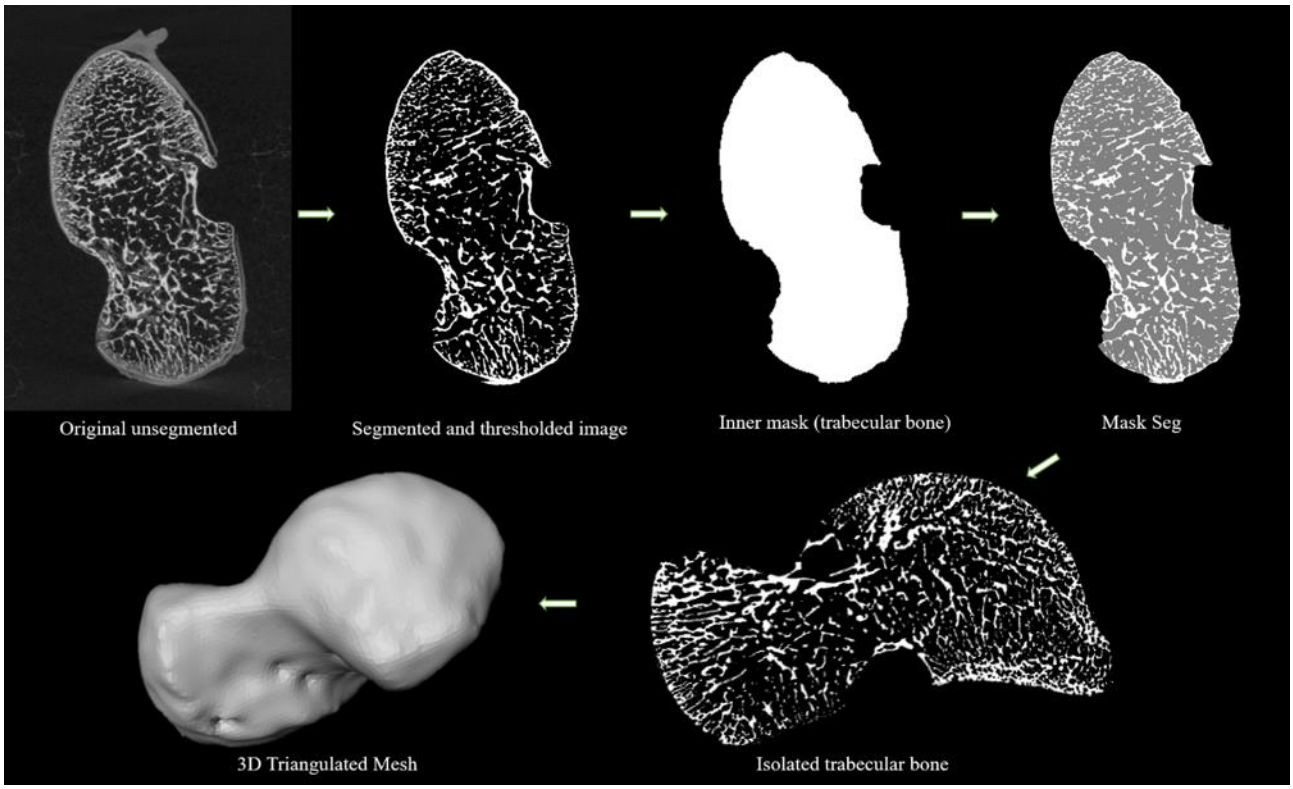

Figure 5 - Trabecular quantification workflow. First, the unsegmented image is segmented and thresholded as described above. Then the masks are created, to separate the trabecular bone.

3D statistical comparisons between groups were perfomed following the Phenotypic PointCloud Analysis protocol proposed by DeMars and collegues (DeMars et al., 2020; Stephens, DeMars et al., 2020) for DA and BV/TV. Briefly, trabecular meshes were aligned using a modified version of the MATLAB auto3dgm package (Tingran, Winchester, and Stephens 2020). The auto3dgm package presents an algorithm which permits the fully automatic placement of corresponcence points on digital models. Then, these pseudolandmarks (i.e. landmark-like points) can be input into standard geometric morphometrics softwares (Boyer et al. 2015). Here, we used a set of 1200 automatically placed pseudolandmarks. Subsequently, we performed a GPA using the GeoMorpho R package (Adams et al. 2018), and we proceeded finding the mean specimen. This step is necessary to obtain a mean mesh by finding the closest-to-the-mean specimens, on which we warped the mean GPA coordinates of all our sample (Stephens, Kivell, Pahr, Hublin, & Skinner, 2018a). The average trabecular mesh obtained was then tetrahedralized using with evenly-spaced (1.75mm) points using TetWild (Hu et al., 2018) and vertices were converted to a point cloud. Individual point clouds were then obtained by interpolating BV/TV and DA scalar values to the vertices of the tetrahedral mesh, which were then aligned by applying the auto3dgm transformation matrixes followed by a rigid, affine, and deformable alignment using a python implementation of the Coherent Point Drift algorithm (Myronenko and Song 2010). BV/TV and DA scalar values were linearly interpolated from each individual point clouds to the corresponding points in the canonical point cloud using SciPy (Virtanen et al. 2020a, 2020b) and the mean, standard deviation, and coefficient of variation for each group were mapped to the average point cloud, and statistically compared across the sample. The homologous points were compared using a two-tailed t-test, with P-values corrected (Friston 1995;

Worsley et al. 1996) and interactively visualized in Paraview with figures being automatically generated using PyVista (Sullivan and Kaszynski 2019).

2.3. Results

2.3.1. External morphology

2.3.1.1. Shape space

Bologna sample

The first three PCs explain 61.7% of the total variance, with PC1 accounting for 40.8% of the total variance. Shapiro normality test indicated that PCs scores were normally distributed (W = 0.9, p-value = >0.5), and Levene test attests for their homoscedasticity (PC1: Test Statistic = 0.15714, p-value = 0.9557; PC2: Test Statistic = 0.32229, p-value = 0.8573; PC3: Test Statistic = 1.7533, p-value = 0.2085). Anova indicated that PC1 scores are significantly different (Df = 3, F-test = 16.06, p-value = 0.0001). This represents ontogenetic allometry, where negative scores account for the small globular morphology of the youngest individuals, while positive scores account for an elongation of the entire body of the talus, due to the development of the neck, and manifestation of the lateral malleolar facet and only partial definition of the posterior trochlear facet. The anterior calcaneal facet is evident in the youngest phases (negative scores), while the posterior calcaneal facet becomes larger, less triangular, and more concave towards PC1 positive. PC2 (10.9%) accounts for a longer lateral ridge that shortens towards the positive PC2 axis in relation to the increase in concavity along the lateral aspect of the talus, the increased talar head size, and continued development of the neck, trochlea, and lateral malleolar facet. Additionally there is a subtle narrowing of the sulcus tali and a clear medial rotation of the talar head. PC3 (10%) negative scores show a more compact shape, that becomes higher along positive values with the development of the posterior calcaneal facet and head.

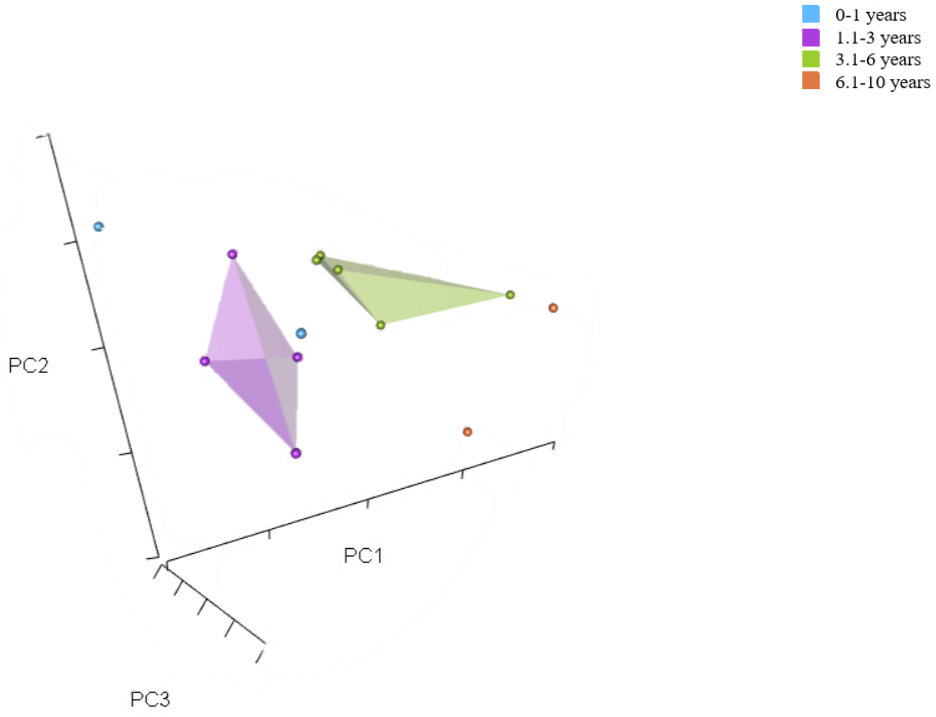

Figure 6 - 3D plot of the control sample (Bologna, Italy).

Bologna and archaeological sample

Shapiro-Wilk normality test shows that the first two PCs are normally distributed (PC1: W = 0.97; p-value = 0.2; PC2: W = 0.98, p-value = 0.7), while PC3 is not normally distributed (W =0.94 , p-values = 0.004). Levene test attests for the homogeneity of variance, with p-values >0.1. The first three PCs account for the 50.1% of the total variance (Figures 7-8), with PC1 explaining the 27.9% of the total variance, where negative scores (i.e. the youngest individuals) describes a small and more bean-like talus, with a small and circular depression in the neck area, showing a not-yet-defined neck. The trochlea is very small, without any lateral or medial rims and no posterior margins. Laterally, the ridge is well defined, clearly separating the head area from the posterior one, separated plantarly by the sulcus tali, a wide a not very deep area between the anterior and posterior developing calcaneal facets that are both not well defined, even though the posterior margin of the anterior calcaneal facet is better marked. Medially, the surface is homogeneous, with no medial malleolar facet. Positive scores showed a great development of the head, less wide than in the youngest specimens, and more anteriorly pronounced and medially rotated. The neck has greatly expanded, with a deep depression with marked rims that clearly separates the neck from the trochlea, head and medial malleolar facet. The trochlea is concave in a mediolateral direction, with well-defined medial and lateral margins, though the posterior rims is still not well defined, while the anteroposterior convexity increases. Laterally, the lateral malleolar facet is almost completely developed, with the antero-posterior reduced ridge that clearly separates the sulcus tali from the neck. The reduction in elongation of the lateral ridge is clearly explained by both the development of the posterior body of the talus and the head, and this is visible also in the sulcus tali area, narrower and deeper due to the expansion and development of both the anterior and posterior calcaneal facets, with the former more advanced in development than the latter, that has yet a concave shape, but it is still developing in the posterior part, with a more triangular-like shape. The groove of the flexor hallucis longus has not developed yet. PC2 (12.1%) account for a global elongation of the talus, that grows in an antero-posterior direction, passing from a globular shape in the youngest individual (i.e. negative scores) to a more slim and defined shape in the oldest individuals (i.e. positive scores). PC3 (9.9%) describes small variances in the lateral surface, with the development of the lateral malleolar process, development of the posterior calcaneal facet, that increase in size and changes in orientation, and the rotation of the head. Analysis of Variance (ANOVA) detected significant differences between groups along PC1 (Df = 3, F-test = 33.11, p = 9.43e-13), while Kruskal-Wallis highlighted differences among groups on PC3 scores (chi-squared = 10.507, df = 3, p-value = 0.01472). Differences between groups among PC2 scores were not significant (Anova: Df = 3, F-test = 0.491, p = 0.69). Tukey's Post-hoc test and Dunn's Post-hoc test (Tables 6 and 7) show the differences between age groups. Pearson's product-moment correlation showed that only PC1 is significantly correlated with size (corr = 0.86; p-value = <2.2e-16), i.e. ontogenetic allometry (Figure 10).

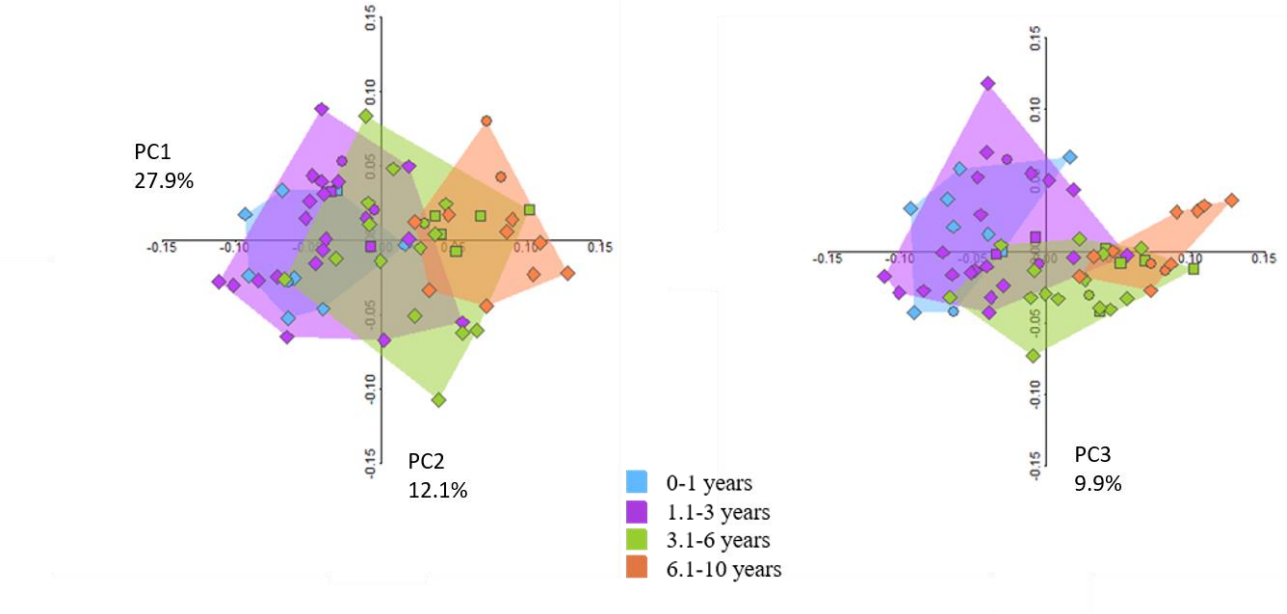

Figure 7 - 2D plot. On the left, PC1 and 2: on the right, PC1 and 3. ***Individuals from Bologna, for which sex was known, are represented by circles (males) and squared symbols (female). Diamonds represent the archaeological samples***

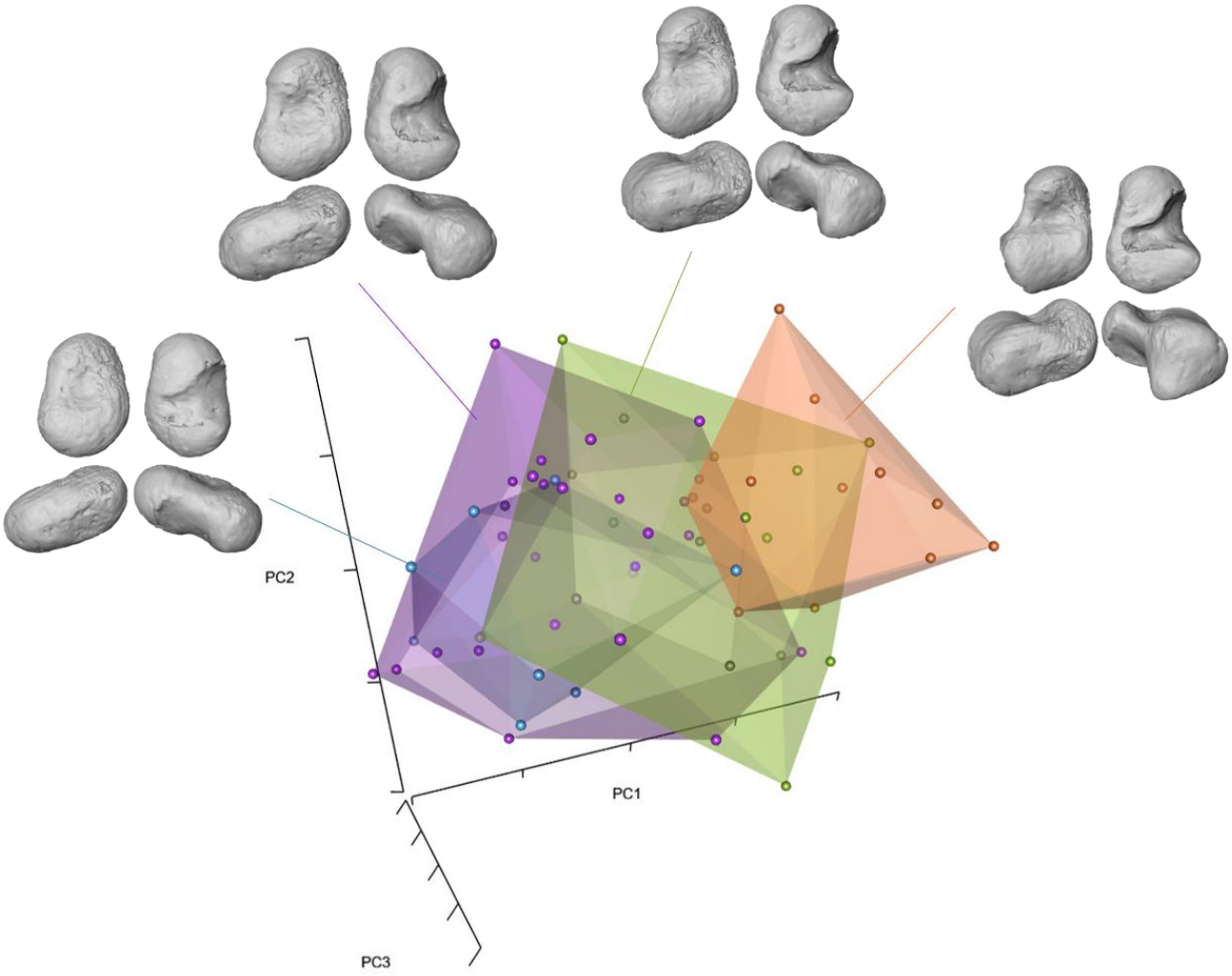

Figure 8 - 3D shape space plot with group means. Each age-group mean is shown in dorsal, plantar, medial, and lateral views.

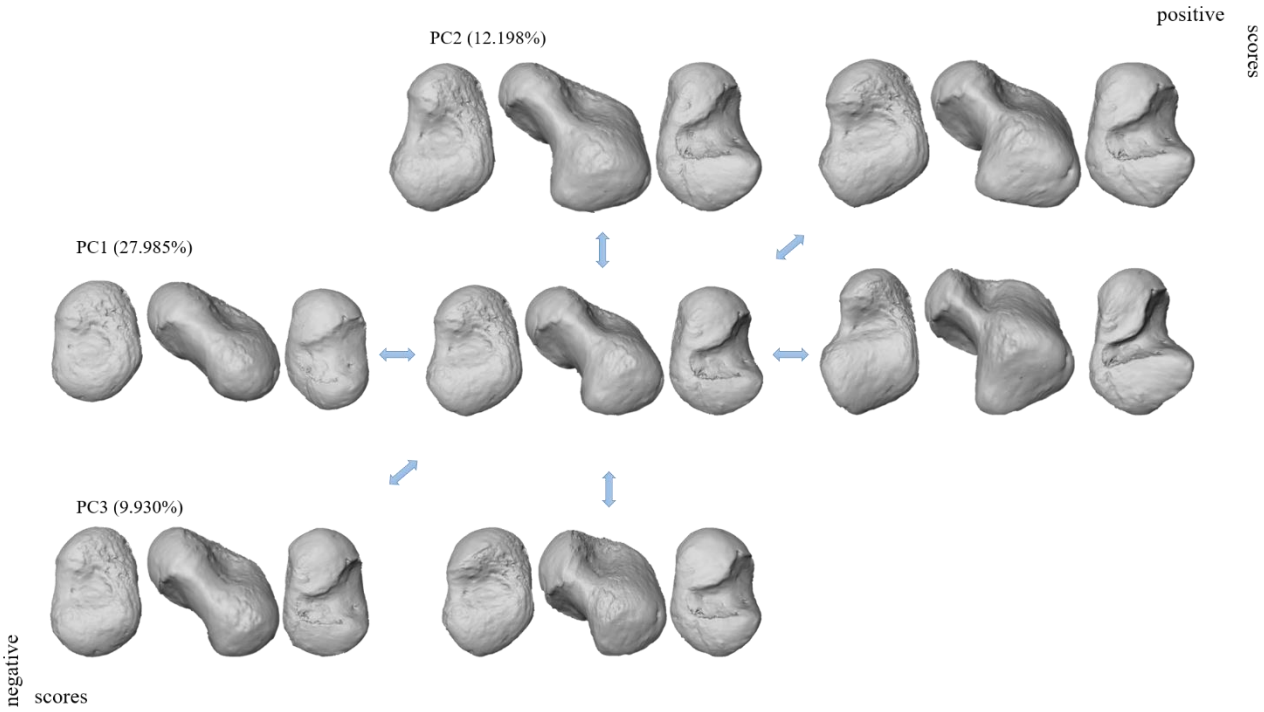

Figure 9 - Shape changes along the first three PCs axes

Table 6 – Results of the Tukey's Post Hoc test for PC1 scores

Age groups	diff	lwr	upr	p adj
1.1-3 vs 0-1	0.01	-0.01	0.053	0.52
3.1-6 vs 0-1	0.07	0.04	0.1	**0.000**
6.1-10 vs 0-1	0.13	0.08	0.17	**0.000**
3.1-6 vs 1.1-3	0.06	0.03	0.08	**0.000**
6.1-10 vs 1.1-3	0.11	0.07	0.14	**0.000**
6.1-10 vs 3.1-6	0.05	0.01	0.08	**0.002**

Table 7 – Results of Dunn's-test for multiple comparisons of independent samples for PC3 scores

	0-1	1.1-3	3.1-6
1.1-3	1.000	-	-
3.1-6	0.053	0.054	-
6.1-10	1.000	1.000	0.157

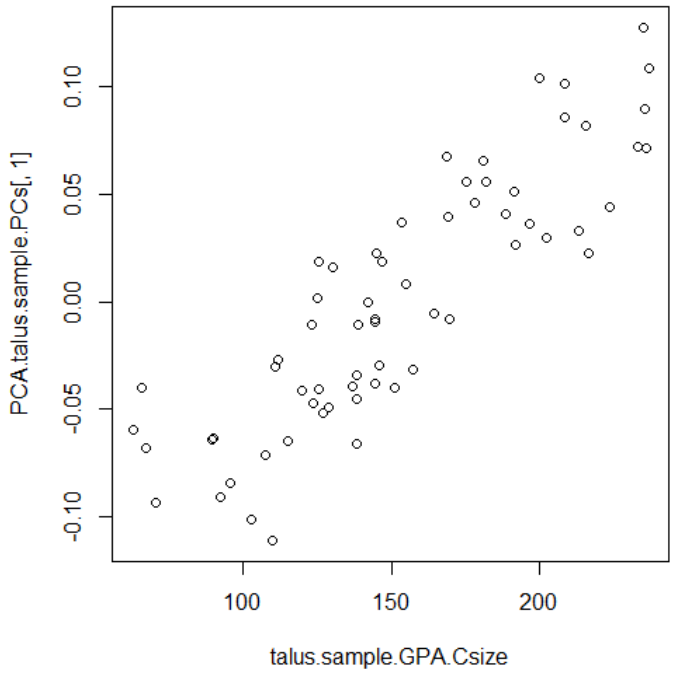

Figure 10 - Correlation with size in shape space (PC1 vs logCn)

2.3.1.2. Form space

The first three PCs account for the 94.47% of total variance (Figure 11). PC1 (92.02%) PC2 (0.12%) and PC3 (0.11%). Shapiro-Wilk normality test assessed the normal distribution of the PC2 and 3 scores. Kruskal-Wallis rank sum test for PC1 showed significant differences (chi-squared = 47.936, df = 3, p-value = 2.198e-10), while ANOVA did not highlight significant differences along PC2 (Df = 3, F-test = 2.4, p-value = 0.07) and PC3 (Df = 3, F-test = 1.6, p-value = 0.1) . Dunn's Post-Hoc test showed differences among each age class (Table 8). Pearson's product-moment correlation showed that PC1 is completely driven by size (corr = 0.98; p-value = <2.2e-16) (Figure 11).

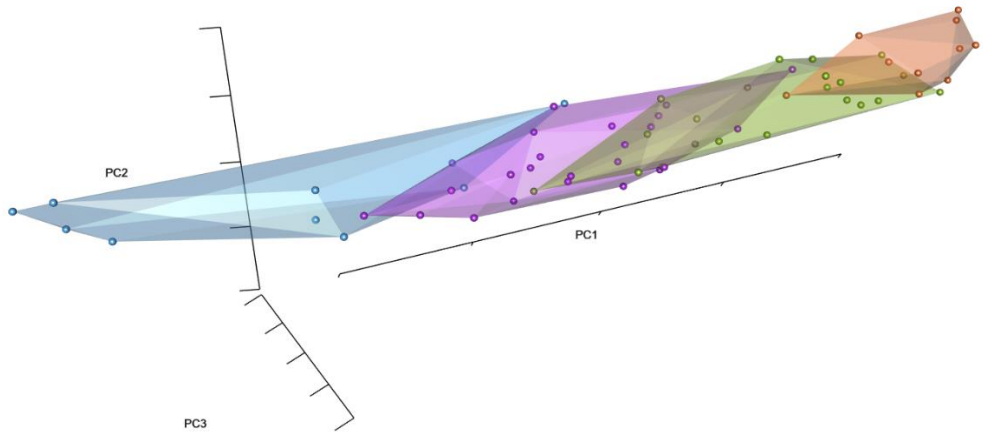

Figure 11 - 3D form space plot. PC1 is completely driven by size, and the result is a "growth axis", with individuals "ordered" by size, from the youngest on the left, to the oldest, on the far right.

Table 8 - Results of the Dunn's Post Hoc test for PC1 scores

	0-1	1.1-3	3.1-6
1.1-3	0.172	-	-
3.1-6	**2.0e-05**	**0.005**	-
6.1-10	**9.9e-09**	**2.1e-06**	0.148

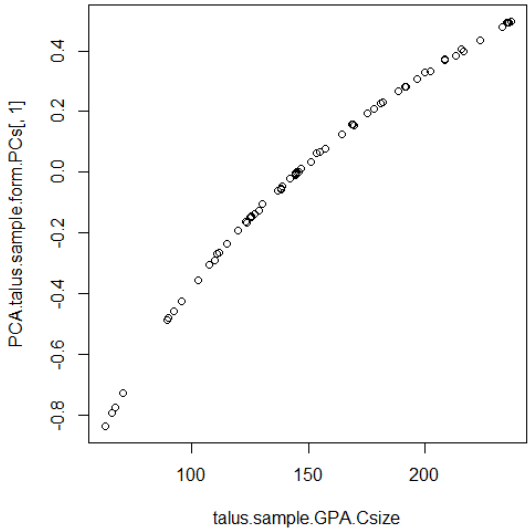

Figure 12 - Correlation between PC1 and centroid size

2.3.2. Internal morphology

Mean values for the age classes are listed in Table 9, while individuals values are listed in Table 10-11. During the first year, the trabecular architecture is very dense, with high BV/TV values, and numerous and thin trabeculae, very close to each other. The mean values, for each age class, show a trend in which, at high BV/TV and Tb.N, correspond low Tb.Th and Tb.Sp. Then, after one year of age, the trend is inverted: BV/TV and Tb.N values decrease, while Tb.Th and Tb.Sp increase progressively until 10 years of age. During the first year of life, BV/TV is relatively homogeneous in all the talus, with slightly higher values in the head and posterior part of the talar body. During the second and third years (age group 1.1-3 years), BV/TV values are generally lower than during the first year, but with relatively higher values in the posterior part of the body, i.e. trochlea, lateral malleolar process, lateral part of the head. Values increase again in the third age group (i.e. 3.1-6 years). The pattern is similar to the one described for the 1.1-3 years cohort, but with differences in magnitude, which is higher, with values slightly lower than the ones registered in the youngest group. In the oldest group, BV/TV pattern is once again similar to the latter description, but with differences in magnitude, i.e. the highest values in the sample (Figure 13). DA values increase after the first year of life. At about 1.5 years, the areas that show higher DA values is the trochlea, neck and dorsal part of the head, and posterior subtalar facet. At about 4 years of age, DA increases also in the future medial malleolar facet, while at about

5-6 years, increased values can be noticed in the most distal part of the head, i.e. navicular facet, posterior subtalar joint and lateral malleolar process. This pattern remains constant after 7-8 years (Figure 14).

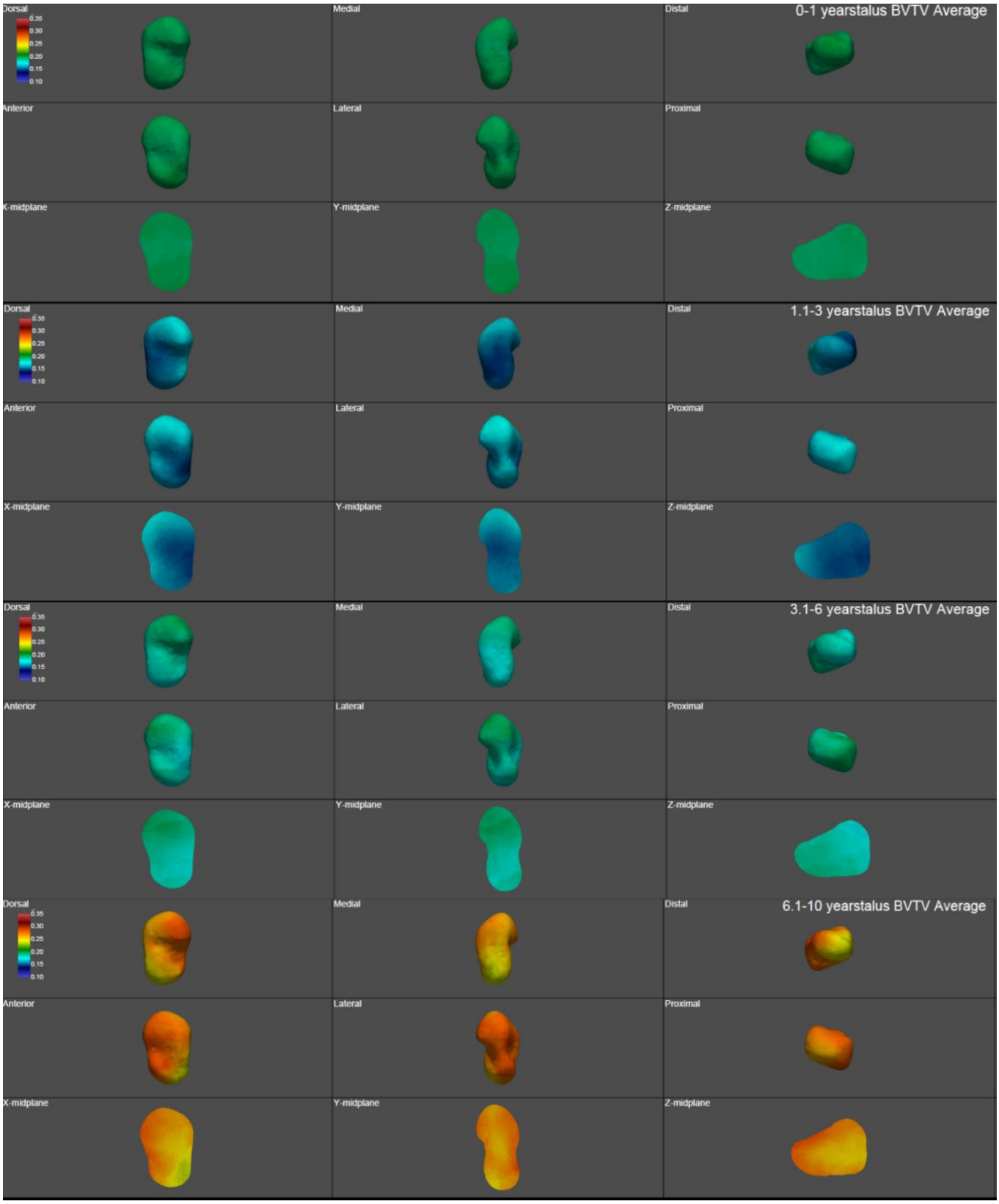

Figure 13 - BV/TV group averages. Colormaps show the different BV/TV values among age classes, which are high and relatively homogenous during the first year of life; after the onset of the bipedal locomotion (>1 year) BV/TV decrease and the magnitude is differentiated among the bone. BV/TV values start increasing again after 3 years old.

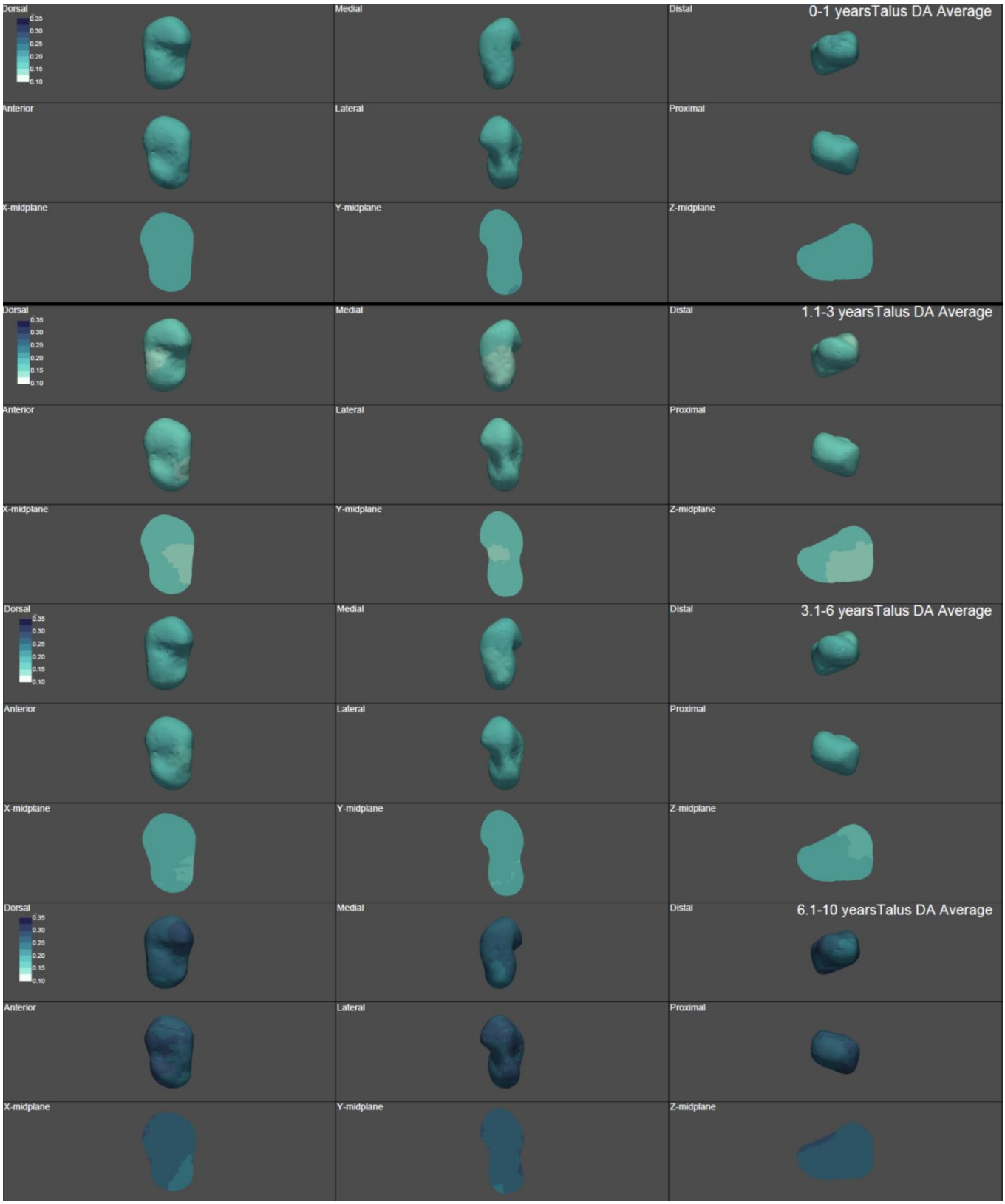

Figure 14 - DA age groups averages. DA is low during the first year of life, i.e. the talus is relatively isotropic. Anisotropy starts increasing slowly after the onset of the bipedal locomotion, at about 1 year of age, reaching the highest values after 6 years of age.

Table 9 – Mean values for age classes

Age Class	DA	BV/TV	Tb.N	Tb.Sp	Tb.Th
0-1 year	0.18	17.71	1.54	0.54	0.14
1.1-3 years	0.22	15.99	1.15	0.70	0.19
3.1-6 years	0.22	17.51	1.20	0.65	0.20
6.1-10 years	0.22	22.83	1.15	0.65	0.23

Table 10 – Individuals' averages for BV/TV and DA

Site	Specimen	Age Class	Age at death	BV/TV (%)	DA
Velia	T305.	Neonates and toddlers	0-3 months	21.65	0.16
Norris Farms	821369.		8 weeks	9.82	0.12
Norris Farms	821045.		0-6 months	23.68	0.11
Velia	T300.		0-6 months	12.41	0.26
Velia	T441.		0-6 months	21.92	0.17
Norris Farms	821051.		7.5 months	18.53	0.16
Velia	T442.		6-9 months	18.12	0.19
Velia	T368.		0.75-1 year	18.95	0.17
Velia	T289.		9-12 months	18.47	0.16
Bologna	58_M.		11 months	23.24	0.16
Bologna	60_F.		11 months	20.12	0.26
Norris Farms	820614.		12 months	5.7	0.24
Velia	T415.	Early Infancy	1-1.5 years	20.66	0.13
Velia	T434.		1-1.5 years	18.6	0.27
Bologna	14_M.		1year and 5 months	11.8	0.23
Norris Farms	821014.		1.5 years	28.42	0.17
Norris Farms	821046.		1.5 years	14.84	0.20
PerkataNyuli	655.		1-3 years	10.93	0.24
Velia	T286.		1.5-2 years	21.31	0.16
Bologna	14_F.		1.9 years	13.82	0.26
Bologna	48_F.		3 years	15.247	0.25
Norris Farms	820683.		3 years	19.14	0.26
Norris Farms	821026.		2 years	10.58	0.20
Norris Farms	821207.		2 years	10.51	0.21
Norris Farms	821214.		3 years	8.71	0.25
PerkataNyuli	516.		1.5-3 years	17.18	0.21
Ilok	G22.		2-3 years	10.5	0.19
Norris Farms	821069.		2.5 years	19.6	0.27
Norris Farms	821113.		2.5 years	12.76	0.26
Velia	T411.		2-3 years	18.39	0.20
Beli Manastir	G6.		2-3.5 years	21.12	0.17
PerkataNyuli	639.		2.5-3	13.98	0.26
Bologna	7_M.		2.9 years	16.3683	0.25
PerkataNyuli	3421.		2.5-3.5 years	17.48	0.24
Norris Farms	819938.	Late Infancy	3 years	12.27	0.25
Ilok	G70.		3-4 years years	14.09	0.16
Ilok	G72.		3-4 years	15.39	0.16
Paks	1166.		3-5 years	27.02	0.17
Paks	997.		3-5 years	16.58	0.25

Velia	T209.		4 years	13.85	0.30
Velia	T342.		4 years	15.82	0.22
Paks	1846.		4-5 years	20.88	0.20
PerkataNyuli	4263.		4-5 years	21.43	0.20
Bologna	4_F.		5 years	18.5	0.21
Bologna	5_F.		5 years	16.22	0.22
Norris Farms	821012.		5 years	10.1	0.30
Parma	7_F.		5 years	22.41	0.26
Velia	T375.		5 years	17.68	0.21
Paks	1164.		5-6 years	16.7	0.26
Velia	T390.		5-6 years	15.18	0.22
Bologna	1_M.		5.8 years	16.94	0.22
Beli Manastir	G20.		5.5-6 years	22.14	0.20
Bologna	BO6_F.		5 years and 10 months	19.61	0.22
Bologna	11_F.		6 years	17.55	0.21
PerkataNyuli	435.		6-7 years	16.31	0.27
Velia	T333.		6-7 years	22.81	0.23
Bologna	6_M.		7 years	16.85	0.28
PerkataNyuli	1575.		6-8 years	24	0.26
Beli Manastir	G31.		7-8 years	24.37	0.18
Paks	1865.	Childhood	7-8 years	25.51	0.19
PerkataNyuli	2123.		7-8 years	26.66	0.22
PerkataNyuli	752.		7-8 years	18.18	0.20
Velia	T320.		7-8 years	28.38	0.21
Bologna	40_M.		9 years	13.36	0.22
Velia	T138.		9-10 years	34.78	0.18

Table 11 – Individuals' averages for Tb.N, Tb.Sp and Tb.Th

Name	Age Class	Age at death		Mean Tb.N	Mean Tb.Sp (SD)	Mean Tb.Th (SD)
VeliaT305.	Neonates and toddlers	0-3 months	1.98	0.38	0.22 (0.13)	0.08 (0.03)
NF821369.		8 weeks	1.73	0.48	0.20 (0.10)	0.05 (0.03)
NF821045.		0-6 months	2.22	0.32	0.17 (0.13)	0.05 (0.05)
VeliaT300.		0-6 months	1.15	0.73	0.36 (0.14)	0.08 (0.03)
VeliaT441.		0-6 months	1.86	0.41	0.21 (0.13)	0.08 (0.03)
NF821051.		7.5 months	1.12	0.68	0.33 (0.21)	0.11 (0.07)
VeliaT442.		6-9 months	1.57	0.49	0.24 (0.14)	0.07 (0.03)
VeliaT368.		0.75-1 year	1.56	0.51	0.23 (0.13)	0.07 (0.03)
VeliaT289.		9-12 months	1.36	0.58	0.25 (0.16)	0.07 (0.04)
BO58_M.		11 months	1.53	0.47	0.18 (0.18)	0.08 (0.05)
BO60_F.		11 months	1.38	0.58	0.27 (0.14)	0.08 (0.04)
NF820614.		12 months	1.06	0.81	0.30 (0.13)	0.11 (0.02)

VeliaT415.	Early Infancy	1-1.5	1.41	0.53	0.23 (0.17)	0.07 (0.05)
VeliaT434.		1-1.5	1.28	0.58	0.20 (0.20)	0.12 (0.04)
BO14_M.		1yrs and 5 mths	1.22	0.68	0.24 (0.14)	0.08 (0.04)
NF821014.		1.5	1.20	0.58	0.25 (0.25)	0.11 (0.07)
NF821046.		1.5	1.14	0.69	0.33 (0.19)	0.11 (0.05)
PerkataNyuli655.		1-3.	0.90	0.92	0.50 (0.19)	0.13 (0.04)
VeliaT286.		1.5-2	1.23	0.63	0.33 (0.18)	0.07 (0.05)
BO14_F.		1.9	1.30	0.61	0.23 (0.16)	0.08 (0.05)
BO48_F.		3	1.22	0.67	0.27 (0.15)	0.08 (0.05)
NF820683.		3	1.11	0.69	0.28 (0.21)	0.11 (0.06)
NF821026.		2	0.91	0.92	0.53 (0.18)	0.11 (0.05)
NF821207.		2	0.95	0.87	0.35 (0.19)	0.11 (0.05)
NF821214.		3	1.04	0.81	0.36 (0.15)	0.11 (0.04)
PerkataNyuli516.		1.5-3	1.08	0.70	0.27 (0.23)	0.13 (0.08)
IlokG22.		2-3.	1.21	0.68	0.26 (0.15)	0.07 (0.04)
NF821069.		2.5	1.19	0.64	0.30 (0.20)	0.11 (0.05)
NF821113.		2.5	1.11	0.72	0.23 (0.18)	0.11 (0.05)
VeliaT411.		2-3.	1.18	0.64	0.24 (0.21)	0.12 (0.05)
BeliManastirG6.		2-3.5	1.25	0.61	0.30 (0.19)	0.07 (0.06)
PerkataNyuli639.		2.5-3	1.07	0.72	0.26 (0.21)	0.13 (0.06)
BO7_M.		2.9	1.12	0.71	0.33 (0.19)	0.08 (0.06)
PerkataNyuli3421.		2.5-3.5	1.13	0.67	0.26 (0.21)	0.13 (0.04)
NF819938.	Late Infancy	3	1.18	0.68	0.25 (0.17)	0.11 (0.05)
IlokG70.		3-4	1.24	0.65	0.28 (0.16)	0.07 (0.05)
IlokG72.		3-4.	1.59	0.49	0.21 (0.14)	0.07 (0.04)
Paks1166.		3-5.	0.94	0.79	0.60 (0.28)	0.13 (0.08)
Paks997.		3-5.	1.25	0.61	0.22 (0.19)	0.13 (0.04)
VeliaT209.		4	1.11	0.70	0.28 (0.20)	0.12 (0.05)
VeliaT342.		4	1.15	0.67	0.26 (0.20)	0.12 (0.05)
Paks1846.		4-5.	1.07	0.68	0.25 (0.25)	0.13 (0.07)
PerkataNyuli4263.		4-5.	1.15	0.62	0.21 (0.25)	0.13 (0.09)
BO4_F.		5	1.23	0.62	0.28 (0.19)	0.08 (0.06)
BO5_F.		5	1.29	0.61	0.25 (0.17)	0.08 (0.05)
NF821012.		5	1.01	0.81	0.34 (0.17)	0.11 (0.05)

PARMA7_F.		5	1.22	0.60	0.26 (0.22)	0.11 (0.07)
VeliaT375.		5	1.27	0.60	0.20 (0.19)	0.12 (0.04)
Paks1164.		5-6.	1.24	0.61	0.24 (0.19)	0.13 (0.04)
VeliaT390.		5-6.	0.96	0.81	0.31 (0.23)	0.12 (0.07)
BO1_M.		5.8	1.02	0.79	0.39 (0.19)	0.08 (0.06)
BeliManastirG20.		5.5-6	1.25	0.60	0.24 (0.20)	0.07 (0.08)
BO6_F.		5.10mths	1.49	0.50	0.20 (0.17)	0.08 (0.05)
BO11_F.		6	1.27	0.60	0.25 (0.19)	0.11 (0.06)
PerkataNyuli435.	Childhood	6-7.	1.07	0.74	0.33 (0.20)	0.13 (0.03)
VeliaT333.		6-7.	1.08	0.68	0.28 (0.24)	0.12 (0.06)
BO6_M.		7	1.29	0.60	0.23 (0.18)	0.11 (0.05)
PerkataNyuli1575.		6-8.	0.98	0.76	0.41 (0.26)	0.13 (0.09)
BeliManastirG31.		7-8.	1.35	0.57	0.26 (0.17)	0.07 (0.06)
Paks1865.		7-8.	1.01	0.71	0.33 (0.28)	0.13 (0.09)
PerkataNyuli2123.		7-8.	1.14	0.61	0.27 (0.26)	0.13 (0.08)
PerkataNyuli752.		7-8.	1.16	0.66	0.25 (0.21)	0.13 (0.04)
VeliaT320.		7-8.	1.22	0.56	0.23 (0.26)	0.12 (0.07)
BO40_M.		9	1.23	0.65	0.28 (0.16)	0.11 (0.04)
VeliaT138.		9-10.	1.14	0.56	0.23 (0.31)	0.12 (0.09=

2.3.2.1. Statistical results

T-tests for individual points in the pointclouds showed that there are significant differences between age classes. P-values are listed in Table 12. Results showed that BV/TV differs significantly between the first two age groups (0-12 months and 1.1-3 years) in the medial side and part of the medial portion of the head, while between the first group and the 6.1-10 years-cohort, BV/TV significantly differs in a small portion of the distal part of the head, on the lateral malleolar process and most lateral-anterior part of the trochlea. BV/TV values are also significantly higher between the cohorts 3.1-6 vs 6.1-10, in particular in the lateral part of the talus, lateral part of the head and sulcus tali.

For the DA, T-test scores showed significant results among age classes. In particular, the first group significantly differs from all the other age groups, in particular in the medial side and head (vs 1.1-3), head, lateral and medial part of the trochlea (vs 3.1-6) and almost completely on the dorsal part, lateral malleolar process, medial side and anterior calcaneal facet (vs 6.1-10). Significant differences emerged also between the groups 1.1-3 vs 6.1-10, specifically in the lateral and anterior part of the trochlea, lateral margin, lateral side of the neck and medal-anterior part of the trochlea. All the significant results of the T-tests are reported in Figures 15 and 16.Coefficient of variance are represented in Figures 17 and 18.

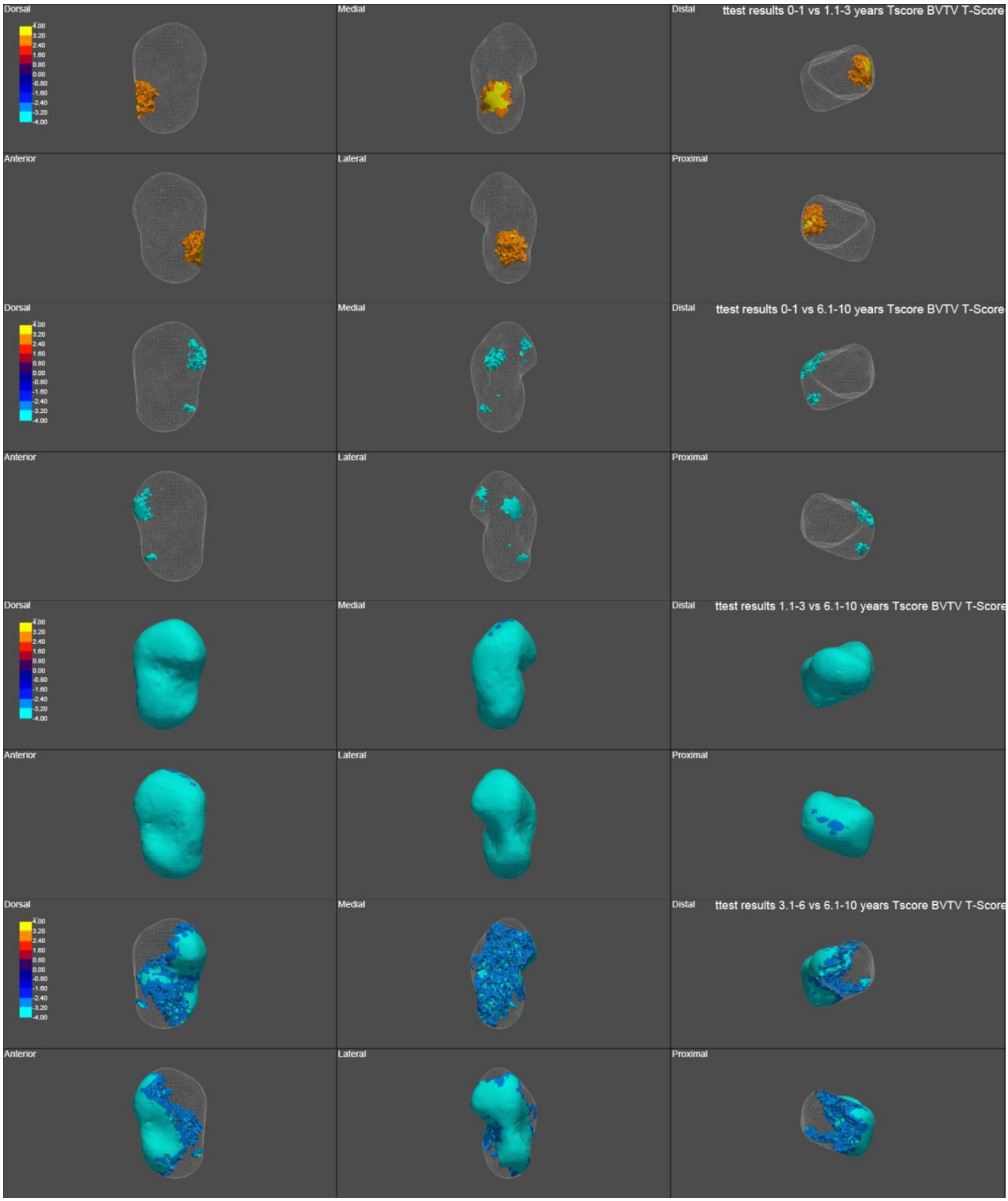

Figure 15 - BV/TV T-Scores. Only the significant results are represented. Warm colors indicate the youngest group in each comparison. Warm colors in the first two rows indicates that the youngest individuals, i.e. 0.-1 years, have significant higher values in the medial side of the head than the 1.1-3 years age group. T-test results between the group 1.1-3 and 6.1-10 reveal that the oldest individuals have significant higher BV/TV values in the medial side of the trochlea, while t-test results between the oldest age group in the sample (6.1-10 years) and 1.1-3 and 3.1-6 years show, respectively, that individuals older than 6 years of age have significant higher values in all the talus and in the lateral side of the talus.

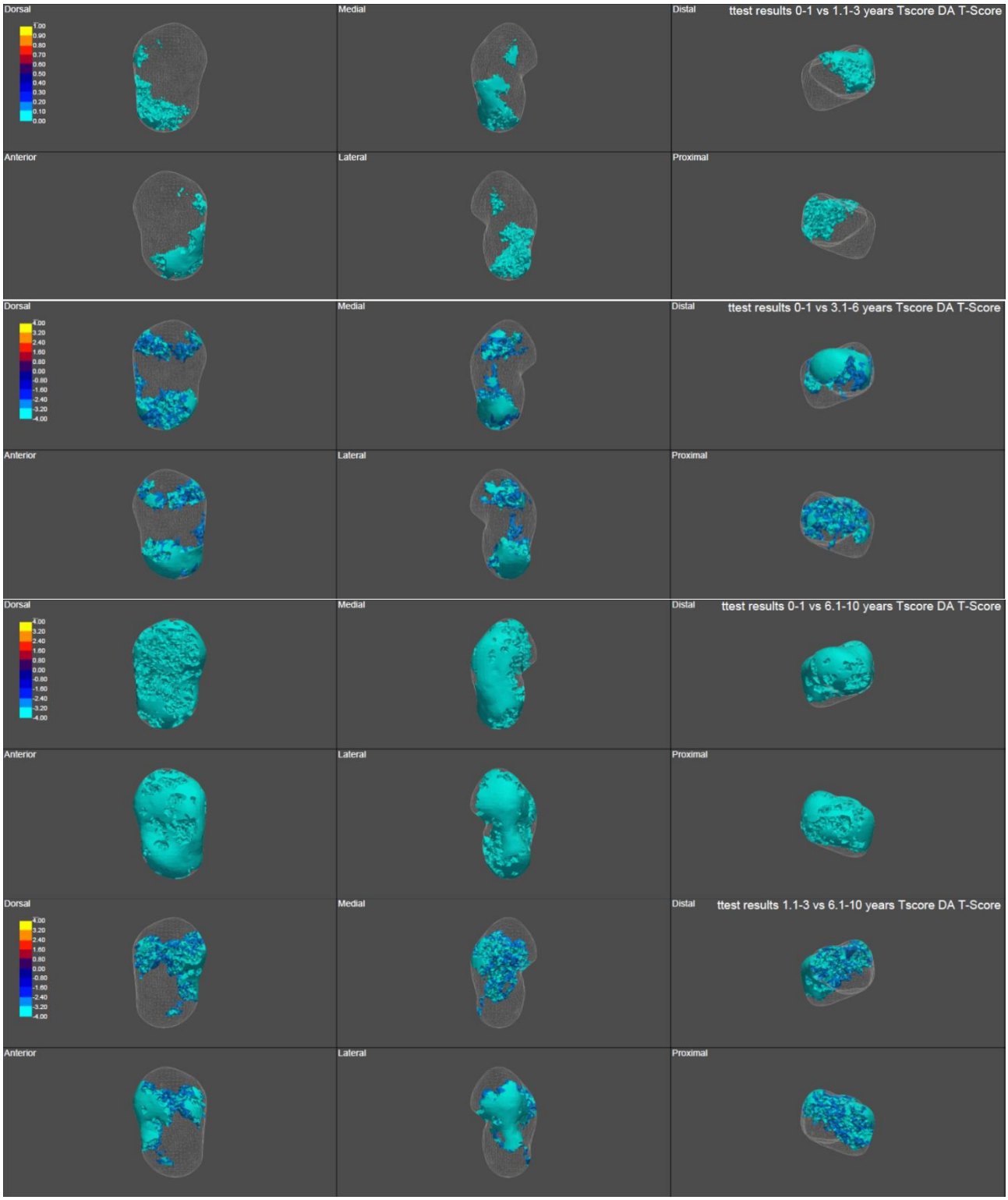

Figure 16 - DA T-Score. Cold colours represent the oldest age group in each comparison. T-test results for the DA show that DA significantly increase since the first years, after the onset of locomotion. In fact, age group 1.1-3 years has significantly higher DA values in the medial side of the head (first two rows), while DA is significantly higher in the 6.1-10 years age group than in the 1.1-3 group, in the anterior part of the trochlea and lateral side of the neck.

Table 12 – T-test scores

		BV/TV	DA
0-1 vs 1.1-3	0-1 vs 1.1-3	**<0.05**	**<0.05**
0-1 vs 3.1-6	0-1 vs 3.1-6	>0.05	**<0.05**
0-1 vs 6.1-10	0-1 vs 6.1-10	**<0.05**	**<0.05**
1.1-3 vs 63.1-6	1.1-3 vs 3.1-6	>0.05	>0.05
1.1-3 vs 6.1-10	1.1-3 vs 6.1-10	**<0.05**	**<0.05**
3.1-6-6.1-10	3.1-6 vs 6.1-10	**<0.05**	>0.05

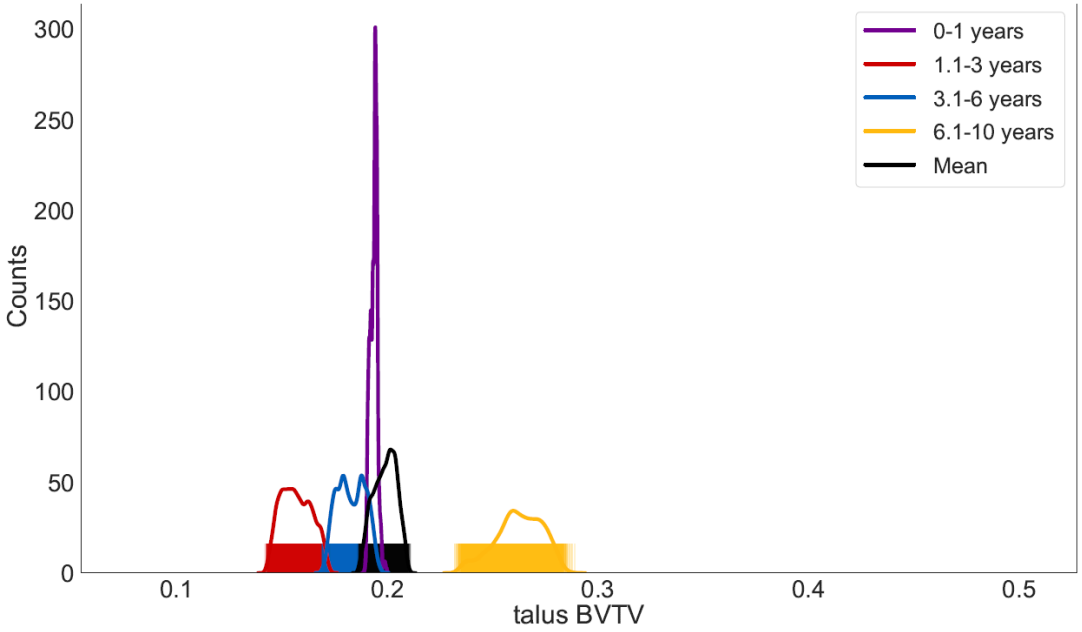

Figure 17 - BV/TV coefficient of variance. The kernel density estimate plot shows the distribution of the frequency of points for a given bone volume fraction value based on the results from the pointlcloud analysis.

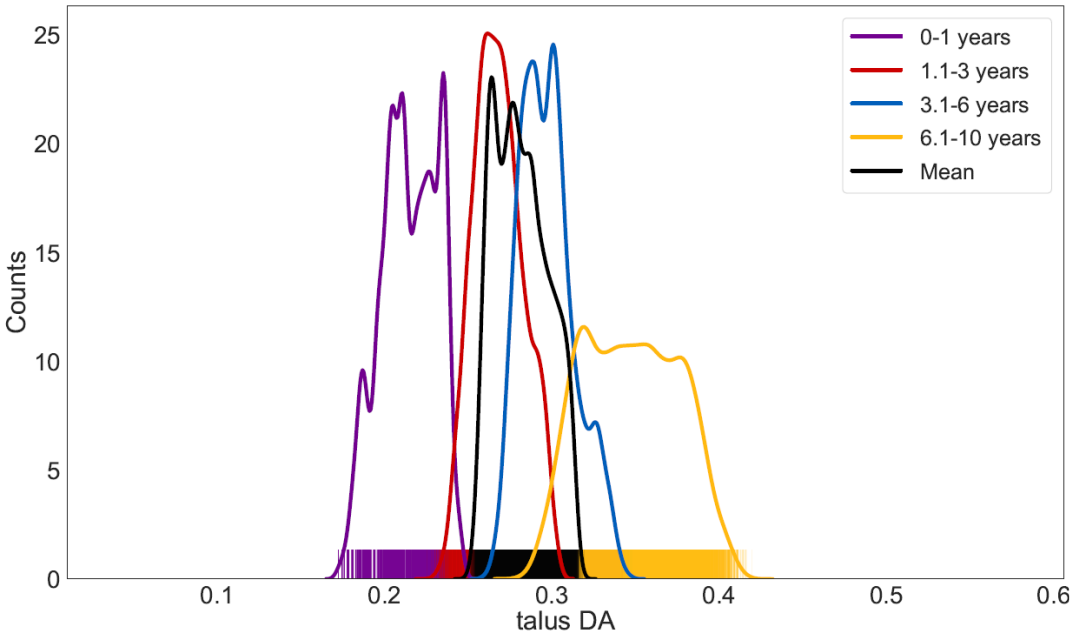

Figure 18 - DA coefficient of variance The kernel density estimate plot shows the distribution of the frequency of points for a given DA value based on the results from the pointlcloud analysis.

2.4. Discussion and Conclusions

This work investigates the internal structure and external shell of the growing human talus, from birth to about 10 years of age. We find out that both differs significantly during growth at different stages, both in location and magnitude, potentially reflecting the different joint position and load distribution during the development of bipedal locomotion. These results are consistent with previous ontogenetic studies of other skeletal elements (Colombo et al. 2019; Saers, Ryan, and Stock 2020) and talus (Hellier and Jeffery 2006). This study is part of a wider project focusing on talar ontogenetic changes linked to the development of human bipedal locomotion. Here we present results showing how talar external shell and internal architecture changes from the early stages of human bipedalism through a more mature and adult-like gait.

2.4.1. External morphology

Significant differences were noted among age classes along PC1 and PC3 scores. The first age class show a more shapeless talus, with a round and shallow future neck area, a round head and a small body, with a very short and not yet marked trochlea. Medial and lateral malleolar facets are not present, while the anterior and posterior calcaneal facets are distinguishable, but not yet well developed. By age one, though, there is a great advancement in the development of the lateral malleolar process, and the head commences its medial rotation, while the neck area starts to lean and lengthen. This is very important, as this age range (1.1 - ≤ 3 years) is the phase where most of the development locomotor milestones happen. The anterior calcaneal facet starts to develop earlier than the posterior one. This is probably due to the fact that, during the earlier locomotor phases, children have not developed yet a proper heel strike. After age three, the elongation of the talus is more evident, the trochlea develop a slight concavity and the medial and lateral rims are visible. The head continues to rotate medially, and the lateral malleolar process starts to develop. As the talus grows in a dorsal-plantar direction, the sulcus tali becomes deeper, while the anterior and posterior calcaneal facets continue to develop, the former ahead, the latter starts to develop its characteristic concavity and becomes more triangular in shape, characteristic that is even more pronounced after age six. A slight rotation of the trochlea is visible, which becomes more evident after six years. During this phase (6.1 – 10 years) the talus has a more mature overall morphology, with the lateral and medial malleolar facets more defined. Only the posterior part of the body, e.g. the posterior rim of the trochlea and posterior rim of the posterior subtalar facets have not yet reached the adult morphology. In shape space, each age group differs significantly from the others along PC1 scores, with the sole exception of the first two classes, i.e., 0-1 and 1.1-3. In PC3, though, age group 3.1-6 years differs significantly from the 0 – 1, which is expected, and 1.1-3 years. The differences along PC1 scores may be justified not only by the changes in shape, but also by the ontogenetic allometry, i.e. morphological changes strictly correlated with increase in size, while the changes along PC3 scores may be explained by the changes in the shape of trochlea and the development of the lateral malleolar process. Statistical differences between 1.1-3 and 3.1-6 years denoted brusque changes in talar shape, probably explainable by development of the lateral malleolar process, the increase in trochlear curvature and the increased rotation of the head. During this

timeframe, in fact, a heel-strike pattern is already present, and the adult-like transfer of forces from the lateral to the medial side is developed, while the rotation of the malleoli of the ankles is completed around 5-6 years (Fritz and Mauch 2013). The infant foot is characterized by a flat arch profile, with large contact areas and large amount of subcutaneous fat, which change with the development of the longitudinal arch. Longitudinal arch reaches adult levels between 5 and 6 years (Bertsch et al. 2004), even though the foot maintains a "flatter appearance" until 10 years of age (see Waseda et al 2014; Staheli, Chew, and Corbett 1987). Its development is driven by both genetic and epigenetic factors, such as body weight, physical activity and footwear (Fritz and Mauch 2013). In addition, the development of the lateral and medial facets changes the aspect of the trochlea, with an increase in the lateral and medial rims and a deeper concavity. This, in addition with the increase in trochlear surface area, makes this surface more efficient in receiving the body weight from the tibia. All these enormous changes may be explained by the maturation of the bipedal locomotion, and the correlated changes that happened in the mechanic of gait. In addition, we observed the changes in the articular facets, i.e. increase in size and orientation, with consequent reduction of the non-articular areas, e.g. sulcus tali, neck. Hellier and Jeffery (2006) described the plasticity of juvenile talus, in which articular facets responds to increase in loading by altering the shape and orientation, ultimately changing the direction of the force passing through them. They tested their hypothesis on a sample of juvenile tali from 8 to 18 years. We observed that this phenomenon is present, even though in a lighter way, also before the age of 8. In fact, we are able to observe how the talar facets start to change their orientation to cope with the forces that passes through its body, neck and head. Between three and six years, the trochlea and head start to change their orientation. From age six, also the posterior subtalar facet starts to change orientation, rotating to a more medio-plantar direction. This is probably linked to the fact that, when loaded, the trochlea receives compressive forces from the tibia, which pass directly to the posterior calcaneal facet, downwards, and forwards to the neck (Hellier & Jeffery, 2006). From here, the compressive forces are converted into tensile forces, and change direction to pass to the head, from where they are transmitted to the navicular and to the calcaneus. When standing, the forces are not distributed homogeneously but a larger amount of forces are transmitted medially, to the metatarsals, particularly to the hallux (Hellier & Jeffery, 2006).

Form space, though, showed significant differences between all the age classes along PC1 scores, which is completely driven by size. These differences are explained by the great increase in size during growth, particularly during the first years, when the size of the foot changes enormously. At birth, the foot has reached about 1/3 of its final length (Maier and Killmann 2003; Fritz and Mauch 2013; Dimeglio 2001), and most of the foot growth occurs during the first three years of life, with the achievement of about 2/3 of the final length (Maier and Killmann 2003; Volpon 1994; Fritz and Mauch 2013). This is due to the fact that the foot has to grow fast to be prepared to bear the increasing body weight, making the foot the first body segment to complete the growth process (DiMeglio, 2001). According to Bertsch et al. (2004), half the adult foot length is achieved around 12-18 months of age, probably to increase stability by augmenting the foot contact areas, e.g. the base support size (Price et al. 2018). According to Scheuer and Black (2004), the talar facets are not delineate until age 6. We were able to track the early formation of some of the talar facets between birth and 10 years of age.

This work poses another piece of information to the talar growth puzzle and, to the knowledge of the authors, this is the first time that both internal and external talar morphologies are explored, adding information on postnatal talar development.

2.4.2. Biomechanics

Trabecular results show that the architecture of the talus changes through ontogeny during the development of human bipedal locomotion. From being a dense and non-specialized structure, with a high number of thin and closely spaced struts, with an isotropic structure, talar architecture becomes a specialized structure, with less and thicker trabeculae, more widely spaced, and with an anisotropic structure. These changes are in line with what has been observed in other studies on the ontogeny of trabecular bone, even though in other skeletal elements and with different methodologies (e.g. by the utilization of VOIs). There are statistical differences in BV/TV and DA values among age classes. BVTV differs significantly between the first two cohorts in the medial part of the head, but no statistical differences emerged between 0-1 and 3.1-6 years groups, while between the former and the 6.1-10 groups, there is a significant difference in the distal part of the head, lateral malleolar process and most lateral-anterior part of the trochlea. Between the 3.1-6 and 6.1-10 groups, BV/TV significantly differs in the lateral side of the talus, sulcus tali and lateral side of the head. The high bone density at birth may reflect a gestational overproduction (Acquaah et al. 2015; Milovanovic et al. 2017). Denser bone in neonates may be likely the result of the endochondral ossification, when bone is laid down quickly following a genetic blueprint and the rapid growth of the cartilage anlagen (Milovanovic et al. 2017). Subsequent remodeling may be genetically driven and also adaptive as a consequence of mechanical strain, e.g. muscle contractions. It is supposed to adapt later to forces produced by bipedal gait, and our results confirm this pattern. In fact, after the third year of age, BV/TV starts to increase, consistently with the weight gain and consequently to the increase in compressive and tensile forces that passes through the talus, with the highest values in the oldest age cohort, i.e. 6.1-10 years. Interestingly, the highest values are found in the lateral side of the talus.

DA differs significantly between the first group and all the other age groups, in particular in the medial side and head (vs 1.1-3), lateral and medial part of the trochlea and head (vs 3.1-6) and almost completely on the dorsal part, lateral malleolar process, medial side and anterior calcaneal facet (vs 6.1-10). Significant differences emerged also between the groups 1.1-3 vs 6.1-10, specifically in the lateral and anterior part of the trochlea, lateral margin, lateral side of the neck and medal-anterior part of the trochlea.

In general, results suggest that trabecular architecture models under the effect of mechanical strain during development of mature bipedal locomotion. Results are consistent with previous studies on different skeletal elements (Colombo et al., 2019; Gosman & Ketcham, 2009; Milovanovic et al., 2017; Raichlen et al., 2015; Ryan & Krovitz, 2006; Saers et al., 2020). During the first year of life, trabeculae are very dense, as seen in the first chapter, and then modeling begins to change the structure, by trabecular resorption, which become more uniformly oriented, thicker, and more widely spaced. Excessive bone laid out during gestational period is important as it serves as a calcium reservoir (Acquaah et al. 2015) during the postnatal period, when the

reduced quantities in breast milk may not be sufficient to provide for the infant needs (Ilich and Kerstetter 2013), but it becomes soon excessive, and reabsorbed. After the onset of bipedal locomotion, there is a constant increase in loading and bone responds stopping the trabeculae removal, e.g. BV/TV stops decreasing (Saers, Ryan, and Stock 2020). Changes occur locally, and the areas of the bone that are more affected by the increase in loading show thicker trabeculae and increased DA. The most significant changes are observable before the development of mature gait, around 7-8 years. Our results are in line with what Saers and colleagues (2020) found out in the calcaneus, with bone laid out isotropically, that becomes more anisotropic with increase in loading. This pattern is different from what Ryan & Krovitz found in the proximal femur, where in one of the two VOIs under study, the initial structure was anisotropic, highlighting a probable genetic blueprint (Cunningham and Black 2009a,b).

The role of the talus is to sustain the weight of the body and transmits this weight in two main directions, i.e. to the calcaneus and to the navicular, and it is subject to both compressive and tensile forces, with the former acting on the body and the latter converted in the neck and passed forward to the head of the talus. These forces act indirectly on the talus, which does not have any attachments, e.g. muscle, tendon, aponeurosis. This makes the talus an important hub of the forces that passes through it; hence, the trabecular orientations should reflect this role. Trabeculae in the talus body are oriented mainly vertically arranged postero-anteriorly (Pal and Routal 1998), facilitating the transmission of the weight from the tibia, which rolls over the trochlea surface during walking. In the head they are arranged in semi-arches, parallel to each other, making it easier to transmit forces through the middle and anterior calcaneal facets and distally to the navicular facet. The neck is a complex area, with a more irregular network that serve different directions (Pal and Routal 1998).

2.4.3. Does the internal and external changes track the locomotor milestones?

Cortical bone has a slower modeling rate than trabecular bone, making the internal architecture more sensitive to catch functional signals, and it is even more true in the case of the articular facets, since subchondral bone is even more conservative. This is also true during ontogenetic development, when the modeling rates are even faster than in adults. As we were able to see in our results, the most interesting biomechanical changes happened before the age of 5, with the changing in orientation and bone density seen soon after the onset of bipedal gait. Though, the slower development of the external talar shell continues to give information about functional use. Taken together, these pieces of information may be of paramount interest. The changes in the internal architecture of the talus correspond to changes in the external dimensions.

During the first year of life, especially during the first half of the first year, the talus is “unspecialized” both in the external shell shape and in trabecular architecture. When looking at the external morphology, the globular and almost facet-free talus shape tells us that the bone is not yet ready to sustain its role of receiver and distributor of forces. And the trabecular architecture confirms it, showing a very unspecialized architecture, with dense and isotropic structure which does not show any evidence of real loading yet. In fact, during this period, children usually engage in a series of movements which does not comprehend the full loading of the

foot (sitting, crawling, full erect posture for brief period of time, with a support). DA is relatively low, showing a homogenous isotropic pattern.

Things start to change between the end of the first year and after the start of the second year. In fact, during this time frame, children usually start to walk, engaging in an initial unstable locomotion, with high step-to-step variation. This pattern slowly tends to improve with both practice and neuromuscular maturation, leading to a more mature gait at the end of the third year, with a full heel-strike and toe-off, allowed thanks to the muscle maturation. Talar shape shows this improvements, with slight changes in head medial-orientation, trochlea surface, lateral malleolar process, which confirms our initial predictions. Trabecular architecture, consequently, records the change in strain with a decrease in BV/TV, with lower number of trabeculae, which are thicker and more widely spaced. Trabeculae which are not loaded are resorbed, promoting the modeling of oriented struts. In particular, the lower density values are recorded in the medial-anterior side of the talus. DA values increase, particularly in the medial side and head.

After the achievement of a more mature and stable gait, the longitudinal arch continues to develop. In the age class 3.1-6, talar shape has improved, increasing the concavity of the trochlea, development of the facets, elongation of the bone. Trabecular bone tracks this changes, and BV/TV starts to increase again in the same areas that has shown the most an increase in size/surface and orientation/morphology: trochlea, subtalar posterior facet, lateral malleolar process and the most distal portion of the head. DA increase, with higher values in the trochlea and head.

Finally, at 6.1 – 10 years, when the gait reaches an adult-like pattern, the morphology has showed great changes in the trochlea, with an increase in medial-lateral concavity and lateral and medial rims, a proximo-distal elongation of the surface with an increase in curvature and orientation, which becomes more medially oriented, as the head. This may be linked to the achieved adult-like transfer of weight from the lateral side, after heel-strike, to the medial side in preparation for the push-off. The re-orientation of the trochlea and head coincides with the slight orientation of the posterior calcaneal facet, which shows a great increase in size and concavity, and a change in shape, i.e. not triangular anymore. In the same areas which shows the greatest changes in shape, corresponds an increase in BV/TV magnitude. DA continues to increase in the most dorsal parts of trochlea, neck, head, lateral and medial malleolar facets, and also posterior calcaneal facets. Our results confirm the initial predictions, confirming a slight change in the articular facets orientation, which increases with increase in age and gait maturation, a steady decrease in BV/TV values and an increase after 3 years of age, and an increase in DA values after the onset of bipedal locomotion.

2.4.4. Methodological limitations

There is a general consensus about the timing of achievement of the locomotor milestones. However, slight differences are noted between different individuals and different populations. These differences may be cultural, as different studies found out that African children start to sit unaided and to walk before the European counterparts (Cowgill and Johnston 2018). In this study, the sample is very variegate, and varies both

geographically, culturally, and chronologically, and this may affect the work. In fact, we do not to what extents genetic and cultural differences may act on the talus.

Another problem that may affect the strength of this work is the use of an archaeological sample, with the sole exception of the Bologna sample – which is limited, concerning children that died before complete the processes of growth. Therefore, we did not know whether the causes of death affected their behavior or their locomotor development. We are well aware of the fact that, besides this drawbacks, archaeological sample are pivotal in this studies. Additionally, the sample, when subsets are concerned, is too small to permit the analysis on a year-by-year basis. This would be helpful, in future, with the increase of the sample.

2.5. Conclusion

When considered together, the results of the changes in both external shell and internal architecture are very informative. During the first few years, i.e. 0-3 years, shape changes are slower than trabecular ones, which demonstrate to be more accurate in capturing the differences in loading. On the contrary, shape changes between the 1.1-3 vs 3.1-6 years and 3.1-6 vs 6.1-10 are greater, and due to the obvious development of the external shape, driven by both genetic and epigenetic factors (e.g., growth in size, general growth, vs a reorientation of articular facets), while DA seems to stabilize after the second year, and steadily increase after six years.

The results of this work show the important information that a holistic approach can provide to the ontogenetic investigations linked to the studies of bipedal locomotion. This approach may help in shedding lights in the long search of origin of human bipedal deambulation, most importantly when the study of fossils is concerned. Our research shows, in fact, that the plasticity of human talus, even though driven by a genetic blueprint, may display the presence of an epigenetic influence and, when accompanied by the study of the faster-in-remodeling trabecular bone, may open the doors to a whole new investigation strategy which may, ultimately, help to discover new information about hominin behavior.

Chapter Three
At the dawning of bipedalism: morphological and trabecular changes during the locomotion shift

3.1. Introduction

Loading of the skeleton is crucial to reach and uphold an adequate and functional bone mass. This is ascribable to highly regulated mechanisms, that allow bone modeling and remodeling through site-specific activation of osteoblastic and osteoclastic cells (Pivonka, Park, and Forwood 2018). During the first two years of life, the modeling rate is higher than in adults, with estimates of neonatal remodeling at 50% per annum, compared to just 5% per annum in the adult life (Walker 1991). Movements starts in utero and continues during the postnatal life. Studies on prenatal movements contributed in shedding lights into the types of movements, intensity, duration and gestational periods they occurred into (DiPietro et al. 2010; Einspieler, Marschik, and Prechtl 2008). It is also well known that the intrauterine environment is drastically different from the extrauterine one, being the former a protected space with virtually no gravity and no loads, since the fetus lives immerse in the amniotic fluid; though, the movements generate forces that are fundamental in the process of growth, aiding in shaping the bones into the adult morphology (Carter and Beaupre 2001). Mechanical stimuli in utero and during early postnatal life are vital for the normal bone development, as may serve to reinforce both bone shape and structure (Cunningham and Black 2009a,b). The external shape of bones clearly reflects a genetic blueprint and functional morphology, as the fact that shape, size, and orientation of articular facets strongly correlate with joint mobility, body mass, and are phenotypic stable (Chris Ruff 1988; Lieberman, Devlin, and Pearson 2001). The external morphology retains also phylogenetic history, i.e. shared similarities between species (Kivell, 2016), which makes it even more difficult to discern the functional aspects from genetic ones (Kivell, 2016). Internal bone structure, however, may help to have a more complete picture. Cancellous bone is believed to be deposed by following genetic patterns, but later, also thanks to the higher rates of bone modeling, it adapts to mechanical loads, giving better insight than the external morphology into the mechanical loading patterns (Kivell, 2016). In fact, adult trabecular bone structure is the result of the loading history that affect bone growth during ontogeny (Gosman & Ketcham, 2009; Ryan & Krovitz, 2006). During development, bone reacts to external stimuli, both changing the dimensions and orientation of articular facets (Hellier and Jeffery 2006) and adapting the trabecular struts by remodeling in response to changing load bearing (Cunningham & Black, 2009b). Skedros et al. (2007) showed that the final skeletal structure derived by a combination of both genetic and epigenetic factors. Ontogenetic studies of both internal and external structures are of paramount importance for deepening our understanding of the processes that lead to the adult morphology. To thoroughly comprehend this process, it is necessary to disclose the growth patterns, which otherwise may remain obscured, heading to misleading interpretations (Kivell, 2016; Saers, Ryan, & Stock, 2020). The origin of bipedalism is still one of the most burning question which still needs some answers. Numerous studies tried to complete the puzzle of the evolution of the human locomotion, each one adding an important piece to the whole picture (for

example, Raichlen et al. 2010; DeSilva and Devlin 2012; Thorpe, Holder, and Crompton 2007; Sockol, Raichlen, and Pontzer 2007; Schmitt 2003; Sylvester 2006). Lower limbs experience thousands of cycles of loading and unloading every day, and magnitude and orientation strictly depends on the location within the bone (Carter 1984). The importance of the foot has been broadly investigated (Harcourt-Smith and Aiello 2004; Fernández et al. 2018; Mcnutt and Zipfel 2018; Smith et al. 2018;. DeSilva and Devlin 2012; DeSilva et al. 2013; DeSilva et al. 2019). It is the element that makes contact with the ground, accommodates irregularities of the ground while maintaining balance. Also, it supports the body weight, while serving both as a shock-absorber and a lever for transmission of propulsive forces (Hallemans, De Clercq, Dongen, & Aerts, 2006). The adult human foot is well adapted and highly specialized to perform perfectly all these tasks, without us noticing. Additionally, studies highlighted that the adult human ankle joint (i.e. distal tibia, fibula and talus), shows different trabecular properties from other nonhuman primates, possibly reflecting the habitual loading patterns (Su, 2011; Barak et al., 2013; Su, Wallace, & Nakatsukasa, 2013; Su & Carlson, 2017; but see also Desilva & Devlin, 2012), and it has been demonstrated that there are links between neuromuscular development and trabecular bone growth (Raichlen et al., 2015). Infant foot, on the other hand, is anatomically different and, therefore, functionally different (e.g. absence of the typical "heel-to-toe" roll-over pattern, see for example Zeininger et al. 2018). During early infancy, the foot consists mostly of ossific nuclei and cartilage, connected by soft tissues. At about 1 year of age, when toddlers start walking, talus, calcaneus, cuboid and some of the phalanges contain their primary ossification centers, still surrounded by cartilaginous tissues (Hallemans et al. 2003). Although studies on the ontogenetic changes linked to the modifications in load-bearing forces that act on the foot are still rare, both on humans (Saers, Ryan, & Stock, 2020; Zeininger, Schmitt, Jensen, & Shapiro, 2018) and nonhuman (Tsegai et al. 2018; Gorissen et al. 2018), studies on the growing talus are even rarer (Hellier & Jeffery, 2006; on the development of the talocrural joint: Turley & Frost, 2014; Turley, Simons, & Frost, 2018), and do not take into account the early phases of talar growth. The talus ossifies from one center of ossification, and its secondary center is not always present (Cunningham, Scheuer, & Black, 2016). This makes the talus a perfect "recorder", as it may account for all the developing stages, being present from the late gestational phase. Tarsals bones ossify through endochondral ossification, e.g. by the calcification of a cartilage anlagen, with talus starting chondrification at 8 prenatal weeks, following the calcaneus, and it is the first talar bone to present signals of vascularization. Lower limb buds appears at 4 weeks of age, and then digital plate starts development (Uhthoff, Kawashima, and Uhthoff 1990).

Being the foot a highly derived and functionally significant region for investigating ontogenetic changes linked to the development of bipedal locomotion, this chapter will focus on the early human talar growth in the attempt to add information about the development of this important anatomical district.

3.1.2. Aims of the study

Aware of the fact that the fetal talus is not yet fully ossified at birth, we aim to study the morphological changes of the talus (i.e. from the ossific nucleus) from the 36-38 prenatal weeks to three years of age. The goals of this study are twofold: 1) to explore the global early talar growth, describing the changes that occur in the

human talus from the last prenatal weeks to three years old, both in the internal structure and in the external shell morphology to broaden the knowledge on the anatomical changes during early development; 2) and secondly to quantify and compare the differences that may exist in the talus before the start of the mechanical loads, before 6 months circa, and after the mechanical load, as the children start sitting, moving, and exploring the space around him/her, first crawling and cruising, and then walking. In fact, improvements appear to mature rapidly in the first 3 to 6 months after the beginning of independent locomotion, and then they tend to slow down (Adolph, Vereijken, and Shrout 2003). Based on previous literature(Ryan and Krovitz 2006; Saers, Ryan, and Stock 2020; Colombo et al. 2019) we hypothesize that in the younger cohort, representing the pre-loading individuals, the trabecular bone will be densely packed and uniformly oriented, with a high number of trabecular struts and low spacing, while in the older cohort the fabric orientation will be more anisotropic and less dense, with lower values of bone density and trabecular numbers, more widely spaced. We also predict, based on the fact that there is a rapid improvements after 3-6 months of practice, after the onset of independent walking (Bril and Ledebt, 1998; for more information, see the first chapter), that the values of DA will drastically increase in the older cohort, while BV/TV values will decrease steadily, due to the fast modeling rates of the trabecular bone.

3.2. Material and Methods
3.2.1. Sample

This study analyzes the early development of the talus in a sample consisting of 40 modern juvenile tali aged between 36 prenatal weeks and 3 postnatal years. Six individuals belonged to the Bologna collection, with known age at death, sex, and cause of death (Belcastro et al., 2017). The collection comprehends Italian skeletal remains from the Emilia-Romagna region and from Sardinia, which were collected mostly from 1908 to 1953 (Belcastro et al., 2017). The largest part of the Emilia-Romagna cohort was buried in Bologna La Certosa cemetery, the biggest cemetery of the city. The importance of this collection is given by the presence of ante mortem data, information about socioeconomical backgrounds, the generally good state of preservation, and the relatively high number of children in the collection. The cohort under study comprehend individuals from Bologna. All the children in this collection died for acute diseases. The absence of chronic pathologies, that might have lasted through time, leads us to believe that this cohort has not had locomotory difficulties for prolonged periods of time, possibly affecting the development of locomotion.

The rest of the study sample has been selected from different archaeological samples, with a timespan that goes from Neolithic to modern age. All the individuals' information are listed in Table 13

One individual is from the site of Beli Manastir, located near the eponymous city, in Osijek-Baranja County, eastern Croatia. The rescue excavations took place in 2014 and 2015 and covered a surface of approximately 37,000 square meters. Two main cultural layers were identified at the site: a prehistoric layer consisting of several Neolithic and Chalcolithic strata, and a Roman period layer. The prehistoric layers of interest are dated to the early and middle Neolithic periods in which the remains of a large settlement and 39 inhumation burials were found. According to the available radiocarbon dates a huge majority of Neolithic burials from this site can be dated to the Middle Neolithic, i.e. between 4800 and 4500 BCE. Most of the burials were found in a contracted position on either left or right side with different orientations. In several cases, one or more ceramic vessels were placed by the head of the deceased.

Two individuals came from the site of Ilok – Krstbajer, located in the eastern part of the town, about 200 m from the border crossing between Ilok (Croatia) and Bačka Palanka (Serbia). The site was partially destroyed during the exploitation of sand for construction purposes in 2011, so Ilok Municipal Museum in cooperation with the Institute of Archaeology carried out the rescue archaeological excavation. Between 2015 and 2017 three research seasons were conducted. The excavated area covers approximately 84 square meters. Within this area, 188 graves and part of prehistoric objects were explored. The archaeological context, artefacts, and radiocarbon analysis date the use of the cemetery between the end of the 12th and the transition from the 15th to the 16th century. These burials most probably belong to the parish cemetery around the church of St. Helen the Queen (Krznar & Rimpf 2018).

11 individuals came from the site of Norris Farms #36 (Illinois, USA), housed at the Pennsylvania State University, for which the age at death was estimated based on tooth crown formation and dental eruption stages (Milner and Smith 1990). This remains are part of the Oneota culture and dated back to 1300 AD (Millner & Smith, 1990).

16 individuals came from the Imperial Roman site of Velia. The site, originally founded by Greeks in 540BC (Morel, 2006), is located on the Italian west coast, near Salerno (Campania, Italy). Numerous archaeological campaigns have been held, and, during the 2003-2006 campaigns (Fiammenghi, 2003), a necropolis with over 330 burials was discovered. This necropolis, dated back to the I and II centuries AD, yielded both cremation and inhumations, with numerous juvenile burials. The age at death was analyzed based on the dental and skeletal maturation.

Four individuals came Perkáta-Nyúli dűlő, Hungary, and are stored at the Natural History Museum in Budapest. Five individuals came from the sites of Paks and nine from Perkáta-Nyúli dűlő. The two sites are located in – (Hungary), and are stored at the Natural History Museum in Budapest. The cemetery and settlement at Perkáta-Nyúli dűlő represents a population of a Cuman settlement in the Transdanubian region of Hungary, which at the same time preserved a population from the transition period of the Cuman integration (Hathàzi, 2004). The site was found during a motorway constructions works, between 2009 and 2010 by the Field Service for Cultural Heritage. The cemetery counts more than 4,000 graves. All the individuals dated back to the 14th-16th centuries AD, except for on (3421) that dated back to the 10th-12th centuries AD. Age-at-death was estimated based on the development of the deciduous and permanent teeth (Moorrees et al., 1963a,b; Smith, 1991). When no teeth were available, diaphyseal length (Stoukal and Hanakovà, 1978) and also epiphyseal fusion (Ferembach et al., 1980) were used (László, 2008; László, 2018; Mesterházy-Ács, Zs. 2015; Szeniczey et al., 2019).

The church around the cemetery of Paks- Cseresznyés was excavated between April of 2008 and 2009 by the Field Service for Cultural Heritage. According to the buildings and to the archaeological material of the village, it can be dated to the 14th and 16th centuries, which probably became deserted due to the expansion of the Ottoman Empire. The anthropological analysis have been conducted between 2009-2010. The specimens, with a very good state of preservation, belong to 504 individuals, 263 of which were infants (László 2012, 2018).

Table 13 - Archaeological sample and analysis information. Individuals are listed by populations

Site (location)	Specimen	Period	Age at death	Cause of Death	GMM	Biomechanics
BeliManastir (Croatia)	G6	Early/Middle Neolithic	2-3.5 years		✓	✓
Bologna (Italia)	58_M	XX c.	11 months	Bronchitis		✓
	60_F		11 months	Acute meningitis (brain fever)		✓
	14_M		1 years 5 months	Chronic enteritis	✓	✓
	14_F		1 year 9 months	Enteritis	✓	✓
	7_M		2 year 9 months	Intestinal gastroenteritis	✓	✓
	48_F		3 years	Meningitis	✓	✓
Ilok (Croazia)	G_70	XX c.	2-. year			✓
	G22	XIII-XV c.	2-3 year		✓	✓
Norris Farm (Illinois, USA)	821045	1300 AD	3 months			✓

	821369		8 weeks		✓
	820614		12 months		✓
	821051		7.5 months	✓	✓
	821046		1.5 years	✓	✓
	821026		2 year	✓	✓
	821207		2 years	✓	✓
	821069		2.5 years	✓	✓
	821113		2.5 years	✓	✓
	820683		3 years	✓	✓
	821214		3 years	✓	✓
Perkáta-Nyúli dűlő (Hungary)	516	XIV-XVI c.	1.5-3 years	✓	✓
	655		1-3 years	✓	✓
	639		2.5-3 years		✓
	3421	X-XII c.	2.5-3 years		✓
Velia (Italy)	T344us1566	Roman (Imperial Age, I-II c. AD)	perinate	✓	✓
	T417us2355		perinate		✓
	T350us1594		perinate	✓	✓
	T322us1436		Perinate (36-39 weeks)		✓
	T315us1398		perinate(36-40 weeks)	✓	✓
	T383us2175		perinate(38 weeks ca)	✓	✓
	T305us1344		0-3 months	✓	✓
	T300us1167		0-6 months	✓	✓
	T441us2538		0-6 months		✓
	T368us2069		0.75-1 years	✓	✓
	T398us2239		6-8 months	✓	
	T289us1098		9-12 months		✓
	T442us2545		6-9 months		✓
	T286us1071		1.5-2 years		✓
	T434us2454		1-1.5 years	✓	✓
	T415us2344		1-1.5 years	✓	✓
	T379us2143		2-3 years		
	T411us2319		2-3 years	✓	✓
	27	**40**			

All the specimens were selected based on their good condition, with minimal or no damages. Specimens with pathological signs (e.g., osteopenia) were excluded from the analyses. The left side was preferred; when missing or incomplete, the right one was selected instead, and mirrored. Four age classes were created, following the classification made by Swan (2020) and then adapted to our sample, and then they were grouped in two main subsets for further analyses, as listed in Table 14:

1) pre-loading group (perinates - 6 postnatal months) comprehends infants who are not able to independently locomote and rely entirely on their caregivers for transportation (Young and Shapiro, 2018), and the lower limbs are minimally loading. Children in this phase are not able to fully propel themselves, but progressively they start to hold the head upright, sit, with support, in an upright position. This group comprehend the youngest age classes, e.g. the late fetal/perinates and the neonates/early toddlers from birth to 6 postnatal months.
2) Post-loading group (6 postnatal months – 3 years old). Children start to sit upright without support, start crawling and, finally, walking unaided at about twelve months. Then, the achievement of the mature gait is refined through the slower and progressive stabilization of the pattern of gait. In this group are included the individuals from the two oldest age cohorts: from 6 months to 12 months, and from 1.1 years and ≤3 years.

The sample that underwent the GM analysis was really small. This is why the four age classes are used to described thoroughly the morphological changes with greater intervals (four, instead of two), but we did not use them for the statistical analysis due to the imbalance. Consistently, we analyzed the same two groups for the trabecular biomechanics analyses, and we showed the age groups averages to better explain the changes along the growth.

Table 14 – Age classes and loading subsets

Age classes	*Loading group*	*Individuals per classes*	*Total*
Perinates/prenatal	Pre-loading	6	11
0-6 months	Pre-loading	5	
6-12 months	Post-loading	7	29
1.1-3 years	Post-loading	22	

3.2.2. Data 3D acquisition and segmentation

All the samples were microCT scanned in different facilities (see Table 15). Scans were reconstructed as 16-bit TIFF stacks, and Image J was used to inspect the scans and evaluate their quality. When the trabecular bone showed signs of damage or rarefaction due to pathological or diagenetic causes, the specimen was excluded from the analyses. Avizo 9.3 (Visualization Sciences Group, SAS) was used to pre-process the reconstructed scan data (e.g. crop or resample). Where heavy sediment or mummified tissues were present, they were removed in Avizo 9.3 using a Wacom board and the Avizo paint-brush tool in the labels-field. A White Hat filter was applied (to the Norris Farms#36, some specimens from BeliManastir, Ilok, and Velia) to improve the contrast between bone and the heavy sediment present into the bone. Segmentation of the image data was

first performed using the MIA clustering method (Dunmore et al., 2018). In short, this method uses a K-means algorithm to cluster the CT images into specific classes determined a priori by the user. This clustering is based on voxel or pixel intensity. Therefore, a fuzzy c-means algorithm (Dunn, 1973; Bezdek, 1987) is applied to cope with the scanning artifacts or different levels of mineralization of the specimen or the soil (Dunmore et al., 2018); lastly the class membership probabilities are calculated. Finally, voxels are attributed to the class with the highest membership probability. All the process results in a segmented dataset. All the output used here are raw files, linked to MetaImage files (ITK). In some cases, the MIA clustering method failed in determining the class belonging. In those cases, a novel domain-enriched deep network architecture (Yazdani et al. 2019) was preferred.

Table 15 - Micro-CT information

Sample	Facility	Voxel size (µ)
Bologna	Center for Quantitative Imaging (CQI), Pennsylvania State University, PA (USA)	20-38
Norris Farms	Center for Quantitative Imaging (CQI), Pennsylvania State University, PA (USA)	12-26
Velia	The Abdus Salam International Centre for Theoretical Physics, Trieste, Italy	18-30
Beli Manastir	University of Zagreb, School of Medicine, Zagreb, Croatia	18-29
Paks and Perkata	The Abdus Salam International Centre for Theoretical Physics, Trieste, Italy	18-30

3.2.3. Geometric Morphometrics Analysis

To cope with the many morphological differences of the growing talus, a minimal template of 146 (semi) landmarks (5 anatomical landmarks, 30 curve semilandmarks, and 111 surface semilandmarks, as shown in Figure 1) was created in Viewbox 4 (dHAL Software), on a perinate talus (Velia T383us2175). The aim of this template is to follow the morphological changes in the gross morphology, related to the ontogeny, from the late postnatal weeks to three years old (Figure 19, Table 16-17). Unfortunately, not every specimen showed an intact cortical bone, making it impossible to apply the configuration of (semi)landmarks on them. Several tali had to be excluded from the GM analysis, as reported in Table 1.

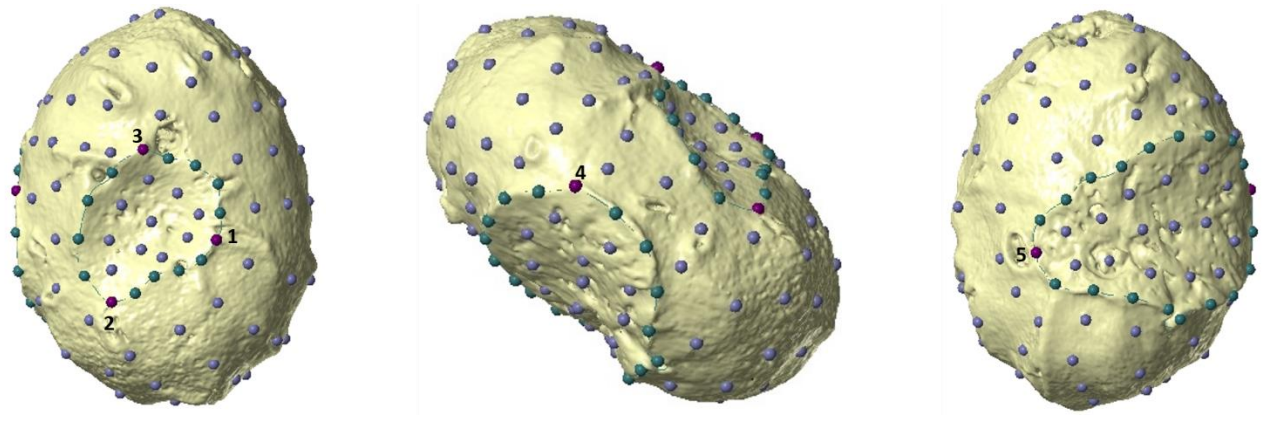

Figure 19- (semi)landmarks configuration. From left to right: dorsal, lateral and palmar view. Landmarks are shown in purple, curve semilandmarks are the green sphere, surface semilandmarks are represented in violet.

¤Table 16 – Configuration of landmarks. Type of landmarks based on (Bookstein 1997)

	Description	*Type of landmark*
1	The most medial point of the neck	III
2	The most lateral point of the neck	III
3	The most anterior point of the neck	III
4	The most anterior point of the lateral bridge	III
5	The most medial point of the sulcus tali	III

Table 17 - Semilandmarks

Semilandmarks on curves	N
Curve L1-L2: Posterior part of the neck	4
Curve L2-L3: Lateral and Anterior part of the neck	4
Curve L3-L1: Medial part of the neck	4
Curve L4-L5: Posterior margin of the Sulcus Tali	9
Curve L5_L4: Sulcus tali and bridge	9
Semilandmarks on surface	N
Head and anterior calc surface	35
Medial side surface	20
Posterior and lateral surface	31
Sulcus Talis surface	15
Neck surface	10

The (semi)landmark configurations were applied to the targets. To be considered geometrically homologous (Gunz & Mitteroecker, 2013), semilandmarks were allowed to slide on the curves and surface, to minimize thin-plate-spline bending energy (Slice, 2006) between template and targets. Then, semilandmarks were allowed to slide against recursive updates of the Procrustes consensus (Gunz, Mitteroecker, & Bookstein, 2005; Mitteroecker & Gunz, 2009). Then, a Generalized Procrustes Analysis (GPA) was run in R 3.6.2 (R Core Team, 2020; Rohlf and Slice, 1990), using geomorph (Adams & Otárola-Castillo, 2013). A shape and form space Principal Component Analysis (PCA) was carried out on the Procrustes coordinates to explore talar shape variation during growth using the R package Morpho (Schlager, 2017). Shapiro Normality Test was performed to assess the distribution of the data, while the homoscedasticity was assessed using a Levene's test for the homogeneity of variance. Analysis of Variance (ANOVA) or Kruskal-Wallis test were used to determine whether mean group values along each PCs differed from each other. Pearson's product moment correlation of PCs scores was run against the natural logarithm of the centroid size (lnCS) to asses if shape variations were related to ontogenetic allometry.

3.2.4. Biomechanical analyses

After the above-mentioned segmentation processes, the trabecular and cortical bone were separated following the protocol outlined by Gross and colleagues (2014) using Medtool 4.3 (Dr Pahr Ingenieurs e.U, 2017). Briefly, opening and closing filters (kernel size varies from 3 to 5, depending on the specimen) with a "region

growing" function were applied using a customized python-based script within Medtool to remove cortical porosity and facilitate the creation of a uniform shell that is then filled to create three different masks, namely outer (i.e. the outer shell of cortical bone), and inner (i.e. the boundary between cortex and trabecular region), which separates cortical from trabecular bone (Gross et al. 2014; N. B. Stephens et al. 2016, 2018a). Then, the inner mask is subtracted from the outer one, creating the cortical thickness mask. For this study, only the inner region, i.d. trabecular bone, was used. Finally, a tetrahedral mesh of trabecular bone was generated using the computational geometry algorithms library CGAL (www.cgal.org), a mesher that creates a 3D finite element model using Delauney triangulation (Delaunay, 1934; Gross et al., 2014; Klomza and Skinner, 2019). Quantification of bone volume fraction (BV/TV), which is the ratio of trabecular bone voxels relative to the total volume of voxels (Fajardo et al., 2007: Kivell, 2016), and Degree of Anisotropy (DA) which describe the degree of orientation of the trabecular struts (Klomnza and Skinner, 2019), was carried out on the trabecular mesh by moving a sampling 5 mm sphere along a background grid with 2.5 mm spacing for each scan (Pahr and Zysset, 2009; Gross et al., 2014). BV/TV (bone voxels/total voxels) is expressed as a percentage, DA is calculated as (1-[eigenvalue3/eigenvalue1]) and is scaled between 1 and 0, where 1 is highly anisotropic and 0 isotropic, following the Mean Intercept Length (MIL). The resulted colormaps were then visualized in Paraview 3.14.1 (Sandia Corporation, Kitware Inc). Mean trabecular thickness (Tb.Th, mm), trabecular numbers (Tb.N), and mean trabecular spacing (Tb.Sp, mm) were calculated (Hildebrand and Ruegsegger, 1997; Stephens et al., 2017).

3.2.5. PointCloud Analysis

In order to statistically compare the results between the two groups, we followed the Phenotypic PointCloud Analysis proposed by DeMars et al. (2020). Briefly, we align all the trabecular volumes using a modified version of the auto3dgm R package (Boyer et al. 2015) to automatically position the pseudolandmarks, i.e. landmark-like points, each of one has a consistent biological identity across all bones in the sample (Boyer, Yapuncich, Butler, Dunn, & Seiffert, 2015), making them homologous. Though, they are not classified by classical the landmarks criteria (e.g. type I, II, or III) nor by the semi-landmarks categories (Mitteroecker and Gunz, 2009). Therefore, the authors called them "pseudolandmarks". Due to the slightly different morphologies, e.g. immature and slightly more mature shape, we used 600 and 1200 pseudolandmarks. After a generalized Procrustes analysis using the GeoMorpho R package (Adams, Collyer, & Kaliontzopoulou, 2018), an average mean of the trabecular meshes was created and warped on the mean coordinates of all the coordinates sample obtained after the GPA. This average trabecular mesh was then filled with the evenly-spaced (1.75mm) points to create the average point cloud (e.g. canonical). The individuals' point clouds were then obtained by interpolation of the individuals' scalar values for BV/TV and DA to the mesh. All the point clouds were aligned on the auto3dgm alignment matrix, and considered homologous. Subsequently, a rigid, affine, and deformable alignment was performed, using the Coherent Point Drift algorithm (Myronenko & Son, 2010), and the individuals' BV/TV and DA scalar values were linearly interpolated from each individual point clouds to the corresponding points in the canonical point cloud using SciPy (Virtanen et al., 2020).

Finally, the obtained group's averages were mapped onto the canonical point cloud, to statistically compare BV/TV and DA across the sample. The homologous point were compared using a two-tailed t-test, with P-values corrected (Friston et al., 1995; Worsley et al., 1996). Results are visualized in Paraview.

3.3.Results

3.3.1. External morphology

3.3.1.1. Shape space

Shape space results of the first three PCs are shown in Figures 20-21. Shapiro normality test show that the first three PCs (52.3% of the total variance) were normally distributed (PC1: W= 0.95, p-value= 0.2196; PC2: W=0.97, p-value=0.69; PC3: W0.98, p-value=0.96) while the Levene test attested for equality of variance, with p-values >0.1 for all the first three PCs. Most of the morphometric variation is explained by PC1 (28.3%), i.e. ontogenetic allometry, which clearly separate the two groups, where negative scores account for small (Figure 5), globular morphology (the youngest individuals), that well represents the not completely ossify neonatal talar morphology (e.g. ossific nuclei), where it is already possible to recognize the talar head and the neck, as a circular depression, and the sulcus tali that is well defined. The impressions of the cartilage canals are still visible in the posterior part of the talus body. Positive scores account for a more mature talar body, with a clear elongation of the entire talus, due to the development of the neck, that shows an increase in concavity and area, a clear development, though not yet complete, of the trochlea and lateral malleolar facet, with the articular facet not yet defined. The area of the sulcus tali is larger and more defined, as well as the lateral ridge. The head is slightly rotated medially, and its shape is more similar to the mature talar head. The anterior calcaneal facet is more defined, while the posterior calcaneal facet has grown, with a characteristic triangular shape, but is not well demarcated yet. PC2 (13.1%) separate the two groups (Figures 20-21), and account for a better distinct and deeper sulcus tali and lateral ridge, with a general “sliminess” of the shape, that is less globular. The lateral ridge shortens along positive values, due to the growth of the head. PC3 (10.8%) negative scores show a wider and concave neck, as seen in PC1, but larger, that grows narrower and with sharper margins along positive values, with the general elongation of the talar body and development of the trochlea and head. ANOVA results showed significant differences between the two groups (Df = 1, F-test=39.73, p-value 1.35e-06) along PC1 scores, while differences along PC2 and PC3 were not significant (PC2: Df=1, F-test = 3.5, p-value = 0.07; PC3: Df = 1, F-test = 0.003, p-value = 0.9). The shape variation described by PC1 is significantly related to size, although not completed guided by it (r=0.75, p-value=5.78e-06). Figures 22, 23 and 24 show the mean shape of the four age classes, and the mean shape of the two loading groups.

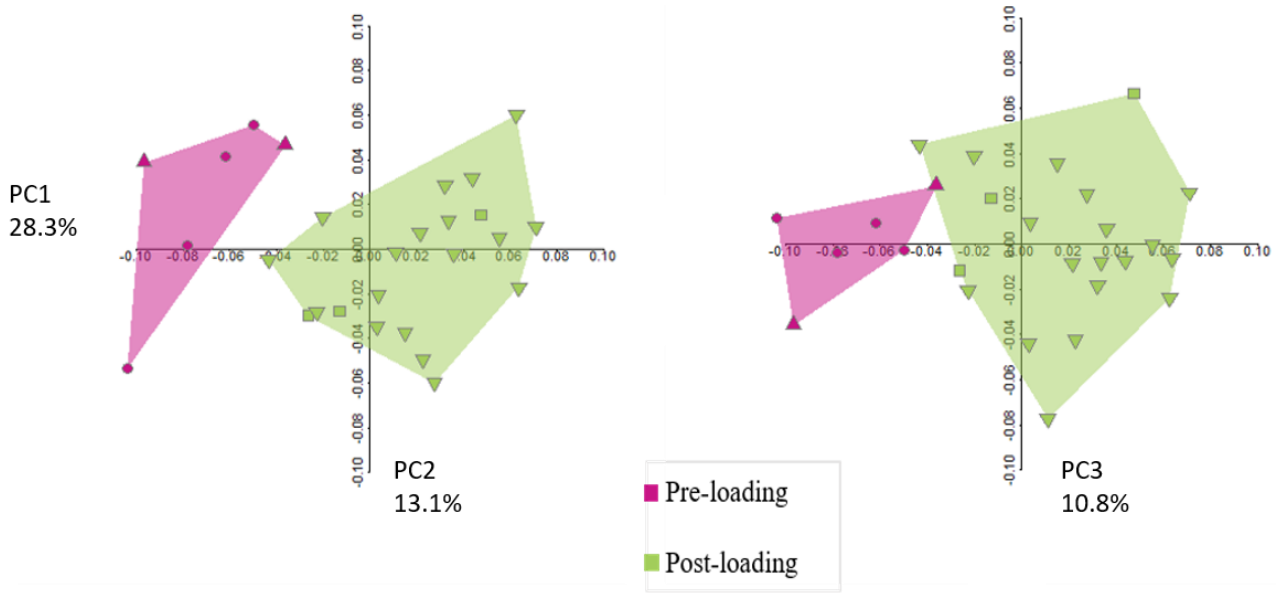

Figure 20 - 2D shape space plot. PC1 and PC2, on the left. PC1 and PC3 on the right. The two groups are well separated. Individuals from Bologna, for which sex was known, are represented by circles (males) and squared symbols (female). Diamonds represent the archaeological samples.

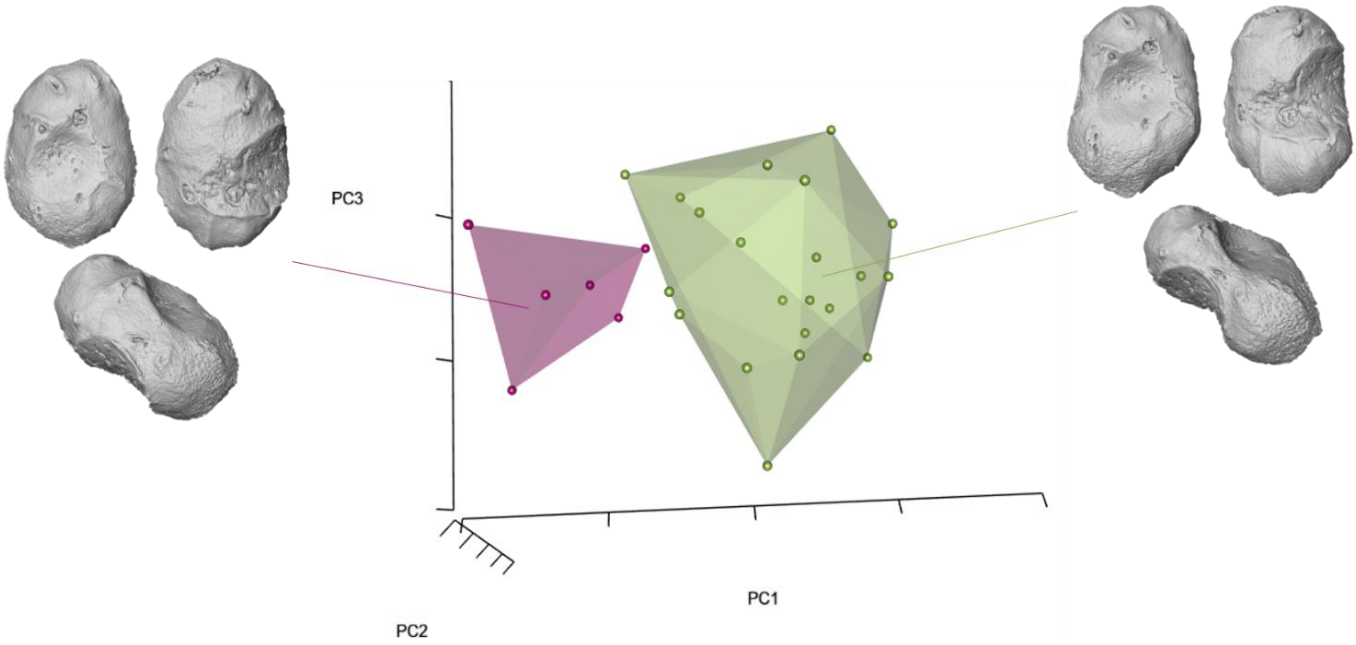

Figure 21 - 3D shape space plot. Group means are represented for each age class in dorsal, plantar and lateral views. Pink represents the youngest cohort (pre-loading) while green represents the post-loading cohort. Age group means are represented in dorsal, plantar, and lateral views (clockwise).

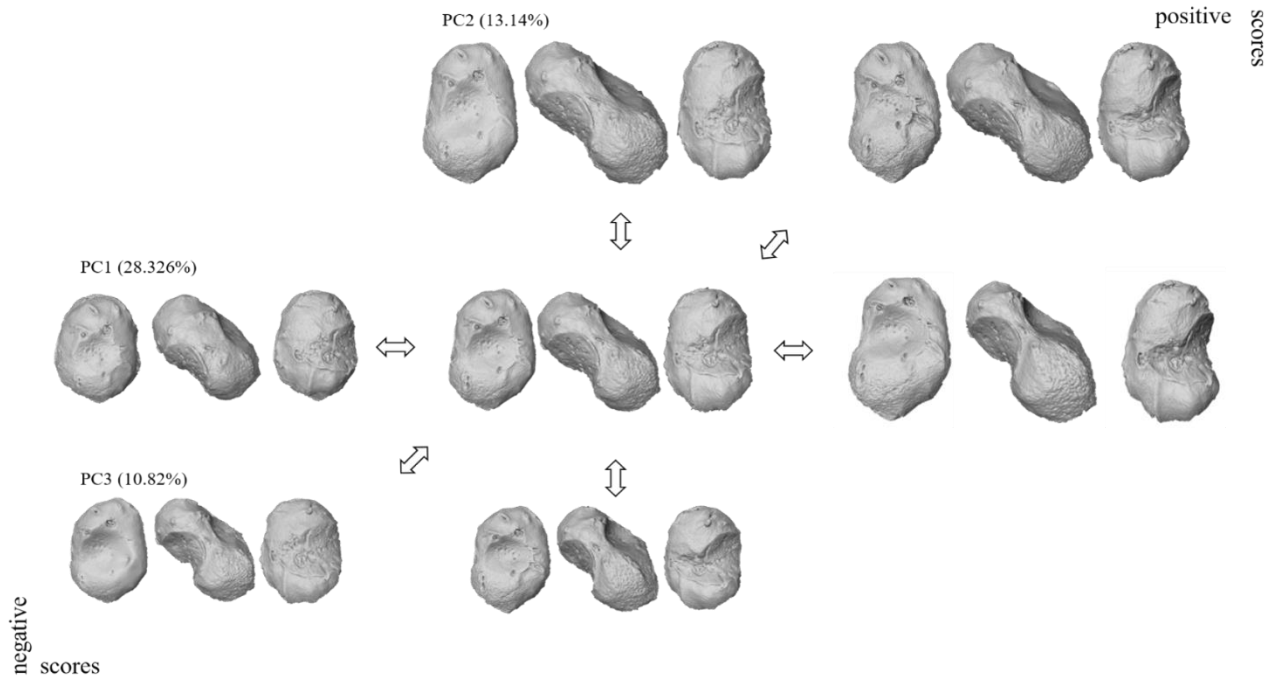

Figure 22 - Shape changes along the first three PCs in (from left to right) dorsal, lateral, and palmar view.

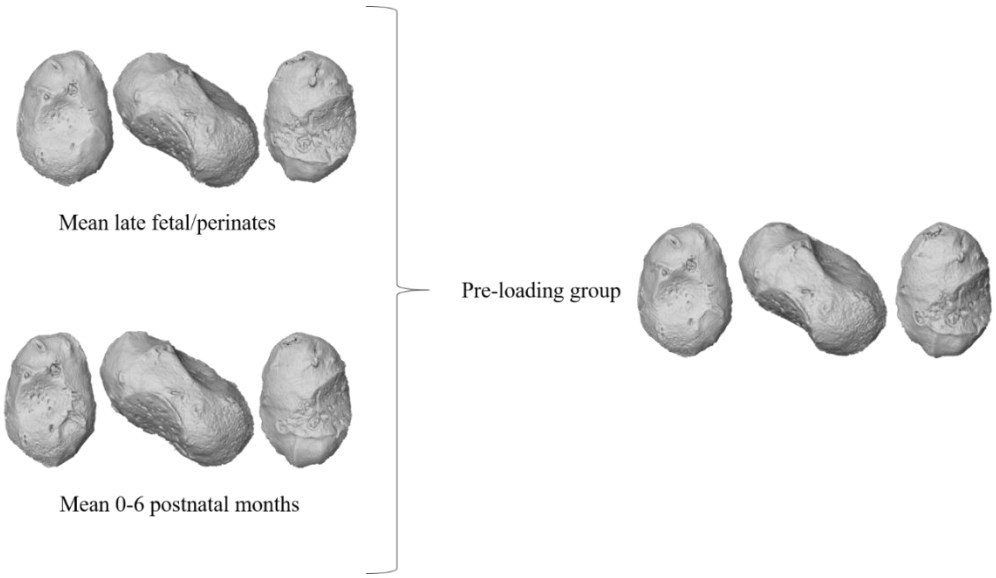

Figure 23 - Mean shapes for age classes and pre-loading mean groups (from left to right: dorsal, lateral, and plantar views)

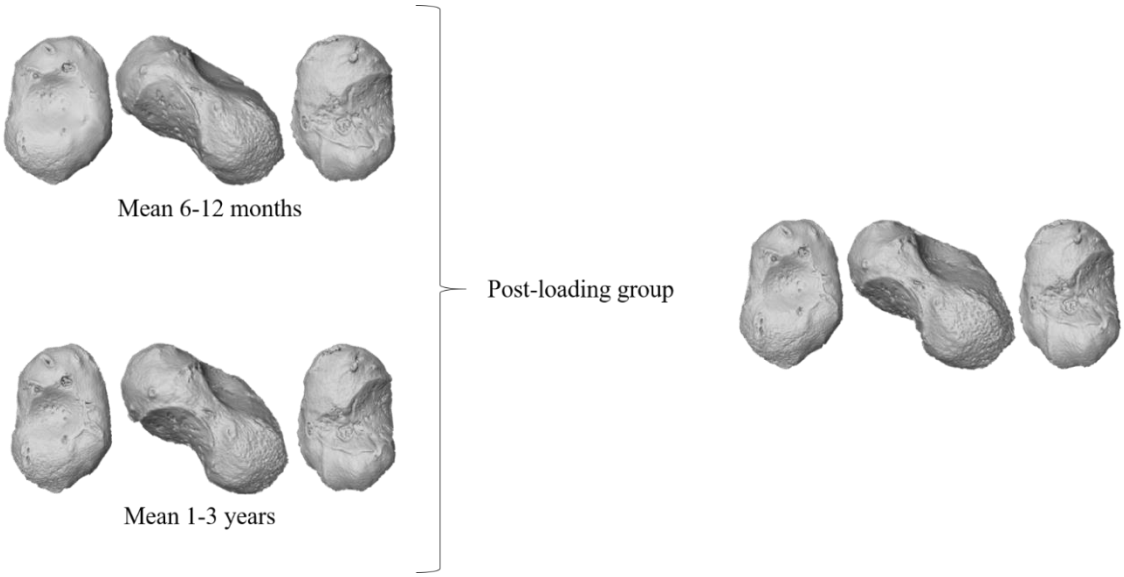

Figure 24 - Mean shapes for the age classes included in the post-loading group (from left to right: dorsal, lateral, and plantar views)

3.3.1.2.Form Space

The morphometric variations is explained almost completely by PC1 (Figure 25), that accounts for the 93.5%, and the two groups are clearly separated along the x axis (PC1), e.g. strong size difference. Shapiro-Wilk normality test shows that only PC1 scores were not normally distributed (PC1:W = 0.8815, p-value = 0.005176; PC2: W = 0.9803, p-value = 0.8692; PC3: W = 0.97888, p-value = 0.8363), while Levene test attested for the equality of variance (PC1: Test Statistic = 4.7981, p-value = 0.03803; PC2: Test Statistic = 0.075207, p-value = 0.7862; PC3: Test Statistic = 0.13598, p-value = 0.7154). A Kruskal-Wallis rank sum test was performed for PC1 scores, with significant results (chi-squared =13.5, df = 1, p-value = 0.0002). PC2 and PC3 were not significant (PC2: df = 1, F-test = 0.2, p-value = 0.6; PC3: df = 1, F-test = 1.4, p-value = 0.2). As expected, PC1 is strongly correlated with size (r = 0.99, p-value = <2.2e-16), showing a "growth axis", while the other PCs are not correlated (PC2, r=0.03, p-value = 0.8; PC3, r=0.05, p-value = 0.8) with size. The first three PCs account for the 95.8% of the total variance.

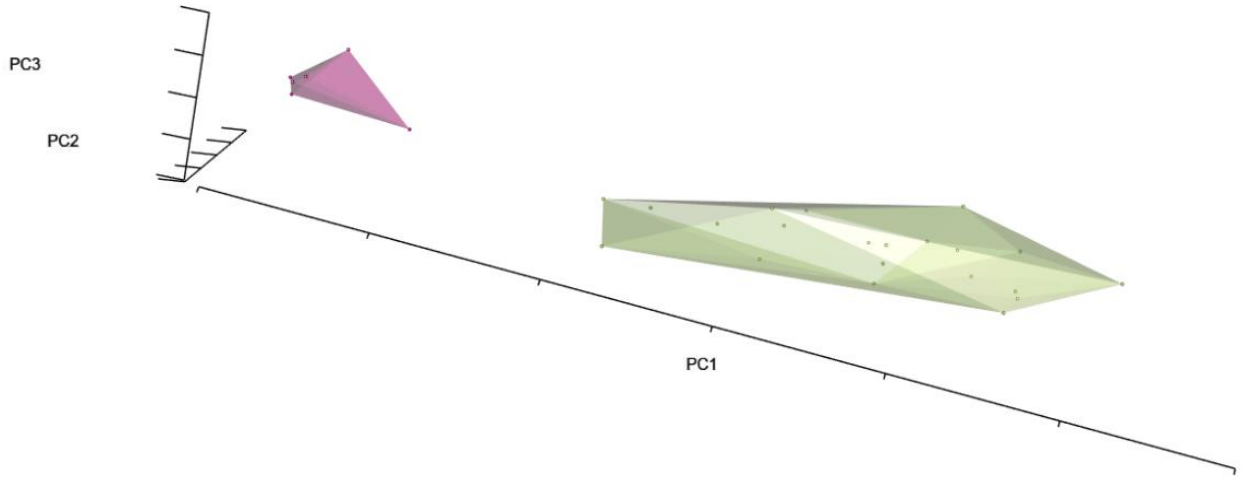

Figure 25 - 3D form space plot with loading groups. The two groups are well separated also in form space. Pink represents the pre-loading cohort, while green represents the post-loading group.

3.3.1.3.Internal morphology

Trabecular results showed that the architecture in the human talus changes through ontogeny. Mean values for the two cohorts are listed in Tables 18-19 and shown in Figures 26-29. Around birth, the structure is very "dense" with high values for Tb.N (mean for the perinates = 1.92, min = 1.53, max = 2.41), that slightly decrease during the first postnatal months (mean 0-6 postnatal months = 1.78), and is almost halved after 1 year (mean 1.1-3 years = 1.14, min = 0.89). Trabecular spacing increased during growth, passing from a dense and packed architecture, with high number of trabeculae with low spacing (mean for the perinates = 0.3, min = 0.2, max = 1.4) that become more widely spaced apart (mean group 1.1-3 = 0.69, min = 0.53, max = 0.92), while thickness decrease slightly from birth (around birth) to 3 years. Bone volume fraction greatly decreases from around birth (mean for the perinates = 24.52%) to the first 6 postnatal months, then it steadily diminishes until 3 years (mean 1.1-3 years = 15.9%). Anisotropy increases steadily, from a more isotropic architecture around birth (mean for the perinates = 0.15) to a more anisotropic structure during the second year of life (mean 1.1-3 years = 0.22). DA values increases, in the posterior-medial portion of the trochlea, around 1 year of age. At about 1.5 years, it increases also in the neck area. The medial side shows an increase in DA at around 2 years of age. Individuals' mean values are listed in Table 20-21.

T-tests results for BV/TV and DA for the two categories, e.g. pre- and post-loading, are shown in Figures 30 and 31. Results showed, in general, that BV/TV is significantly higher in the pre-loading talus, while DA increases significantly in the post-loading group. In the pre-load individuals, BV/TV is higher in in the medial side, medial portion of trochlea and neck, and head, with low values in the lateral part of the neck and head, and lateral malleolar surface. The pattern in the post-loading group is different both in location and magnitude. The highest values are located in the trochlea and posterior calcaneal facet and lateral side of the head, while the lowest are located in the sulcus tali, medial side of the head, and anterior calcaneal facet, with significant

differences located in the medial side of the head and anterior calcaneal facet. DA shows higher values in the post-loading group, with the highest values in the talar head, trochlea, medial side, and posterior calcaneal facet, with the lowest in the sulcus tali and lateral malleolar facet. Similarly, in the pre-loading cohort the values are higher in the trochlea and head, but the lowest values are located not only in the sulcus tali, but also in the medial side. The differences, in the area of the trochlea, the most proximal part of the posterior calcaneal facet, neck, and superior part of the head, are statistically significant.

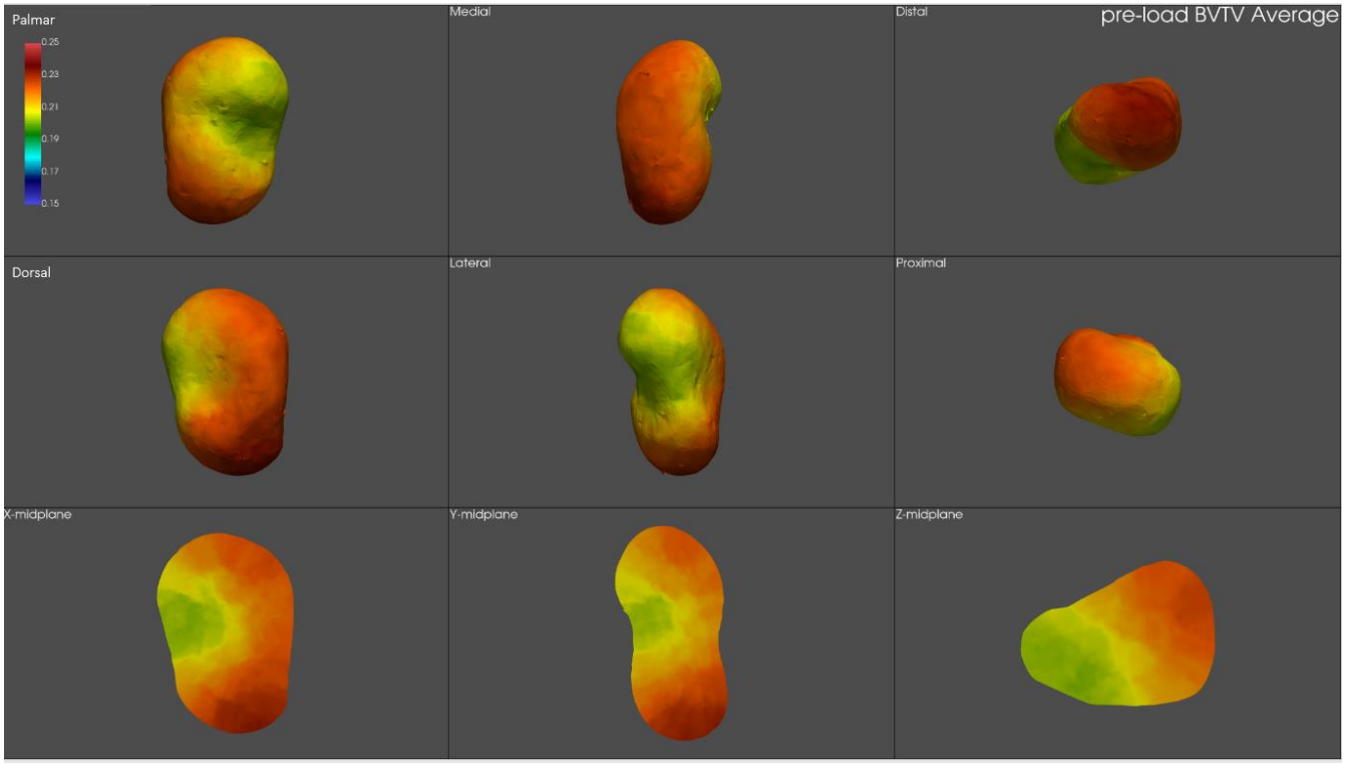

Figure 26 - BV/TV pre-loading average. Colormaps represent BV/TV values, which are high, describing a dense trabecular architecture, with highest values in the medial side of the talus and head.

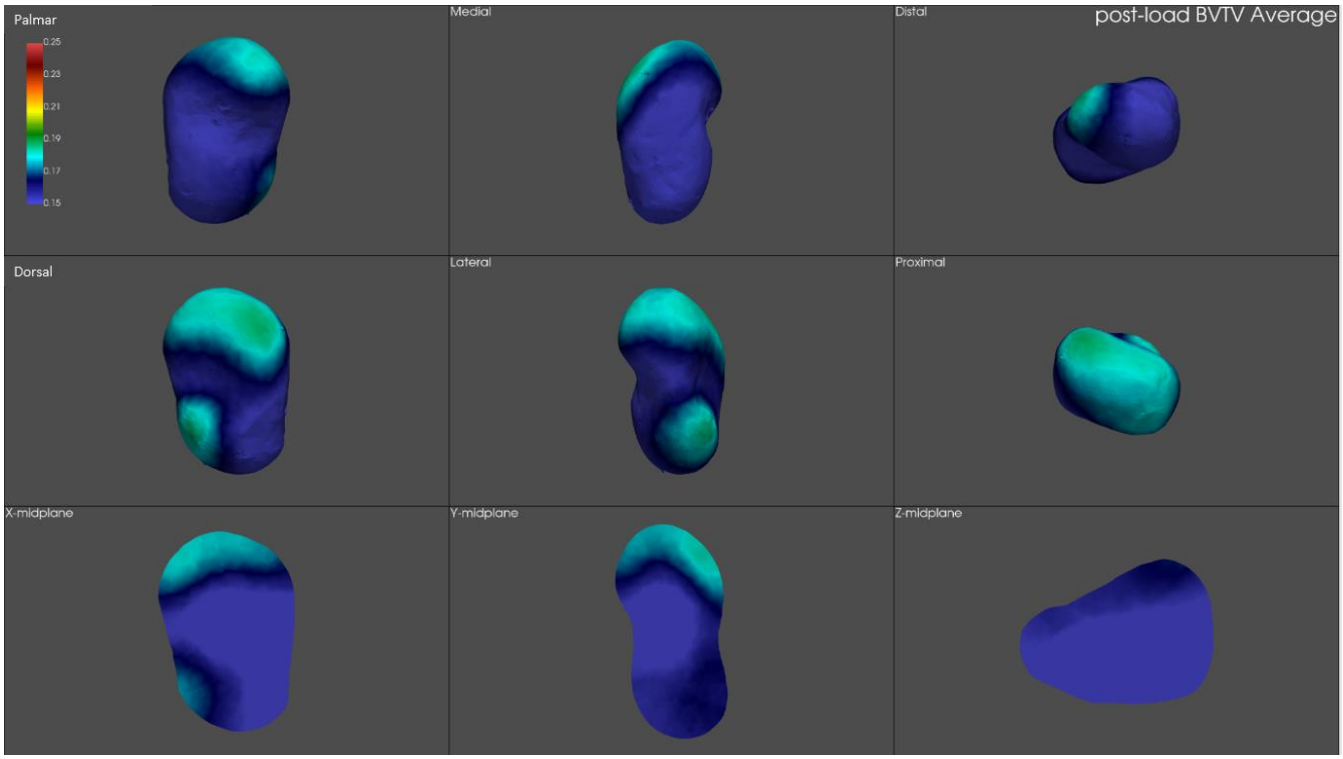

Figure 27 - BV/TV post-loading average. Colormaps represent BV/TV values, which are relatively low, with the highest values in the posterior part of the trochlea.

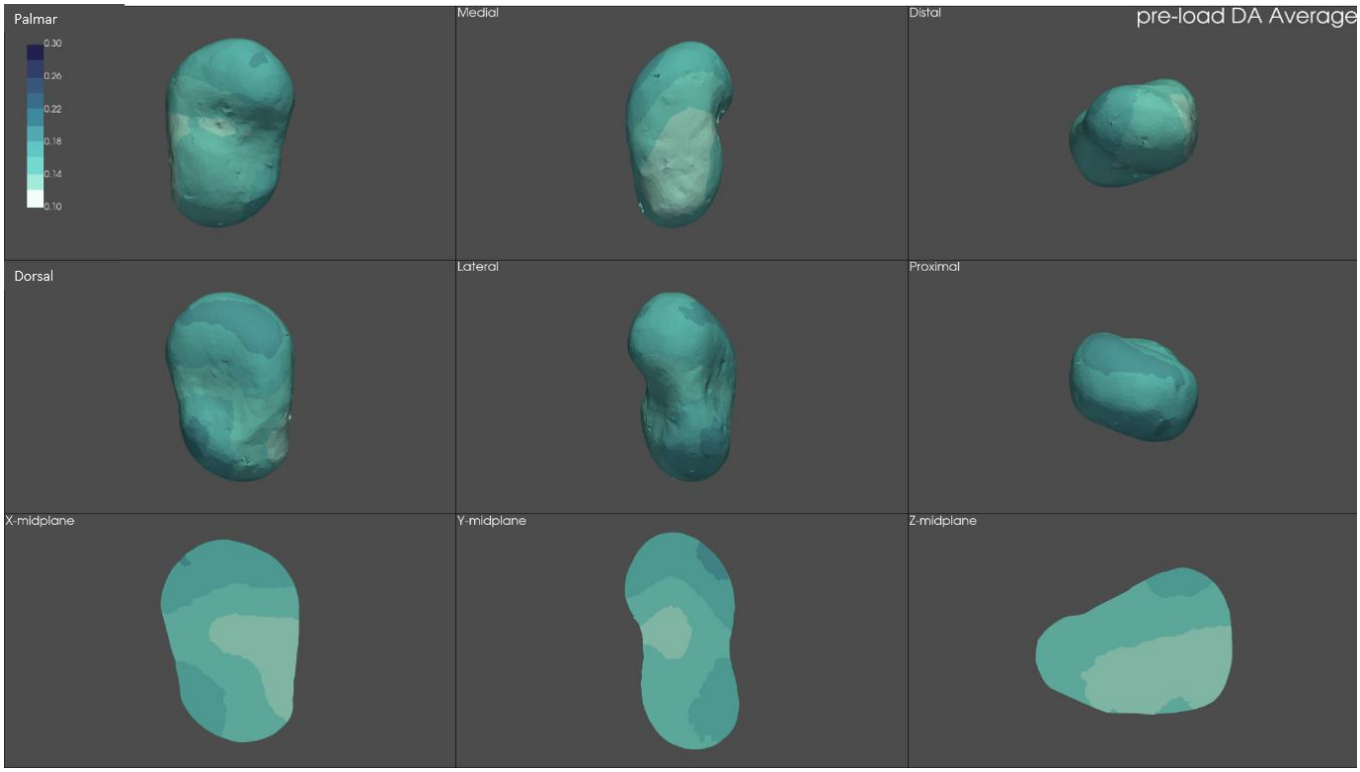

Figure 28 - DA pre-loading average. Colormaps represent DA values, which are low, with the lowest values being in the medial side of the head.

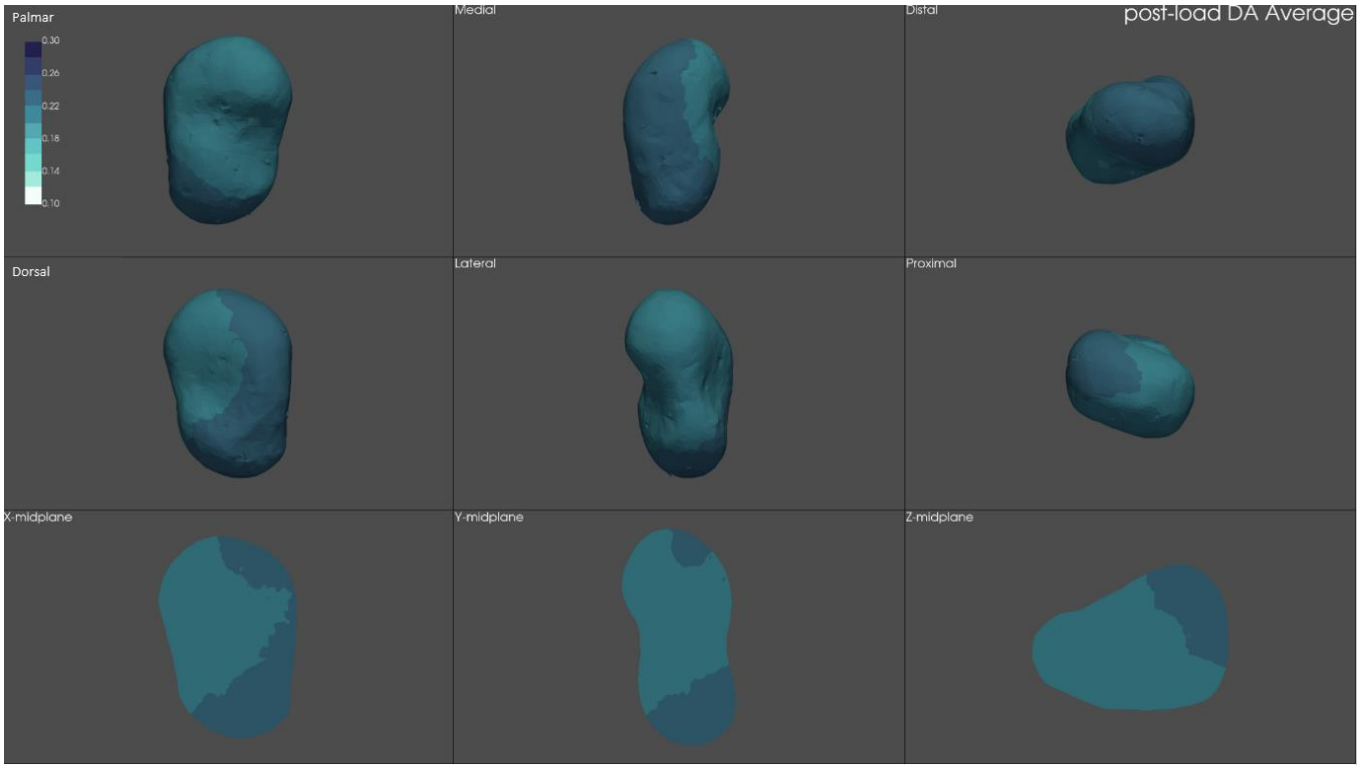

Figure 29 - DA post-loading average. Colormaps represent DA values, which start increasing after the onset of bipedal locomotion. The highest values are in the medial side of the talus, especially in the head and medial-posterior side of the trochlea.

Table 18 – Mean age group and loading group values for Tb.N, Tb.Sp and Tb.Th values

		Tb.N	Tb.Sp	Tb.Th
Pre-loading	Perinates	1.92	0.39	0.14
	0-6 months	1.79	0.46	0.13
	Pre-loading	1.86	0.42	0.14
Post-loading	6-12 months	1.37	0.59	0.16
	1.1-3 years	1.15	0.70	0.19
	Post-loading	1.20	0.67	0.18

Table 19 - Mean age group and loading group values for BV/TV e DA

		BV/TV(%)	DA
Pre-loading	Perinates	24.53	0.16
	0-6 months	17.90	0.17
	pre-loading	21.51	0.16
Post-loading	6-12 months	17.59	0.20
	1.1-3 years	15.93	0.23
	post-loading	16.34	0.22

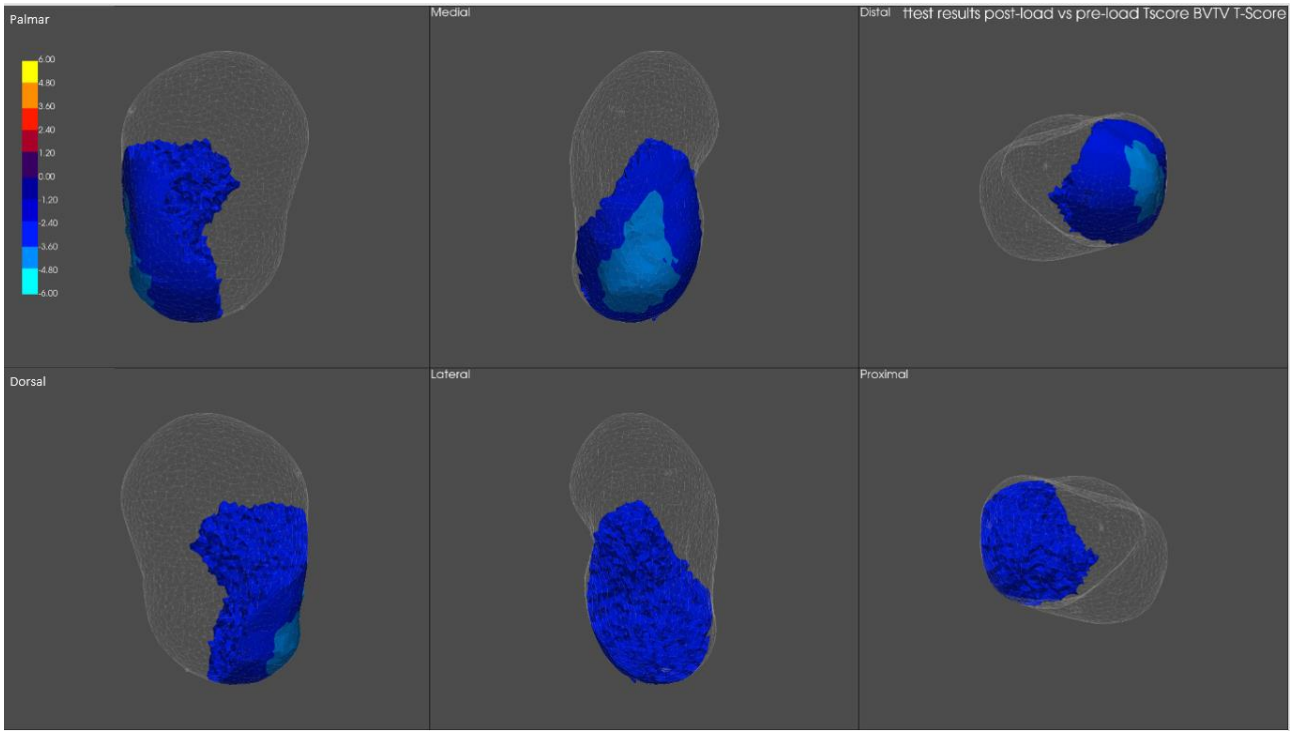

Figure 30 - BV/TV t-test results showing the significantly different areas between the two groups. Warm colors represent the pre-load group, cold colors the post-load group. The blue areas showed the areas which significantly differs between the two groups, i.e. the pre-loading subset has significantly higher BV/TV values in the medial side.

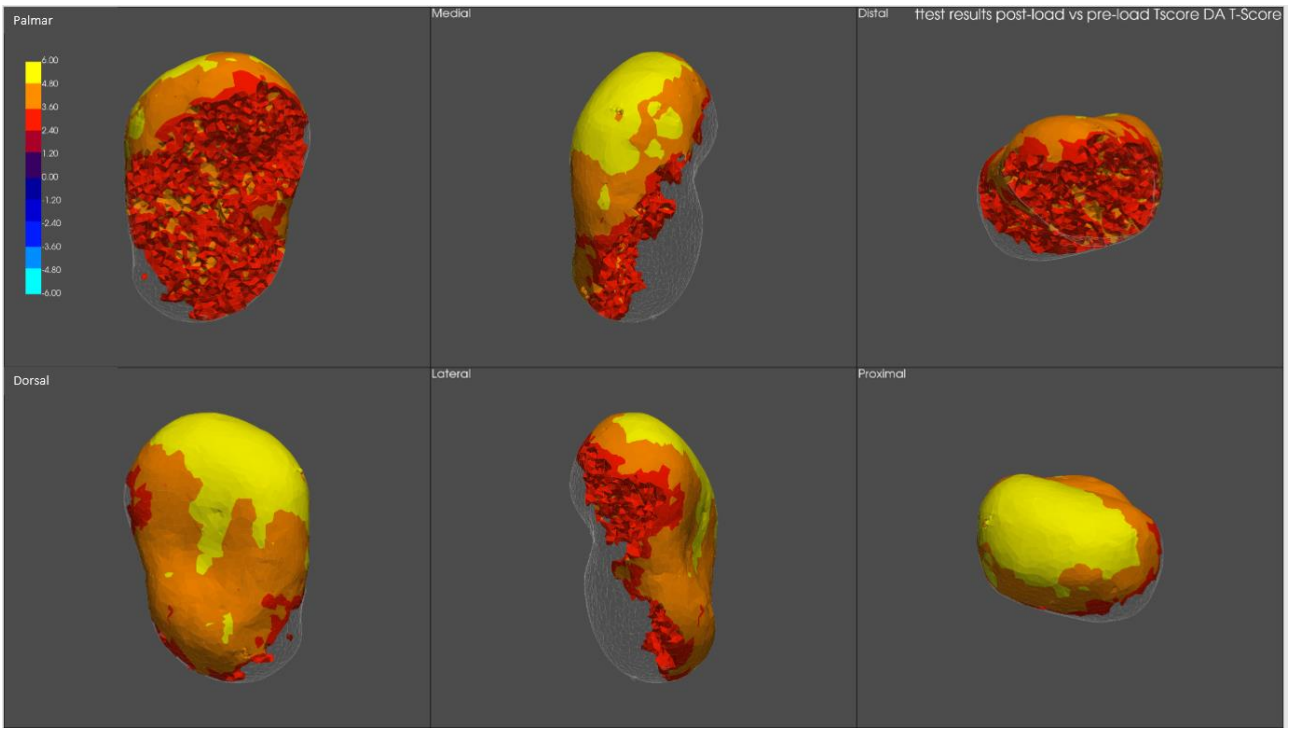

Figure 31 - DA t-test results showing the significantly different areas between the two groups. Warm colors represent the pre-load group, cold colors the post-load group. The highest DA values in the post-loading group are located in the trochlea, neck and most dorsal part of the head.

Table 20 – Individuals' averages for Tb.N, Tb.Sp, Tb.Th

Name	Age Class	Loading group	Age at death	Tb.N mean	Tb.Sp mean (SD)	Tb.Th mean
VeliaT322.	Perinates	Pre-load	36-39 weeks	1.72	0.4 (0.22)	0.14 (0.04)
VeliaT315.		Pre-load	36-40 weeks	1.87	0.37 (0.15)	0.15 (0.04)
VeliaT344.		Pre-load	perinates	2.09	0.31 (0.13)	0.16 (0.05)
VeliaT350.		Pre-load	perinates	1.53	0.5155 (0.2455)	0.13 (0.04)
VeliaT383.		Pre-load	38 weeks ca	1.88	0.40 (0.17)	0.12 (0.02)
VeliaT417.		Pre-load	perinates	2.41	0.26 (0.12)	0.14 (0.03)
VeliaT305.	0-6 postnatal months	Pre-load	0-3 months	1.98	0.37 (0.21)	0.12 (0.02)
NF821369.		Pre-load	8 weeks	1.72	0.47 (0.20)	0.10 (0.02)
NF821045.		Pre-load	0-6 months	2.21	0.32 (0.17)	0.12 (0.04)
VeliaT300.		Pre-load	0-6 months	1.14	0.73 (0.36)	0.13 (0.03)
VeliaT441.			0-6 months	1.86	0.40 (0.21)	0.13 (0.02)
NF821051.	6.1-12 months	Post-load	7.5 months	1.11	0.68 (0.32)	0.21 (0.06)
VeliaT442.		Post-load	6-9 months	1.57	0.49 (0.23)	0.14 (0.03)
VeliaT368.		Post-load	0.75-1 year	1.55	0.51 (0.23)	0.13 (0.02)
VeliaT289.		Post-load	9-12 months	1.36	0.57 (0.25)	0.15 (0.03)
BO58_M.		Post-load	11 months	1.53	0.47 (0.18)	0.17 (0.04)
BO60_F.		Post-load	11 months	1.37	0.58 (0.26)	0.14 (0.03)
NF820614.		Post-load	12 months	1.05	0.81 (0.29)	0.13 (0.02)
VeliaT415.	1.1-3 years	Post-load	1-1.5 years	1.41	0.53 (0.22)	0.17 (0.04)
VeliaT434.		Post-load	1-1.5 years	1.27	0.58 (0.20)	0.20 (0.04)
BO14_M.		Post-load	1 years and 5 months	1.21	0.68 (0.24)	0.13 (0.03)

NF821014.	Post-load	1.5 years	1.19	0.58 (0.24)	0.25 (0.06)
NF821046.	Post-load	1.5 years	1.14	0.68 (0.33)	0.18 (0.04)
PerkataNyuli655.	Post-load	1-3 years	0.89	0.92 (0.50)	0.19 (0.03)
VeliaT286.	Post-load	1.5-2 years	1.22	0.63 (0.32)	0.18 (0.04)
BO14_F.	Post-load	1.9 years	1.30	0.61 (0.22)	0.15 (0.04)
BO48_F.	Post-load	3 years	1.22	0.66 (0.26)	0.15 (0.04)
NF820683.	Post-load	3 years	1.10	0.69 (0.27)	0.21 (0.05)
NF821026.	Post-load	2 years	0.90	0.92 (0.52)	0.18 (0.04)
NF821207.	Post-load	2 years	0.94	0.86 (0.35)	0.18 (0.05)
NF821214.	Post-load	3 years	1.04	0.80 (0.35)	0.15 (0.03)
PerkataNyuli516.	Post-load	1.5-3 years	1.07	0.70 (0.26)	0.22 (0.07)
IlokG22.		2-3 years	1.20	0.68 (0.25)	0.14 (0.04)
NF821069.	Post-load	2.5 years	1.19	0.63 (0.30)	0.20 (0.05)
NF821113.	Post-load	2.5 years	1.11	0.71 (0.22)	0.18 (0.04)
VeliaT411.	Post-load	2-3 years	1.17	0.64 (0.23)	0.20 (0.05)
BeliManastirG6.	Post-load	2-3 years	1.25	0.61 (0.30)	0.18 (0.05)
PerkataNyuli639.	Post-load	2.5-3 years	1.06	0.72 (0.25)	0.21 (0.06)
BO7_M.	Post-load	2.9 years	1.11	0.70 (0.32)	0.18 (0.06)

Table 21 – Individuals' averages for BV/TV and DA

Name	Age Class	Loading group	Age at death	BV/TV (%)	Degree of Anisotropy
VeliaT322.	Perinates	Pre-load	36-39 weeks	21.49	0.09
VeliaT315.		Pre-load	36-40 weeks	26.54	0.18
VeliaT344.		Pre-load	Perinate	29.14	0.13

VeliaT350.	0-6 months	Pre-load	Perinate	14.14	0.31
VeliaT383.		Pre-load	38 weeks ca	20.41	0.13
VeliaT417.		Pre-load	Perinate	35.44	0.07
VeliaT305.		Pre-load	0-3 months	21.65	0.16
NF821369.		Pre-load	8 weeks	9.82	0.12
NF821045.		Pre-load	0-6 months	23.68	0.11
VeliaT300.		Pre-load	0-6 months	12.41	0.26
VeliaT441.		Pre-load	0-6 months	21.92	0.17
NF821051.	6.1-12 months	Post-load	7.5 months	18.53	0.16
VeliaT442.		Post-load	6-9 months	18.12	0.19
VeliaT368.		Post-load	0.75-1 year	18.95	0.17
VeliaT289.		Post-load	9-12 months	18.47	0.16
BO58_M.		Post-load	11 months	23.24	0.16
BO60_F.		Post-load	11 months	20.12	0.26
NF820614.		Post-load	12 months	5.70	0.24
VeliaT415.		Post-load	1-1.5 years	20.66	0.13
VeliaT434.		Post-load	1-1.5 years	18.6	0.27
BO14_M.		Post-load	1 years and 5 months	11.8	0.23
NF821014.		Post-load	1.5 years	28.42	0.17
NF821046.		Post-load	1.5 years	14.84	0.20
PerkataNyuli655.		Post-load	1-3 years	10.93	0.24
VeliaT286.		Post-load	1.5-2 years	21.31	0.16
BO14_F.		Post-load	1 years and 9 months	13.82	0.26
BO48_F.		Post-load	3 years	15.24	0.25
NF820683.	1.1-3 years	Post-load	3 years	19.14	0.26
NF821026.		Post-load	2 years	10.58	0.20
NF821207.		Post-load	2 years	10.51	0.21
NF821214.		Post-load	3 years	8.71	0.25
PerkataNyuli516.		Post-load	1.5-3 years	17.18	0.21
IlokG22.		Post-load	2-3 years	10.5	0.19
NF821069.		Post-load	2.5 years	19.6	0.27
NF821113.		Post-load	2.5 years	12.76	0.26
VeliaT411.		Post-load	2-3 years	18.39	0.20
BeliManastirG6.		Post-load	2-3 years	21.12	0.17

PerkataNyuli639.	Post-load	2.5-3 years	13.98	0.26
BO7_M.	Post-load	2 years and 9 months	16.368	0.25

3.4.Discussion

The main goal of this study was to describe the growing changes that occurred in the talus from the last prenatal weeks to three years old (i.e. until the end of the second year of age), to better explore this time frame during which the most important locomotor milestones occur, and try to catch any bony signal that could be linked to the gradually developing bipedalism. Here, we discuss first separately the results, and then we try to link the external and internal talar changes during growth.

3.4.1.External morphology

This study explore the considerable changes in the morphology of the talus during ontogeny, by means of geometric morphometric methods, i.e. exploring not only the changes correlated with size, namely ontogenetic allometry, but also the differences in pure shape. PC1 clearly separates the sample in two main groups, separating the individuals younger than 6 months of age from those older than 6 months, showing that numerous morphological changes take place during the first year of life. This timeframe is pivotal, since fundamental milestones occur (e.g. sitting upright, crawling, cruising, supported locomotion and, finally, independent locomotion), and the foot is prepared to support the impending change in mechanical loading. The globular neonatal talus started changing shortly after birth, with the expansion of the neck surface and an almost imperceptible initial torsion of the head, with a more elongated shape. But the most important and visible changes happened after 6 postnatal months. Probably, with a more mature neuromuscular system and with the aid of external stimuli, e.g. by caregivers, children start to explore and practice, and the foot experiences more and more loading, even though is not fully loaded yet. After six months the neck area has greatly expanded, with more defined margins and the more pronounced torsion of the head, with a more marked lateral ridge and a first sign of the lateral malleolar area expansion. The development is more pronounced after the first year, when the child experiences the unsupported deambulation. The sulcus tali is well marked and wider, and the anterior and posterior calcaneal facets are visible, the head is more defined and, most importantly, the trochlea has expanded. Though the shape is not mature yet, far from the adult morphology, between 2 and 3 years, the locomotion pattern gradually assume an adult-like arrangement. We did not test for the correlation with body weight, but it is plausible that the weight gain played a pivotal role in the changes described here, during the early maturation. The changing in orientation of the articular facets described by Hellier & Jeffery (2006) is not yet observable, since the sample in their study was older than 8 years. However, it is known that during the stance and swing phases of locomotion, the compressive forces act on the trochlear surface, and from here are transmitted downwards to the calcaneus, through the posterior calcaneal facet, and anteriorly through the neck - where they are converted in tensile forces (Pal and Routal 1998a) - and the head, on to the navicular. This transmission could be linked to the early development of the trochlea, which shows a smooth but clear increase in the antero-posterior curvature, and in the gradually sharpening of the margins of the subtalar facets. The posterior one, in particular, begins to form starting from a very smooth morphology, and it grows almost triangular in shape, along with the elongation of the talar body. As noted by Hellier &

Jeffery (2006), the inferior talar articular facets do not equally distribute the forces while standing. A larger force is transmitted to the navicular than to the cuboid (via the calcaneus) and hence, metatarsals are loaded increasingly in a medial direction (Manter 1946; Salathé, Arangio, and Salathé 1986). Also, the heel strike is not developed, yet, and the child touches the ground with a flat foot. This may explain why the posterior part of the talus, e.g. posterior side of the trochlea and posterior calcaneal facets, continue developing after 3 years of age. This investigation shows how the talar morphology changes in concomitance with the onset of bipedal locomotion. Slower changes characterized the first 6 postnatal months, with a morphology that is not yet ready to bear loads; in the second half of the second year, though, changes are more noticeable, and pivotal areas (e.g. trochlea, head, neck) underwent great modifications, preparing the foot to bear the full body weight. After the onset of locomotion, the hinted increased in trochlear curved-shape and the expansion of its area suggest that the trochlea is finally ready to perform its role, i.e. to receive and distribute the body weight from the tibia. Moreover, the slight increase in orientation of the head suggest that the foot is not yet performing a full medial weight transfer, and this is consistent with the not-yet-developed heel-strike and toe-off, and medial arch. Though, Straus (1927) found out that a medial torsion of the head was present in the prenatal talus, which decreases during growth. Our results showed the opposite process. The torsion of the head is pivotal for the correct medial transmission of the forces, though the immature foot does not need yet to transmits the forces medially, therefore the talar head does not show yet the medial rotation. As the body weight increases, and the gait matures, the torsion of the talar head increases, aiding this medial weight transfer. This characteristic is thought to be linked to the ontogenetic adduction of the hallux, i.e. an important phylogenetic signal (Straus,1927). This is the first time that the early talar anatomical changes are explored by means of geometric morphometrics methods, and we were able to fill an existing gap in the literature. This contribute may help, with an increased sample, in identifying differences in human ontogenetic trajectories, and better explore the dynamics that guide the early talar development, e.g. how much the genetic blueprint contributes in this phase. The pre- and post-locomotion morphologies separates well, and it may well help in distinguish these two fundamental phases. It may reflect a programmed development. In addition, comparing the different external morphologies may also help in interpreting the shape of fossils talar remains.

3.4.2.Internal morphology

In this study, we examined 40 juvenile talar bone, to explore how trabecular bone changes along with development of locomotion. In order to do so, we first investigate how trabecular architecture cope with the early loading increase by exploring architectural differences in four age classes; then, we statistically tested the differences between two different groups: the first one with allegedly no efficient loading in the foot zone, and the second one with an increasing loading of the foot. We predicted that the trabecular structure would change, adapting its architecture gradually along with the maturation of the neuromuscular system and, consequently, with the gradually increasing loading of the foot, passing from no load, to full bipedal load. Results showed that our initial hypotheses were corrected. At birth and during the first postnatal months, trabeculae are closely-packed, revealing a very dense architecture, with numerous and thin trabeculae and a

rather isotropic structure. In the first year of life, bone is rapidly remodeled. Space between trabeculae rapidly increases as trabeculae are removed and the remaining trabeculae gradually thicken. In the second half of the first year of life, BV/TV values decreased, probably as a result of trabecular resorption, with fewer and thicker struts and an increased spacing between each other. After 1 year of age, therefore after the onset of unaided locomotion, the values of BV/TV decrease, while DA starts to increase slowly. According to previous study (Carter & Beaupré, 2001; Ryan and Krovitz 2006; Reissis and Abel 2012; Ryan and Shaw 2015), a dense and generalized trabecular structure is deposited during endochondral ossification, and this non-specialized structure subsequently reorganizes into fewer, thicker, and directionally organized systems of trabeculae. During fetal life, the fetus usually punch and kick against the uterine wall, which represents a mechanical resistance (Acquaah et al. 2015). After birth, these movements decrease, in the light of the new environment, e.g. more space and absence of uterine wall as a constraint. Moreover, hormones play a key role in bone development (Bonjour et al. 2012; Swan et al. 2020; Gosman, Stout, and Larsen 2011), with the maternal estrogen that, in combination with the fetal movements influence bone development. Furthermore, a "gestational overproduction" (Acquaah et al. 2015) with a high bone mass may constitute a postnatal calcium reservoir, helping maintain mineral homeostasis. Trabecular architecture remodels under mechanical loading during gait maturation, as suggested by previous studies (Colombo et al., 2019; Gosman & Ketcham, 2009; Raichlen et al., 2015; Ryan & Krovitz, 2006; Saers, Ryan, & Stock, 2020). Saers et al. (2020) proposed that unnecessary bone deposited during endochondral ossification would be resorbed during the first year of life, if insufficiently loaded, following the mechanostat model (Frost 2003). The decrease in bone volume fraction may be explained by the removal of unloaded or underloaded struts (Ryan and Krovitz, 2006). Many studies found that, while bone volume fraction and trabecular thickness increase, the number of trabeculae decreases during development (Byers et al. 2000; Tanck et al. 2001; Salle et al. 2002; Nuzzo et al. 2003; Nafei et al. 2000; Parfitt et al. 2000; Halloran et al. 2002; Wolschrijn and Weijs 2004; Mulder et al. 2005). It appears that initial mechanical adaptation is achieved first by adding bone mass, and then by remodeling to gain efficiency later.

BV/TV continues to decrease during all the first year of life, consistently with a trabecular structure that is not being strained above a certain threshold, as pointed out by (Pivonka, Park, and Forwood, 2018), indicating that the talar architecture responds to variation in loading magnitude from the second half of the first year of life, and then it slightly increases in the posterior part of the trochlea and posterior subtalar joint after 2 years of life, while DA progressively increases after six postnatal months. This is in accordance with the previous literature, which describes the presence of a dense and generalized structure initially deposited during endochondral ossification, and later remodeling to cope with the functional role of the talus. The role that mechanical loading has in shaping trabecular bone morphology has been already demonstrated (Barak, Lieberman, and Hublin 2011). Specifically, values are significantly higher in the trochlea, most proximal part of the posterior calcaneal facet, neck, and superior part of the head, showing an early remodeling following strain. This may be linked to an early remodeling due to the increase in body weight. Trabeculae are remodeled according to the directions of loading, and as the foot is loaded, struts start to remodel according to the direction

of forces, i.e. compressive and tensile forces, respectively in the trochlea and neck areas. Interestingly, DA increases first in the posterior and medial portion of the trochlea, i.e. the area which receives the full weight from the tibia. The young walkers, at this stage, touch the ground with a flat feet, and the medial arch is not fully developed yet. At about 1.5 years, it increases also in the neck area. The lateral side shows an increase in DA at around 2 years of age, while anisotropy increases in the head during the second half of the second year of age, probably reflecting a more mature locomotion, and a more adult-like pattern due to the action of the tensile forces in the neck area.

This study confirms the predictions, demonstrating that in the early stages of growth the talus responds adapting to mechanical strain. This work fills the existing gap in literature, exploring how trabecular bone in the juvenile talus starts (re)modeling at early stages, showing once again the fast response of the trabecular bone to mechanical stimuli.

3.4.3. Linking internal and external morphological changes

Taken together, the internal and external modifications tell us a story. External morphology shows us how the foot, i.e. talus, could be loaded during different growth stages. It is mostly driven by a genetic blueprint, and the immature configuration tells us that, at this stage, children are not ready to walk properly. With the increase in weight, maturation in neuromuscular system, and biological growth of the children, the talar morphology commences to show the readiness to walk, firstly by increasing the trochlear surface, then starting developing the subtalar joints and changing the orientation of the head. Talar shell reflects the immaturity of gait, and the genetic and epigenetic influences are probably strictly linked together. If the external morphology tells us what the infant could be able to do at that time, the internal architecture could provide precious information about how actually the bone is loaded, and it tells us that the immature shell well correspond to the immature and not loaded trabecular architecture. Interestingly, BV/TV is higher in the “most-expanding” areas such as the trochlea, the lateral process and the subtalar facets, which have a great increase in growth after the first year. Trabecular changes may correspond to the ontogenetic changes that we explore on the external talar shell. These changes, also, may be linked to the development of mature gait in juveniles. As we saw, the important milestones (i.e. sitting upright at about six months, crawling at approximately nine months, independent bipedal deambulation at about twelve months) may reflect the changes seen in this study, possibly capturing the locomotion shift. After the achieving of the independency, gait continue to develop, with changing in lateral stability and step length, until about 7 years (Sutherland et al. 1980; Sutherland 1997), but the most important shift remain the conquer of the independent bipedal gait at about 1 year, reflected by important remodeling of the trabecular bone. Though, at differences in the external shell corresponding differences in the internal architecture, which is mostly driven by actual modeling due to strain and changing in forces and use.

This is the first time that the early talar changes are explored in such a holistic way. We showed also that the exploration of both external and internal morphologies offer a valuable key to the interpretation of plastic

changes. Our findings may help in shedding light into the early human foot development, and they could be a useful instrument when the juvenile fossil record is concerned.

3.4.4. Limits of the study and future directions

Unfortunately, a few drawbacks needs to be highlighted. First of all, the relatively small sample size that limits the analyses, which is further limited in the cortical analysis, due to the often unpreserved cortical bone, as a consequence of, for example, post-depositional damages. Moreover, the youngest classes are even worse represented. We are aware of the fact that fetal and perinatal individuals are rare to find, but these categories deserve deeper investigations.

Secondly, locomotor and cultural behaviors for these individuals are not known, and the unbalanced populations here represented may mask slightly interpopulation differenced, e.g. cultural and genetic.

Finally, while the age range is good, there are some gaps and, more importantly, the usage of an archaeological sample, with age estimation, brings with it another margin of error, which is though intrinsic. The hope is to increase the sample and, potentially, limits the number of populations. Despite these drawbacks, this study demonstrates that the pre-walking phase is clearly reflected in talar morphology, both in the internal and external morphology. This findings may help in shedding lights in talar developmental trajectories, both in the archaeological and fossil samples. Changes in bone morphologies were consistent with the locomotor milestones, showing a more immature morphology, i.e. globular shape with developing articular facets which develops consistently with the “walking needs” and a dense and isotropic structure, while the post-walking morphology shows a more mature talus, which starts showing fairly its plasticity, i.e. in changing the orientation of the facets to cope with the direction of forces and, at the same time, a less dense and more anisotropic trabecular architecture, which responds to the changes in loading after the onset of unassisted walking. The talus, as well, is suitable to be used to track gait maturation in juvenile humans. Future works should take into account the other foot bones, to create a “development map” that follows the development of bipedalism in all the foot, which can be of paramount importance in evolutionary studies. Also, experimental works are needed in controlled samples, to establish the actual cause-effect.

Chapter Four
Becoming adults: the last steps of the journey. Exploring talar changes during the last years of growth

4.1. Introduction

Human talus must cope with the increasing body weight, during growth, but must remain congruent to efficiently perform its critical role of sustain and distribute weight. Talus has seven articulations with four bones. Being part of the talocrural joint, talus articulates with tibia and fibula, forming a very mobile joint which permits a wide range of movements, e.g. eversion and inversion, dorsiflexion and plantarflexion, pronation and supination. Downwards and forwards, it articulates also with the calcaneus and navicular, forming the subtalar and talonavicular joints. Though, due to spatial limitations derived by the conformation of the articulations, like for example the ankle mortise, talar facets are prevented from overexpanding in size in response to load increase. This is true for all the tarsals bone, which must cope with great forces despite having relatively small articular surface respect to, for example, the wider femoral condylar surface (Lieberman, Devlin, and Pearson 2001b). This implies a different way to cope with increasing forces. Talar facets respond with a change in orientation, to efficiently receive and distribute stress. Talar plasticity has been previously assessed by several studies on adults (Turley, White, and Frost 2015; Kevin Turley and Frost 2014, 2013; Sorrentino, Belcastro, et al. 2020; Sorrentino, Carlson, et al. 2020) and on ontogenetic samples (Hellier and Jeffery 2006; Turley and Frost 2014). During childhood, in fact, children steadily gain weight but it is with the pubertal growth spurt that body weight increases suddenly, and in a relatively short period of time, about 50% of the adult body weight is gained (Barnes 1975). Articular surfaces are plastically responsive to stress during growth (Hellier and Jeffery 2006; Russo and Kirk 2013) by changing the shape, size, and orientation of their surfaces. After completion of skeletal development, though, response to stress is granted by the bone shafts, which respond increasing the diaphyseal cross-section (Ruff, Scott, and Liu 1991). As explained by Hellier and Jeffery (2006), changes in facet shape and orientation as opposed to changes in surface area may offer a better adaption to increased load bearing in a bone, providing a solution to the spatial constriction. The relatively small articular facets of the human talus adjust to the mechanical requirements of long term loading changes over ontogeny. Talar development is affected by its role of weight-bearer and its wide range of mobility. Talar articular surfaces adaptions throughout ontogeny, i.e. during increasing demand of load, are of paramount importance, as changes prevent talus from deforming under weight, and permits to perform its critical role in sustain human body (Hellier and Jeffery, 2006). Singular articular surfaces may also have the potential to distinguish features associated with bipedal locomotion from other forms of habitual locomotion (Rita Sorrentino, Carlson, et al. 2020), making them useful to interpret different locomotor behavior in fossil tali. The investigation of how and when articular facets develop may thus offer new pieces of information when trying to explore the different locomotor behaviors in the past.

Here we try to explore talar plasticity on a sample aged between 4-5 and 15 years, observing the development of talar facets and how and when they start to reorient in response to increase in weight bearing, following their growth pattern until adolescence, when the foot is supposed to reach its adult size (Fritz and Mauch 2013). Also, based on previous studies on the ontogenetic trajectories of trabecular architecture (Saers, Ryan, and Stock 2020; Colombo et al. 2019; Ryan and Krovitz 2006), we suppose that anisotropy will slightly increase until around 7-8 years, and then reach a plateau when the locomotion is supposed to have reached an adult-like pattern. After the plateau has been reached, due to the more one-way direction of the compressive forces passing through the head and the posterior calcaneal facet, it is supposed that the highest DA values will be reached in these two areas, while lower DA values are expected to be found in the trochlea and anterior calcaneal facets, as they receive stress from calcaneus and navicular. BV/TV values are expected to be higher in the lateral side, as it receives more strain from the tibia.

4.2 Materials and Methods

This work analyzes the late postnatal development of the human talus, with a focus on the development of the articular facets. The sample consists of 41 modern juvenile tali aged between 5 and 15 year old. Eleven individuals (F=6; M=5), aged between 5 and 11 years, came from the Collection of Bologna, Italy, which sex, age at death, and cause of death is known (Belcastro et al. 2017; see Table 22). The collection comprehend Italian skeletal remains from the Emilia-Romagna region and from Sardinia, and they were collected mostly from 1908 to 1953 (Belcastro et al., 2017). The largest part of the Emilia-Romagna cohort was buried in Bologna La Certosa cemetery, the biggest cemetery of the city. The importance of this collection is given by the presence of ante mortem data, information about socioeconomical backgrounds, the generally good state of preservation and the relatively high number of children in the collection. The birth year ranged between 1814 and 1922 (with the majority born after 1850) and they died between 1898 and 1944. For the large part of the individuals, the place of birth were also known. As for the jobs, women were mostly housewives and sewer, while men were employed in different occupations, i.e., farmer, laborer, and mason with more frequency. The great number of non-adults who died before the first year of life highlights the high infant mortality during the mid-19th century (Belcastro et al., 2017), with a decrease of children in the collection from the age of 3. The cohort under study comprehend individuals from Bologna and Parma.

The rest of the study sample has been selected from different archaeological samples, with a timespan that goes from Upper Paleolithic (Epigravettian) to modern age.

Seven individuals came from Beli Manastir. The site is located near eponym town in Osijek-Baranja County in eastern Croatia. The rescue excavations took place in 2014 and 2015 and covered a surface of approximately 37,000 square meters. Two main cultural layers were identified at the site: a prehistoric layer consisting of several Neolithic and Chalcolithic strata, and a Roman period layer. The prehistoric layers of interest are dated to the early and middle Neolithic periods in which the remains of a large settlement and 39 inhumation burials were found. According to the available radiocarbon dates a huge majority of Neolithic burials from this site can be dated to the Middle Neolithic, i.e. between 4800 and 4500 BCE. Most of the burials were found in a contracted position on either left or right side with different orientations. In several cases, one or more ceramic vessels were placed by the head of the deceased.

Three individuals came from the site of Ilok – Krstbajer, located in the eastern part of the town, about 200 m from the border crossing between Ilok (Croatia) and Bačka Palanka (Serbia). The site was partially destroyed during the exploitation of sand for construction purposes in 2011, so Ilok Municipal Museum in cooperation with the Institute of Archaeology carried out the rescue archaeological excavation. Between 2015 and 2017 three research seasons were conducted. The excavated area covers approximately 84 square meters. Within this area, 188 graves and part of prehistoric objects were explored. The archaeological context, artefacts, and radiocarbon analysis date the use of the cemetery between the end of the 12th and the transition from the 15th to the 16th century. These burials most probably belong to the parish cemetery around the church of St. Helen the Queen (Krznar & Rimpf 2018).

Two individuals belong to the Norris Farms #36 (Illinois, USA) sample, housed at the Pennsylvania State University, for which the age at death was estimated based on tooth crown formation and dental eruption stages (Millner and Smith, 1990). This remains are part of the Oneota culture and dated back to 1300 AD (Millner and Smith, 1990).

Six individuals came from the Imperial Roman site of Velia. The site, originally founded by Greeks in 540BC (Morel, 2006), is located on the Italian west coast, near Salerno (Campania, Italy). Numerous archaeological campaigns have been held, and, during the 2003-2006 campaign (Fiammenghi, 2003), a necropolis with over 330 burials. This necropolis, dated back to the I and II centuries AD, yielded both cremation and inhumations, with numerous juvenile burials. The age at death was analyzed based on common anthropological methods which take into account skeletal and dental maturation.

Four individuals came from the sites of Paks and seven from Perkáta-Nyúli dűlő. The two sites are located in Hungary, and are stored at the Natural History Museum in Budapest. The cemetery and settlement at Perkáta-Nyúli dűlő represents a population of a Cuman settlement in the Transdanubian region of Hungary, which at the same time preserved a population from the transition period of the Cuman integration (Hathàzi, 2004). The site was found during a motorway constructions works, between 2009 and 2010 by the Field Service for Cultural Heritage. The cemetery counts more than 4,000 graves. All the individuals dated back to the 14^{th}-16^{th} centuries AD, except for on (3421) that dated back to the 10^{th}-12^{th} centuries AD. Age-at-death was estimated based on the development of the deciduous and permanent teeth (Moorrees et al., 1963a,b; Smith, 1991). When no teeth were available, diaphyseal length (Stoukal and Hanakovà, 1978) and also epiphyseal fusion (Ferembach et al., 1980) were used (László, 2008; László, 2018; Mesterházy-Ács, Zs. 2015; Szeniczey et al., 2019).

The church around the cemetery of Paks- Cseresznyés was excavated between April of 2008 and 2009 by the Field Service for Cultural Heritage. According to the buildings and to the archaeological material of the village, it can be dated to the 14^{th} and 16^{th} centuries, which probably became deserted due to the expansion of the Ottoman Empire. The anthropological analysis have been conducted between 2009-2010. The specimens, with a very good state of preservation, belong to 504 individuals, 263 of which were infants (László, 2018).

Finally, one individual from Grotta Paglicci (Italy) was included in the analysis. The young male is aged 12-13 years, and had been buried with a rich funeral tool kit and many ornaments (Ronchitelli et al. 2015).

Table 22 – Study sample. Individuals are listed in order of population.

Site	Specimen	Period	Age at death (in years)	GMM	Biomechanics
BeliManastir	G20	Early/Middle Neolithic	5.5-6.5	✓	✓
BeliManastir	G1	Early/Middle Neolithic	7-9	✓	
BeliManastir	G4	Early/Middle Neolithic	12-14	✓	✓
BeliManastir	G2	Early/Middle Neolithic	12-14	✓	
BeliManastir	G5	Early/Middle Neolithic	13-15	✓	
BeliManastir	G9	Early/Middle Neolithic	13-15	✓	
BeliManastir	G31	Early/Middle Neolithic	7-8		✓

Bologna	BO4_F	XX Century	5		✓
Bologna	BO5_F	XX Century	5	✓	✓
Bologna	Parma7_F	XX Century	5	✓	✓
Bologna	BO6_F	XX Century	5 years 10 and months	✓	✓
Bologna	BO1_M	XX Century	5 years and 8 months	✓	✓
Bologna	BO11_F	XX Century	6	✓	✓
Bologna	BO40_M	XX Century	9	✓	✓
Bologna	BO6_M	XX Century	7		✓
Bologna	BO39_M	XX Century	11	✓	✓
Bologna	BO81_M	XX Century	11	✓	✓
Bologna	Parma10_F	XX Century	13	✓	✓
Ilok	G72	13th-15th century	4		✓
Ilok	G23	13th-15th century	12-15	✓	
Ilok	G26	13th-15th century	14-15	✓	
Norris Farm	821012	1300 AD	5	✓	✓
Paglicci	Paglicci	UP	12-13 years	✓	✓
Paks TO-18	1846	14-16th c.	4-5	✓	✓
Paks TO-18	1164	14-16th c.	5-6	✓	✓
Paks TO-18	1865	14-16th c.	7-8	✓	✓
Paks TO-18	1156	14-16th c.	13-14	✓	✓
Perkáta-Nyúli dűlő	4263	10-12th c.	4-5		✓
Perkáta-Nyúli dűlő	435	14-16th c.	6-7		✓
Perkáta-Nyúli dűlő	1575	10-12th c.	6-8	✓	✓
Perkáta-Nyúli dűlő	752	14-16th c.	7-8	✓	✓
Perkáta-Nyúli dűlő	2123	10-12th c.	7-8	✓	✓
Perkáta-Nyúli dűlő	116	14-16th c.	11-12	✓	✓
Perkáta-Nyúli dűlő	734	14-16th c.	13-15	✓	✓
Velia	T375us2129	Roman	5		✓
Velia	T320us1431	Roman	7-8		✓
Velia	T390us2207	Roman	5-6	✓	✓
Velia	T333us1489	Roman	6-7	✓	✓
Velia	T138us1636	Roman	9-10	✓	✓
Velia	T365us2028	Roman	12-15	✓	✓

All the specimens were selected based on their good condition, with minimal or no damages. The left side was preferred; when the left talus was missing or incomplete, the right one was selected instead, and mirrored. Specimens were scanned (see Table 23), and scans were reconstructed as 16-bit TIFF stacks, and ImageJ was used to inspect the scans and evaluate their quality. When the trabecular bone showed signs of damage or rarefaction due to pathological or diagenetic causes, the specimen was excluded from the analyses. Avizo 9.3 (Visualization Sciences Group, SAS) was used to pre-process the reconstructed scan data (e.g. crop or resample). Where heavy sediment or mummified tissues were present, they were removed in Avizo 9.3 using

a Wacom board and the Avizo paint-brush tool in the labels-field. A White Hat filter was applied (to the Norris Farms#36, Beli Manastir, and Velia samples) to improve the contrast between bone and the heavy sediment present into the bone. In the cases in which this contrast was impossible to improve, the specimens were excluded from the analyses. Segmentation of the image data was performed using the MIA clustering method (Dunmore et al., 2018). In short, this method uses a K-means algorithm to cluster the CT images into specific classes determined a priori by the user. This clustering is based on voxel or pixel intensity. Therefore, a fuzzy c-means algorithm (Dunn, 1973; Bezdek, 1987) is applied to cope with the scanning artifacts or different levels of mineralization of the specimen or the soil (Dunmore et al., 2018), and the class membership probabilities are calculated. Finally, voxels are attributed to the class with the highest membership probability. All the process results in a segmented dataset. All the output used here are raw files, linked to MetaImage files (ITK).

4.2.1. Age Classes

The sample was then subset in four age classes (Table 24) as follows (Swan et al., 2020):

- Late infancy (4.1-6 years). In this subset, infants engage in an intermediate phase between immature and mature gait. Early infancy (1.1-3 years). This stage includes infants who are able to walk independently, engaging in an immature toddling gait.
- Childhood (6.1-10). This stage comprehends children who achieved mature locomotion.
- Adolescence (10.1-15). This stage comprehends the late ontogenetic growth phase in the human foot. The growth pace slows down and the talus achieves the adult morphology.

Table 23 - Micro-CT information

Sample	Facility	Voxel size (μ)
Bologna	Center for Quantitative Imaging (CQI), Pennsylvania State University, PA (USA)	20-38
Norris Farms	Center for Quantitative Imaging (CQI), Pennsylvania State University, PA (USA)	12-26
Velia	The Abdus Salam International Centre for Theoretical Physics, Trieste, Italy	18-30
Beli Manastir and Ilok	University of Zagreb, School of Medicine, Zagreb, Croatia	18-29
Paks and Perkata	The Abdus Salam International Centre for Theoretical Physics, Trieste, Italy	18-30
Paglicci	University of Bologna, Department of Physics, Bologna, Italy	40

Table 24 - Age classes

Age classes	***Group Name***	***Individuals per classes***
4.1-6 yrs	Late infancy	15
6.1-10	Childhood	12
10.1-15	Adolescence	14
Total		41

4.2.2. Geometric Morphometrics Analysis

To cope with the different morphologies of the growing talus, a template of 254 (semi) landmarks (11 anatomical landmarks, 89 curve semilandmarks, and 154 surface semilandmarks) was created in Viewbox 4 (dHAL Software), on a 5 year-old female specimen (Parma7-F). The aim of this template is to follow the morphological changes in the gross morphology, related to the ontogeny, and the development of the articular facet, linked also to the locomotion, from the late infancy throughout adolescence. (Figures 32-33; Tables 25-26). The (semi)landmark configurations were applied to all the targets in which facets were clearly visible. To be considered geometrically homologous (Gunz & Mitteroecker, 2013), semilandmarks were allowed to slide on the curves and surface, to minimize thin-plate-spline bending energy (Slice, 2006) between template and targets. Then, semilandmarks were allowed to slide against recursive updates of the Procrustes consensus (Rohlf and Slice, 1990). The coordinates were then registered with a Generalized Procrustes Analysis (GPA) where the size was removed and the specimens were scaled and translated. The GPA was performed in R, using geomorph (Adams & Otárola-Castillo, 2013).

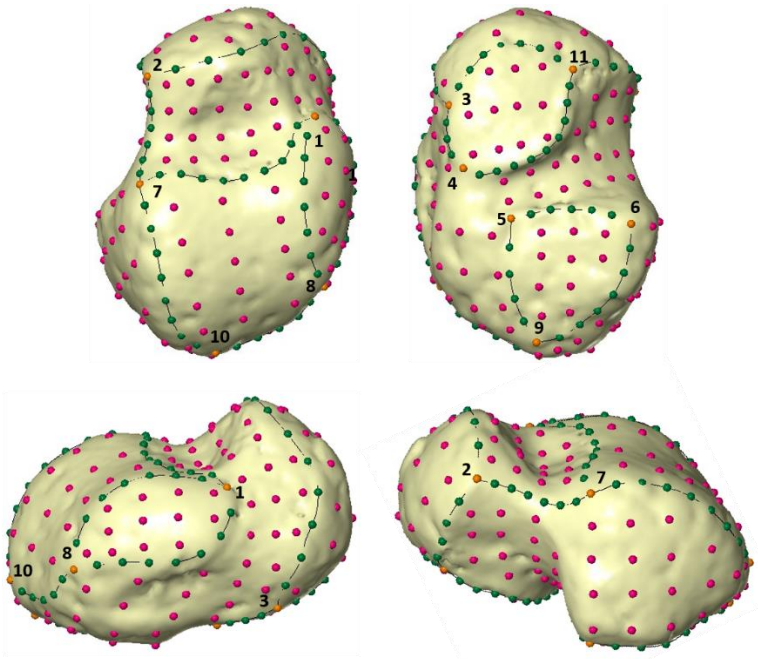

Figure 32 - (semi)landmark configuration. Landmarks are represented in orange. Curve semilandmarks are represented in green, surface semilandmarks in magenta.

Table 25 – Configuration of landmarks. Type of landmarks assigned according to Bookstein (1997).

Description	*Type of landmark*
01 Most distal point of contact between the medial malleolar facet and the trochlea	III
02 Most lateral point of the head	III
03 Most medial point of the head	III
04 Most medial point of the anterior calcaneal facet	III
05 Most proximo-medial point of the posterior calcaneal facet	III
06 Most lateral point of the posterior calcaneal facet	III
07 Most lateral point of contact between trochlea and neck	III

08 Most proximal point of contact between the medial malleolar facet and the trochlear surface	III
09 Most posterior point on the posterior calcaneal facet	III
10 Most lateral-posterior point of the trochlea	III
11 Most lateral point on the anterior calcaneal facet	III

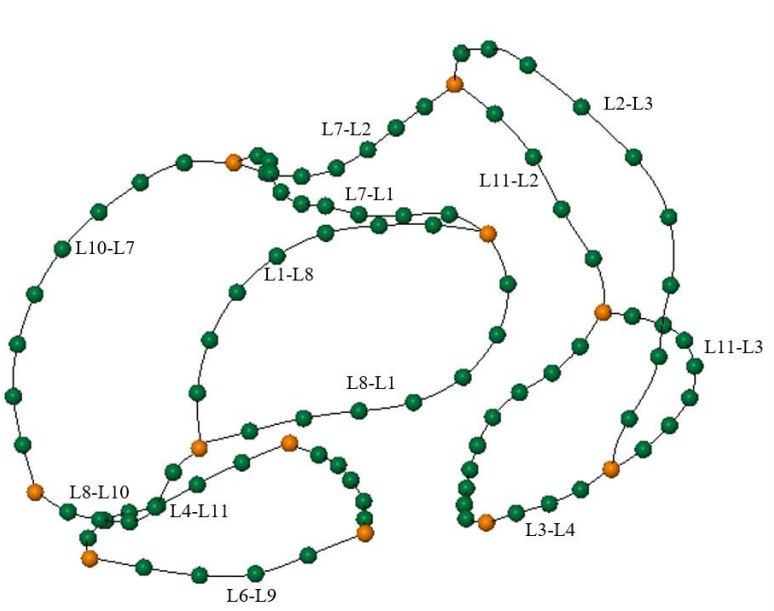

Figure 33 - Configuration of (semi)landmarks. Anatomical landmarks (orange) and curve semilandmarks (green) are represented. Curves are described in Table 26.

Table 26 - semilandmarks

Semilandmarks on curves	N
Curve L1-L8: Medial margin of the trochlea	7
Curve L2-L3: Head	9
Curve L3-L4: Medial margin of the anterior calcaneal facet	3
Curve L4-L11: Posterior margin of the anterior calcaneal facet	9
Curve L6-L9: Lateral margin of the posterior calcaneal facet	6
Curve L7-L1: Distal margin of the trochlea	9
Curve L7-L2: Lateral ridge	6
Curve L8-L10: Posterior margin of the trochlea	4
Curve L9-L5: Posterior margin of the posterior calcaneal facet	4
Curve L8-L1: Inferior margin of the medial malleolar facet	7
Curve L10-L7: Lateral margin of the trochlea	8
Curve L11-L2: Most inferior margin of the head	4
Curve L11-L3: Most anterior margin of the anterior calcaneal facet	7
Semilandmarks on surface	N
Neck	15
Head	30
Posterior Calcaneal facet	10
Sulcus Tali	20
Trochlea	15
Medial malleolar facet	12

Anterior calcaneal facet	11
Lateral surface	20
Posterior suface	11
Medial surface	10

A shape and form space Principal Component Analysis (PCA) was carried out on the Procrustes coordinates to explore talar shape variation during growth using Morpho (Schlager, 2017). First, a Shapiro Normality Test and a Levene test were performed, to assess the distribution of the data and its homoscedasticity. Then, based on the fulfillment of the assumption, the respective parametric or non-parametric tests (Analysis of Variance (ANOVA), Kruskal-Wallis rank sum test, Tukey's post-hoc test, and Dunn's test) were run to find any significance variance between group means along the first three PCs. Pearson's product moment correlation was perform to asses if shape variations were related to size. A form-space PCA (i.e., shape + size) was carried out by augmenting the Procrustes shape coordinates by the natural logarithm of CS. Visualization of shape changes along the principal axes was obtained by TPS deformation (Bookstein 1997) of the Procrustes grand mean shape surface in Avizo 7.1 (Visualization Science Group Inc.). The analyses were performed for both the whole talar shape and separately for each articular facet, except for the lateral malleolar facet, which develop after 6 years and it was not possible to include all the specimens in the study sample, to study the facet development from the early beginning. As a consequence, (semi)landmarks of each articular facet were extrapolated; then, a GPA and the above analysis were performed for each facet, to thoroughly analyze the shape changes. In addition, a two-block partial least square analysis (Rohlf and Corti 2000) was run to assess the degree of association between two blocks of Procrustes-aligned coordinates, i.e. different articular facets. In addition, a multivariate effect size describing the strength of the effect is estimated from the empirically-generated sampling distribution (Adams et al. 2018).

4.2.3.Biomechanical analyses

After the above-mentioned segmentation processes, the trabecular and cortical bone were separated following the protocol outlined by Gross and colleagues (2014) using Medtool 4.3 (Dr Pahr Ingenieurs e.U, 2017). Briefly, opening and closing filters (kernel size varies from 3 to 5, depending on the specimen) with a "region growing" function were applied using a customized python-based script within Medtool to remove cortical porosity and facilitate the creation of a uniform shell that is then filled to create three different masks, namely outer (i.e. the outer shell of cortical bone), and inner (i.e. the boundary between cortex and trabecular region), which separates cortical from trabecular bone (Gross et al. 2014; N. B. Stephens et al. 2016, 2018a). Then, the inner mask is subtracted from the outer one, creating the cortical thickness mask. For this study, only the inner region, i.d. trabecular bone, was used. Finally, a tetrahedral mesh of trabecular bone was generated using the computational geometry algorithms library CGAL (www.cgal.org), a mesher that creates a 3D finite element model using Delauney triangulation (Delaunay, 1934; Gross et al., 2014; Klomza and Skinner, 2019). Quantification of bone volume fraction (BV/TV), which is the ratio of trabecular bone voxels relative to the

total volume of voxels (Fajardo et al., 2007: Kivell, 2016), and Degree of Anisotropy (DA) which describe the degree of orientation of the trabecular struts (Klomnza and Skinner, 2019), was carried out on the trabecular mesh by moving a sampling 5 mm sphere along a background grid with 2.5 mm spacing for each scan (Pahr and Zysset, 2009; Gross et al., 2014). BV/TV (bone voxels/total voxels) is expressed as a percentage, DA is calculated as (1-[eigenvalue3/eigenvalue1]) and is scaled between 1 and 0, where 1 is highly anisotropic and 0 isotropic, following the Mean Intercept Length (MIL). The resulted colormaps were then visualized in Paraview 3.14.1 (Sandia Corporation, Kitware Inc). Mean trabecular thickness (Tb.Th, mm), trabecular numbers (Tb.N), and mean trabecular spacing (Tb.Sp, mm) were calculated (Hildebrand and Ruegsegger, 1997; Stephens et al., 2017).

3D statistical comparisons between groups were performed following the Phenotypic PointCloud Analysis protocol proposed by DeMars et al. (2020; Stephens, DeMars et al., 2020) for DA and BV/TV. Briefly, trabecular meshes were aligned using a modified version of the MATLAB auto3dgm package (Tingran, Winchester, and Stephens 2020). The auto3dgm package presents an algorithm which permits the fully automatic placement of corresponcence points on digital models. Then, these pseudolandmarks (i.e. landmark-like points) can be input into standard geometric morphometrics softwares (Boyer et al. 2015). Here, we used a set of 1200 automatically placed pseudolandmarks. Subsequently, we performed a GPA using the GeoMorpho R package (Adams et al. 2018), and we proceeded finding the mean specimen. This step is necessary to obtain a mean mesh by finding the closest-to-the-mean specimens, on which we warped the mean GPA coordinates of all our sample (Stephens, Kivell, Pahr, Hublin, & Skinner, 2018a). The average trabecular mesh obtained was then tetrahedralized using with evenly-spaced (1.75mm) points using TetWild (Hu et al., 2018) and vertices were converted to a point cloud. Individual point clouds were then obtained by interpolating BV/TV and DA scalar values to the vertices of the tetrahedral mesh, which were then aligned by applying the auto3dgm transformation matrixes followed by a rigid, affine, and deformable alignment using a python implementation of the Coherent Point Drift algorithm (Myronenko and Song 2010). BV/TV and DA scalar values were linearly interpolated from each individual point clouds to the corresponding points in the canonical point cloud using SciPy (Virtanen et al. 2020b, 2020a) and the mean, standard deviation, and coefficient of variation for each group were mapped to the average point cloud, and statistically compared across the sample. The homologous points were compared using a two-tailed t-test, with P-values corrected (Friston 1995; Worsley et al. 1996) and interactively visualized in Paraview with figures being automatically generated using PyVista (Sullivan and Kaszynski 2019).

4.3. Results

4.3.1. External morphology

4.3.1.1. Shape space

The first three PCs explain the 57.9% of the total variance (Figures 34 and 35). Shapiro-Wilk normality test show that the first two PCs were not normally distributed (PC1: W = 0.9, p-value = 0.005; PC2: W = 0.9, p-value = 0.04; PC3: W = 0.9, p-value = 0.3) while the Levene test attested for equality of variance, with p-values for all the first three PCs (PC1: Test Statistic = 0.7695, p-value = 0.4722; PC2: Test Statistic = 0.98537, p-value = 0.3851; PC3: Test Statistic = 0.097289, p-value = 0.9076). Most of the morphometric variation is explained by PC1 (38.9%), i.e. ontogenetic allometry. Negative scores account for a more immature morphology, with the articular facets barely noticeable, the trochlea has already started to expand and increase its concavity, while the medial and lateral rims have started to grow. The calcaneal facets are still developing, but their morphology is still immature, with a larger sulcus tali between them and a triangular-like shape of the posterior facet. Positive values describe an adult morphology, with well develop articular facets. The trochlea is well defined, is elongated in a medial-distal orientation and its concavity is well defined, with the lateral and medial rims well delineated. The lateral and medial malleolar facets are adult like in shape, as the subtalar facets, with the posterior one which clearly shows its rotation and deep concavity. Space between articular facets is reduced, and the head is medially orientated. PC2 (12.4%) shows a clear development of the trochlea along positive values, and a more demarcation of the anterior subtalar facet, while PC3 scores (6.5%) captured the increase in medial orientation of the head. The shape scores for PC1 are significantly different (Kruskal-Wallis chi-squared = 24.002, p-value = 6.138e-06), while differences along PC2 and PC3 scores are not significant (PC2: chi-squared = 1.9, df = 2, p-value = 0.3; PC3: df = 2, F-test = 0.5, p-value = 0.5). Dunn's post-hoc test results are shown in Table 27. There are significant differences between each age group. From 4.1-6 year to 6.1-10 years, the head shows a great increase of the medial rotation, while the trochlea greatly expands and change in shape, becoming more squared in dorsal view, and with an increase in rotation. Articular facets are, in general, more delineated, even though, especially the posterior calcaneal facet, is still triangular in shape and has not yet developed its concavity. The most astounding changes are visible in the 10.1-15 years age group, with an adult-like morphology, as captured by PCs positive values (Figure 35). The shape variation described by PC1 is significantly related to size (r=0.92, p-value= 7.573e-14), while the correlation with size for PC2 and 3 is not significant (p-value >0.5). Figure 5 shows the mean shape of the age classes. Figures 36 and 37 illustrates changes along PCs axes and mean groups.

Table 27 - Results of Dunn's-test Post-hoc for PC1 scores

	4.1-6 years	6.1-10 years
6.1-10 years	**0.28**	-
10.1-15 years	**2.6e-06**	**0.02**

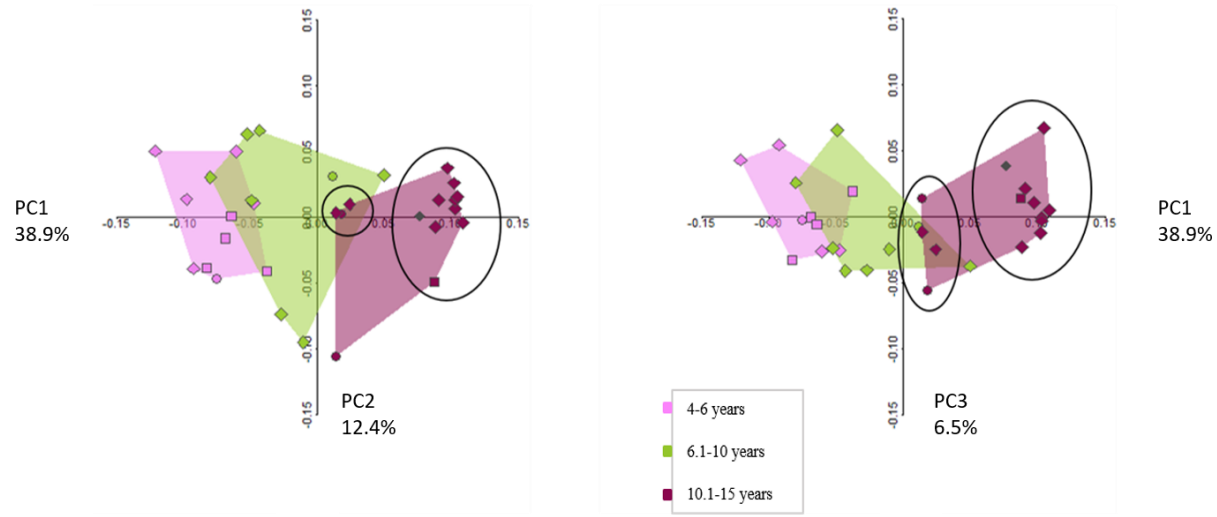

Figure 34 - 2D plot in shape space. Circles highlight the separation within the oldest group, i.e. between 10-11 and 12-15 years. Individuals from Bologna, for which sex was known, are represented by circles (males) and squared symbols (female). Diamonds represent the archaeological samples The black point represents Paglicci individual.

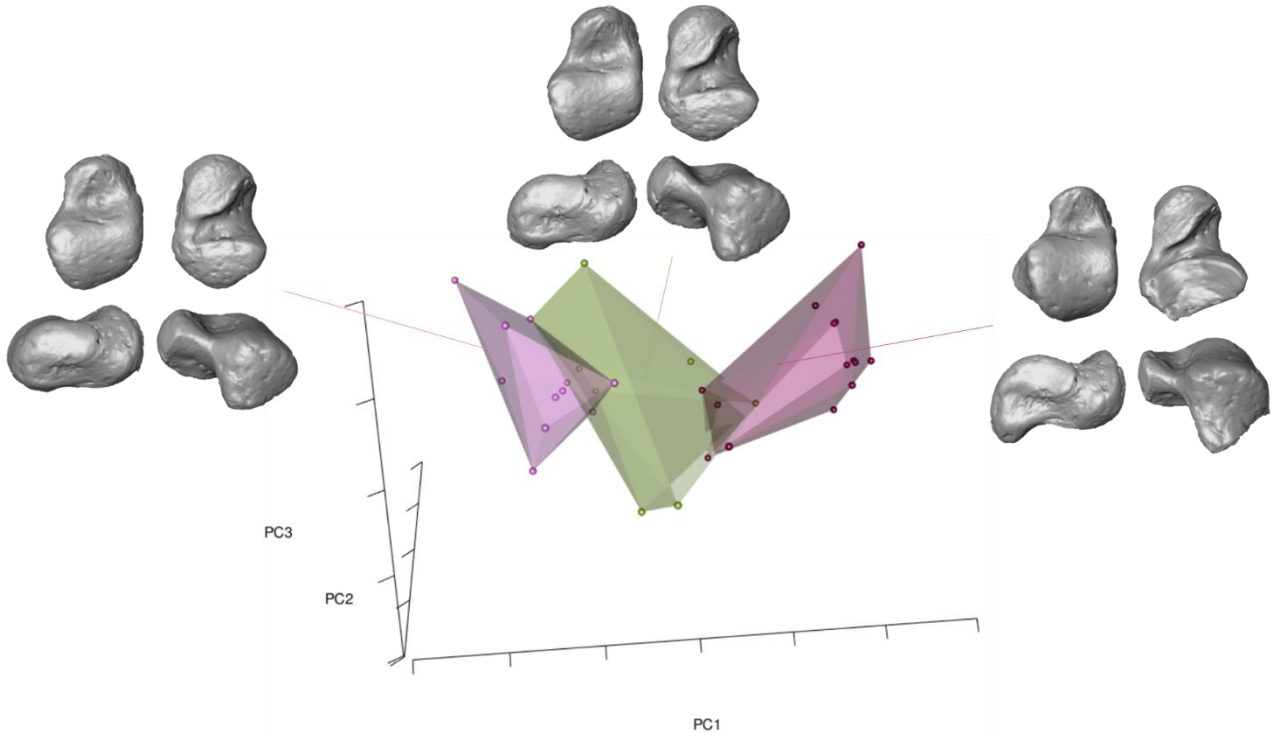

Figure 35 - Shape space 3D plot. Group means are represented for each age class. Mean shapes are represented, for each age group, in dorsal, palmar, medial, and lateral view.

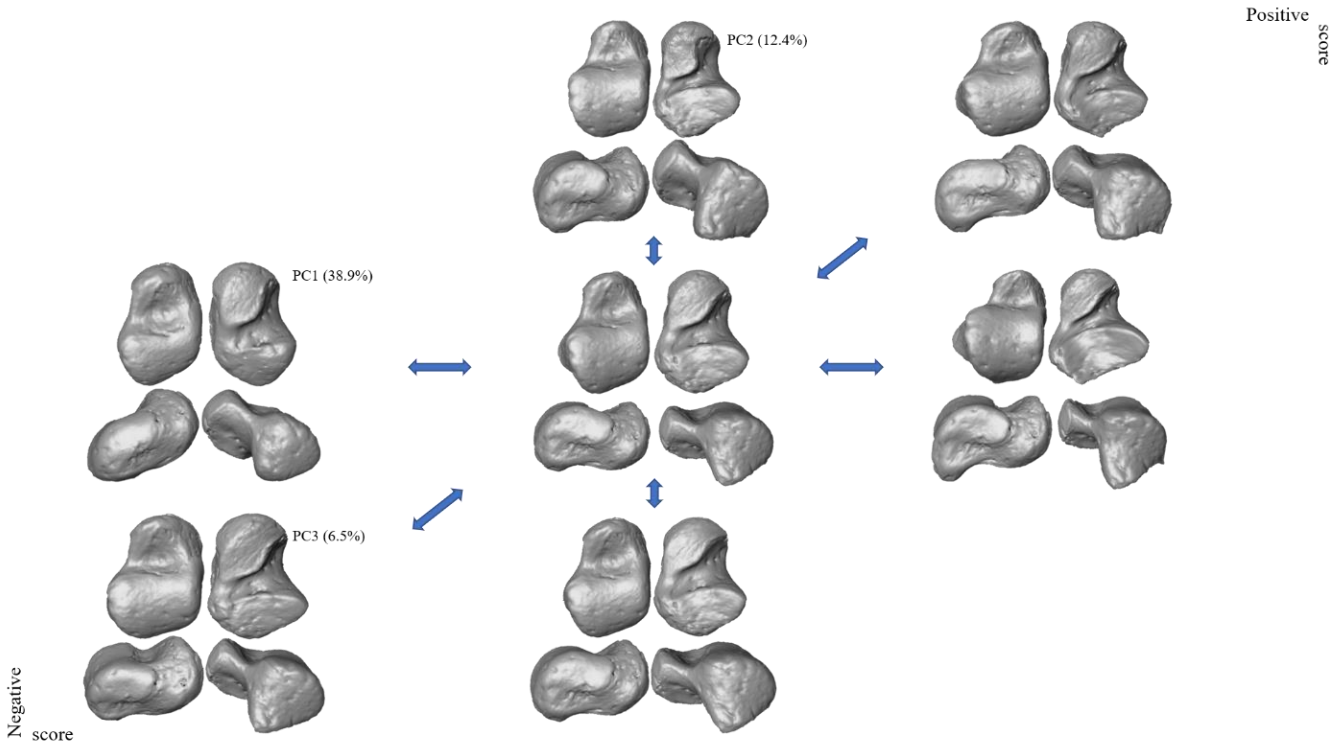

Figure 36 - Shape variation along the first three PCs axes. Tali are represented in dorsal, palmar, medial, and lateral views.

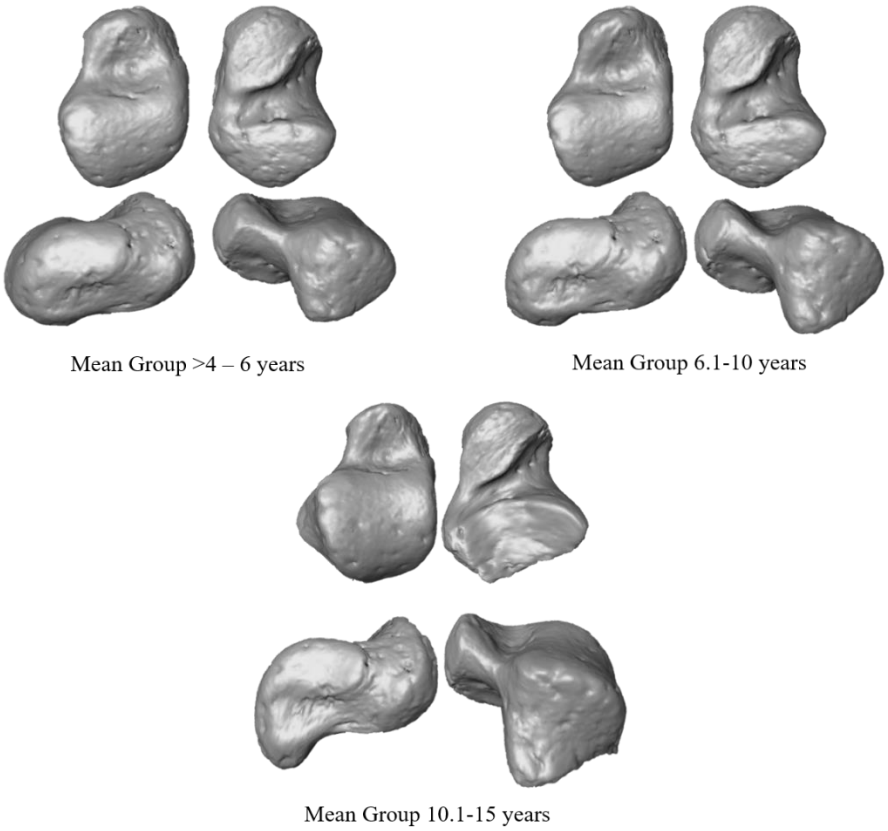

Figure 37 - Mean group shapes. ○Tali are represented in dorsal, palmar, medial, and lateral views.

Partially Least square results are summarized in Table 28, and plots for each analysis are shown in Figures 38-40. Results show that the association between shape is significant for the navicular facet in association with both trochlea and anterior calcaneal facet, for the trochlea in association with both the posterior calcaneal facet and medial malleolar facet and for the posterior calcaneal facet and medial malleolar facet.

Table 28 – PLS results for the association between articular facets

	r-PLS	P-value	Effect size
Navicular facet vs trochlea	0.58	**0.02**	2.20
Navicular facet vs Anterior calcaneal facet	0.90	**0.001**	6.32
Navicular facet vs posterior calcaneal facet	0.50	0.18	0.91
Navicular facet vs medial malleolar facet	0.40	0.69	0.59
Trochlea vs anterior calcaneal facet	0.46	0.20	0.73
Trochlea vs posterior calcaneal facet	0.86	**0.001**	5.72
Trochlea vs medial malleolar facet	0.91	**0.001**	6.19
Anterior calcaneal facet vs posterior calcaneal facet	0.47	0.40	0.19
Anterior calcaneal facet vs medial calcaneal facet	0.50	0.22	0.73
Posterior calcaneal facet vs medial malleolar facet	0.86	**0.001**	5.31

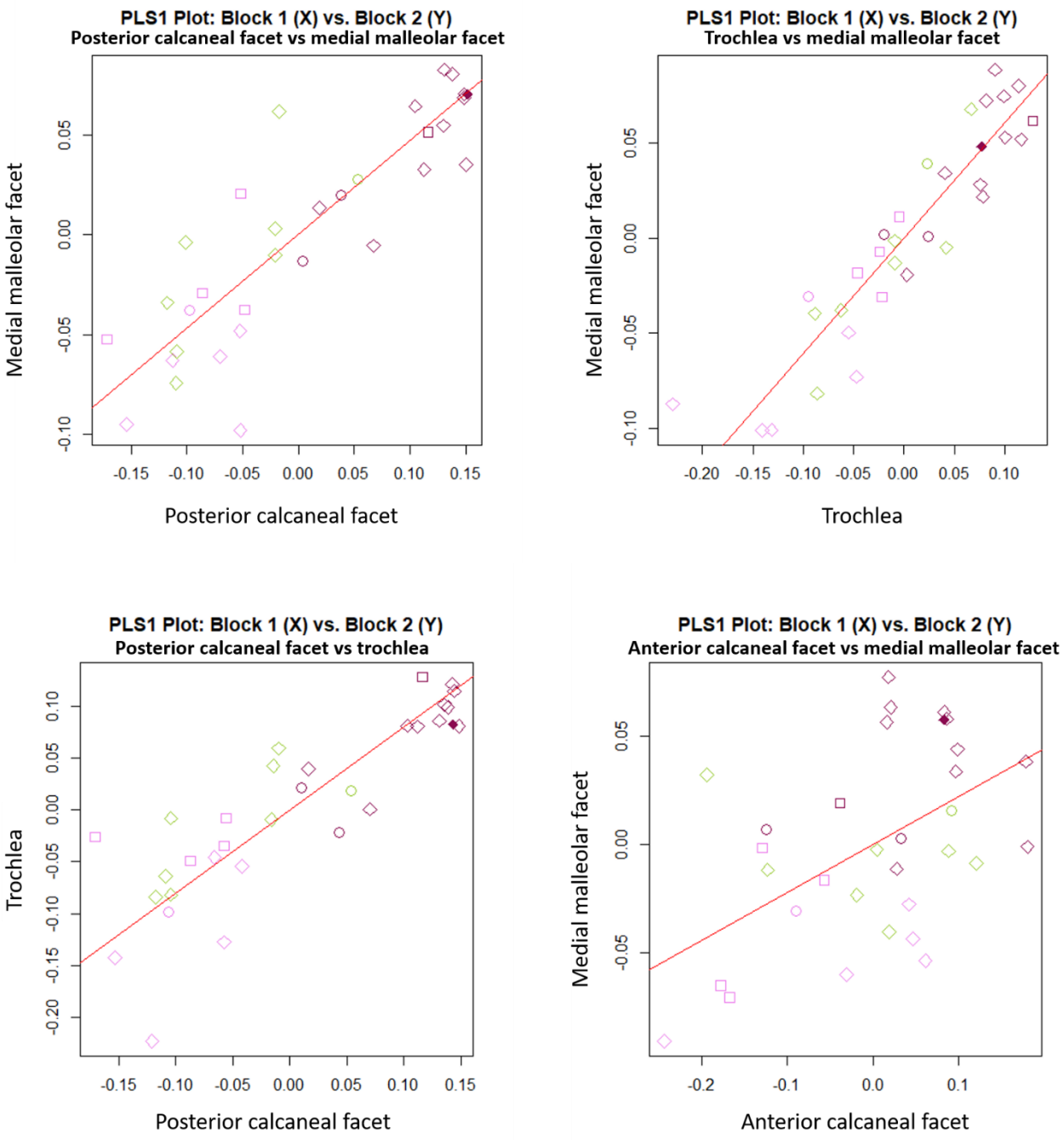

Figure 38 – 2D plot of the two-block pls results. In each plot, individuals from Bologna, for which sex was known, are represented by circles (males) and squared symbols (female). Diamonds represent the archaeological samples The filled point represents Paglicci individual. Pink represents the 4.1-6 year-old age group; green represents the 6.1-10 year-old age group; purple represents the 10.1-15 year-old age group.

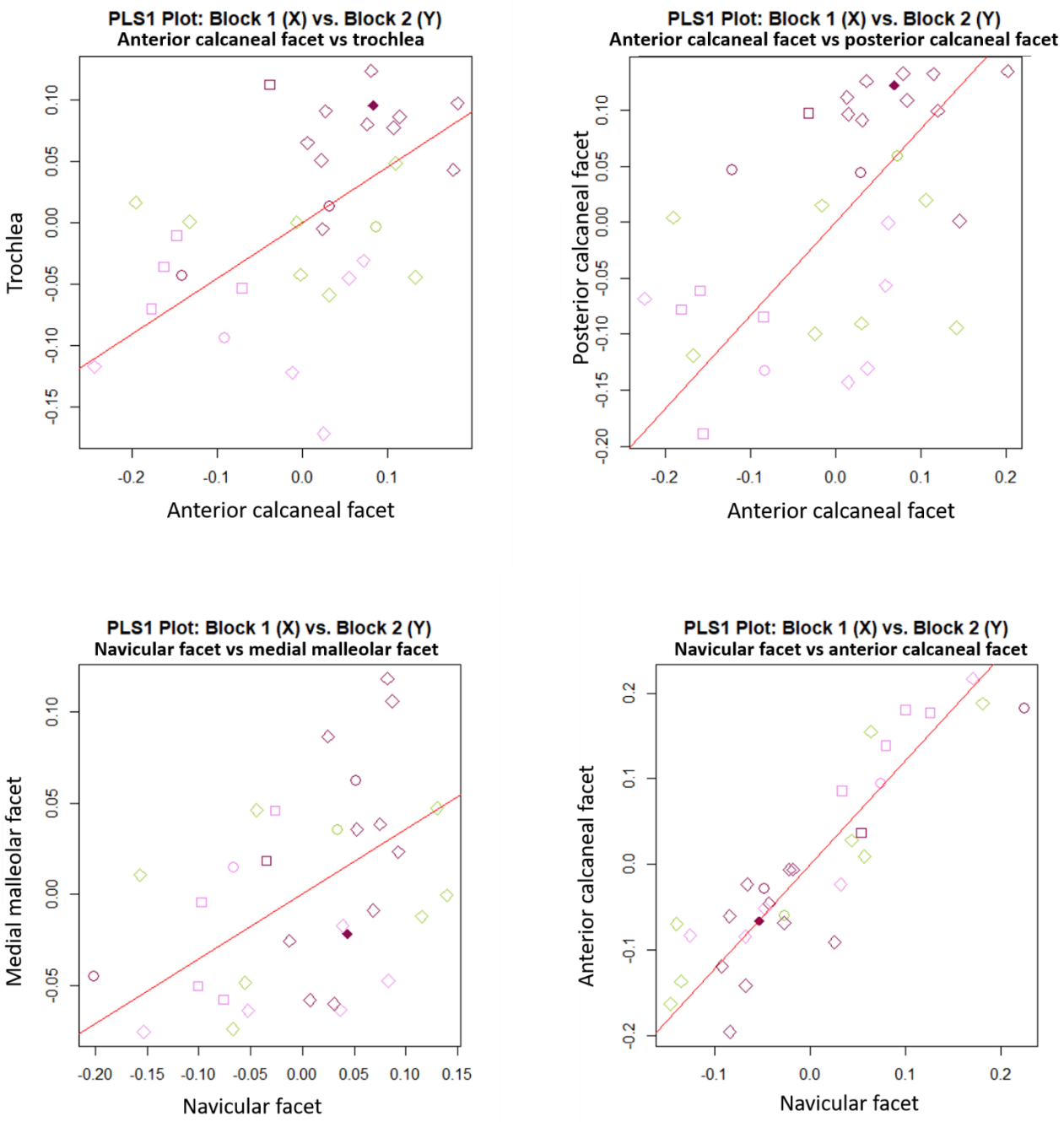

Figure 39 - 2D plot of the two-block pls results. In each plot, individuals from Bologna, for which sex was known, are represented by circles (males) and squared symbols (female). Diamonds represent the archaeological samples The filled point represents Paglicci individual. Pink represents the 4.1-6 year-old age group; green represents the 6.1-10 year-old age group; purple represents the 10.1-15 year-old age group.

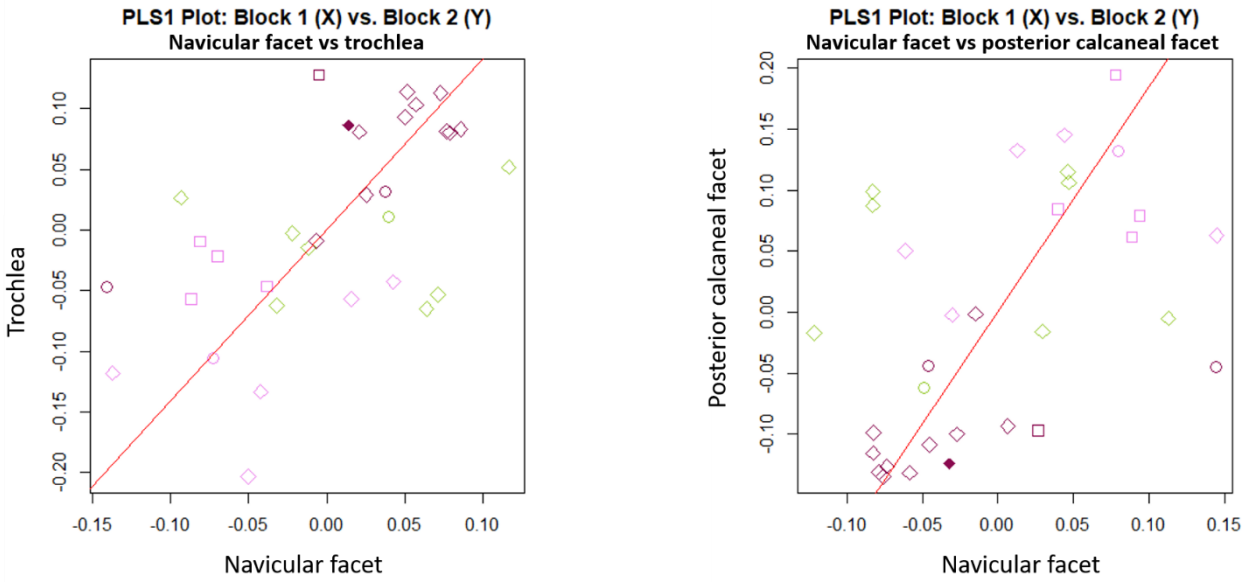

Figure 40 – 2D plot of the two-block pls results. In each plot, individuals from Bologna, for which sex was known, are represented by circles (males) and squared symbols (female). Diamonds represent the archaeological samples The filled point represents Paglicci individual. Pink represents the 4.1-6 year-old age group; green represents the 6.1-10 year-old age group; purple represents the 10.1-15 year-old age group.

4.3.1.2. Form space

The first three PCs explain the 89.4% of the total variance (Figure 41). Shapiro-Wilk normality test reveals that only PC1 and PC3 present a normal distribution (PC1: W = 0.9, p-value = 0.4; PC2: W = 0.9, p-value = 0.008; PC3: W = 0.9, p-value = 0.5) while the Levene test attested for equality of variance for all the first three PCs (PC1: Test Statistic = 0.90735, p-value = 0.4144; PC2: Test Statistic = 0.40931, p-value = 0.6678; PC3 Test Statistic = 0.16177, p-value = 0.8514). Most of the morphometric variation is explained by PC1 (84.27%),which is completely driven by size (Pearson r=0.99, p-value= < 2.2e-16) while the correlation with size for PC2 (3.02%) and 3 (2.14%), is not significant (p-value >0.5), and account for minor morphological changes. The oldest group is clearly separated from the youngest group. The shape scores for PC1 are significantly different (ANOVA: df = 2, F-test = 53.4, p-value = 4.3e-10), while differences along PC2 (Kruskal-Wallis chi-squared = 1.1058, df = 2, p-value = 0.5753) and PC3 (ANOVA df = 2, F-test = 1.3, p-value = 0.2) were not significant. Tukey post-hoc test results are shown in Table 29

Table 29 - Tukey posthoc test results in form space

Age classes	diff	lwr	upr	p adj
4-6years vs 6.1-10 years	0.18	0.05	0.30	**0.003**
10.1-15 years vs 4-6years	0.45	0.34	0.55	**0.000**
10.1-15 years vs 6.1-10 years	0.26	0.14	0.38	**0.000**

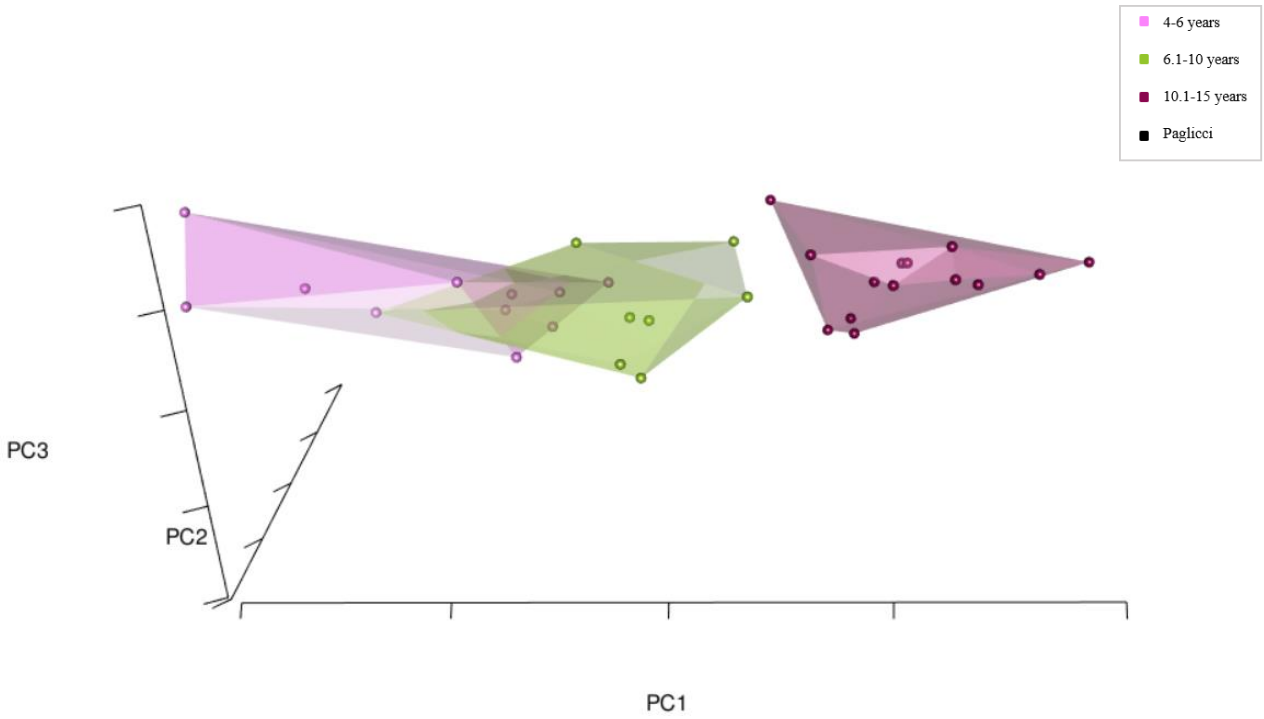

Figure 41 - 3D plot in form space. The increase in size clearly separates the oldest age group from the two youngest cohorts.

4.3.1.3. Separate facets

Anterior calcaneal facet

The first three PCs explain the 78.7% of the total variance (Figure 42). The three groups are not separated. PC1 (49.9%) account for a more immature shape (i.e. negative values), less rhomboidal in shape and with a smooth anterior margin, almost invisible, while positive values (i.e. oldest individuals) show a more define facet, with clearly marked anterior margin and an antero-posterior elongation. PC2 (21.1%) describe an enlargement of the facet along positive values, while PC3 (7.6%) captures a slight change in the anterior surface of the facet, which becomes less flat. Shapiro Normality test shows that the first three PCs are are normally distributed (PC1: w = 0.9, p-value = 0.07; PC2: w = 0.9, p-value = 0.2; PC3: w.9, p-value = 0.5). ANOVA shows significant difference along PC1 (Df=2, F = 3.7, p-value = 0.03) and PC3 values (Df = 2, F = 5.7, p-value = 0.007), while differences along PC2 are not significant (df = 2, F-test = 0.6, p-value = 0.5). Tukey Post-hoc test results are shown in Tables 30 and 31. PC1 is correlated with size (r = 0.29; p-value = 0.0003).

Table 30 - Tukey's post-hoc test results for PC1

	diff	wr	upr	p adj
4-6years vs 6.1-10 years	-0.06	-0.19	0.05	0.37
10.1-15 years vs 4-6years	-0.11	-0.22	-0.01	**0.02**
10.1-15 years vs 6.1-10 years	-0.04	-0.16	0.06	0.57

Table 31 - Tukey's post-hoc test results for PC3

	diff	lwr	upr	p adj
4-6years vs 6.1-10 years	0.02	-0.01	0.07	0.28
10.1-15 years vs 4-6years	-0.02	-0.06	0.009	0.15
10.1-15 years vs 6.1-10 years	-0.05	-0.10	-0.01	**0.006**

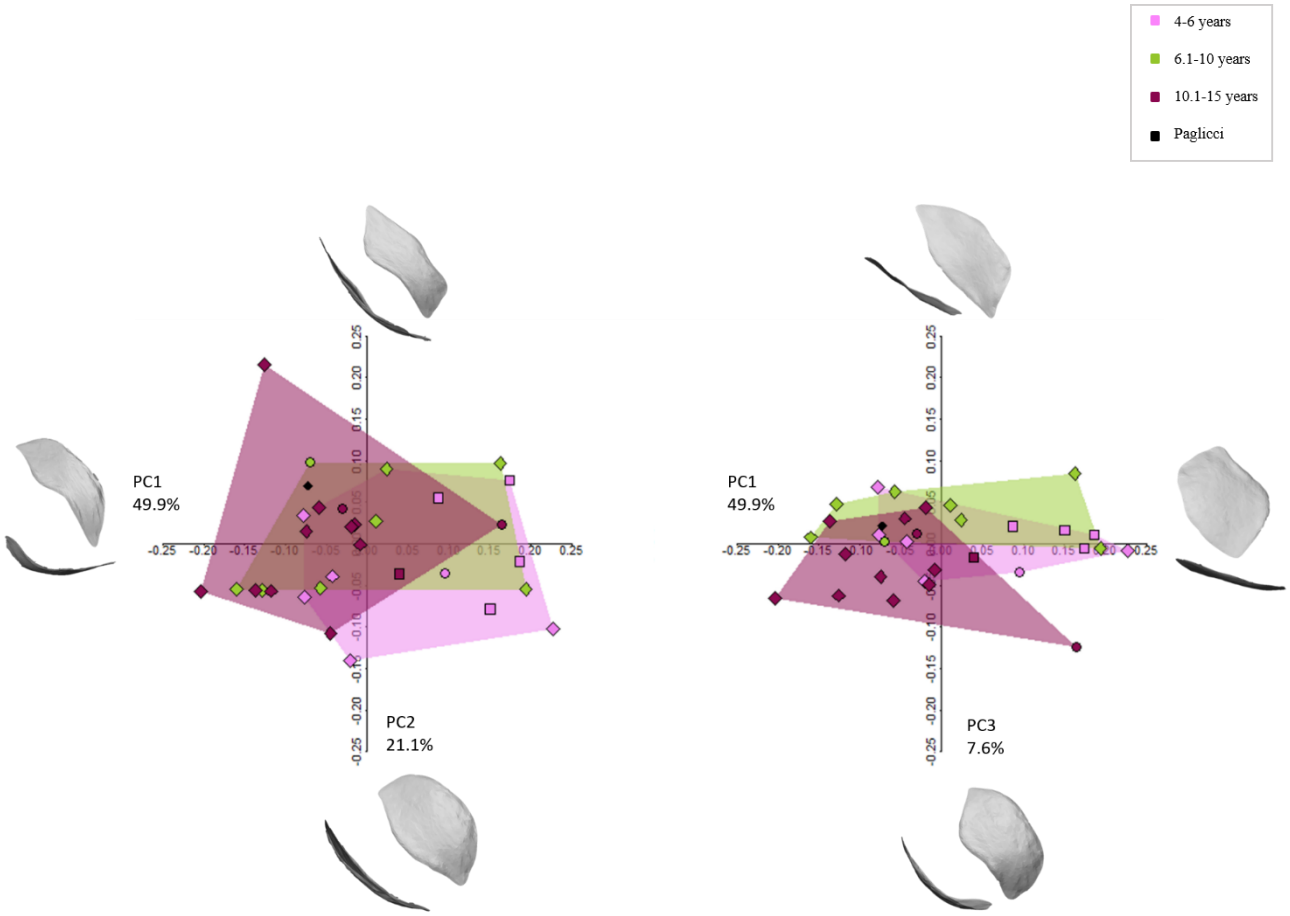

Figure 42 - PCA plots. On the left, PC1 and PC2. On the right, PC1 and PC3. Shape space plots of the anterior calcaneal facet do not separate age classes. Individuals from Bologna, for which sex was known, are represented by circles (males) and squared symbols (female). Diamonds represent the archaeological samples The black point represents Paglicci individual.

Form space

The first three PCs explain he 92.6% of the total variance (Figure 43). PC1 account for the 79.2% of the variance, while PC2 and PC3 account for the8.2% and 5.1% of the variance, respectively. Shapiro test show that the first three PCs scores are normally distributed (PC1: w = 0.9, p-value = 0.06; PC2: w = 0.9, p-value = 0.6; PC3: w = 0.9, p-value = 0.1). ANOVA shows that significant differences are present only along PC1 scores (PC1: df = 2, F = 21.8, p-value = 1.38e-06; PC2: df = 2; F-test = 0.23; p-value = 0.7; PC3: df = 2; F-test = 0.35; p-value = 0.7). Tukey's post-hoc test highlight differences among each age class (Table 32), related to the great increase in size (Pearson, r = 0.98; p-value = < 2.2e-16).

Table 32 – Tukey's post-hoc test results for PC1

	diff	lwr	upr	adj
4.1-6years vs 6.1-10 years	0.21	0.00	0.42	**0.04**
10.1-15 years vs 4.1-6years	0.49	0.30	0.67	**0.000**
10.1-15 years vs 6.1-10 years	0.27	0.07	0.47	**0.006**

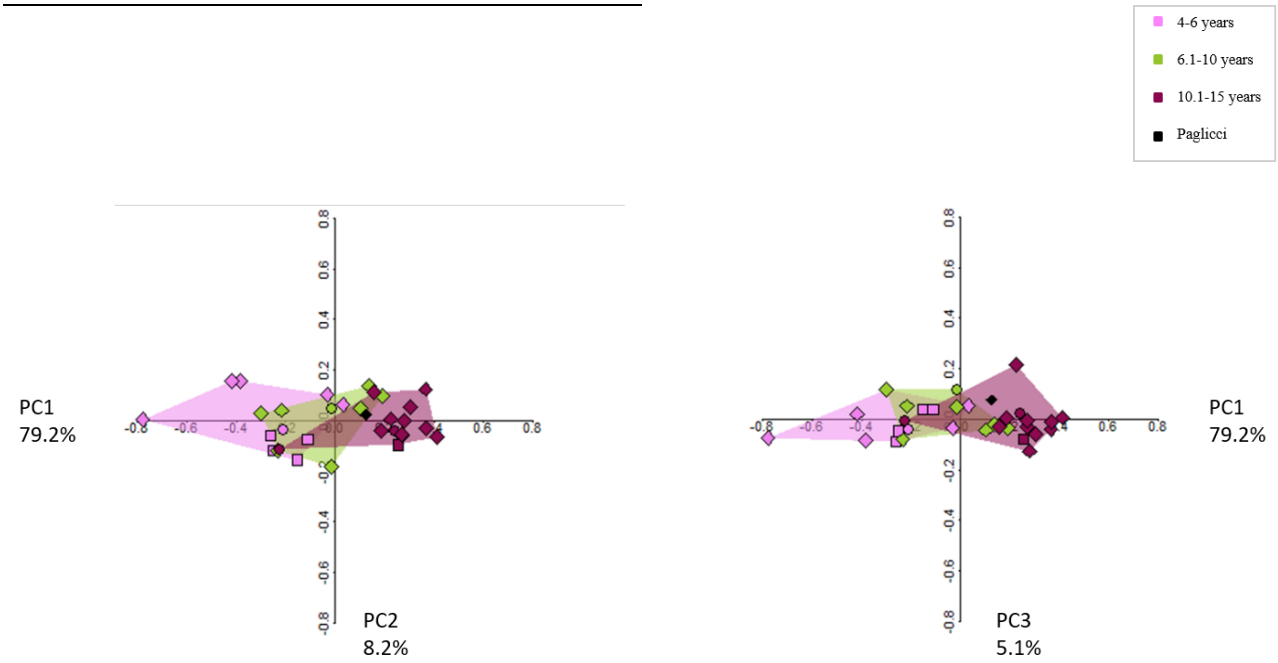

Figure 43 - 2D form space plots. The first three PCs do not separate age classes. Individuals from Bologna, for which sex was known, are represented by circles (males) and squared symbols (female). Diamonds represent the archaeological samples The black point represents Paglicci individual.

Navicular facet

The first three PCs explain the 74.21% of the total variance (Figure 44) and do not separate age classes. PC1 (52.8%) account for a more globular head morphology, which shows an increase in medial-lateral elongation along positive scores, with a more prominent superior margin and a flatter profile. PC2 (13.3%) and PC3 (8.07%) describes both increases in head medial elongation, with PC3 accounting for ontogenetic allometry. The first three PCs' scores are normally distributed (Shapiro-Wilk normality test: PC1: w = 0.9, p-value = 0.3; PC2: w = 0.9, p-value = 0.2; PC3: w = 0.9, p-value = 0.1). ANOVA shows significant difference along PC2 (df = 2, F-test = 3.9, p-value = 0.03) and PC3 values (df = 2, F-test = 7.23, p-value = 0.002), while differences along PC1 are not significant (df = 2, F-test = 1.04, p-value = 0.3). Tukey Post-hoc test results are shown in Tables 33 and 34. PC3 is correlated with size (r = 0.5; p-value = 0.001).

Table 33 – Tukey's post-hoc test results for PC2

	diff	lwr	upr	p adj
4-6years vs 6.1-10 years	0.05	0.00	0.1	**0.02**
10.1-15 years vs 4-6years	0.03	-0.01	0.07	0.21
10.1-15 years vs 6.1-10 years	-0.02	-0.07	0.02	0.38

Table 34 – Tukey's post-hoc test results for PC3

	diff	lwr	upr	p adj
4-6years vs 6.1-10 years	0.02	-0.01	0.06	0.21
10.1-15 years vs 4-6years	0.04	0.01	0.08	**0.001**
10.1-15 years vs 6.1-10 years	0.02	-0.01	0.05	0.24

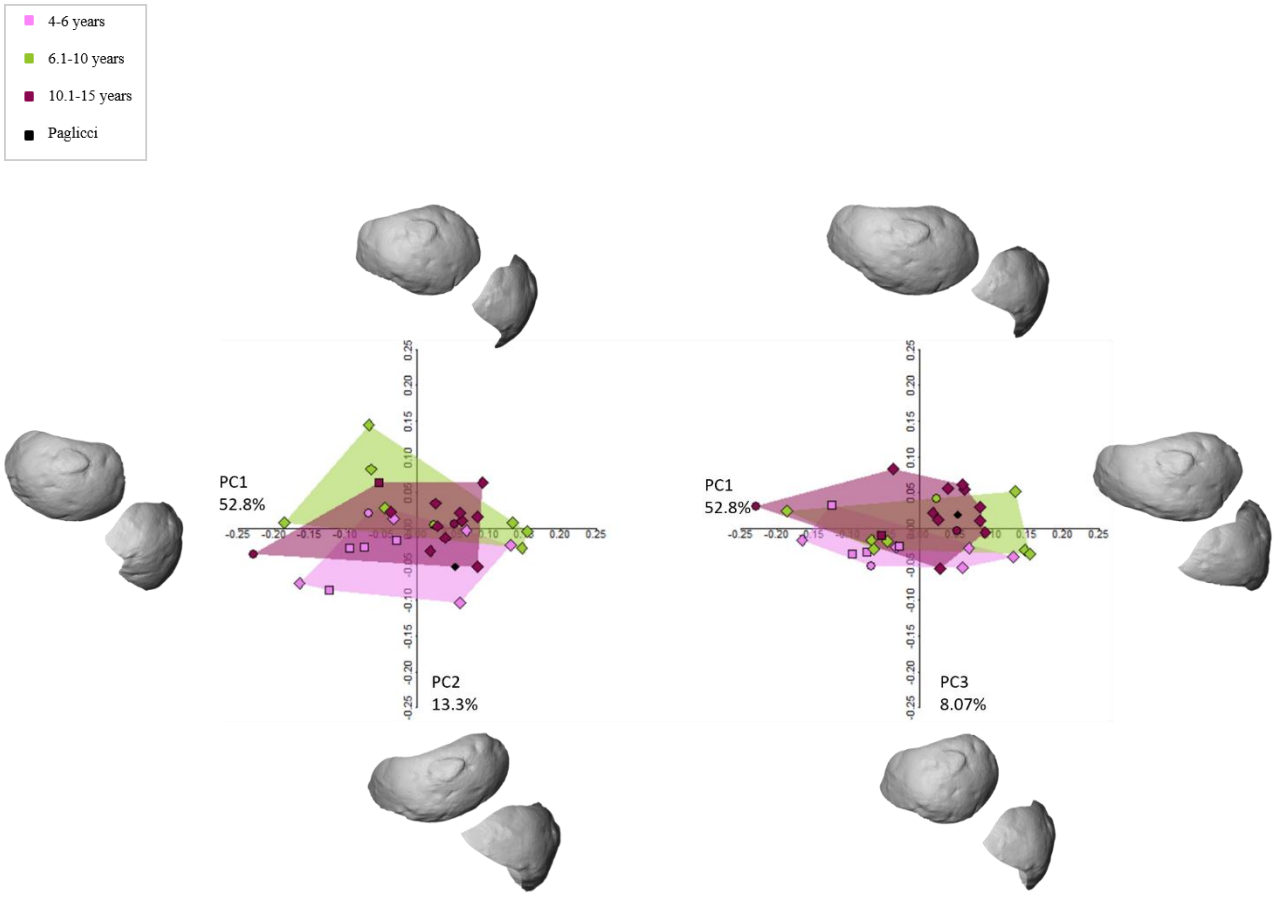

Figure 44 - 2D shape space plots. The first three PCs do not contribute in separating the three age groups in shape space. Individuals from Bologna, for which sex was known, are represented by circles (males) and squared symbols (female). Diamonds represent the archaeological samples The black point represents Paglicci individual.

Form space

When size is included, the first three PCs account for the 91.07% of the total variance (Figure 45), with PC1 explaining the 72.3% of the variability (PC2 = 14.9%; PC3 = 3.7%). The oldest group is well separated from the youngest groups. Shapiro-Wilk normality test shows that the first three PCs are normally distributed (PC1: w = 0.9, p-value = 0.2; PC2: w =0.9, p-value = 0.3; PC3: w = 0.9, p-value = 0.1). ANOVA shows significant differences between groups along PC1 (Df = 2, F-test = 42.1, p-value = 1.94e-09; PC2: df = 2, F-test =0.14, p-value = 0.8; PC3: df = 2, F-test = 2.7, p-value = 0.07), and Tukey's post-hoc test highlight significant differences between each group (Table 35). PC1 is highly correlated with size (r = 0.99; p-value = < 2.2e-16).

Table 35 – Tukey's post-hoc test for PC1

	diff	lwr	upr	p adj
4-6years vs 6.1-10 years	0.16	0.04	0.29	**0.006**
10.1-15 years vs 4-6years	0.40	0.29	0.5	**0.000**
10.1-15 years vs 6.1-10 years	0.23	0.11	0.35	**0.0001**

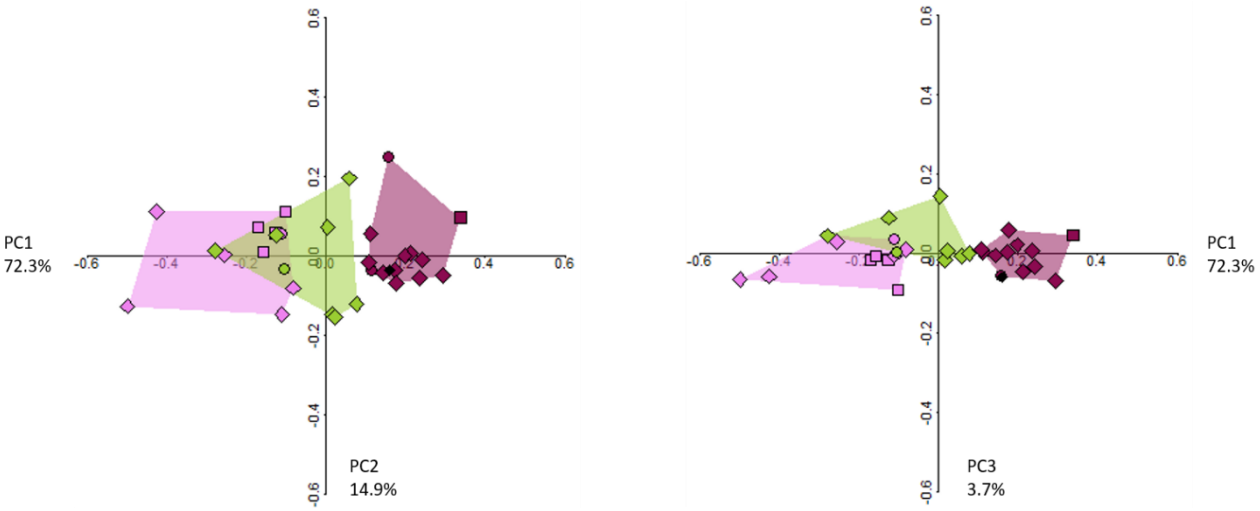

Figure 45 - 2D form space plot. Individuals from Bologna, for which sex was known, are represented by circles (males) and squared symbols (female). Diamonds represent the archaeological samples The black point represents Paglicci individual.

Medial malleolar facet

The first three PCs describe the 71.1% of the total variance (Figure 46), with PC1 (37.8%) describing an immature medial malleolar facet (i.e. negative values), with slightly visible rims and a flatter profile. Along positive values, the superior profile increase in heights as the trochlea develops, producing a more arched facet superior profile and a more pointed proximal surface. The facet becomes more concave. PC2 (20.4%) account for an increase in size, while PC3 (12.9%) account for slight changes in the anterior margin, which becomes more defined along positive values. Shapiro-Wilk normality test accounts for the normal distribution of the first three PCs scores (PC1: w=0.9, p-value = 0.5; PC2: w = 0.9, p-value = 0.1; PC3: w = 0.9, p-value = 0.5). Anova highlight significant between groups along PC2 scores (df = 2, F-test = 20.5, p-value = 2.44e-06; PC1: df = 2, F-test = 0.14, p-value = 0.8; PC3: df =2, F-test = 0.05, p-value = 0.9). Tukey's post-hoc are shown in Table 36. PC2 is highly correlated with size (Pearson r=0.7 p-value = 1.299e-06).

Table 36 – Tukey's post-hoc test for PC2

	diff	lwr	upr	p adj
4-6years vs 6.1-10 years	0.03	-0.004	0.07	0.08
10.1-15 years vs 4-6years	0.09	0.05	0.12	**0.00001**
10.1-15 years vs 6.1-10 years	0.05	0.01	0.09	**0.004**

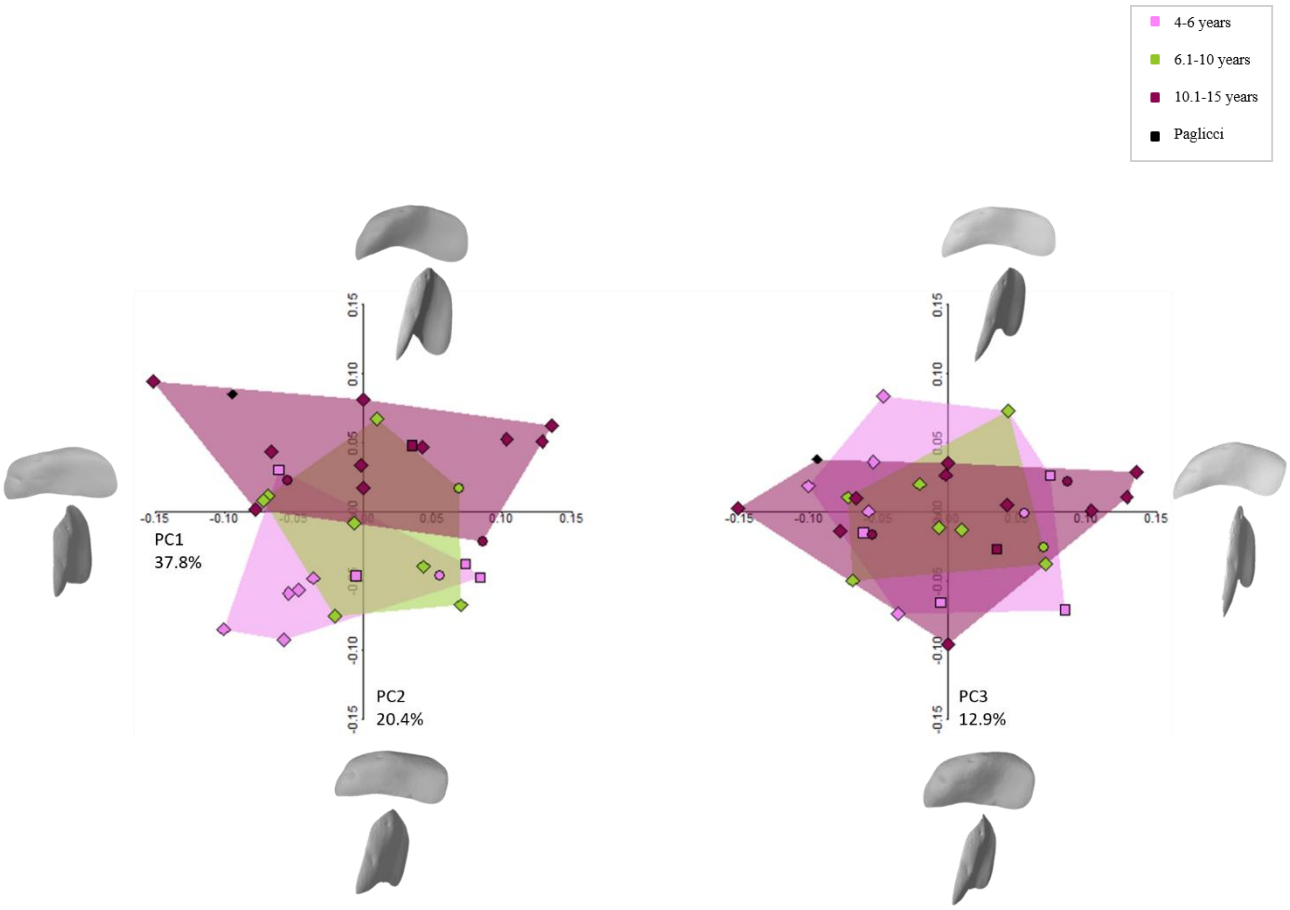

Figure 46 - 2D plot in shape space. Age groups do not contribute in separating the sample. Individuals from Bologna, for which sex was known, are represented by circles (males) and squared symbols (female). Diamonds represent the archaeological samples The black point represents Paglicci individual.

Form space

The first three PCs account for the 92.4% of total variance (Figure 47), with PC1 explaining the 82.06%, while PC2 and PC3 account for the 7.6% and 2.3% of the variance, respectively. Shapiro-Wilk normality test attests the normal distribution of the first three PCs scores (PC1: w = 0.9, p-value =0.5; PC2: w = 0.9, p-value = 0.3; PC3: w =0.9, p-value = 0.3) ANOVA shows statistical differences among PC1 values (df= 2, F-test = 40.6, p-value = 2.89e-09), while differences among groups are not significant along PC2 and PC3' scores (PC2: df = 2, F-test = 0.1, p-value = 0.8; PC3: df = 2, F-test = 0.3, p-value = 0.7). Tukey's post-hoc test results are shown in Table 37. PC1 is highly correlated with size (Pearson r = 0.99; p-value = < 2.2e-16).

Table 37 – Tukey's post-hoc test for PC3.

	diff	lwr	upr	p adj
4-6years vs 6.1-10 years	0.17	0.03	0.31	**0.009**
10.1-15 years vs 4-6years	0.43	0.31	0.55	**0.000**
10.1-15 years vs 6.1-10 years	0.25	0.12	0.39	**0.0001**

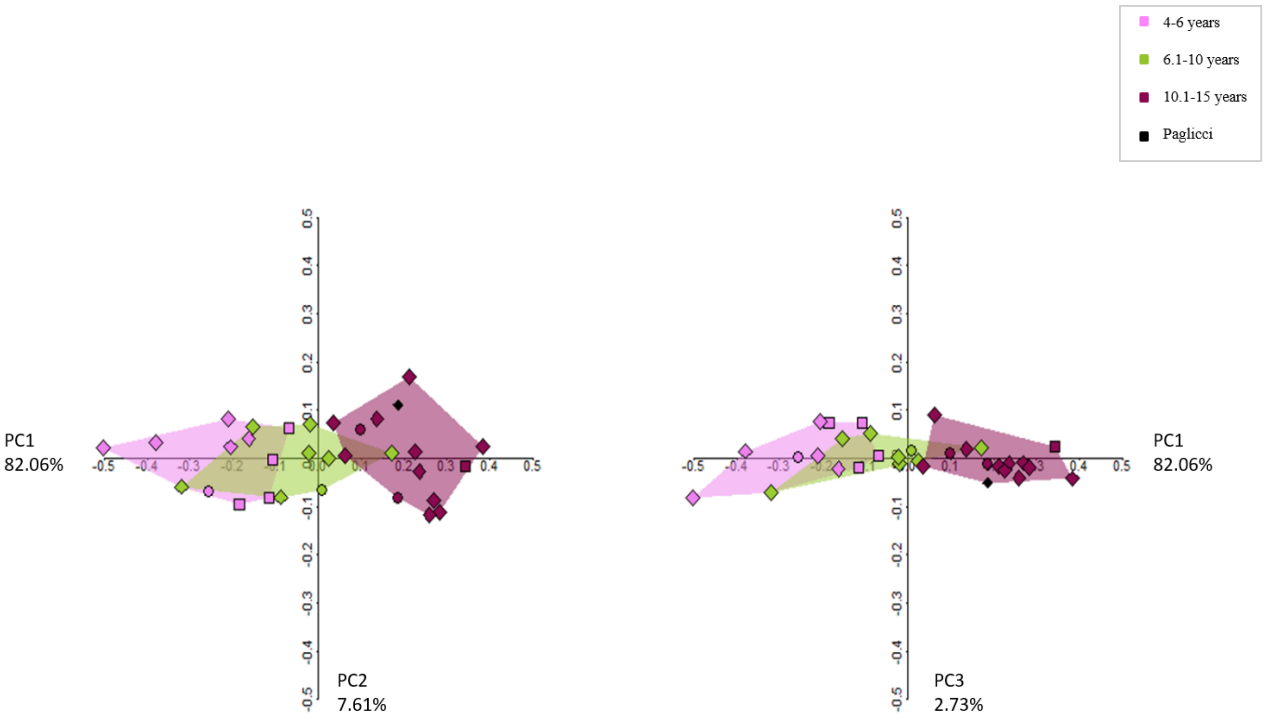

Figure 47 - 2D form space plot. The first three PCs do not clearly separate the three groups. Individuals from Bologna, for which sex was known, are represented by circles (males) and squared symbols (female). Diamonds represent the archaeological samples The black point represents Paglicci individual.

Posterior calcaneal surface

The first three PCs account for the 78.8% of the total variance (Figure 48) captured the medial increase in rotation of the articular facet. PC1 (44.07%) account for a more triangular shape in the youngest cohort, which increase in size along positive scores, changing into a more rectangular shape. PC2 and PC3 (18.1% and 16.9%, respectively) describe slight morphological changes the elongation of the medial margin in a proximal-distal direction, and the increase in convexity of the facet. Shapiro-Wilk normality test attests the normal distribution of PC2 (w=0.9, p-value = 0.6) and PC3 (w = 0.9, p-value = 0.2), while PC1 scores are not normally distributed (w= 0.9, p-value = 0.05). Kruskal-Wallis highlight significant differences among PC1 values (chi-squared = 22.896, df = 2, p-value = 1.067e-05), while Anova shows not significant differences among PC2 and PC3 (PC2: df) 2, F-test = 2.28, p-value = 0.11; PC3: df = 2, F-test = 0.764, p-value = 0.4). Pearson's product-moment correlation shows a high correlation between PC1 and size (r =0.99; p-value = <2.2e-16). Dunn's post-hoc test results are shown in Table 38.

Table 38 – Dunn's post-hoc test results for PC1

	4.1-6 years	6.1-10 years
6.1-10 years	1.0000	-
10.1-15 years	**2.3e-05**	**0.0024**

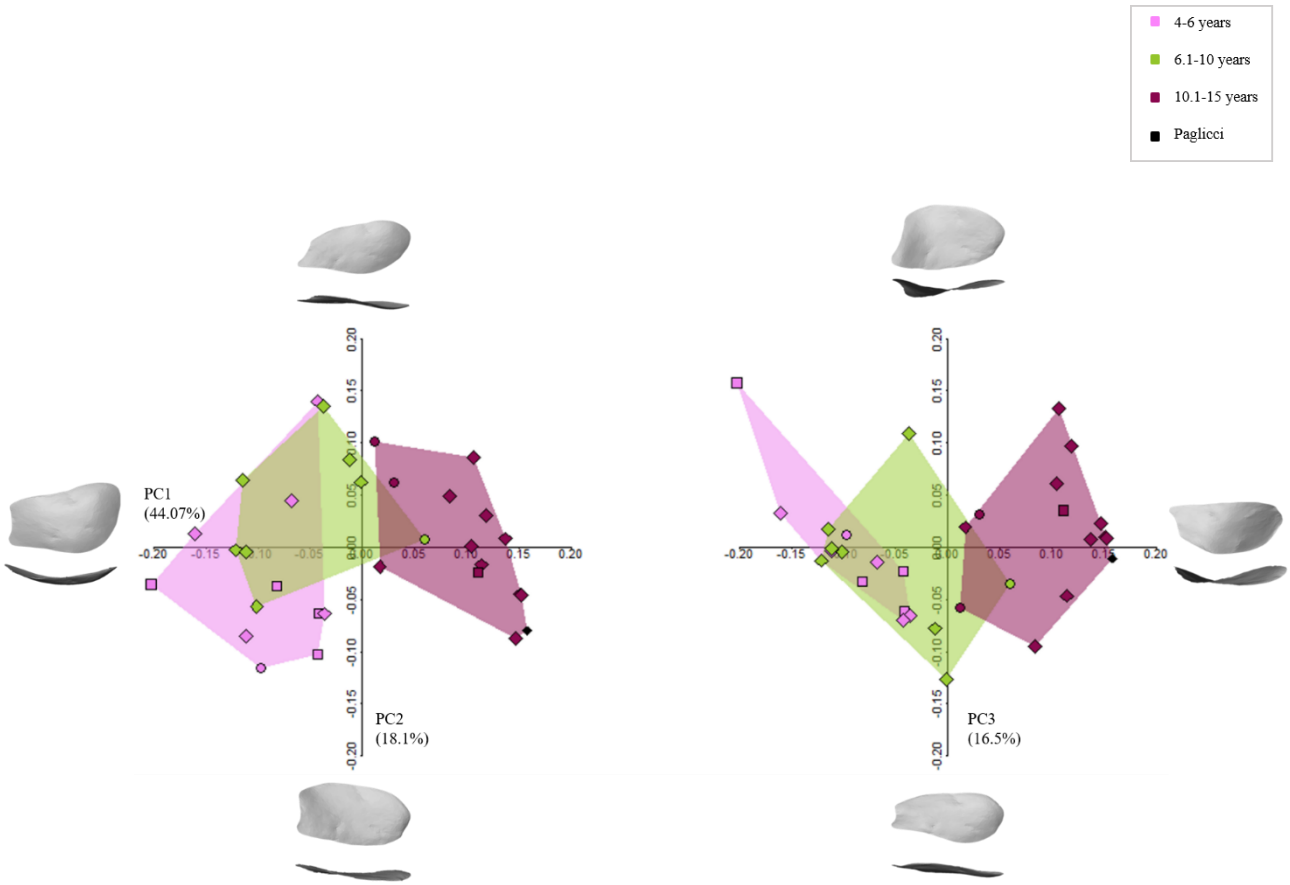

Figure 48 - 2D shape space plots. Age groups are not clearly separated along axes. Individuals from Bologna, for which sex was known, are represented by circles (males) and squared symbols (female). Diamonds represent the archaeological samples The black point represents Paglicci individual.

Form space

The first three PCs explain the 92.6% of the total variance (Figure 49), and do not contribute in separating the age groups. PC1 explains the 79.2% of the total variance, while PC2 and PC3 explain the 8.2% and the 5.1%, respectively, of the total variance. Shapiro-Wilk normality test attests the normality distribution of the first three PCs score (PC1: w = 0.9, p-value = 0.06; PC2: w = 0.9, p-value = 0.6; Pc3: w = 0.9, p-value = 0.1). PC1 is highly correlated with size (Pearson, r = 0.82; p-value = 6.835e-09). Anova shows significant differences are present among PC1 scores (Df = 2, F = 21.8, p-value = `1.38e-06`), while differences among PC2 and PC3 scores are not significant (PC2: df = 2, F-test = 0.23, p-value = 0.7; PC3: df = 2, F-test = 0.35, p-value = 0.7). Tukey's post-hoc test results are shown in Table 39

Table 39 – Tukey's post-hoc test results for PC1

	diff	lwr	upr	p adj
4-6years vs 6.1-10 years	0.21	0.003	0.42	**0.04**
10.1-15 years vs 4-6years	0.49	0.30	0.67	**0.00**
10.1-15 years vs 6.1-10 years	0.27	0.07	0.47	**0.006**

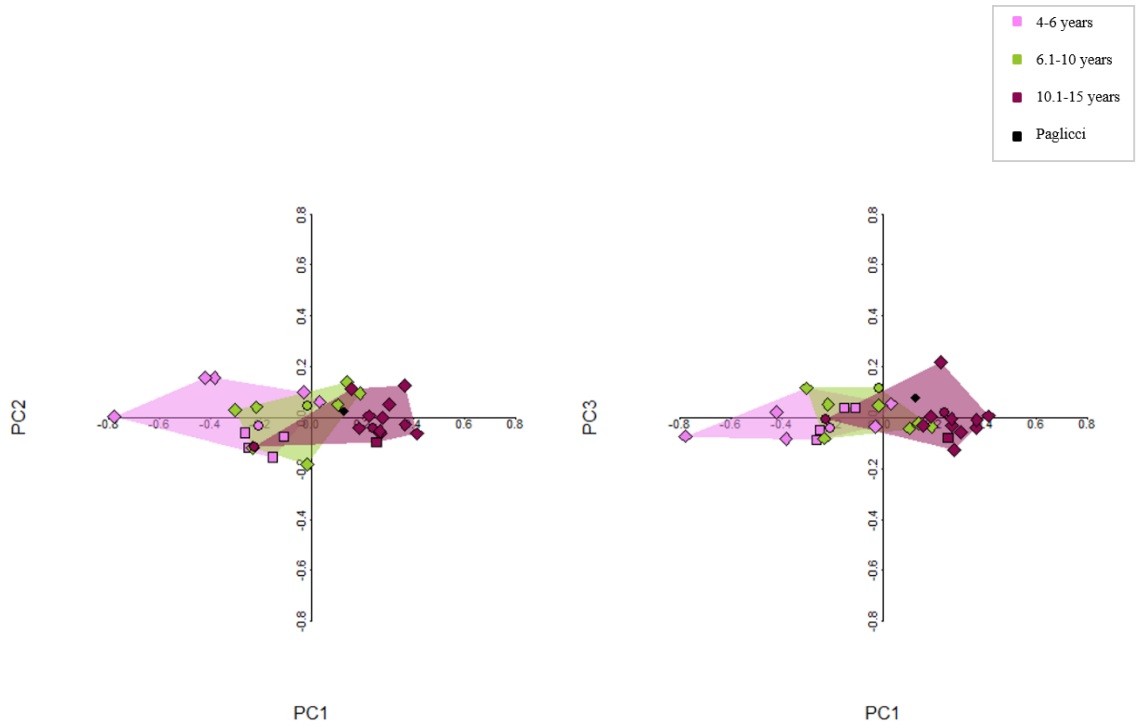

Figure 49 - 2D form space plots. The first three PCs do not contribute in separate the age groups. Individuals from Bologna, for which sex was known, are represented by circles (males) and squared symbols (female). Diamonds represent the archaeological samples The black point represents Paglicci individual.

Trochlea

The first three PCs account for the 74.4% of the total variance (Figure 50) and do not contribute in separating the age groups. PC1 (58.8%) account for a small and not elongated trochlea along negative values, with an almost flat profile, due to the only hinted medial and lateral rims, and a smooth posterior margin, which changes along positive values, with a great increase in antero-posterior elongation of the surface, higher lateral and medial rims, increase concavity of the surface and a great increase in trochlear curvature. The anterior and posterior margins are more defined. PC2 (11.9%) and PC3 (8.6%) both capture slight changes in trochlear curvature. Shapiro-Wilk normality test show that only PC2 scores were not normally distributed (PC:1W = 0.95748, p-value = 0.2191; PCs2:W = 0.93436, p-value = 0.04667; PC3:W = 0.98688, p-value = 0.9527). Significant differences between groups are present among PC1 scores (ANOVA: Df = 2, F = 23.6, p-value = 6.8e-07), while PC2 (chi-squared = 0.61617, df = 2, p-value = 0.7349) and PC3 (df = 2, F-test = 0.56, p-value = 0.5). Tukey's post-hoc test results are described in Table 40. Pearson correlation test highlight that PC1 is highly correlated with size, describing ontogenetic allometry morphological variations (r = 0.91; p-value = 4.855e-14).

Table 40 – Tukey's post-hoc test results for PC1

	diff	lwr	upr	p adj
4-6years vs 6.1-10 years	0.06	0.001	0.129	**0.042**
10.1-15 years vs 4-6years	0.15	0.098	0.209	**0.000**
10.1-15 years vs 6.1-10 years	0.08	0.026	0.148	**0.003**

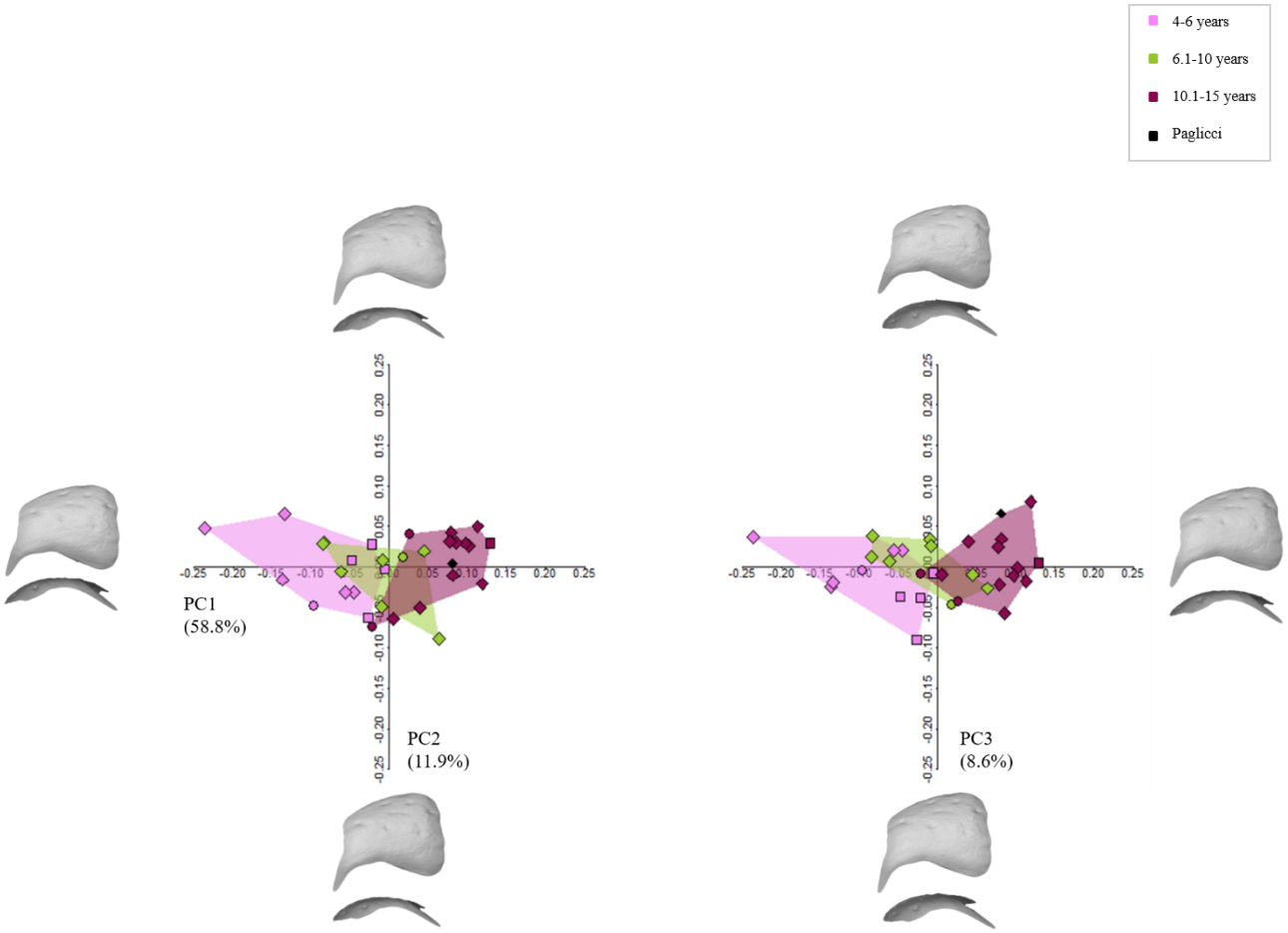

Figure 50 - 2D shape space plots. Individuals from Bologna, for which sex was known, are represented by circles (males) and squared symbols (female). Diamonds represent the archaeological samples The black point represents Paglicci individual.

Form space

When size is included, the first three PCs account for the 93.8% of the total variance (Figure 51), clearly separating the oldest group from the youngest ones. PC1 (89.5%) captures all the size information, while PC2 (2.4%) and PC3 (1.8%) describe minimal shape differences. Shapiro-Wilk normality test shows that only PC2 scores were not normally distributed (PC1: W = 0.97172, p-value = 0.5481; PC2: W = 0.90696, p-value = 0.009357; PC3: W = 0.96912, p-value = 0.4755). ANOVA shows significant differences among PC1 scores (df = 2, F-test = 49.6, p-value 4.3e-10), while differences between groups along PC2 (chi-squared = 1.0975, df = 2, p-value = 0.5777) and PC3 (df = 2, F-test = 1.17, p-value = 0.3) are not significant. Tukey's post-hoc test results are shown in Table 41. PC1 is highly correlated with size (Pearson, r = 0.98 p-value = < 2.2e-16).

Table 41 – Tukey's post-hoc test results for PC1

	diff	lwr	upr	p adj
4-6years vs 6.1-10 years	0.05	0.00	0.09	**0.025**
10.1-15 years vs 4-6years	0.09	0.05	0.12	**0.000**
10.1-15 years vs 6.1-10 years	0.03	-0.00	0.08	0.078

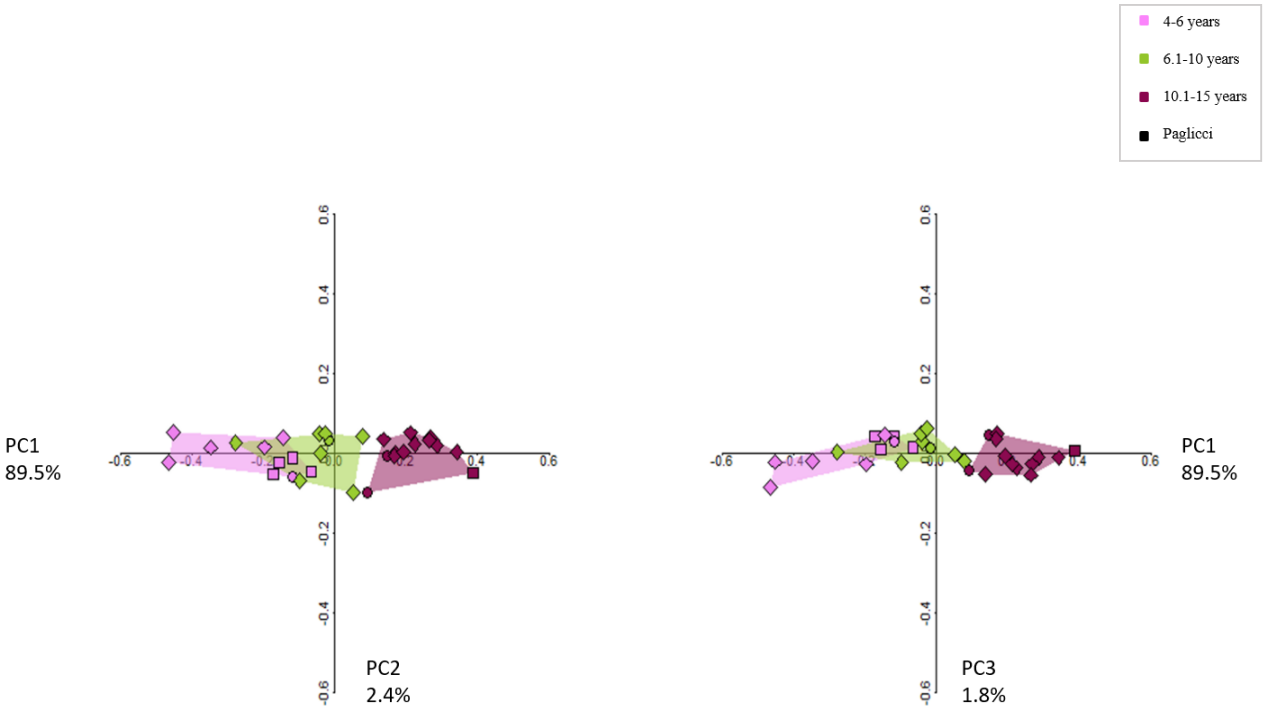

Figure 51 – 2D form space plot. The oldest group is well separated from the youngest ones. Individuals from Bologna, for which sex was known, are represented by circles (males) and squared symbols (female). Diamonds represent the archaeological samples The black point represents Paglicci individual.

4.3.2. Internal morphology

Mean values for age classes are listed in Table 42 (individual's values are listed in Table 43-44) and represented in Figures 52-54. At about 4.1-6 years old, the trabecular architecture shows lower BV/TV values than in the oldest age groups, with thinner trabeculae which are more densely packed between them than in the oldest age groups. The highest average BV/TV values are in the age range 6.1-10 years. The number of the trabeculae decreases between 6.1-10 years, with an increase of spacing and thickness. After 10.1 years, talar architecture shows less and thicker trabeculae, while the spacing decreases again. BV/TV values increases, with different magnitude in the different talar areas. Between 4.1 and 6 years, BV/TV values are relatively low, with higher values in the trochlea, superior and most distal part of the head, posterior calcaneal facet and lateral malleolar process. Between 6.1 and 10 years, the pattern is similar, with different magnitude, i.d. higher values. After 10 years, BV/TV values are the highest in almost all the talar body, except for the medial and inferior part of the head, most distal part of the anterior calcaneal facet, and postero-lateral part of the trochlea. DA is more stable, showing lower values in the first age group, specifically at about 4.1-6 years of age. Then, values slightly increase until they reach a plateau, and remain stable until 10.1-15, when they slightly decrease (Figure 55-57).

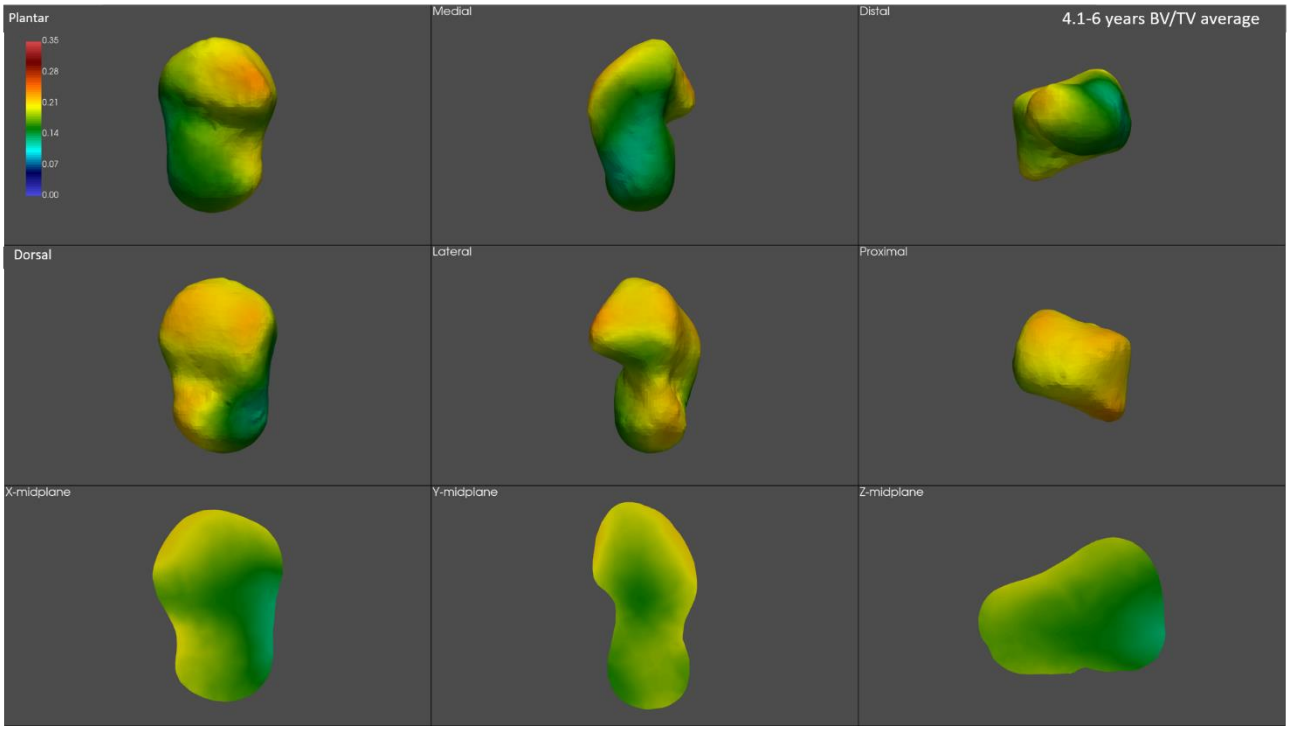

Figure 52 - BV/TV average of the 4.1-6 years-old group. Warm colors represent high values

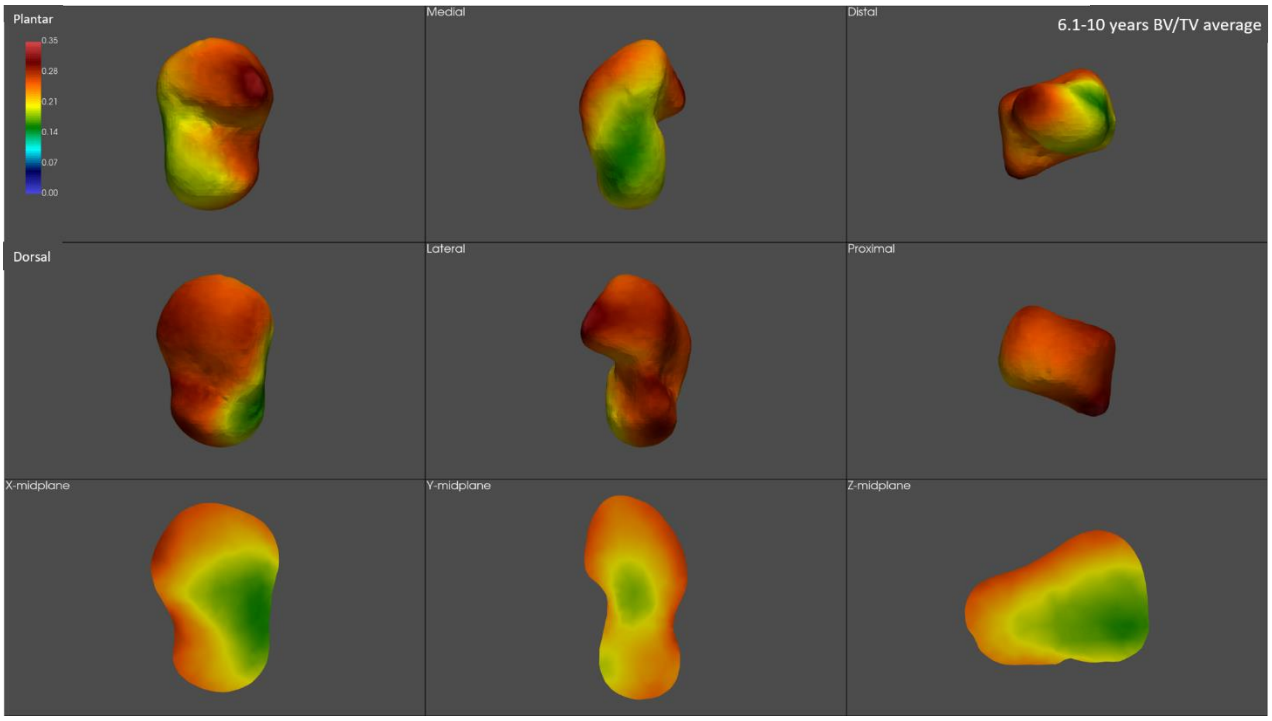

Figure 53 - BV/TV average of the 6.1-10 years-old group. Warm colors represent high values

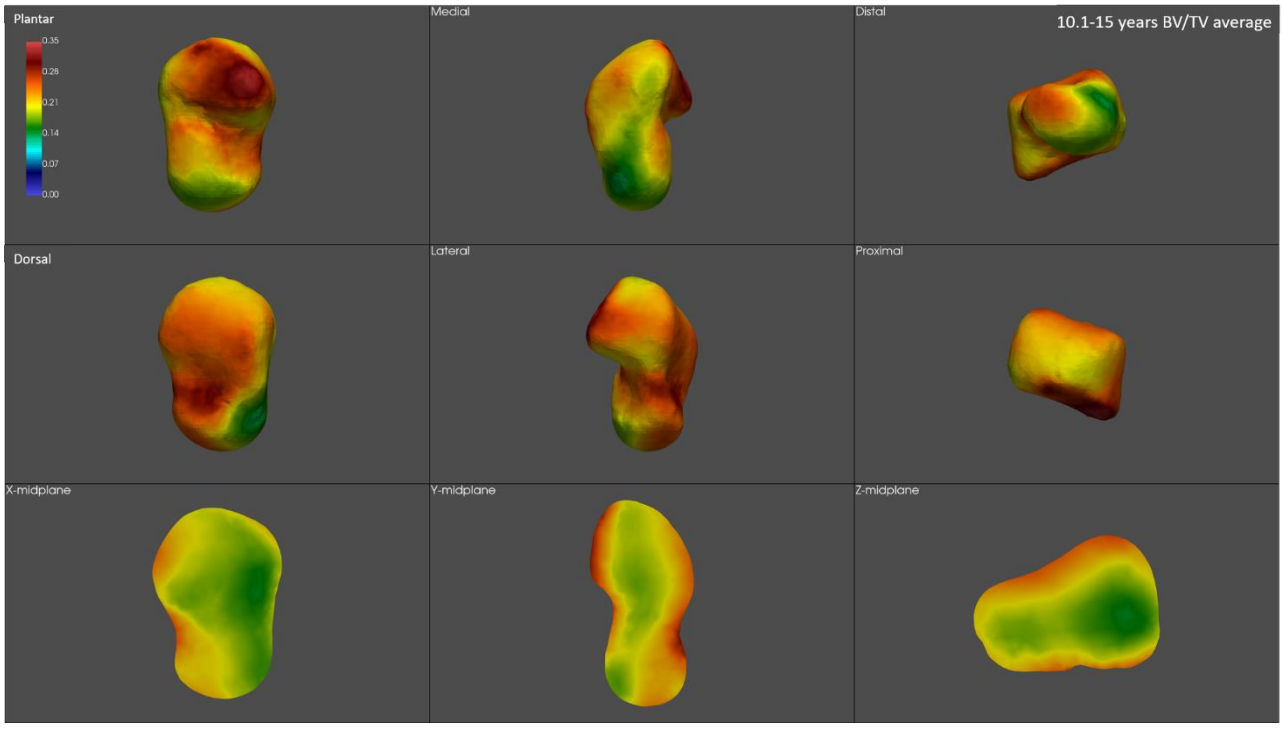

Figure 54 - BV/TV average of the 10.1-15 years-old group. Warm colors represent high values

Table 42 – Mean age-groups values

Age Class	BVTV	DA	Tb.N	Tb.Sp	Tb.Th
4.1-6 years	17.79	0.23	1.20	0.65	0.20
6.1-10 years	22.84	0.23	1.15	1.15	0.23
10.1-15 years	21.29	0.22	1.05	0.71	0.25

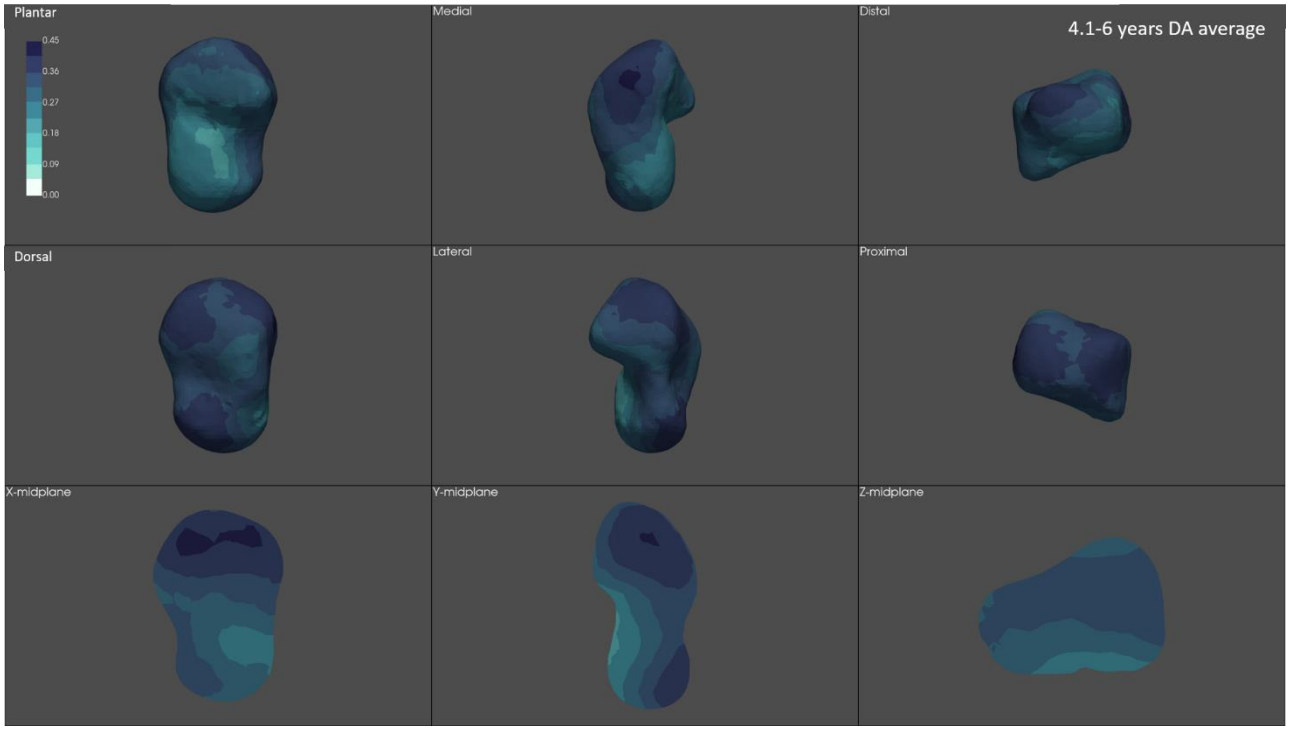

Figure 55 - 4.1-6 years group DA average. Darker colors represent high values

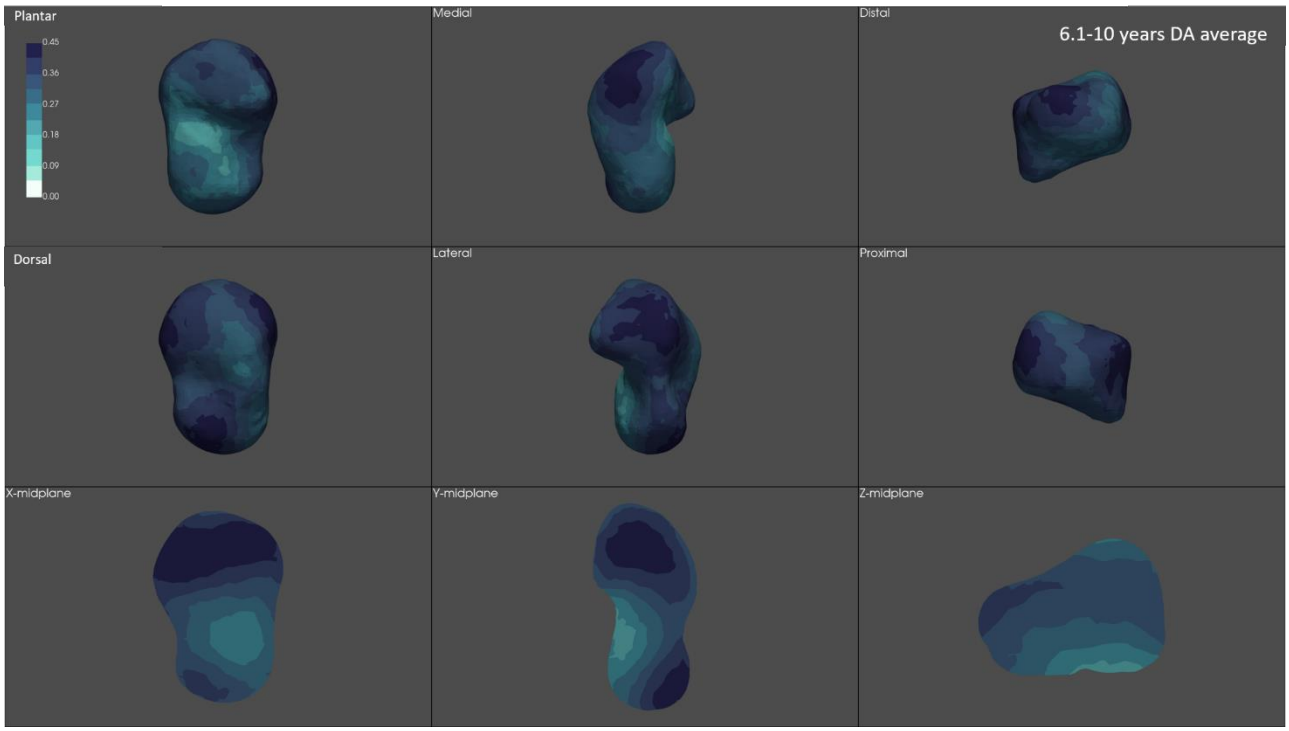

Figure 56 - 6.1-10 years group DA average. Darker colors represent high values

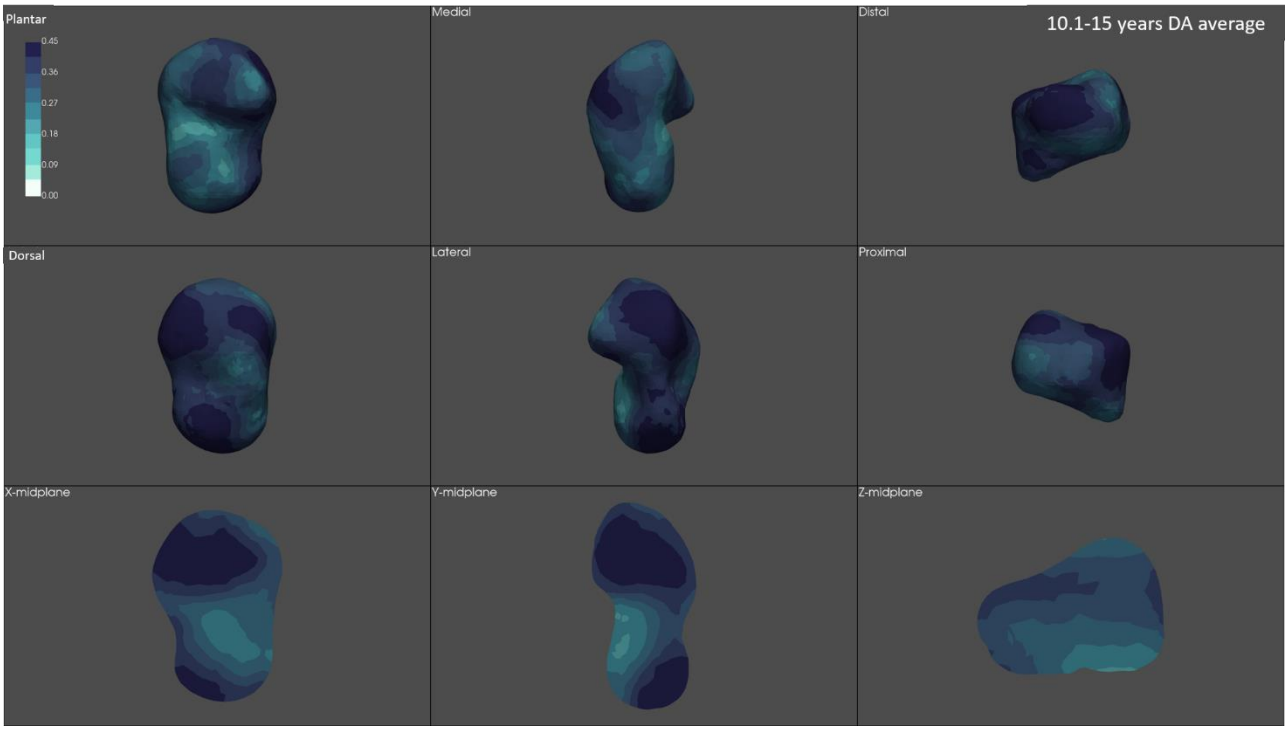

Figure 57 - 10.1-15 years group DA average. Darker colors represent high values

Paglicci juvenile shows a similar DA pattern and magnitude as the other individuals of the same age, i.e. 10.1-15 years; BV/TV values reach the highest values in the lateral malleolar surface, most distal part of the head, and posterior calcaneal surface, and lower values in the trochlea surface. The lowest BV/TV is found in the medial side and anterior subtalar facet (Figure 58)

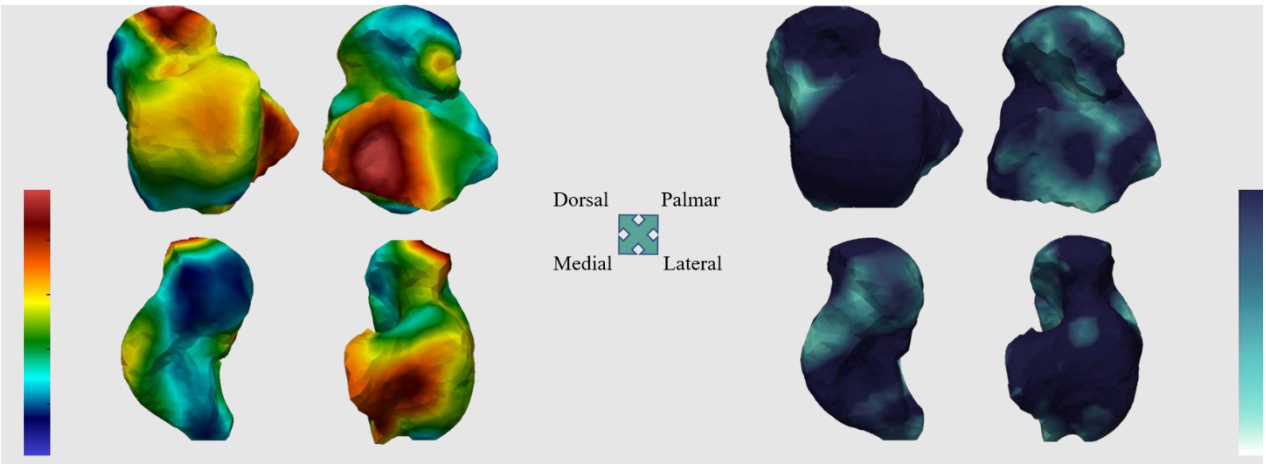

Figure 58 - BV/TV (left) and DA colormaps of the juvenile Upper Palaeolithic individual from Grotta di Paglicci (Italy). BV/TV and DA values are in lines with the age group 10.1-15.

T-test for individual points in the pointclouds showed that there are significant differences between age mean age classes. Results showed that BV/TV differs significantly between the first two age groups (4.1-6 vs 6.1-10 years, Figure 59) in the lateral side and part of the lateral portion of the head, lateral portion of the trochlea and lateral malleolar, with higher values in almost all the significantly-different-areas in the 6.1-10 years group

(yellow-marked areas in the picture) while between the first group and the 10.1-15 years-cohort (Figure 60). No significant differences have been found between the two oldest classes.

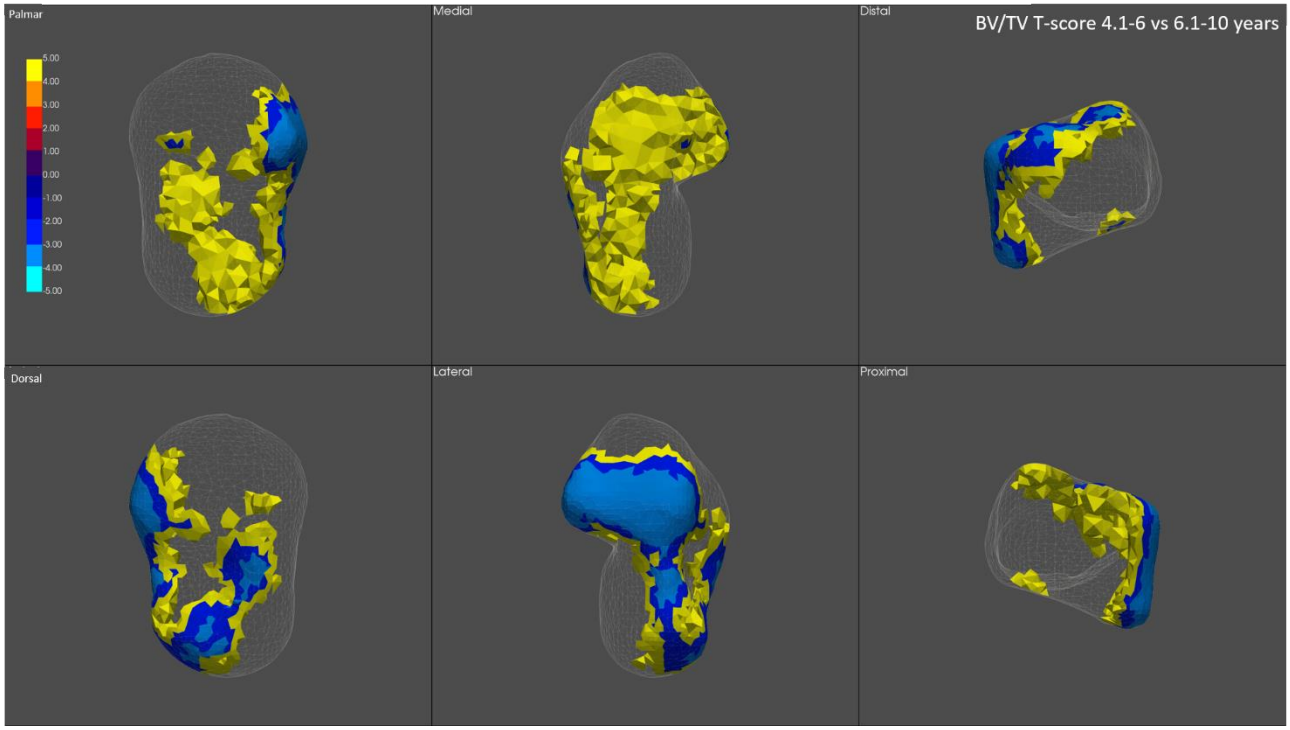

Figure 59 - BV/TV T-Scores. Yellow indicates the higher significant values in the youngest age group, while blue represents the higher values in the oldest group, in this comparison. Youngest individuals have higher BV/TV values in the lateral side of the talus and trochlea, and in the neck and lateral head, which significantly increase particularly in the lateral malleolar process and lateral part of the head in the 6.1-10 years group.

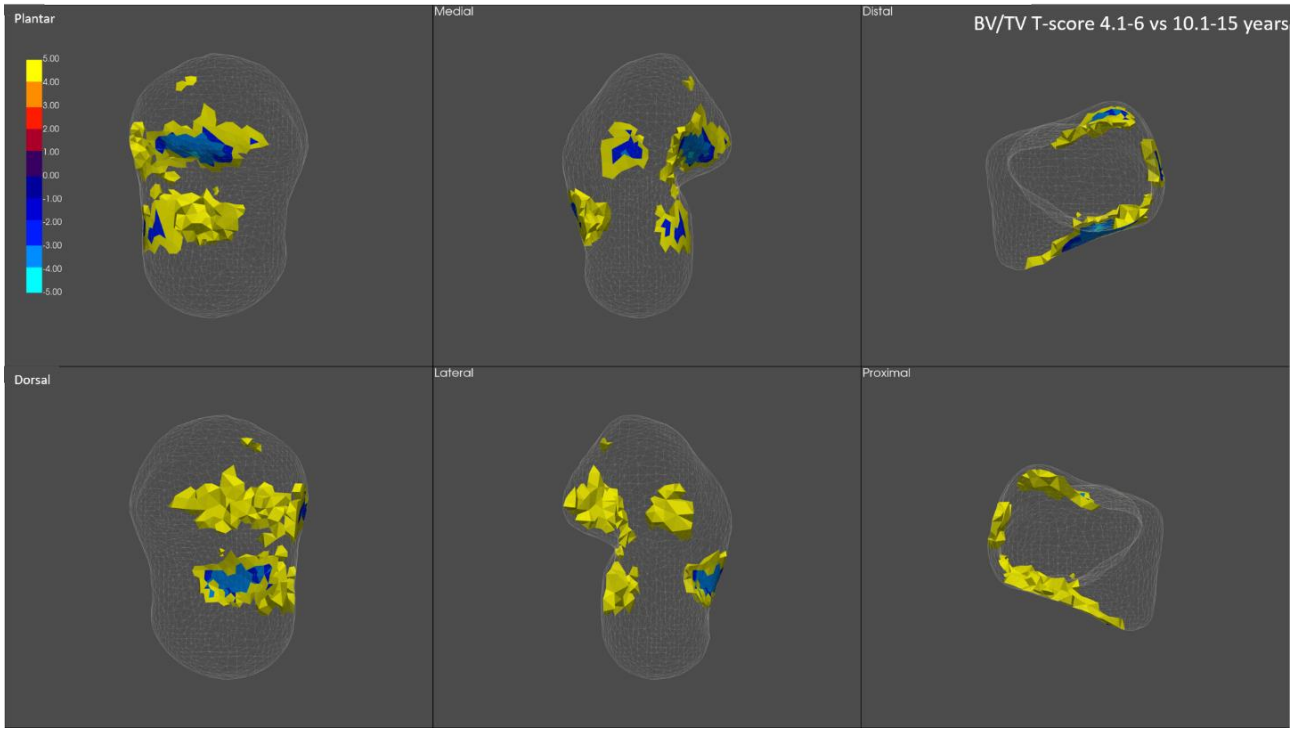

Figure 60 - BV/TV T-Scores. Yellow indicates the higher significant values in the youngest age group, while blue represents the higher values in the oldest group, in this comparison.

For the DA, T-test scores showed significant results among age classes. In particular, the first group significantly differs from all the other age groups, in particular in the lateral side of the trochlea (vs 6.1, Figure 58), lateral and most plantar portion of the trochlea (vs 10.1-15). Significant differences emerged also between the groups 6.1-10 vs 10.1-15 years, specifically in the lateral and anterior part of the trochlea. All the significant results of the T-tests are reported in Figures 61-63.

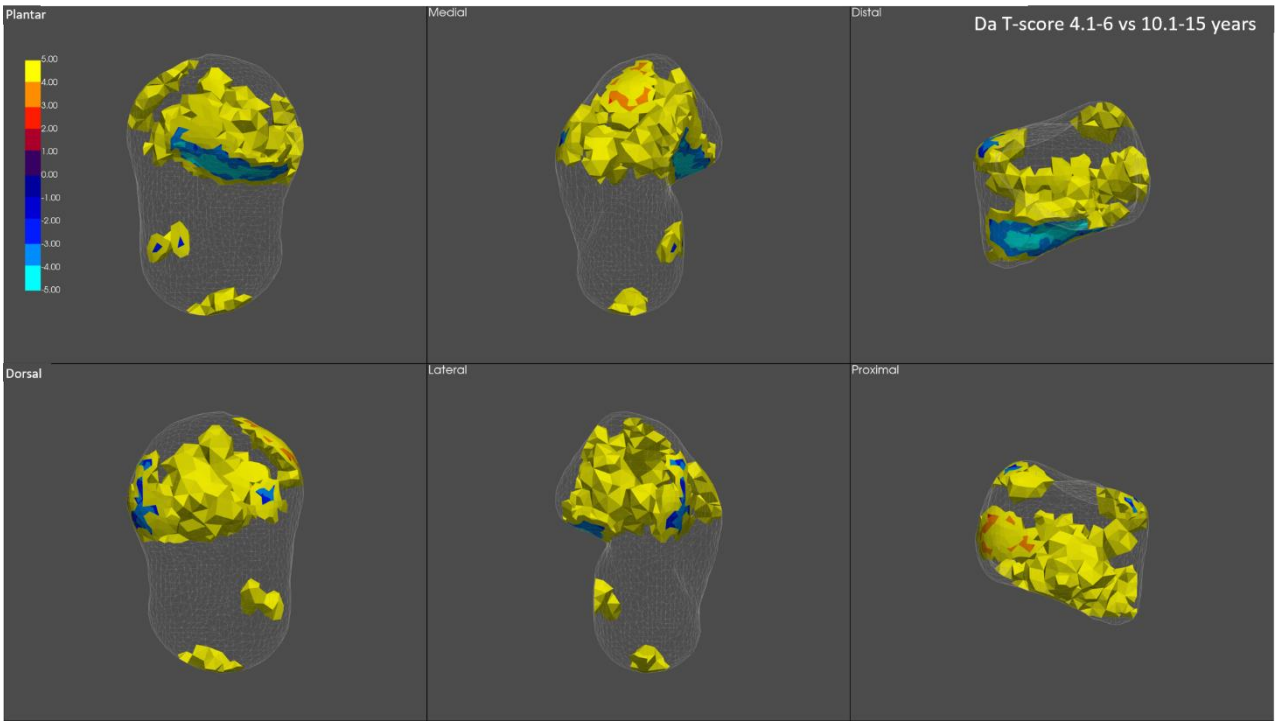

Figure 61 - DA T-Score. Cold colours represent the oldest age group in each comparison. T-test results for the DA show that DA is significantly higher in the posterior part of the talus.

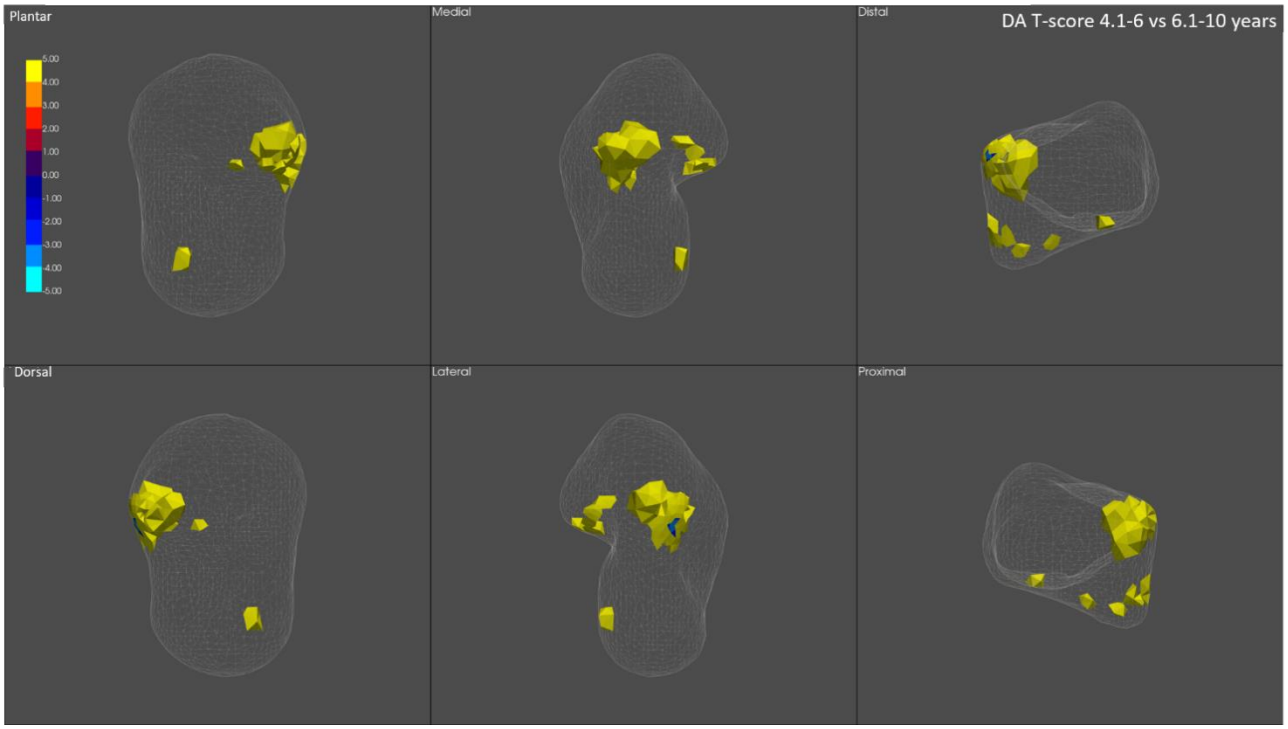

Figure 62 - DA T-Score. Cold colours represent the oldest age group in each comparison. T-test results for the DA show that DA is significantly higher in a small portion of the lateral side of the trochlea.

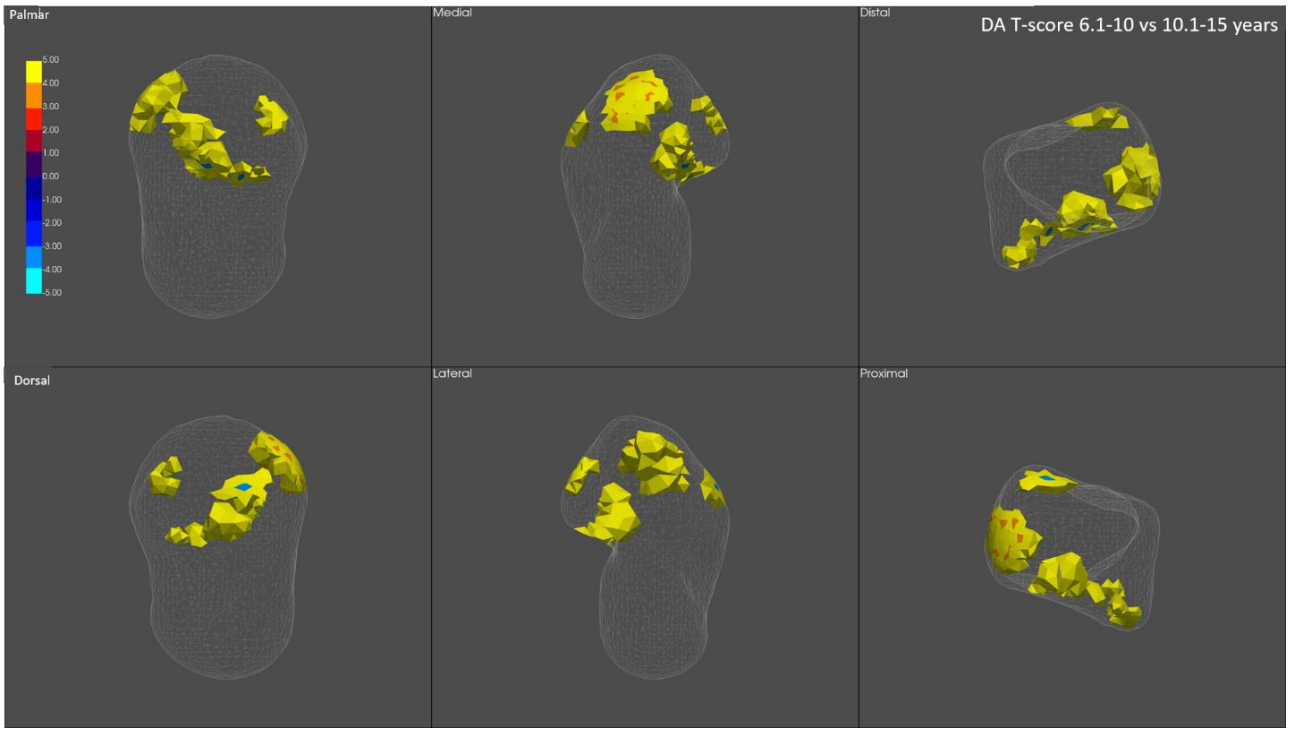

Figure 63 - DA T-Score. Cold colours represent the oldest age group in each comparison. T-test results for the DA show that DA is significantly higher in a small lateral portion of the posterior calcaneal facet, and a small portion on the anterior-medial side of the trochlea.

Table 43 – individuals' averages for BV/TV and DA

Name	Age Class	Age in years	Period	BV/TV (%)	DA
IlokG70	4-6 years	4	13th-15th century	14.09	0.16
IlokG72		4	13th-15th century	15.39	0.17

Paks1166		4	14-16th c.	27.02	0.18
Paks997		4	14-16th c.	16.58	0.26
VeliaT209		4	Roman	13.85	0.30
VeliaT342		4	Roman	15.82	0.22
Paks1846		4.4	14-16th c.	20.88	0.20
PerkataNyuli4263		4.4	10-12th c.	21.43	0.21
BO4_F		5	XX Century	18.5	0.22
BO5_F		5	XX Century	16.22	0.22
NF821012		5	1303 AD	10.1	0.30
PARMA7_F		5	XX Century	22.41	0.26
VeliaT375		5	Roman	17.68	0.22
Paks1164		5.4	14-16th c.	16.7	0.27
VeliaT390		5.4	Roman	15.18	0.23
BO1_M		5.6	XX Century	16.94	0.23
BeliManastirG20		5.7	Early/Middle Neolithic	22.14	0.20
BO6_F		5.8	XX Century	19.61	0.22
BO11_F		6	XX Century	17.55	0.22
PerkataNyuli435		6.4	14-16th c.	16.31	0.28
VeliaT333		6.4	Roman	22.81	0.23
BO6_M		7	XX Century	16.85	0.28
PerkataNyuli1575		7	10-12th c.	24	0.27
BeliManastirG31		7.4	Early/Middle Neolithic	24.37	0.18
Paks1865	6.1-10 years	7.4	14-16th c.	25.51	0.19
PerkataNyuli2123		7.4	10-12th c.	26.66	0.23
PerkataNyuli752		7.4	14-16th c.	18.18	0.20
VeliaT320		7.4	Roman	28.38	0.22
BO40_M		9	XX Century	13.36	0.22
VeliaT138		9.4	Roman	34.78	0.19
BO39_M		11	XX Century	15.35	0.22
BO81_M		11	XX Century	16.21	0.24
PerkataNyuli116		11.4	14-16th c.	17.77	0.24
BeliManastirG4	10.1-15 years	13	Early/Middle Neolithic	32.78	0.21
PARMA10_F		13	XX Century	22.94	0.23
Paks1156		13.4	14-16th c.	20.9	0.24
VeliaT365		13.4	Roman	25.21	0.11
PerkataNyuli734		14	14-16th c.	19.13	0.24
UPPaglicci.	10.1-15 years	12-13	Upper Palaeolithic	21.7	0.25

Table 44 – Individuals' averages for Tb.N, Tb.Sp, and Tb.Th

Name	**Age Class**	**Age in years**	**Period**	**Mean Tb.N**	**Mean Tb.Sp (SD)**	**Mean Tb.Th (SD)**
NF819938		3	1300 AD	1.18	0.68 (0.25)	0.17 (0.05)
IlokG70	4-6 years	3.4	13th-15th century	1.24	0.65 (0.28)	0.16 (0.05)
IlokG72		3.4	13th-15th century	1.59	0.49 (0.21)	0.14 (0.04)

Paks1166		4	14-16th c.	0.94	0.79 (0.60)	0.28 (0.08)
Paks997		4	14-16th c.	1.25	0.61 (0.22)	0.19 (0.04)
VeliaT209		4	Roman	1.11	0.70 (0.28)	0.20 (0.05)
VeliaT342		4	Roman	1.15	0.67 (0.26)	0.20 (0.05)
Paks1846		4.4	14-16th c.	1.07	0.68 (0.25)	0.25 (0.07)
PerkataNyuli4263		4.4	10-12th c.	1.15	0.62 (0.21)	0.25 (0.09)
BO4_F		5	XX Century	1.23	0.62 (0.28)	0.19 (0.06)
BO5_F		5	XX Century	1.29	0.61 (0.25)	0.17 (0.05)
NF821012		5	1303 AD	1.01	0.81 (0.34)	0.17 (0.05)
PARMA7_F		5	XX Century	1.22	0.60 (0.26)	0.22 (0.07)
VeliaT375		5	Roman	1.27	0.60 (0.20)	0.19 (0.04)
Paks1164		5.4	14-16th c.	1.24	0.61 (0.24)	0.19 (0.04)
VeliaT390		5.4	Roman	0.96	0.81 (0.31)	0.23 (0.07)
BO1_M		5.6	XX Century	1.02	0.79 (0.39)	0.19 (0.06)
BeliManastirG20		5.7	Early/Middle Neolithic	1.25	0.60 (0.24)	0.20 (0.08)
BO6_F		5.8	XX Century	1.49	0.50 (0.20)	0.17 (0.05)
BO11_F		6	XX Century	1.27	0.60 (0.25)	0.19 (0.06)
PerkataNyuli435		6.4	14-16th c.	1.07	0.74 (0.33)	0.20 (0.03)
VeliaT333		6.4	Roman	1.08	0.68 (0.28)	0.24 (0.06)
BO6_M		7	XX Century	1.29	0.60 (0.23)	0.18 (0.05)
PerkataNyuli1575		7	10-12th c.	0.98	0.76 (0.41)	0.26 (0.09)
BeliManastirG31	6.1-10 years	7.4	Early/Middle Neolithic	1.35	0.57 (0.26)	0.17 (0.06)
Paks1865		7.4	14-16th c.	1.01	0.71 (0.33)	0.28 (0.09)
PerkataNyuli2123		7.4	10-12th c.	1.14	0.61 (0.27)	0.26 (0.08)
PerkataNyuli752		7.4	14-16th c.	1.16	0.66 (0.25)	0.21 (0.04)
VeliaT320		7.4	Roman	1.22	0.56 (0.23)	0.26 (0.07)
BO40_M		9	XX Century	1.23	0.65 (0.28)	0.16 (0.04)
VeliaT138.		9.4	Roman	1.14	0.56 (0.23)	0.31 (0.09)
BO39_M		11	XX Century	1.05	0.74 (0.28)	0.21 (0.07)
BO81_M		11	XX Century	1.09	0.71 (0.33)	0.21 (0.08)
PerkataNyuli116		11.4	14-16th c.	1.07	0.73 (0.29)	0.20 (0.04)
BeliManastirG4	10.1-15 years	13	Early/Middle Neolithic	1.13	0.57 (0.22)	0.32 (0.14)
PARMA10_F		13	XX Century	0.89	0.81 (0.36)	0.31 (0.11)
Paks1156		13.4	14-16th c.	1.02	0.72 (0.28)	0.27 (0.09)
VeliaT365		13.4	Roman	1.12	0.65 (0.28)	0.24 (0.08)
PerkataNyuli734		14	14-16th c.	1.04	0.73 (0.28)	0.23 (0.06)
UPPaglicci.	10.1-15 years	12-13	Upper Paleolithic	1.19	0.60 (0.19)	0.24 (0.06)

4.4. Discussion

This work investigates the internal and external morphology of the growing human talus, from about 4-5 years of age to the end of the foot growth period, at about 15 years of age, to observe how talar morphologies changes during the last phases of growth. In the previous chapters, we found out that both morphologies differs greatly during growth at different stages, potentially reflecting the different joint position and load distribution during the last phases of the achievement of an adult-like bipedal locomotion, focusing on the development of the articular surfaces. These results are consistent with previous ontogenetic studies of other skeletal elements, e.g. tibia, calcaneus (Raichlen et al., 2015; Saers, Ryan, & Stock, 2020) and talus (Hellier and Jeffery 2006). In this chapter, the last growth phases are the focus of the investigation. Overall, the results show that there are considerable changes in size of the overall talus, and great changes in shape and orientation of the talar facets. Variations described by negative scores, i.e. the youngest cohort, describe an already functional but still relatively immature shape, with barely visible articular surfaces, which are developing and have already started to rotate minimally. Along positive values, i.e. adolescents, the talar shape shows complete maturation, with all the articular facets and posterior processes well developed. With the great expansion of the talar surfaces, the facet-free space between them greatly reduces. The head, trochlea, and posterior calcaneal facets are now medially oriented, increasing the functional weight transfer through the medial part of the foot during push-off, i.e. the forces which go to the hallux passing through the navicular and cuboid through the calcaneus. There are significant changes in talar shape among age groups. PC1 accounts for ontogenetic allometric changes, and the greatest differences are found between the oldest group and the 6.1-10 years group. In fact, it is possible to notice a continual and progressive growth between the first two cohorts, with the shape changing progressively, but maintaining a similar morphology, while after 10-11 years the growth pace is faster, and the morphological changes are greater, with increase not only in size but in shape and orientation of the talar facets. Even though PC1 does not separate the three groups, which overlaps one another in the morphospace, it is possible to notice a clear separation inside the oldest group, with the youngest individuals, i.e. 10-11 years-old, overlapping with the 6.1-10 years group, highlighting a great increase in size and morphology (i.e. a more mature morphology) around 11-12 years old. At about twelve-thirteen years, in fact, talar shape reaches its adult-like morphology, with the development of the posterior processes and the groove of the flexor hallucis longus. Moreover, even though the most important and biggest changes in foot shape happen during early childhood, considerable changes happen also until late adolescence (Stavlas et al. 2005), and one of the most important modification is the increase in height of the medial longitudinal arch. In fact, even though the medial longitudinal arch develops relatively early during childhood, the foot may appear flat until puberty, and the arch height reaches its normal height during adolescence (Waseda et al. 2014). Waseda and colleagues (2014) found out, in their study based on the foot structure of 10,155 children, that the arch height ratio was almost flat, in both males and females, until 10 years, and then significantly increase between 11 and 13 years. This low-arched foot may be related to a more laxity of the ligaments during childhood, which improves during the late phases of growth (Staheli, Chew, and Corbett 1987), as the ossification process leads to a more stable structure, which is more capable to bear the body weight (Van Boerum and Sangeorzan 2003).

In form space, PC1 is a “growth axis”, capturing all the size increase, which well separates the oldest group (10.1-15 years) from the two youngest cohorts, and differences may be easily explainable by the great increase in talar size, also linked to the puberal growth spurt (Lewis 2007).

When the singular facets are concerned, significant differences among all the three groups are visible, even though they do not help differentiating the age groups in the morphospace. In general, talar facets are all clearly visible from about 5 years, though they grow at different time and pace. The subtalar joints, i.e. anterior and posterior, start developing earlier than the others, and they are more easily seen in the first group, i.e. 4.1-6 years, while the posterior margin of the trochlea and medial malleolar facet develop later, in particular in the posterior margins. The lateral malleolar facet is the latter to develop, and it was not included in the singular facet analysis because it late development would have excluded most of the sample. In general, the adult-like pattern is not reached until 10.1-15 years, when the morphology is adult. Anterior calcaneal facet has a really smooth anterior margin in the youngest individuals, and morphological changes are relative mostly to the anterior-posterior elongation, while the medial facet is not always distinguishable. Navicular facet, and the head, changes in size and orientation along positive scores. PCs clearly separate the oldest group from the others, in form space, describing a clear growth of the head. Medial malleolar facet is visible at around 5 years, showing the greatest increase in size and morphology after 10 years of age, with the development of the trochlear rims and the posterior apex. Significant differences highlight the greatest changes after 10 years of age. Posterior calcaneal facet greatly increase in orientation and shape, becoming more rectangular-like after 10 years, and passing from a flat surface, to a concave one. Significant differences are present between each age group both in shape and form space, denoting a continuous increase in size and shape changes until adolescence. Also the trochlea changes greatly in shape, size, and orientation. The changes here described may be linked to the increase in body weight, which are consistent with previous studies, even though a genetic programmed development is probably still playing a big role (Hellier and Jeffery, 2006). The change in shape of the trochlea could be in part an adaptation, responding plastically to the increase weight received mostly from the tibia: an enlarged surface, and more convex, facilitates the absorption and distribution of forces through the trochlear surfaces. Then, they passed through the trabecular bone and to the posterior calcaneal facet directly to the calcaneus, and forward to the neck, where they are converted in tensile forces and pass to the talonavicular and anterior subtalar joint (Hellier and Jeffery, 2006; Pal and Routal 1998). Forces pass then to the medial side of the foot, during stance and push-off. The change in orientation of the trochlea is thought to be a biomechanical adaptation to better perform its role of receiver and distributor of forces (Hellier and Jeffery, 2006). The talonavicular and posterior calcaneal facets change their orientation to improve the response to the biomechanical demands. To ameliorate the transmission of the forces to the other tarsals, the head must rotate medially and plantarly. As a response, the posterior calcaneal facet rotates medially, to facilitate a more efficient transmission of the forces to the calcaneus, i.e. heel. The posterior subtalar joint experiences the highest loading of the calcaneus. Interestingly, when covariation was tested, trochlea shape changes were significant linked to the shape changes of the navicular, medial malleolar, and posterior calcaneal facet, while the navicular facet shows a strong covariation with the trochlea and anterior calcaneal facet.

Posterior calcaneal facet changes in shape were significantly linked to the medial malleolar facet. These changes highlight the correlation in shape changes of the talar articular facets during growth.

On the other hand, trabecular changes vary between age classes, passing from an architecture with high values of Tb.N and Tb.Sp and thinner struts, to an architecture with lower Tb.N and Tb.Sp values, and thicker struts. BV/TV seems to decrease after 5 years of age, probably also due to the increase in bone surface with growth. While BV/TV changes during this timeframe, DA is relatively stable, with small variations. The highest BV/TV values were found in the lateral side of the talar head, trochlea, and posterior calcaneal facet. In the trochlea, values are higher in the medial and lateral sides, and lower in the central part of the surface, partially confirming the predictions, even though magnitude changes a little with age, with a fluctuation which shown BV/TV values decreasing after 6 years of age and then increase suddenly after 11 years. At heel strike, all of the load is initially transmitted from the posterior part of the trochlear surface to the posterior subtalar joint (Pal and Routal 1998). During midstance, loadings are transmitted to the heel through the posterior and anterior calcaneal facets, and distally towards the navicular through the talar head. From heel rise to toe-off the weight of the body is transmitted to the forefoot while the talar neck and head are subjected to tensile forces. During heel rise, forces from the triceps surae are exerted on the calcaneus producing a proximal/anterior force on the plantar side of the talus (Pal and Routal 1998). The lowest BV/TV values are found in the medial side and anterior calcaneal facet. Changes captured in the trabecular structure after the age of 6 are supposedly linked to the changes in body size and proportions, i.e. allometry. After adolescence growth spurt started, at around 10-12 years, body mass and bone deposition increase at faster rates and socially, adolescent are supposed to participate in adult activities and work. Trabecular structures is supposed to follow allometric scaling patterns (Shaw and Ryan 2012; Saers, Ryan, and Stock 2019b), expecting an increase in BV/TV. Growth spurt onset changes depending on sex: females are supposed to increase growth rates earlier than boys, at about 10 years, while growth spurt in boys commences at about 12 years (Lewis 2007). We hypothesized that DA will have increase slightly in the second group, after around 7-8 years of age. Indeed, we found out that DA reached a plateau in the first age group. Though, as supposed, the highest values are reached in the head and posterior part of the talar body. BV/TV increases reaching the highest values in the second age group, i.e. 6.1-10 years, and then slightly decreases. We hypothesized that the highest magnitude was expected in the lateral side of the trochlea and head, and we were able to see this pattern in our results. Hence our hypotheses were supported.

Taken together, these results may help understanding talar growth, and how it adapts to changes in locomotion behaviours and increase in body mass. Though, there are few drawbacks in this study. First of all, it was not possible to explore dimorphic differences in growth, which are known to exist. Second of all, the sample was not homogeneous, being composed by different populations not represented in the same way. This make it impossible trying to find differences linked to mobility or substrate. Estimated age at death may not be accurate, and the combination of more populations prevent to make more accurate assumptions. This problem is common, when using archaeological populations.

Nonetheless, this is the first study to explore the late talar growth by examining both internal and external morphologies. Results may help to better understand talar plasticity, helping in the interpretations of adult

human tali. Future study may consider to deepen this investigation by adding new known populations, i.e. with sex and age known, to explore the dimorphism linked to the puberty growth spurt.

Chapter Five
Dissertation conclusion and future directions

The aim of this dissertation was to explore talar changes during growth linked to the acquisition of bipedal locomotion, focusing on the functional adaptation in the human talus, by means of two different methods: geometric morphometrics and trabecular biomechanics. The use of both methods enables the investigation of the changes in the external morphology and in the internal architecture. In addition, this work uniquely combines innovative methods, such as the whole bone trabecular analysis and, in particular, the statistical approach which permits to statistically compared all the bone areas among different age groups. This is the first study to investigate both the internal and external morphologies in the human talus in an ontogenetic sample, and the first to take into account the three-dimensional trabecular structure of the whole developing human talus.

The difficulties in finding a good sample study, i.e. numerous individuals belonging to few populations, with known age at death and homogeneously represented among age-groups are common, when archaeological samples are concerned. Moreover, even though a plastic response of the articular facets has been hypothesized, experimental studies are needed to accurately discern plastic adaptation from programmed development.

Nevertheless, this work contribute to a growing corpus of data pointing out that the analysis of the developing human bones has a terrific potential to help anthropologists to paint more detailed picture of the past. This work may help untangle how the bone responds to stress during growth, thus helping to interpret fossil foot bones. In fact, obligate bipedalism is a hallmark of human species, yet its early appearance and development is still debated. Fossil record provides a complex picture of the evolution of the locomotion, and foot bones are of paramount importance to complete this complex mosaic. External morphology is more strictly related to genetics but, together with the analysis of trabecular bone architecture, can be of great help in the interpretation of the changes linked to the development of bipedal locomotion, creating a framework which can be helpful in interpreting the fossil record. Trabecular bone structure, has already proven its strong relationship with mobility, even though it is influenced by numerous other variables.

In the second chapter, the analysis of the postnatal growth showed that the changes are linked to the development of bipedalism, demonstrating that it would be possible to discern information about behaviour and locomotion through the analysis of both the internal and external morphology of juvenile tali.

In the third chapter, I focused on the differences between unloaded (or minimally loaded) talar morphologies, and loaded talar morphology, with the aim of capture the differences between the pre- and post-locomotion morphologies. Both the structure, internal and external, showed a different and more adapted architecture, with an external shell still immature but ready to be loaded, i.e. with the development and a slight medial rotation of the head, and the internal architecture promptly responds to the load, mainly changing the orientation of the trabeculae (i.e. increasing in anisotropy) and in their number, thickness, and spacing.

In the last analysis, the study focused on the development of talar articular facets, and the last stage of growth, highlighting the plasticity of the talus while coping with the increase in body weight.

This work may constitute a framework for comparisons with the fossil record. Future directions will consider the inclusion of other populations, to better explore differences among growth phases in different cultures, and will consider the investigation of other tarsal bones, to map the whole foot. Moreover, future investigation will comprise the study of different species, including different human and non-human species.

Literature Cited

Abitbol, M M. 1993. “Quadrupedalism and the Acquisition Bipedalism in Human Children Of,” 189–95.

Acquaah, Frank, Katharine A. Robson Brown, Farah Ahmed, Nathan Jeffery, and Richard L. Abel. 2015. “Early Trabecular Development in Human Vertebrae: Overproduction, Constructive Regression, and Refinement.” *Frontiers in Endocrinology* 6 (MAY): 1–9. https://doi.org/10.3389/fendo.2015.00067.

Adams, D C, M L Collyer, A Kaliontzopoulou, and E Sherratt. 2018. “Geomorph: Software for Geometric Morphometric Analyses, R Package v. 3.0. 6.” Vienna, Austria: R Foundation.

Adams, Dean C, and Erik Otárola-Castillo. 2013. “Geomorph: An R Package for the Collection and Analysis of Geometric Morphometric Shape Data.” *Methods in Ecology and Evolution* 4 (4): 393–99.

Adolph, Karen E., and Anthony M. Avolio. 2000. “Walking Infants Adapt Locomotion to Changing Body Dimensions.” *Journal of Experimental Psychology: Human Perception and Performance* 26 (3): 1148–66. https://doi.org/10.1037/0096-1523.26.3.1148.

Adolph, Karen E., Beatrix Vereijken, and Mark A. Denny. 1998. “Learning to Crawl.” *Child Development* 69 (5): 1299–1312. https://doi.org/10.1111/j.1467-8624.1998.tb06213.x.

Adolph, Karen E., Beatrix Vereijken, and Patrick E. Shrout. 2003a. “What Changes in Infant Walking and Why.” *Child Development* 74 (2): 475–97. https://doi.org/10.1111/1467-8624.7402011.

Adolph, Karen E, Bennett I Bertenthal, Steven M Boker, Eugene C Goldfield, Eleanor J Gibson, and Eleanorj Gibson. 1997. “Learning in the Development of Infant Locomotion” 62 (3).

Assaiante, C., and B. Amblard. 1993. “Ontogenesis of Head Stabilization in Space during Locomotion in Children: Influence of Visual Cues.” *Experimental Brain Research* 93 (3): 499–515. https://doi.org/10.1007/BF00229365.

Barak, Meir M., Daniel E. Lieberman, and Jean Jacques Hublin. 2011a. “A Wolff in Sheep’s Clothing: Trabecular Bone Adaptation in Response to Changes in Joint Loading Orientation.” *Bone* 49 (6): 1141–51. https://doi.org/10.1016/j.bone.2011.08.020.

Barak, Meir M., Daniel E. Lieberman, David Raichlen, Herman Pontzer, Anna G. Warrener, and Jean Jacques Hublin. 2013. “Trabecular Evidence for a Human-like Gait in Australopithecus Africanus.” *PLoS ONE* 8 (11). https://doi.org/10.1371/journal.pone.0077687.

Barak, Meir M. 2019. “Bone Modeling or Bone Remodeling: That Is the Question.” *American Journal of Physical Anthropology*. https://doi.org/10.1002/ajpa.23966.

Barnes, H. V. 1975. “Physical Growth and Development during Puberty.” *Medical Clinics of North America* 59 (6): 1305–17. https://doi.org/10.1016/S0025-7125(16)31931-9.

Belcastro, M. G., B. Bonfiglioli, M. E. Pedrosi, M. Zuppello, V. Tanganelli, and V. Mariotti. 2017. “The History and Composition of the Identified Human Skeletal Collection of the Certosa Cemetery (Bologna, Italy, 19th–20th Century).” *International Journal of Osteoarchaeology* 27 (5): 912–25. https://doi.org/10.1002/oa.2605.

Bell, M A, and N A Fox. 1998. “Crawling Experience Is Related to Changes in Cortical Organization during Infancy: Evidence Form EEG Coherence.” *Developmental Psychology* 29 (551–561): 551–61.

Bennett, Matthew R., John W.K. Harris, Brian G. Richmond, David R. Braun, Emma Mbua, Purity Kiura, Daniel Olago, et al. 2009. “Early Hominin Foot Morphology Based on 1.5-Million-Year-Old Footprints from Ileret, Kenya.” *Science* 323 (5918): 1197–1201. https://doi.org/10.1126/science.1168132.

Berger, Wiltrud, Eckart Altenmueller, and Vincent Dietz. 1984. “Normal and Impaired Development of Children’s Gait.” *Human Neurobiology* 3 (3): 163–70.

Bernstein, Ira M., Jeffrey D. Horbar, Gary J. Badger, Arne Ohlsson, and Agneta Golan. 2000. “Morbidity and Mortality among Very-Low-Birth-Weight Neonates with Intrauterine Growth Restriction.” *American Journal of Obstetrics and Gynecology* 182 (1): 198–206. https://doi.org/10.1016/S0002-9378(00)70513-8.

Bertenthal, Bennett I, Joseph J Campos, and Karen Caplovitz Barrett. 1984. “Self-Produced Locomotion.” In *Continuities and Discontinuities in Development*, 175–210. Springer.

Bertsch, Carola, Heidi Unger, Winfried Winkelmann, and Dieter Rosenbaum. 2004. “Evaluation of Early Walking Patterns from Plantar Pressure Distribution Measurements. First Year Results of 42 Children.” *Gait and Posture* 19 (3): 235–42. https://doi.org/10.1016/S0966-6362(03)00064-X.

Bezdek, James C, Richard J Hathaway, Michael J Sabin, and William T Tucker. 1987. “Convergence Theory for Fuzzy C-Means: Counterexamples and Repairs.” *IEEE Transactions on Systems, Man, and Cybernetics* 17 (5): 873–77.

Boerum, Drew H Van, and Bruce J Sangeorzan. 2003. “Biomechanics and Pathophysiology of f Lat Foot.” *Foot and Ankle Clinics* 8: 419–30. https://doi.org/10.1016/S1083-7515(03)00084-6.

Bonjour, Jean-Philippe, Thierry Chevalley, Serge Ferrari, and Rene Rizzoli. 2012. “Chapter 9 - Peak Bone Mass and Its Regulation.” In *Pediatric Bone (Second Edition)*, edited by Francis H Glorieux, John M Pettifor, and Harald Jüppner, Second Edi, 189–221. San Diego: Academic Press. https://doi.org/https://doi.org/10.1016/B978-0-12-382040-2.10009-7.

Bookstein, Fred L. 1997. “Landmark Methos for Forms without Lendmarks: Morphometrics of Group Difference in Outline Shape.” *Medical Image Analysis* 1 (3): 225–43. http://www.ncbi.nlm.nih.gov/pubmed/9873908.

Bookstein 1991. *Morphometric Tools for Landmark Data: Geometry and Biology*. Cambridge University Press.

Boyer, Doug M, Gabriel S Yapuncich, Jared E Butler, Rachel H Dunn, and Erik R Seiffert. 2015. “Evolution of Postural Diversity in Primates as Reflected by the Size and Shape of the Medial Tibial Facet of the Talus.” *American Journal of Physical Anthropology* 157 (1): 134–77. https://doi.org/10.1002/ajpa.22702.

Brenière, Y, and B Bril. 1988. “[Why Do Children Walk When Falling down While Adults Fall down in Walking?].” *Comptes Rendus de l’Academie Des Sciences. Serie III, Sciences de La Vie* 307 (11): 617–22. https://europepmc.org/abstract/med/3142643.

Bril, Blandine, and Yvon Brenière. 1991. “Timing Invariances in Toddlers’ Gait.” *Advances in Psychology* 81 (C): 231–44. https://doi.org/10.1016/S0166-4115(08)60768-2.

Bril, Blandine, and Annick Ledebt. 1998. “Head Coordination as a Means to Assist Sensory Integration in Learning to Walk.” *Neuroscience and Biobehavioral Reviews* 22 (4): 555–63. https://doi.org/10.1016/S0149-7634(97)00044-4.

Burnett, Carolyn N., and Ernest W. Johnson. 1971. “Development of Gait in Childhood. Part I: Method.” *Developmental Medicine & Child Neurology* 13 (2): 196–206. https://doi.org/10.1111/j.1469-8749.1971.tb03245.x.

Byers, S., A. J. Moore, R. W. Byard, and N. L. Fazzalari. 2000. “Quantitative Histomorphometric Analysis of the Human Growth Plate from Birth to Adolescence.” *Bone* 27 (4): 495–501. https://doi.org/10.1016/S8756-3282(00)00357-4.

Campos, Joseph J, Bennett I Bertenthal, and Rosanne Kermoian. 1992. “Early Experience and Emotional Development: The Emergence of Wariness of Heights.” SAGE Publications Sage CA: Los Angeles, CA.

Carlson, Kristian J., and Stefan Judex. 2007. “Increased Non-Linear Locomotion Alters Diaphyseal Bone Shape.” *Journal of Experimental Biology* 210 (17): 3117–25. https://doi.org/10.1242/jeb.006544.

Carter, D R, and G S Beaupre. 2001. “Skeletal Form and Function.” Cambridge: Cambridge University Press. 1Validity of the Sts.

Carter, Dennis R. 1984. “Mechanical Loading Histories and Cortical Bone Remodeling.” *Calcified Tissue International* 36 (1 Supplement). https://doi.org/10.1007/BF02406129.

Chagas, P S C, M C Mancini, S T Fonseca, and T B C Soares. 2006. “Neuromuscular Mechanisms and Anthropometric Modifications in the Initial Stages of Independent Gait” 24: 375–81. https://doi.org/10.1016/j.gaitpost.2005.11.005.

Clark, Jane E., Jill Whitall, and Sally J. Phillips. 1988. “Human Interlimb Coordination: The First 6 Months of Independent Walking.” *Developmental Psychobiology* 21 (5): 445–56. https://doi.org/10.1002/dev.420210504.

Colombo, A., N. B. Stephens, Z. J. Tsegai, M. Bettuzzi, M. P. Morigi, M. G. Belcastro, and J.-J. Hublin. 2019. “Trabecular Analysis of the Distal Radial Metaphysis during the Acquisition of Crawling and Bipedal Walking in Childhood: A Preliminary Study.” *Bulletins et Mémoires de La Société d’Anthropologie de Paris* 31 (1–2): 43–51. https://doi.org/10.3166/bmsap-2018-0041.

Cowgill, Libby W, and Rob A Johnston. 2018. “Biomechanical Implications of the Onset of Walking *.” *Journal of Human Evolution* 122: 133–45. https://doi.org/10.1016/j.jhevol.2018.06.003.

Crompton, Robin H., S. K.S. Thorpe, Weijie Wang, R. C. Payne, Russell Savage, Tanya Carey, Peter Aerts, et al. n.d. “The Biomechanical Evolution of Erect Bipedality.”

Cunningham, Craig A., and Sue M. Black. 2009a. “Anticipating Bipedalism: Trabecular Organization in the Newborn Ilium.” *Journal of Anatomy* 214 (6): 817–29. https://doi.org/10.1111/j.1469-7580.2009.01073.x.

Cunningham, Craig A., and Sue M. Black.. 2009b. “Development of the Fetal Ilium - Challenging Concepts of Bipedality.” *Journal of Anatomy* 214 (1): 91–99. https://doi.org/10.1111/j.1469-7580.2008.01005.x.

Cunningham, Craig, Louise Scheuer, and Sue Black. 2016a. *Developmental Juvenile Osteology: Second Edition*. *Developmental Juvenile Osteology: Second Edition*.

Delaunay, Boris. 1934. “Sur La Sphere Vide.” *Izv. Akad. Nauk SSSR, Otdelenie Matematicheskii i Estestvennyka Nauk* 7 (793–800): 1–2.

DeMars, Lily J.D., Nicholas B. Stephens, Jaap P.P. Saers, Adam Gordon, Jay T Stock, and Timothy M Ryan. 2020. “Using Point Clouds to Investigate the Relationship between Trabecular Bone Phenotype and Behavior: An Example Utilizing the Human Calcaneus.” *American Journal of Human Biology*, no. January: 1–16. https://doi.org/10.1002/ajhb.23468.

DeSilva, Jeremy M. 2009. “Functional Morphology of the Ankle and the Likelihood of Climbing in Early Hominins.” *Proceedings of the National Academy of Sciences of the United States of America* 106 (16): 6567–72. https://doi.org/10.1073/pnas.0900270106.

DeSilva, Jeremy M., and Maureen J. Devlin. 2012. “A Comparative Study of the Trabecular Bony Architecture of the Talus in Humans, Non-Human Primates, and Australopithecus.” *Journal of Human Evolution* 63 (3): 536–51. https://doi.org/10.1016/j.jhevol.2012.06.006.

DeSilva, Jeremy M., Kenneth G Holt, Steven E Churchill, Kristian J Carlson, Christopher S Walker, Bernhard Zipfel, and Lee R Berger. 2013. “The Lower Limb and Mechanics of Walking in Australopithecus Sediba.” *Science* 340 (6129): 1232999. https://doi.org/10.1126/science.1232999.

DeSilva, Jeremy, Ellison McNutt, Julien Benoit, and Bernhard Zipfel. 2019. “One Small Step: A Review of Plio-Pleistocene Hominin Foot Evolution.” *American Journal of Physical Anthropology* 168 (July 2018): 63–140. https://doi.org/10.1002/ajpa.23750.

DETENBECK, L E E C, and PATRICK J KELLY. 1969. “Total Dislocation of the Talus.” *JBJS* 51 (2): 283–88.

Dimeglio, Alain. 2001. “Growth in Pediatric Orthopaedics.” *Journal of Pediatric Orthopaedics* 21 (4): 549–55.

DiPietro, Janet A., Katie T Kivlighan, Kathleen A Costigan, Suzanne E Rubin, Dorothy E Shiffler, Janice L Henderson, and Joseph P Pillion. 2010. “Prenatal Antecedents of Newborn Neurological Maturation.” *Child Development* 81 (1): 115–30. https://doi.org/10.1111/j.1467-8624.2009.01384.x.

Drapeau, Michelle S.M., and Elizabeth H. Harmon. 2013. “Metatarsal Torsion in Monkeys, Apes, Humans and Australopiths.” *Journal of Human Evolution* 64 (1): 93–108. https://doi.org/10.1016/j.jhevol.2012.10.008.

Dunmore, Christopher J, Gert Wollny, and Matthew M Skinner. 2018. “MIA-Clustering: A Novel Method for Segmentation of Paleontological Material.” *PeerJ* 2018 (2): 1–18. https://doi.org/10.7717/peerj.4374.

Dunn, Joseph C. 1973. “A Fuzzy Relative of the ISODATA Process and Its Use in Detecting Compact Well-Separated Clusters.”

Einspieler, Christa, Peter B Marschik, and Heinz F.R. Prechtl. 2008. “Human Motor Behavior: Prenatal Origin and Early Postnatal Development.” *Journal of Psychology*. https://doi.org/10.1027/0044-3409.216.3.147.

Eriksen, E. F. 1986. “Normal and Pathological Remodeling of Human Trabecular Bone: Three Dimensional Reconstruction of the Remodeling Sequence in Normals and in Metabolic Bone Disease.” *Endocrine Reviews* 7 (4): 379–408. https://doi.org/10.1210/edrv-7-4-379.

Eriksen, Erik Fink. 2010. “Cellular Mechanisms of Bone Remodeling.” *Reviews in Endocrine and Metabolic Disorders*. https://doi.org/10.1007/s11154-010-9153-1.

Fajardo, Roberto J., Ralph Müller, Rich A. Ketcham, and Matthew Colbert. 2007. “Nonhuman Anthropoid Primate Femoral Neck Trabecular Architecture and Its Relationship to Locomotor Mode.” *Anatomical Record* 290 (4): 422–36. https://doi.org/10.1002/ar.20493.

Farris, Dominic James, Luke A. Kelly, Andrew G. Cresswell, and Glen A. Lichtwark. 2019. “The Functional Importance of Human Foot Muscles for Bipedal Locomotion.” *Proceedings of the National Academy of Sciences of the United States of America* 116 (5): 1645–50. https://doi.org/10.1073/pnas.1812820116.

Fazzalari, N. L., A. J. Moore, S. Byers, and R. W. Byard. 1997. “Quantitative Analysis of Trabecular Morphogenesis in the Human Costochondral Junction during the Postnatal Period in Normal Subjects.” *Anatomical Record* 248 (1): 1–12. https://doi.org/10.1002/(SICI)1097-0185(199705)248:1<1::AID-AR1>3.0.CO;2-Z.

Ferembach, Denise. 1980. “Recomendations for Age and Sex Diagnosis of Skeletons.” *Journal of Human Evolution* 9: 517–49.

Fernández, Peter J., Carrie S. Mongle, Louise Leakey, Daniel J. Proctor, Caley M. Orr, Biren A. Patel, Sergio Almécija, Matthew W. Tocheri, and William L. Jungers. 2018. “Evolution and Function of the Hominin Forefoot.” *Proceedings of the National Academy of Sciences* 115 (35): 201800818. https://doi.org/10.1073/pnas.1800818115.

Fiammenghi, C A. 2003. “La Necropoli Di Elea-Velia: Qualche Osservazione Preliminare.” *Elea-Velia. Le Nuove Ricerche. Quaderni Del Centro Studi Magna Grecia* 1: 49–61.

Forssberg, H. 1985. “Ontogeny of Human Locomotor Control I. Infant Stepping, Supported Locomotion and Transition to Independent Locomotion.” *Experimental Brain Research* 57: 480–93. https://doi.org/0014-4819.

Frelat, Mélanie A., Stanislav Katina, Gerhard W. Weber, and Fred L. Bookstein. 2012. “Technical Note: A Novel Geometric Morphometric Approach to the Study of Long Bone Shape Variation.” *American Journal of Physical Anthropology* 149 (4): 628–38. https://doi.org/10.1002/ajpa.22177.

Frelat, Mélanie A., Colin N. Shaw, Simone Sukhdeo, Jean-Jacques Hublin, Stefano Benazzi, and Timothy M. Ryan. 2017. “Evolution of the Hominin Knee and Ankle.” *Journal of Human Evolution* 108: 147–60. https://doi.org/10.1016/j.jhevol.2017.03.006.

Friston, Karl J. 1995. “Statistical Parametric Mapping: Ontology and Current Issues.” *Journal of Cerebral Blood Flow & Metabolism* 15 (3): 361–70.

http://www.ncbi.nlm.nih.gov/entrez/query.fcgi?cmd=Retrieve&db=PubMed&dopt=Citation&list_uids=7713993%5Cnhttp://www.ncbi.nlm.nih.gov/pubmed/7713993%5Cnhttp://www.nature.com/doifinder/10.1038/jcbfm.1995.45.

Fritz, B., and M. Mauch. 2013. "Foot Development in Childhood and Adolescence." In *Handbook of Footwear Design and Manufacture*, 49–71. https://doi.org/10.1533/9780857098795.1.49.

Frost, Harold M. 2003. "Bone's Mechanostat: A 2003 Update." *The Anatomical Record Part A: Discoveries in Molecular, Cellular, and Evolutionary Biology: An Official Publication of the American Association of Anatomists* 275 (2): 1081–1101.

Gao, Tingran, Julie Winchester, and Nick Stephens. 2020. "NBStephens/Auto3dgm-Matlab-Gorgon: Auto3dgm with Transformation Matrices," September. https://doi.org/10.5281/ZENODO.4010432.

Gardner, Ernest, Ronan O'Rahilly, and D J Gray. 1959. "The Prenatal Development of the Skeleton and Joints of the Human Foot." *JBJS* 41 (5): 847–76.

Gorissen, B. M.C., C. F. Wolschrijn, B. van Rietbergen, L. Rieppo, S. Saarakkala, and P. R. van Weeren. 2018. "Trabecular and Subchondral Bone Development of the Talus and Distal Tibia from Foal to Adult in the Warmblood Horse." *Journal of Veterinary Medicine Series C: Anatomia Histologia Embryologia* 47 (3): 206–15. https://doi.org/10.1111/ahe.12341.

Gosman, James H. 2007. "Patterns in Ontogeny of Human Trabecular Bone from Sunwatch Village in the Prehistoric Ohio Valley." The Ohio State University. https://doi.org/10.1002/ajpa.20931.

Gosman, James H., and Richard A. Ketcham. 2009. "Patterns in Ontogeny of Human Trabecular Bone from SunWatch Village in the Prehistoric Ohio Valley: General Features of Microarchitectural Change." *American Journal of Physical Anthropology* 138 (3): 318–32. https://doi.org/10.1002/ajpa.20931.

Gosman, James H, Samuel D Stout, and Clark Spencer Larsen. 2011. "Skeletal Biology over the Life Span: A View from the Surfaces." *American Journal of Physical Anthropology* 146 (S53): 86–98.

Gross, Thomas, Tracy L. Kivell, Matthew M. Skinner, N. Huynh Nguyen, and Dieter H. Pahr. 2014. "A CT-Image-Based Framework for the Holistic Analysis of Cortical and Trabecular Bone Morphology." *Palaeontologia Electronica* 17 (3). https://doi.org/10.26879/438.

Gunz, Philipp, and Philipp Mitteroecker. 2013. "Semilandmarks: A Method for Quantifying Curves and Surfaces." *Hystrix* 24 (1). https://doi.org/10.4404/hystrix-24.1-6292.

Hallemans, Ann, Dirk De Clercq, Stefaan Van Dongen, and Peter Aerts. 2006a. "Changes in Foot-Function Parameters during the First 5 Months after the Onset of Independent Walking: A Longitudinal Follow-up Study." *Gait and Posture* 23 (2): 142–48. https://doi.org/10.1016/j.gaitpost.2005.01.003.

Hallemans, Ann, Dirk De Clercq, Bert Otten, and Peter Aerts. 2005. "3D Joint Dynamics of Walking in Toddlers: A Cross-Sectional Study Spanning the First Rapid Development Phase of Walking." *Gait and Posture* 22 (2): 107–18. https://doi.org/10.1016/j.gaitpost.2004.07.010.

Hallemans, Ann, Kristiaan D'Août, Dirk De Clercq, and Peter Aerts. 2003. "Pressure Distribution Patterns under the Feet of New Walkers: The First Two Months of Independent Walking." *Foot and Ankle International* 24 (5): 444–53. https://doi.org/10.1177/107110070302400513.

Halloran, Bernard P., Virginia L. Ferguson, Steven J. Simske, Andrew Burghardt, Laura L. Venton, and Sharmila Majumdar. 2002. “Changes in Bone Structure and Mass with Advancing Age in the Male C57BL/6J Mouse.” *Journal of Bone and Mineral Research* 17 (6): 1044–50. https://doi.org/10.1359/jbmr.2002.17.6.1044.

Harcourt-Smith. 2002. “Form and Function in The.” *Archivio Internazionale Di Studi Neurologici* 1 (September): 409–17.

Harcourt-Smith, W, and Lc Aiello. 2004. “Fossils, Feet and the Evolution of Bipedal Locomotion.” *Journal of Anatomy* 204: 403–16. https://doi.org/10.1111/j.0021-8782.2004.00296.x.

Harcourt-Smith, Will E.H., and L. C. Aiello. 2004a. “Fossils, Feet and the Evolution of Human Bipedal Locomotion.” *Journal of Anatomy* 204 (5): 403–16. https://doi.org/10.1111/j.0021-8782.2004.00296.x.

Hatházi, Gábor. 2004. “A Kunok Régészeti Emlékei a Kelet-Dunántúlon (Die Archäologischen Funde Und Befunde Der Kumanen Im Osten Transdanubiens).” OpHung.

Hellier, C A, and N Jeffery. 2006a. “Morphological Plasticity in the Juvenile Talus.” *Foot and Ankle Surgery* 12 (3): 139–47. https://doi.org/10.1016/j.fas.2006.03.008.

Hildebrand, T., and P. Rüegsegger. 1997. “A New Method for the Model-Independent Assessment of Thickness in Three-Dimensional Images.” *Journal of Microscopy* 185 (1): 67–75. https://doi.org/10.1046/j.1365-2818.1997.1340694.x.

Hilgard, Ernest R., and Myrtle B. McGraw. 1945. “The Neuromuscular Maturation of the Human Infant.” *The American Journal of Psychology* 58 (2): 296. https://doi.org/10.2307/1417865.

Holowka, Nicholas B, and Daniel E Lieberman. 2018. “Rethinking the Evolution of the Human Foot: Insights from Experimental Research.” *Journal of Experimental Biology*. https://doi.org/10.1242/jeb.174425.

Hu, Yixin, Qingnan Zhou, Xifeng Gao, Alec Jacobson, Denis Zorin, and Daniele Panozzo. 2018. “Tetrahedral Meshing in the Wild.” *ACM Trans. Graph.* 37 (4): 60–61.

Ilich, Jasminka Z, and Jane E Kerstetter. 2013. “Nutrition in Bone Health Revisited : A Story Beyond Calcium.” *American Journal of Nutrition* 19 (6): 37–41.

Kivell, Tracy L. 2016a. “A Review of Trabecular Bone Functional Adaptation: What Have We Learned from Trabecular Analyses in Extant Hominoids and What Can We Apply to Fossils?” *Journal of Anatomy* 228 (4): 569–94. https://doi.org/10.1111/joa.12446.

Komza, Klara, and Matthew M. Skinner. 2019. “First Metatarsal Trabecular Bone Structure in Extant Hominoids and Swartkrans Hominins.” *Journal of Human Evolution* 131: 1–21. https://doi.org/10.1016/j.jhevol.2019.03.003.

Landi, Federica, Antonio Profico, Alessio Veneziano, Isabelle De Groote, and Giorgio Manzi. 2020. “Locomotion, Posture, and the Foramen Magnum in Primates: Reliability of Indices and Insights into Hominin Bipedalism.” *American Journal of Primatology* 82 (9): 1–13. https://doi.org/10.1002/ajp.23170.

László, Orsolya. 2008. “Study of Influence of Stress on Skeletal Growth in Non-Adults–Comparative

Analysis of a Subadult Population from a Medieval Hungarian Cemetery, Kána." *MSC Szakdolgozat. Durham University, Durham*.

László, Orsolya. 2018. "Gyermekkorú Maradványok Összehasonlító Biológiai Antropológiai Vizsgálata Történeti Népességekben." *ANTHROPOLOGIAI KÖZLEMÉNYEK* 59: 55–63.

Levine, Mel. 2012. *A Mind at a Time: How Every Child Can Succeed*. Simon and Schuster.

Lewis, Mary E. 2007. *The Bioarchaeology of Children: Perspectives from Biological and Forensic Anthropology*. Vol. 50. Cambridge University Press.

Lewton, Kristi L., and Jeremiah E. Scott. 2017. "Ischial Form as an Indicator of Bipedal Kinematics in Early Hominins: A Test Using Extant Anthropoids." *Anatomical Record* 300 (5): 845–58. https://doi.org/10.1002/ar.23543.

Lieberman, Daniel E., Maureen J. Devlin, and Osbjorn M. Pearson. 2001. "Articular Area Responses to Mechanical Loading: Effects of Exercise, Age, and Skeletal Location." *American Journal of Physical Anthropology* 116 (4): 266–77. https://doi.org/10.1002/ajpa.1123.

Lieberman, Daniel E. 1997. "Making Behavioral and Phylogenetic Inferences from Hominid Fossils: Considering the Developmental Influence of Mechanical Forces." *Annual Review of Anthropology* 26 (1): 185–210.

Long, Fanxin. 2012. "Prenatal Bone Development." In *Pediatric Bone*, Second Edi, 39–53. Elsevier Inc. https://doi.org/10.1016/B978-0-12-382040-2.10003-6.

Maier, Erne, and M Killmann. 2003. "Kinderfuß Und Kinderschuh." *Entwicklung Der Kindlichen Beine Und Füß Und Ihre Anforderungen an Fußgerechte Schuhe*.

Manter, John T. 1946. "Distribution of Compression Forces in the Joints of the Human Foot." *The Anatomical Record* 96 (3): 313–21.

Masao, Fidelis T., Elgidius B. Ichumbaki, Marco Cherin, Angelo Barili, Giovanni Boschian, Dawid A. Iurino, Sofia Menconero, Jacopo Moggi-Cecchi, and Giorgio Manzi. 2016. "New Footprints from Laetoli (Tanzania) Provide Evidence for Marked Body Size Variation in Early Hominins." *ELife* 5 (DECEMBER2016): 29. https://doi.org/10.7554/eLife.19568.

McGraw, MB. 1935. "Growth: A Study of Johnny and Jimmy (Preface by F. Tilney; Introduction by J. Dewey.)." https://psycnet.apa.org/record/1935-06046-000.

McNutt, Ellison J., Bernhard Zipfel, and Jeremy M. DeSilva. 2018. "The Evolution of the Human Foot." *Evolutionary Anthropology*. https://doi.org/10.1002/evan.21713.

Mesterházy-Ács, Zs. 2015. "Párták És Pártaövek Paks-Cseresznyés Lelőhelyről." *Szőllősy, C., Pokrovenszki, K.(Szerk.) Fiatal Középkoros Régészek VI. Konferenciájának Tanulmánykötete. Szent István Király Múzeum, Székesfehérvár*, 191–203.

Milner, George R, and Virginia G Smith. 1990. "Oneota Human Skeletal Remains." *Archaeological Investigations at the Morton Village and Norris Farms* 36 (11).

Milovanovic, Petar, Danijela Djonic, Michael Hahn, Michael Amling, Björn Busse, and Marija Djuric. 2017. "Region-Dependent Patterns of Trabecular Bone Growth in the Human Proximal Femur: A Study of

3D Bone Microarchitecture from Early Postnatal to Late Childhood Period." *American Journal of Physical Anthropology* 164 (2): 281–91. https://doi.org/10.1002/ajpa.23268.

Mitteroecker, Philipp, Philipp Gunz, Markus Bernhard, Katrin Schaefer, and Fred L Bookstein. 2004. "Comparison of Cranial Ontogenetic Trajectories among Great Apes and Humans." *Journal of Human Evolution* 46 (6): 679–98. https://doi.org/10.1016/j.jhevol.2004.03.006.

Mitteroecker, Philipp, Philipp Gunz, Sonja Windhager, and Katrin Schaefer. 2013. "A Brief Review of Shape, Form, and Allometry in Geometric Morphometrics, with Applications to Human Facial Morphology." *Hystrix* 24 (1): 1–8. https://doi.org/10.4404/hystrix-24.1-6369.

Moore, Keith L, and Arthur F Dalley. 2018. *Clinically Oriented Anatomy*. Wolters kluwer india Pvt Ltd.

Moorrees, C. F. A., E. A. Fanning, and Jr. E. E. Hunt. 1963. "Age Variation of Formation Stages for Ten Permanent Teeth." *Journal of Dental Research* 42 (6): 1490–1502. http://core.tdar.org/document/112919/age-variation-of-formation-stages-for-ten-permanent-teeth.

Moorrees, Coenraad F A, Elizabeth A Fanning, and Edward E Hunt Jr. 1963. "Formation and Resorption of Three Deciduous Teeth in Children." *American Journal of Physical Anthropology* 21 (2): 205–13.

Morel, Jean-Paul. 2006. "De Marseille à Velia: Problèmes Phocéens." *Comptes Rendus Des Séances de l'Académie Des Inscriptions et Belles-Lettres* 150 (4): 1723–83.

Mulder, Lars, Jan Harm Koolstra, Wim A. Weijs, and Theo M.G.J. Van Eijden. 2005. "Architecture and Mineralization of Developing Trabecular Bone in the Pig Mandibular Condyle." *Anatomical Record - Part A Discoveries in Molecular, Cellular, and Evolutionary Biology* 285 (1): 659–66. https://doi.org/10.1002/ar.a.20208.

Myronenko, Andriy, and Xubo Song. 2010. "Point Set Registration: Coherent Point Drifts." *IEEE Transactions on Pattern Analysis and Machine Intelligence* 32 (12): 2262–75. https://doi.org/10.1109/TPAMI.2010.46.

Nafei, A., J. Kabel, A. Odgaard, F. Linde, and I. Hvid. 2000. "Properties of Growing Trabecular Ovine Bone Part II: Architectural and Mechanical Properties." *Journal of Bone and Joint Surgery - Series B* 82 (6): 921–27. https://doi.org/10.1302/0301-620X.82B6.9837.

Nuzzo, S, C Meneghini, P Braillon, R Bouvier, S Mobilio, and Françoise Peyrin. 2003. "Microarchitectural and Physical Changes during Fetal Growth in Human Vertebral Bone." *Journal of Bone and Mineral Research* 18 (4): 760–68. https://doi.org/10.1359/jbmr.2003.18.4.760.

Okamoto, Tsutomu, Kayoko Okamoto, and Paul D. Andrew. 2003. "Electromyographic Developmental Changes in One Individual from Newborn Stepping to Mature Walking." *Gait and Posture* 17 (1): 18–27. https://doi.org/10.1016/S0966-6362(02)00049-8.

Pahr, Dieter H., and Philippe K. Zysset. 2009. "A Comparison of Enhanced Continuum FE with Micro FE Models of Human Vertebral Bodies." *Journal of Biomechanics* 42 (4): 455–62. https://doi.org/10.1016/j.jbiomech.2008.11.028.

Pal, Gaya P., and Rohini V. Routal. 1998. "Architecture of the Cancellous Bone of the Human Talus." *Anatomical Record* 252 (2): 185–93. https://doi.org/10.1002/(SICI)1097-

0185(199810)252:2<185::AID-AR4>3.0.CO;2-2.

Palmer, Carroll E. 1944. “Studies of the Center of Gravity in the Human Body.” *Child Development* 15 (2/3): 99–180.

Parfitt, A M, R Travers, F Rauch, and F H Glorieux. 2000. “Structural and Cellular Changes during Bone Growth in Healthy Children.” *Bone* 27 (4): 487–94.

Pedersen, A V, J H Størksen, and B Vereijken. 2002. “Lateral Biases in the Development of Infant Walking.” In *Poster Presentation at the Seventh European Workshop on Ecological Psychology, Bendor, France*.

Pivonka, Peter, Aaron Park, and Mark R Forwood. 2018. “Functional Adaptation of Bone: The Mechanostat and Beyond.” In *Multiscale Mechanobiology of Bone Remodeling and Adaptation*, 1–60. Springer.

Pontzer, H., D. E. Lieberman, E. Momin, M. J. Devlin, J. D. Polk, B. Hallgrímsson, and D. M.L. Cooper. 2006. “Trabecular Bone in the Bird Knee Responds with High Sensitivity to Changes in Load Orientation.” *Journal of Experimental Biology* 209 (1): 57–65. https://doi.org/10.1242/jeb.01971.

Preis, Sabine, Anja Klemms, and Kristiina Müller. 2008. “Gait Analysis by Measuring Ground Reaction Forces in Children: Changes to an Adaptive Gait Pattern between the Ages of One and Five Years.” *Developmental Medicine & Child Neurology* 39 (4): 228–33. https://doi.org/10.1111/j.1469-8749.1997.tb07416.x.

Price, Carina, Stewart C. Morrison, Farina Hashmi, Jill Phethean, and Christopher Nester. 2018. “Biomechanics of the Infant Foot during the Transition to Independent Walking: A Narrative Review.” *Gait and Posture* 59 (December 2016): 140–46. https://doi.org/10.1016/j.gaitpost.2017.09.005.

Raichlen, David A. 2005. “Effects of Limb Mass Distribution on the Ontogeny of Quadrupedalism in Infant Baboons (Papio Cynocephalus) and Implications for the Evolution of Primate Quadrupedalism.” *Journal of Human Evolution* 49 (4): 415–31. https://doi.org/10.1016/j.jhevol.2005.05.004.

Raichlen, David A., and Adam D. Gordon. 2017. “Interpretation of Footprints from Site S Confirms Human-like Bipedal Biomechanics in Laetoli Hominins.” *Journal of Human Evolution* 107: 134–38. https://doi.org/10.1016/j.jhevol.2017.04.002.

Raichlen, David a., Adam D. Gordon, Adam D. Foster, James T. Webber, Simone M. Sukhdeo, Robert S. Scott, James H. Gosman, and Timothy M. Ryan. 2015. “An Ontogenetic Framework Linking Locomotion and Trabecular Bone Architecture with Applications for Reconstructing Hominin Life History.” *Journal of Human Evolution* 81: 1–12. https://doi.org/10.1016/j.jhevol.2015.01.003.

Raichlen, David A., Adam D. Gordon, William E.H. Harcourt-Smith, Adam D. Foster, and Wm Randall Haas. 2010. “Laetoli Footprints Preserve Earliest Direct Evidence of Human-Like Bipedal Biomechanics.” *PLoS ONE* 5 (3): 1–6. https://doi.org/10.1371/journal.pone.0009769.

Reissis, Dimitris, and Richard L Abel. 2012. “Development of Fetal Trabecular Micro-Architecture in the Humerus and Femur.” *Journal of Anatomy* 220 (5): 496–503. https://doi.org/10.1111/j.1469-7580.2012.01487.x.

Rohlf, F. James, and Marco Corti. 2000. “Use of Two-Block Partial Least-Squares to Study Covariation in

Shape." *Systematic Biology* 49 (4): 740–53.

Rohlf, F. James, and Dennis Slice. 1990. "Extensions of the Procrustes Method for the Optimal Superimposition of Landmarks." *Systematic Zoology* 39 (1): 40. https://doi.org/10.2307/2992207.

Ronchitelli, Annamaria, Sonia Mugnaini, Simona Arrighi, Andrea Atrei, Giulia Capecchi, Marco Giamello, Laura Longo, Nadia Marchettini, Cecilia Viti, and Adriana Moroni. 2015. "When Technology Joins Symbolic Behaviour: The Gravettian Burials at Grotta Paglicci (Rignano Garganico - Foggia - Southern Italy)." *Quaternary International* 359: 423–41. https://doi.org/10.1016/j.quaint.2014.08.038.

Ruff, Chris. 1988. "Hindlimb Articular Surface Allometry in Hominoidea and Macaca, with Comparison to Diaphyseal Scaling." *Journal of Human Evolution* 17: 687–714.

Ruff, Christopher B., and Wilson C. Hayes. 1982. "Subperiosteal Expansion and Cortical Remodeling of the Human Femur and Tibia with Aging." *Science* 217 (4563): 945–48. https://doi.org/10.1126/science.7112107.

Ruff, Christopher B., William W. Scott, and Allie Y.-C Liu. 1991. "Articular and Diaphyseal Remodeling of the Proximal Femur with Changes in Body Mass in Adults." *American Journal of Physical Anthropology* 86 (3): 397–413. https://doi.org/10.1002/ajpa.1330860306.

Ruff, Christopher B, Erik Trinkaus, Alan Walker, and Clark Spencer Larsen. 1993. "Postcranial Robusticity in Homo. I: Temporal Trends and Mechanical Interpretation." *American Journal of Physical Anthropology* 91 (1): 21–53.

Ruff, Christopher, Brigitte Holt, and Erik Trinkaus. 2006. "Who's Afraid of the Big Bad Wolff?: 'Wolff's Law' and Bone Functional Adaptation." *American Journal of Physical Anthropology*. https://doi.org/10.1002/ajpa.20371.

Russo, Gabrielle A., and E. Christopher Kirk. 2013. "Foramen Magnum Position in Bipedal Mammals." *Journal of Human Evolution* 65 (5): 656–70. https://doi.org/10.1016/j.jhevol.2013.07.007.

Ryan, Timothy M., Kristian J. Carlson, Adam D. Gordon, Nina Jablonski, Colin N. Shaw, and Jay T. Stock. 2018. "Human-like Hip Joint Loading in Australopithecus Africanus and Paranthropus Robustus." *Journal of Human Evolution* 121: 12–24. https://doi.org/10.1016/j.jhevol.2018.03.008.

Ryan, Timothy M., and Gail E. Krovitz. 2006. "Trabecular Bone Ontogeny in the Human Proximal Femur." *Journal of Human Evolution* 51 (6): 591–602. https://doi.org/10.1016/j.jhevol.2006.06.004.

Ryan, Timothy M, David A Raichlen, and James H Gosman. 2017. "Structural and Mechanical Changes in Trabecular Bone during Early Development in the Human Femur and Humerus." *Building Bones: Bone Formation and Development in Anthropology* 77: 281.

Ryan, Timothy M, and Colin N Shaw. 2015. "Gracility of the Modern Homo Sapiens Skeleton Is the Result of Decreased Biomechanical Loading" 112 (2). https://doi.org/10.1073/pnas.1418646112.

Saers, Jaap P. P. 2017. "Ontogeny and Functional Adaptation of Pedal Trabecular Bone." University of Cambridge.

Saers, Jaap P.P., Timothy M. Ryan, and Jay T. Stock. 2019. "Trabecular Bone Structure Scales Allometrically in the Foot of Four Human Groups." *Journal of Human Evolution* 135: 102654.

https://doi.org/10.1016/j.jhevol.2019.102654.

Saers, Jaap P.P., Timothy M. Ryan, and Jay T Stock. 2020. “Baby Steps towards Linking Calcaneal Trabecular Bone Ontogeny and the Development of Bipedal Human Gait.” *Journal of Anatomy* 236 (3): 474–92. https://doi.org/10.1111/joa.13120.

Salathé, Eric Paul, George A. Arangio, and Eric P. Salathé. 1986. “A Biomechanical Model of the Foot.” *Journal of Biomechanics* 19 (12): 989–1001. https://doi.org/10.1016/0021-9290(86)90116-8.

Salle, B. L., F. Rauch, R. Travers, R. Bouvier, and F. H. Glorieux. 2002. “Human Fetal Bone Development: Histomorphometric Evaluation of the Proximal Femoral Metaphysis.” *Bone* 30 (6): 823–28. https://doi.org/10.1016/S8756-3282(02)00724-X.

Scheuer, Louise, and Sue Black. 2004. *The Juvenile Skeleton*. Elsevier.

Schlager, Stefan. 2017. “Morpho and Rvcg–Shape Analysis in R: R-Packages for Geometric Morphometrics, Shape Analysis and Surface Manipulations.” In *Statistical Shape and Deformation Analysis*, 217–56. Elsevier.

Schmitt, Daniel. 2003. “Insights into the Evolution of Human Bipedalism from Experimental Studies of Humans and Other Primates.” *Journal of Experimental Biology*. https://doi.org/10.1242/jeb.00279.

Shapiro, L. J., and D. A. Raichlen. 2006. “Limb Proportions and the Ontogeny of Quadrupedal Walking in Infant Baboons (Papio Cynocephalus).” *Journal of Zoology* 269 (2): 191–203. https://doi.org/10.1111/j.1469-7998.2006.00082.x.

Shaw, Colin N., and Timothy M. Ryan. 2012. “Does Skeletal Anatomy Reflect Adaptation to Locomotor Patterns? Cortical and Trabecular Architecture in Human and Nonhuman Anthropoids.” *American Journal of Physical Anthropology* 147 (2): 187–200. https://doi.org/10.1002/ajpa.21635.

Skedros, John G., Scott M. Sorenson, Kenneth J. Hunt, and Joshua D. Holyoak. 2007. “Ontogenetic Structural and Material Variations in Ovine Calcanei: A Model for Interpreting Bone Adaptation.” *Anatomical Record* 290 (3): 284–300. https://doi.org/10.1002/ar.20423.

Slice, Dennis E. 2006. *Modern Morphometrics in Physical Anthropology*. Springer Science & Business Media.

Smith, Bh. 1991. “Standards of Human Tooth Formation and Dental Age Assessment.” *Advances in Dental Anthropology*. http://deepblue.lib.umich.edu/handle/2027.42/90867.

Smith, Tanya M., Zarin Machanda, Andrew B Bernard, Ronan M Donovan, Amanda M Papakyrikos, Martin N Muller, Richard W. Wrangham, et al. 2018. “Multivariate Analysis of Variations in Intrinsic Foot Musculature among Hominoids.” *American Journal of Physical Anthropology* 114 (1): 1–12. https://doi.org/10.1111/joa.12780.

Sockol, M. D., D. A. Raichlen, and H. Pontzer. 2007. “Chimpanzee Locomotor Energetics and the Origin of Human Bipedalism.” *Proceedings of the National Academy of Sciences* 104 (30): 12265–69. https://doi.org/10.1073/pnas.0703267104.

Sorrentino, R., N.B. Stephens, K.J. Carlson, C. Figus, L. Fiorenza, S. Frost, W. Harcourt-Smith, et al. 2020. “The Influence of Mobility Strategy on the Modern Human Talus.” *American Journal of Physical*

Anthropology 171 (3). https://doi.org/10.1002/ajpa.23976.

Sorrentino, Rita, Maria Giovanna Belcastro, Carla Figus, Nicholas B. Stephens, Kevin Turley, William Harcourt-Smith, Timothy M. Ryan, and Stefano Benazzi. 2020. "Exploring Sexual Dimorphism of the Modern Human Talus through Geometric Morphometric Methods." *PLoS ONE* 15 (2): 1–17. https://doi.org/10.1371/journal.pone.0229255.

Sorrentino, Rita, Kristian J. Carlson, Eugenio Bortolini, Caterina Minghetti, Francesco Feletti, Luca Fiorenza, Stephen Frost, et al. 2020. "Morphometric Analysis of the Hominin Talus: Evolutionary and Functional Implications." *Journal of Human Evolution* 142: 102747. https://doi.org/10.1016/j.jhevol.2020.102747.

Sorrentino, Rita, Nicholas B. Stephens, Kristian J. Carlson, Carla Figus, Luca Fiorenza, Stephen Frost, William Harcourt-Smith, et al. 2020. "The Influence of Mobility Strategy on the Modern Human Talus." *American Journal of Physical Anthropology* 171 (3): 456–69. https://doi.org/10.1002/ajpa.23976.

Staheli, LYNN T, Deanna E Chew, and MARILYN Corbett. 1987. "The Longitudinal Arch. A Survey of Eight Hundred and Eighty-Two Feet in Normal Children and Adults." *The Journal of Bone and Joint Surgery. American Volume* 69 (3): 426–28.

Stavlas, Panagiotis, Theodoros B Grivas, Constantinos Michas, Elias Vasiliadis, and Vassilios Polyzois. 2005. "The Evolution of Foot Morphology in Children Between 6 and 17 Years of Age : A Cross-Sectional Study Based on Footprints in a Mediterranean Population." *The Journal of Foot & Ankle Surgery*, 424–28. https://doi.org/10.1053/j.jfas.2005.07.023.

Stephens, Nicholas B., Tracy L. Kivell, Thomas Gross, Dieter H. Pahr, Richard A. Lazenby, Jean Jacques Hublin, Israel Hershkovitz, and Matthew M. Skinner. 2016. "Trabecular Architecture in the Thumb of Pan and Homo: Implications for Investigating Hand Use, Loading, and Hand Preference in the Fossil Record." *American Journal of Physical Anthropology* 161 (4): 603–19. https://doi.org/10.1002/ajpa.23061.

Stephens, Nicholas B., Tracy L. Kivell, Dieter H. Pahr, Jean Jacques Hublin, and Matthew M. Skinner. 2018. "Trabecular Bone Patterning across the Human Hand." *Journal of Human Evolution* 123: 1–23. https://doi.org/10.1016/j.jhevol.2018.05.004.

Stephens, Nick. 2020. "NBStephens/Phenotypic_PointCloud_Analysis: Initial_release," August. https://doi.org/10.5281/ZENODO.4006529.

Stloukal, Milan, and Hana Hanáková. 1978. "Length of Long Bones in Ancient Slavonic Populations-with Particular Consideration to Questions of Growth." *HOMO-JOURNAL OF COMPARATIVE HUMAN BIOLOGY* 29 (1): 53–69.

Straus, William L. 1927. "The Growth of the Human Foot and Its Evolutionary Significance." *Contrib Embryol* 101: 93–134.

Su, Anne. 2011. "The Functional Morphology of Subchondral and Trabecular Bone in the Hominoid Tibiotalar Joint." *Stonybrook Thesis*.

Su, Anne, and Kristian J. Carlson. 2017. “Comparative Analysis of Trabecular Bone Structure and Orientation in South African Hominin Tali.” *Journal of Human Evolution* 106: 1–18. https://doi.org/10.1016/j.jhevol.2016.12.006.

Su, Anne, Ian J. Wallace, and Masato Nakatsukasa. 2013. “Trabecular Bone Anisotropy and Orientation in an Early Pleistocene Hominin Talus from East Turkana, Kenya.” *Journal of Human Evolution* 64 (6): 667–77. https://doi.org/10.1016/j.jhevol.2013.03.003.

Sullivan, C Bane, and Alexander A Kaszynski. 2019. “PyVista: 3D Plotting and Mesh Analysis through a Streamlined Interface for the Visualization Toolkit (VTK).” *Journal of Open Source Software* 4 (37): 1450.

Sutherland, D. 1997. “The Development of Mature Gait.” *Gait and Posture* 6 (2): 163–70. https://doi.org/10.1016/S0966-6362(97)00029-5.

Sutherland, D H, R Olshen, L Cooper, and S L Woo. 1980. “The Development of Mature Gait.” *J Bone Joint Surg Am*.

Swan, Karen R, Rachel Ives, Laura A.B. Wilson, and Louise T Humphrey. 2020. “Ontogenetic Changes in Femoral Cross-Sectional Geometry during Childhood Locomotor Development.” *American Journal of Physical Anthropology* 173 (1): 80–95. https://doi.org/10.1002/ajpa.24080.

Sylvester, Adam D. 2006. “Locomotor Decoupling and the Origin of Hominin Bipedalism.” *Journal of Theoretical Biology* 242 (3): 581–90. https://doi.org/10.1016/j.jtbi.2006.04.016.

Szeniczey, Tamás, Antónia Marcsik, Zsófia Ács, Tímea Balassa, Zsolt Bernert, Katalin Bakó, Tamás Czuppon, et al. 2019. “Hyperostosis Frontalis Interna in Ancient Populations from the Carpathian Basin – A Possible Relationship between Lifestyle and Risk of Development.” *International Journal of Paleopathology* 24 (October 2018): 108–18. https://doi.org/10.1016/j.ijpp.2018.10.003.

Tanck, E., J. Homminga, G. H. Van Lenthe, and R. Huiskes. 2001. “Increase in Bone Volume Fraction Precedes Architectural Adaptation in Growing Bone.” *Bone* 28 (6): 650–54. https://doi.org/10.1016/S8756-3282(01)00464-1.

Thatcher, Robert W, G Lyon, J Rumsey, and N Krasnegor. 1996. *Developmental Neuroimaging: Mapping the Development of Brain and Behavior*. Academic Press.

Thelen, Esther. 1992. “Development of Locomotion from a Dynamic Systems Approach.” In *Movement Disorders in Children*, 36:169–73. Karger Publishers.

Thorpe, S. K.S., R. L. Holder, and R. H. Crompton. 2007. “Origin of Human Bipedalism as an Adaptation for Locomotion on Flexible Branches.” *Science* 316 (5829): 1328–31. https://doi.org/10.1126/science.1140799.

Tsegai, Zewdi J., Matthew M. Skinner, Andrew H. Gee, Dieter H. Pahr, Graham M. Treece, Jean Jacques Hublin, and Tracy L. Kivell. 2017. “Trabecular and Cortical Bone Structure of the Talus and Distal Tibia in Pan and Homo.” *American Journal of Physical Anthropology* 163 (4): 784–805. https://doi.org/10.1002/ajpa.23249.

Tsegai, Zewdi J., Matthew M. Skinner, Dieter H. Pahr, Jean-Jacques Hublin, and Tracy L. Kivell. 2018.

"Ontogeny and Variability of Trabecular Bone in the Chimpanzee Humerus, Femur and Tibia." *American Journal of Physical Anthropology*, no. July: 1–24. https://doi.org/10.1002/ajpa.23696.

Turley, K., F. J. White, and S. R. Frost. 2015. "Phenotypic Plasticity: The Impact of Habitat and Behavior (Substrate Use) on Adult Talo-Crural Appositional Articular Joint Shape Both between and within Closely Related Hominoid Species." *Human Evolution* 30 (1–2): 49–67. https://doi.org/10.14673/HE2015121002.

Turley, Kevin, and Stephen R. Frost. 2013 "The Shape and Presentation of the Catarrhine Talus: A Geometric Morphometric Analysis." *Anatomical Record* 296 (6): 877–90. https://doi.org/10.1002/ar.22696.

Turley, Kevin, and Stephen R. Frost. 2014a. "The Ontogeny of Talo-Crural Appositional Articular Morphology among Catarrhine Taxa: Adult Shape Reflects Substrate Use." *American Journal of Physical Anthropology* 154 (3): 447–58. https://doi.org/10.1002/ajpa.22528.

Turley, Kevin, and Stephen R Frost. 2014b. "The Appositional Articular Morphology of the Talo-Crural Joint: The Influence of Substrate Use on Joint Shape." *Anatomical Record* 297 (4): 618–29. https://doi.org/10.1002/ar.22879.

Turley, Kevin, Evan A Simons, and Stephen R Frost. 2018. "Trajectory Analysis among African Hominoids Can Provide Insights into Genetic and Epigenetic Influences during Ontogeny." *American Journal of Physical Anthropology*, no. May: 1–5. https://doi.org/10.1002/ajpa.23625.

Uhthoff, Hans K, T. Kawashima, and H K Uhthoff. 1990. "The Development of the Ankle and Foot." In *The Embryology of the Human Locomotor System*, 22:141–53. https://doi.org/10.1007/978-3-642-75310-7_15.

Virtanen, Pauli, Ralf Gommers, Travis E. Oliphant, Matt Haberland, Tyler Reddy, David Cournapeau, Evgeni Burovski, et al. 2020a. "Author Correction: SciPy 1.0: Fundamental Algorithms for Scientific Computing in Python (Nature Methods, (2020), 17, 3, (261-272), 10.1038/S41592-019-0686-2)." *Nature Methods* 17 (3): 352. https://doi.org/10.1038/s41592-020-0772-5.

Virtanen, Pauli et al., 2020b. "SciPy 1.0: Fundamental Algorithms for Scientific Computing in Python." *Nature Methods* 17 (3): 261–72. https://doi.org/10.1038/s41592-019-0686-2.

Volpon, Jose B. 1994. "Footprint Analysis during the Growth Period." *Journal of Pediatric Orthopedics* 14 (1): 83–85.

Walker, J. M. 1991. "Musculoskeletal Development: A Review." *Physical Therapy* 71 (12): 878–89. https://doi.org/10.1093/ptj/71.12.878.

Ward, Carol V. 2002. "Interpreting the Posture and Locomotion of Australopithecus Afarensis: Where Do We Stand?" *Yearbook of Physical Anthropology* 45: 185–215. https://doi.org/10.1002/ajpa.10185.

Waseda, Akeo, Yasunori Suda, Suguru Inokuchi, and Yuji Nishiwaki. 2014. "Standard Growth of the Foot Arch in Childhood and Adolescence — Derived from the Measurement Results." *Foot and Ankle Surgery* 20 (3): 208–14. https://doi.org/10.1016/j.fas.2014.04.007.

Wolff, Julius. 1893. "Das Gesetz Der Transformation Der Knochen." *Deutsche Medizinische Wochenschrift*

19 (47): 1222–24. https://doi.org/10.1055/s-0028-1144106.

Wolschrijn, Claudia F., and Win A. Weijs. 2004. “Development of the Trabecular Structure within the Ulnar Medial Coronoid Process of Young Dogs.” *Anatomical Record - Part A Discoveries in Molecular, Cellular, and Evolutionary Biology* 278 (2): 514–19. https://doi.org/10.1002/ar.a.20039.

Worsley, K. J., S. Marrett, P. Neelin, A. C. Vandal, K. J. Friston, and A. C. Evans. 1996. “A Unified Statistical Approach for Determining Significant Signals in Images of Cerebral Activation.” *Human Brain Mapping* 4 (1): 58–73. https://doi.org/10.1002/(SICI)1097-0193(1996)4:1<58::AID-HBM4>3.0.CO;2-O.

Yazdani, Amirsaeed, Nicholas B Stephens, Venkateswararao Cherukuri, Timothy Ryan, and Vishal Monga. 2019. “Domain-Enriched Deep Network for Micro-CT Image Segmentation.” In *Conference Record - Asilomar Conference on Signals, Systems and Computers*, 2019-Novem:1867–71. https://doi.org/10.1109/IEEECONF44664.2019.9048654.

Zeininger, Angel Diane. 2013. “Ontogeny of Bipedalism : Pedal Mechanics and Trabecular Bone Morphology.”

Zeininger, Angel, Biren A. Patel, Bernhard Zipfel, and Kristian J. Carlson. 2016. “Trabecular Architecture in the StW 352 Fossil Hominin Calcaneus.” *Journal of Human Evolution* 97: 145–58. https://doi.org/10.1016/j.jhevol.2016.05.009.

Zeininger, Angel, Daniel Schmitt, Jody L. Jensen, and Liza J. Shapiro. 2018. “Ontogenetic Changes in Foot Strike Pattern and Calcaneal Loading during Walking in Young Children.” *Gait and Posture* 59 (September 2017): 18–22. https://doi.org/10.1016/j.gaitpost.2017.09.027.